MODELING NITROGEN CONTROLS ON TERRESTRIAL ECOSYSTEMS

ASSESSING NITROGEN CONTROLS ON TERRESTRIAL CARBON, WATER AND ENERGY FLUXES AND POOLS AT MULTI-SCALES USING THE CLASS-CTEM^{N+} MODEL

By SUO HUANG, B.Sc, M.Sc

A Thesis Submitted to the School of Graduate Studies In Partial Fulfillment of the Requirements For the Degree Doctor of Philosophy

McMaster University

DOCTOR OF PHILOSOPHY (2014) McMaster University
(Environmental Sciences) Hamilton, Ontario

TITLE:

Assessing Nitrogen Controls on Terrestrial Carbon, Water and Energy Fluxes and Pools at Multi-scales Using the Carbon-Nitrogen Coupled CLASS-CTEM^{N+} Model

AUTHOR: Suo Huang, B.Sc., M.Sc.

SUPERVISOR: Professor M. Altaf Arain

NUMBER OF PAGES: 144

ABSTRACT

The carbon and nitrogen coupled dynamic vegetation model, CLASS-CTEM^{N+} combines process-based, large-scale representations of terrestrial vegetation dynamics and land-atmosphere carbon and water exchanges in a modular framework. It prognostically simulates the principal processes of the terrestrial biosphere carbon and kinetic energy exchanges at the soil surface and plants, as well as the dynamic soil-plant nitrogen cycles.

In this study, improvements made in parameterization of different plant functional types (PFTs) were evaluated, and then, model was used to assess the effects of nitrogen controls on simulated terrestrial carbon, water and energy exchanges and carbon pools from the site-level to regional and global scales. Prior to global simulations, standardized hourly meteorological forcing data, eddy covariance (EC) fluxes, and other site-specific observations from 39 FLUXNET sites from the North American Carbon Program (NACP) and the Large Scale Biosphere-Atmosphere Experiment in Amazonia (LBA) projects, spanning 194 site-years and covering 8 major PFTs across the North America and the Amazonian basin, were used to evaluate model performance. Two versions of the model, carbon and nitrogen coupled (C-N) version and carbon-only (C) version were used to simulate diurnal, daily, seasonal and annual values of carbon, water and energy fluxes at each site. Carbon pools and key nitrogen cycling variables were compared to investigate nitrogen controls on carbon, water and energy exchanges at each site.

On the global scale, gridded forcing and initializing data sets developed by the North American Carbon Program (NACP)-Multi-Scale Synthesis and Terrestrial Model Intercomparison Project (MsTMIP) were used in CLASS-CTEM^{N+} simulations at 0.5 × 0.5 degree spatial resolution from 1901 to 2010. Exploratory and diagnostic assessment of the model was conducted at the global multi-decade scale, by comparing results from both versions of the model with observational and modeled estimates from literature to determine the impact of nitrogen availability on spatiotemporal dynamics and distributions of terrestrial carbon, water and energy fluxes and C pools.

Model results revealed satisfactory performance of the model in simulating carbon, water and energy fluxes and carbon stocks, when compared to observations, especially in summer, and at evergreen needleleaf forest ecosystems. In contrast, simulation-observations agreement declined in winter and early spring, and at non-forested sites (crops and grassland), especially in dry periods during the growing season. The C-N coupled model simulated global total mean annual estimates from 1980-2010 for Gross Ecosystem Productivity (GEP, 122.7 Pg C yr^{-1}), Ecosystem Respiration (Re, 119.1 Pg C yr^{-1}), Net Ecosystem Productivity (NPE, 3.46 Pg C yr^{-1}), Net Primary Productivity (NPP, 57.1 Pg C yr^{-1}), Latent Heat (LE, 146.2 ZJ yr^{-1}), Sensible Heat Flux (H, 194.0 ZJ yr^{-1}), Soil Organic Carbon (SOC, 1230.0 Pg C) and Total Vegetation Biomass (Tvg, 608.0 Pg C) were similar to reported values in the literature. Evaluation of nitrogen limitation impacts on global carbon sink and sources dynamics showed considerable variability between and within forest types due to non-linearity of N effects and spatiotemporal heterogeneity of C-N interactions. For the recent 1970-2010 period, the C-N model estimated annual increase rate in the global mean terrestrial carbon uptake, was 0.05 Pg C yr^{-1}, which was less than the 0.12 Pg C yr^{-1} simulated by C-only version of the model, suggesting a strong N attenuation effect compared to the C-only over this period. The consideration of N dynamics in the CLASS-$CTEM^{N+}$ simulations reduces the terrestrial C uptake compared with that of the C-only counterpart in some regions, where N might not be always be sufficiently available for plants to grow, particularly in mid to high latitude regions of boreal forests, tundra and some temperate forest regions, where N is a primary limiting nutrient. While a smaller N limitation effect was observed in the southern temperate and tropical regions where ecosystem production is most likely to be limited by phosphorus (P) rather than N.

Overall, the inclusion of the nitrogen cycle in the CLASS-$CTEM^{N+}$ model improved its prediction accuracy, in particular for forests. This study gives us confidence that CLASS-$CTEM^{N+}$ can predict carbon, water and energy fluxes and carbon stocks quite well in multiple vegetation ecosystems. The inclusion of nitrogen cycle in the model helped in its application at regional and global scales to evaluate nitrogen availability impacts on carbon cycle in terrestrial ecosystems and to determine nitrogen cycle feedbacks on Earth's climate system. This study also suggested the need for a network of long-term monitoring sites to measure changes in the vegetation and soil carbon biomass at the local and regional levels.

ACKNOWLEDGEMENTS

First of all, I would like to express my deepest gratitude to my supervisor, Professor Altaf Arain, for his supportive and insightful leading through my six years of Master and PhD studies at McMaster University. I was truly influenced by his passion and dedication to the academic research. His responsibility toward his students will make everyone feel fortunate to have such a supervisor like him.

I would like to thank the members of my supervisory committee: Dr. Vivek Arora, Dr. Jing M Chen, Dr. Paulin Coulibaly and Dr. Mike Waddington for the encouragement, guidance, and repeated appearances at annual committee meetings despite their tight schedules. I was tremendously inspired by their remarkable sense of research frontiers and scientific thinking.

I would like to acknowledge Dr. Vivek Arora for providing us the CTEM model code with the recent new parameters and thanks to his valuable advice and detailed discussions through all these years' personal communications. Thanks to Dr. Daina Verseghy and Dr. Paul Bartlett for CLASS model code. Thanks to Dr. Fengming Yuan for the contribution to the nitrogen coupling work in CLASS-CTEM.

Dr. Christopher Schwalm, Dr. Kevin Schaefer, Dr. Deborah Huntzinger and Dr. Yaxing Wei are greatly appreciated for their constructive technical support and scientific discussions in our research.

I appreciated the technical training and computational facility assistance from the SHARCNET of Compute Canada. In particular, I would like to thank Dr. Sergey Mashchenko for teaching me everything about the HPCs operations on SHARCNET, as well as for helping me with the optimization and logic design.

Moreover, I want to thank Dr. Jing M Chen and Dr. Mike Waddington by providing insightful scientific discussions and stimulating directions. The fellow researchers from their groups are also acknowledged for their technical expertise and support for our research along the way.

Data from the North American Carbon Program (NACP), Large-Scale Biosphere Atmosphere Experiment in Amazonia (LBA) and NACP-Multi-scale Synthesis and Terrestrial Model Intercomparison Project (MsTMIP) are acknowledged. We acknowledge the eddy covariance flux data acquired from the global FLUXNET.

I would like to show my great appreciation to the 'Climate lab-mates' for their valuable support and discussions, and more importantly, their laughter and bakery made the lab a relaxing and agreeable working place. I was highly motivated by their strength and commitment that they demonstrated toward the research work. Their open-mindedness to embrace new challenges and willingness to help others had significant impact on me. Special thanks going to Dr. Matthias Peichl, Dr. Jason Brodeur and Dr. Myroslava Khomik for their 'vice-supervisory' support. As such, I'd like to recognize you each individually and say that it's been my pleasure: Bin Chen, Rob Thorne, Samantha MacKay, Emily Hayman, Michelle Molon, Michelle Kula, Janelle Trant, Ananta Parsaud and Rachel Skubel.

Finally, I'd like to thank my parents and friends for the incredible love and support, without them I could not have this tough task done in my lifetime.

Table 0.1 List of Abbreviations

C	Carbon	LULCC	Land Use and Land Cover Change
CCCMa	Canadian Centre for Climate Modelling and Analysis	MSC	Meteorological Service of Canada
CGC3M	Canadian Global Coupled Climate-Carbon Model	MsTMIP	The Multi-Scale Synthesis and Terrestrial Model Intercomparison Project
CGCM	Canadian Global Climate Model	N	Nitrogen
CLASS	Canadian Land Surface Scheme	NACP	The North American Carbon Program
CO2	Carbon Dioxide	NCAR	National Center for Atmospheric Research
CRCM	Canadian Regional Climate Model	NCEP	National Centers for Environmental Prediction
CRU	Climatic Research Unit	Ndep	Nitrogen deposition
CTEM	Canadian Terrestrial Ecosystem Model	NEE	Net Ecosystem Exchange
DGVM	Dynamic Global Vegetation Model	NEP	Net Ecosystem Productivity
EC	Eddy Covariance	NH4+	Ammonia
EI	Model Efficiency Index	NIR	Near Infrared Radiation
ESMs	Earth System Models	NO3-	Nitrate
ET	Evapotranspiration	NPP	Net Primary Productivity
FACE	Free-Air Concentration Enrichment	PFTs	Plant functional types
FAO	Food and Agriculture Organization of the United Nations	Ra	Autotrophic respiration
FIA	Forest Inventory Analysis	RCPs	Representative Concentration Pathways
FOM	Fast/short-lived soil organic matter	Re	Terrestrial Ecosystem Respiration
fPAR	Photosynthetically Active Radiation	Rh	Heterotrophic respiration
GEP	Gross Ecosystem Productivity	RMSE	Root Mean Square Error
GHGs	Green House Gases	Rn	Net Radiation
H	Sensible Heat Flux	Runoff	Surface Runoff
IGBP	International Geosphere-Biosphere Programme	SLA	Specific leaf area
IPCC	The Intergovernmental Panel on Climate Change	SOC	Soil Organic Carbon
LAI	Leaf Area Index	SOM	Stable soil organic matter
LBA	Large Scale Biosphere-Atmosphere Experiment in Amazonia	SYNMAP	Synergetic Land Cover Product
LE	Latent Heat Flux	TEM	Terrestrial Ecosystem Model
LSSs	Land Surface Scheme	Tr	Transpiration
LUC	Land Use Change	Tvg	Total Vegetation Biomass

TABLE OF CONTENTS

INDEX OF TABLES

INDEX OF FIGURES

1. CHAPTER 1: INTRODUCTION

Terrestrial ecosystems play an important role in regulating Earth's climate through their biogeophysical and biogeochemical responses and feedbacks in terms of carbon (C), water and energy exchanges. During 2000-2007 period, terrestrial ecosystems have absorbed approximately 25~30% of anthropogenic fossil fuel carbon dioxide (CO_2) emissions (Keeling et al., 1996; Le Quere et al., 2009). However, rapid changes in climate due to human activities, such as the rising levels of greenhouse gases (GHGs) emissions, especially rapidly increasing atmospheric CO_2 levels, mostly caused by fossil fuel burning (IPCC 2007; Le Quere et al. 2009; Dolman et al. 2010; Alexander et al. 2013), land use changes (LUC), fertilizer application and enhanced atmospheric nitrogen (N) deposition, are dramatically altering the dynamics and functions of the terrestrial ecosystems (Nadelhoffer et al., 1999; McGuire et al., 2001; Holland et al., 2005; Denman 2007; Reay et al., 2008).

There is growing evidence that the human-induced enhancement in atmospheric nitrogen (N) deposition on land surfaces have affected terrestrial vegetation ecosystems (Hungate et al. 2003; Luo et al. 2004; Canadell et al. 2007; (Galloway et al., 2008, 2004; Gruber and Galloway, 2008; Gerber et al. 2010; Zaehle et al. 2010; Bonan & Levis 2010). Observations from Free-Air Concentration Enrichment (FACE) experiments suggest that terrestrial ecosystems grown under elevated CO_2 require more N to support enhanced plant growth than is required at ambient CO_2 (Luo et al., 2006). Warmer and wetter soils have the potential to increase the amount of inorganic N in soil through enhanced mineralization associated with decomposition. The improved N availability in soil may lead to enhanced soil microbial activity, which generally increases plant-available N in addition to meeting the N needs of soil organisms. The mineralization of soil N associated with decomposition has the potential to enhance the uptake of CO_2 by vegetation more than the loss of CO_2 from the decomposition (McGuire et al., 2007; Shaver, 1992). Increases in N deposition in industrialized regions have significantly contributed to the terrestrial carbon sink, particularly through enhancing vegetation growth in N limited areas (Holland et al. 1997; Nadelhoffer et al. 1999; Davidson et al. 2004; Churkina et al. 2007; Thornton et al. 2007; Sutton & Vries 2008; de Vries et al. 2009; Quinn Thomas et al. 2011; Fleischer et al. 2013).

Large uncertainties existed in the exact contribution of N deposition (or N fertilization) on the historical and future C sink with the C-N interacted responses and feedbacks towards the future climate change (Heimann and Reichstein, 2008; Reay et al., 2008; Scheffer et al., 2009; Arneth et al. 2011; Erisman et al. 2011; Zaehle et al. 2011). Studies have indicated that N-limitation may suppress maximum photosynthesis rates and hence C uptake, particularly in forests (Vitousek & Howarth 1991; Aber et al. 1998; Nadelhoffer et al. 1999; Schulze

2000; Hungate et al. 2003; IPCC 2007; Bonan 2008; Reich et al. 2008). Leaf N controls on photosynthesis may also affect stomatal conductance, and hence, evapotranspiration and energy balance (Schulze 2000; Dickinson et al. 2002). Warming may increase the availability of mineral N to plants and has the potential to stimulate C storage in plants (Melillo et al., 2002). N limitation may also alter plant respiration due to changes in plant tissue N content (Reich et al., 2008). The impact of increased N availability in soils is even more uncertain, as some studies suggest that soil C may decrease with increased N availability, while others suggest no change or even increases in C storage (Reay et al., 2008a). Therefore, it is currently unclear how changes in N availability would affect C sequestration in vegetated ecosystems under enhanced atmospheric CO_2 concentrations and warmer temperatures (Reay et al., 2008a; Sutton and Vries, 2008). Therefore, understanding of N cycling impacts on C, water and energy exchanges in terrestrial ecosystems is urgently important to accurately predicted future climate changes and associated feedbacks, in particular those related to plant and soil nutrient status.

Despite the close coupling of C and N cycles and the significance of N dynamics in terrestrial C cycle, ecosystem models use descriptive input parameters to establish the physiology, biochemistry, structure, and allocation patterns of vegetation functional types, or biomes. And, for local site-scale simulations, it is possible to measure required data, but as spatial resolution increases, the data availability is limited. Due to the complexity of the C-N interaction in the process-based DGVMs, and because of the availability of very limited observed data for the model parameterization or intercomparison purpose, few terrestrial ecosystem models have incorporated the N dynamics, which are currently the major limitations to global and regional modeling (Cox et al., 2000; Dufresne et al., 2002; Friedlingstein et al., 2006; IPCC, 2007a).

An international scientific endeavor headed by North American and Brazil FLUXNET community (Baldocchi, 2008; Baldocchi et al., 2001) had led to the establishment of the North American Carbon Program (NACP) (Schwalm et al., 2010) and the Large Scale Biosphere-Atmosphere Experiment in Amazonia (LBA) (Avissar, 2002), with a primary goal to understand the interactions between the atmosphere and terrestrial ecosystems. Observed flux and meteorological data from the these initiative have provided a unique data source to evaluate the performance of the LSM and DGVM (Christoffersen et al., 2014; de Gonçalves et al., 2013; von Randow et al., 2013).

In our previous study, N controls on C and water exchanges were analyzed in a temperate conifer forest in Ontario, Canada from 2003 to 2007 using a newly developed C-N coupled model, CLASS-CTEM^{N+} (Huang et al., 2011). Key soil and plant N cycling algorithms including biological fixation, mineralization, nitrification, denitrification, leaching and N controls on plant photosynthesis capacity were incorporated into CLASS-CTEM^{N+}. Simulated values of soil-plant N contents and C and N fluxes were compared with available observation-based estimates for the study period (2003-2007). Model results showed that a proper representation of N controls on photosynthetic uptake and canopy conductance results in more plausible simulations of observed C and water fluxes.

However, CLASS-CTEM^{N+} needs to be further evaluated at multi-sites and at larger spatiotemporal scales, using generalized biome parameterizations. Sensitivity analysis of key model parameters was also required to before its application at regional and global scales. In this study, three independent investigations were conducted as a systematic and continuous extension to the CLASS-CTEM^{N+} development and application at 8 PFTs and then from regional and global scales, over 110 years.

1.1 Objectives

Specifically, the objectives of this PhD work are:

(1) to develop generalize CLASS-CTEM^{N+}'s parameters and improve model processes to simulate carbon, water and energy fluxes and carbon stocks for all plant functional types (PFTs);

(2) to evaluate the performance of the model by comparing simulated carbon, water and energy fluxes and carbon stocks with flux and biometric measurements from forest, crop and grassland sites in Canada and United States in the North America and the Amazon region in Brazil in South America;

(3) to conduct sensitivity analysis of nitrogen use efficacy (NUE) at multiple PFTs under different imposed N deposition levels; and quantify the long-term variability of N effects on simulated C, water and energy fluxes and C pools (4) to investigate climate and N cycling feedbacks on terrestrial ecosystems at regional and global scales by performing model simulations of C, water and energy fluxes and C pools for over ~100 years at 0.5 × 0.5 spatial resolution.

(5) to identify and explore the capabilities, uncertainties and limitations of CLASS-CTEM^{N+} for future applications at regional and global scales.

To achieve these objectives, two versions of the model, a C and N integrated (C-N) version and a carbon-only (C) version, were employed. Model simulations were performed from hourly to monthly time scale at site-level to 0.5 x 0.5 degree global resolutions. Global simulations were performed from 1901 to 2010.

This thesis includes three chapters that are geared toward independent publications. Therefore, there is some overlap or duplication of text related to model and forcing and initialization data sets. Chapter 2 of this thesis describes the CLASS-CTEM^{N+} multi-site evaluation across North America with the NACP project; Chapter 3 describes model assessment with the LBA datasets at Amazonia tropical region; Chapter 4 describes the CLASS-CTEM^{N+} global simulation; and conclusions are given in Chapter 5.

1.2 Reference:

Aber, J., McDowell, W., Nadelhoffer, K., Alison, M., Berntson, G., Kamakea, M., McNulty, S., Currie, W., Rustad, L., Fernandez, I., 1998. Nitrogen Saturation in Temperate Forest Ecosystems. Bioscience 48, 921–934.

Alexander, L. V., Allen, S.K., Bindoff, N.L., Bréon, F.-M., Church, J.A., 2013. Working Group I Contribution to the IPCC Fifth Assessment Report Climate Change 2013: The Physical Science Basis Summary for Policymakers. http://www.climatechange2013.org/ (accessed 6.2.14).

Avissar, R., 2002. Preface to special issue on the Large-Scale Biosphere-Atmosphere Experiment in Amazonia (LBA). J. Geophys. Res. 107, 8034. doi:10.1029/2002JD002507

Baldocchi, D., 2008. "Breathing" of the terrestrial biosphere: lessons learned from a global network of carbon dioxide flux measurement systems. Aust. J. Bot. 56, 1. doi:10.1071/BT07151

Baldocchi, D., Falge, E., Gu, L., Olson, R., Hollinger, D., Running, S., Anthoni, P., Bernhofer, C., Davis, K., Evans, R., Fuentes, J., Goldstein, A., Katul, G., Law, B., Lee, X., Malhi, Y., Meyers, T., Munger, W., Oechel, W., Paw, K.T., Pilegaard, K., Schmid, H.P., Valentini, R., Verma, S., Vesala, T., Wilson, K., Wofsy, S., 2001. FLUXNET: A New Tool to Study the Temporal and Spatial Variability of Ecosystem–Scale Carbon Dioxide, Water Vapor, and Energy Flux Densities. Bull. Am. Meteorol. Soc. 82, 2415–2434. doi:10.1175/1520-0477(2001)082<2415:FANTTS>2.3.CO;2

Bonan, G.B., 2008. Forests and Climate Change: Forcings, Feedbacks, and the Climate Benefits of Forests. Science (80-.). 320, 1444–1449. doi:10.1126/science.1155121

Bonan, G.B., Levis, S., 2010. Quantifying carbon-nitrogen feedbacks in the Community Land Model (CLM4). Geophys. Res. Lett. 37, 1–6. doi:10.1029/2010GL042430

Canadell, J.G., Pataki, D.E., Pitelka, L.F. (Eds.), 2007. Terrestrial Ecosystems in a Changing World, Global Change — The IGBP Series. Springer Berlin Heidelberg, Berlin, Heidelberg. doi:10.1007/978-3-540-32730-1

Christoffersen, B.O., Restrepo-Coupe, N., Arain, M.A., Baker, I.T., Cestaro, B.P., Ciais, P., Fisher, J.B., Galbraith, D., Guan, X., Gulden, L., van den Hurk, B., Ichii, K., Imbuzeiro, H., Jain, A., Levine, N., Miguez-Macho, G., Poulter, B., Roberti, D.R., Sakaguchi, K., Sahoo, A., Schaefer, K., Shi, M., Verbeeck, H., Yang, Z.-L., Araújo, A.C., Kruijt, B., Manzi, A.O., da Rocha, H.R., von Randow, C., Muza, M.N., Borak, J., Costa, M.H., Gonçalves de Gonçalves, L.G., Zeng, X., Saleska, S.R., 2014. Mechanisms of water supply and vegetation demand govern the seasonality and magnitude of evapotranspiration in Amazonia and Cerrado. Agric. For. Meteorol. 191, 33–50. doi:10.1016/j.agrformet.2014.02.008

Churkina, G., Trusilova, K., Vetter, M., Dentener, F., 2007. Contributions of nitrogen deposition and forest regrowth to terrestrial carbon uptake. Carbon Balance Manag. 2, 5. doi:10.1186/1750-0680-2-5

Cox, P.M., Betts, R.A., Jones, C.D., Spall, S.A., Totterdell, I.J., 2000. Acceleration of global warming due to carbon-cycle feedbacks in a coupled climate model. Nature 408, 184–187.

Davidson, E.A., Reis de Carvalho, C.J., Vieira, I.C.G., Figueiredo, R. de O., Moutinho, P., Yoko Ishida, F., Primo dos Santos, M.T., Benito Guerrero, J., Kalif, K., Tuma Sabá, R., 2004. Nitrogen and Phosphorus limitation of biomass growth in a tropical secondary forest. Ecol. Appl. 14, 150–163. doi:10.1890/01-6006

De Gonçalves, L.G.G., Borak, J.S., Costa, M.H., Saleska, S.R., Baker, I., Restrepo-Coupe, N., Muza, M.N., Poulter, B., Verbeeck, H., Fisher, J.B., Arain, M.A., Arkin, P., Cestaro, B.P., Christoffersen, B., Galbraith, D., Guan, X., van den Hurk, B.J.J.M., Ichii, K., Imbuzeiro, H.M.A., Jain, A.K., Levine, N., Lu, C., Miguez-Macho, G., Roberti, D.R., Sahoo, A., Sakaguchi, K., Schaefer, K., Shi, M., Shuttleworth, W.J., Tian, H., Yang, Z.-L., Zeng, X., 2013. Overview of the Large-Scale Biosphere–Atmosphere Experiment in Amazonia Data Model Intercomparison Project (LBA-DMIP). Agric. For. Meteorol. 182-183, 111–127. doi:10.1016/j.agrformet.2013.04.030

Dickinson, R.E., Berry, J.A., Bonan, G.B., Collatz, G.J., Field, C.B., Fung, I.Y., Goulden, M., Hoffmann, W.A., Jackson, R.B., Myneni, R., Sellers, P.J., Shaikh, M., 2002. Nitrogen Controls on Climate Model Evapotranspiration. J. Clim. 15, 278–295.

Dolman, A.J., van der Werf, G.R., van der Molen, M.K., Ganssen, G., Erisman, J.-W., Strengers, B., 2010. A carbon cycle science update since IPCC AR-4. Ambio 39, 402–12.

Dufresne, J.L., Fairhead, L., Le Treut, H., Berthelot, M., Bopp, L., Ciais, P., Friedlingstein, P., Monfray, P., 2002. On the magnitude of positive feedback between future climate change and the carbon cycle. Geophys. Res. Lett. 29.

Friedlingstein, P., Cox, P., Betts, R., 2006. Climate-carbon cycle feedback analysis: Results from the C4MIP model intercomparison. J. ….

Gerber, S., Hedin, L.O., Oppenheimer, M., Pacala, S.W., Shevliakova, E., 2010. Nitrogen cycling and feedbacks in a global dynamic land model. Global Biogeochem. Cycles 24, n/a–n/a. doi:10.1029/2008GB003336

Heimann, M., Reichstein, M., 2008. Terrestrial ecosystem carbon dynamics and climate feedbacks. Nature 451, 289–292.

Holland, E., Braswell, B., Lamarque, J.F., Townsend, A., Sulzman, J., J.-F, M., uuml, ller, 1997. Variations in the predicted spatial distribution of atmospheric nitrogen deposition and their impact on carbon uptake by terrestrial ecosystems. J. Geophys. Res.

Holland, E.A., Braswell, B.H., Sulzman, J., Lamarque, J.-F., 2005. Nitrogen deposition onto the United States and Western Europe: synthesis of observations and models. Ecol. Appl. 15, 38–57. doi:10.1890/03-5162

Huang, S., Arain, M.A., Arora, V.K., Yuan, F., Brodeur, J., Peichl, M., 2011. Analysis of nitrogen controls on carbon and water exchanges in a conifer forest using the CLASS-CTEMN+ model. Ecol. Modell. 222, 3743–3760. doi:10.1016/j.ecolmodel.2011.09.008

Hungate, B.A., Dukes, J.S., Shaw, M.R., Luo, Y., Field, C.B., 2003. ATMOSPHERIC SCIENCE: Nitrogen and Climate Change. Science (80-.). 302, 1512–1513. doi:10.1126/science.1091390

IPCC, 2007. Climate Change 2007: The Physical Science Basis, Contribution of Working Group I to the Fourth Assessment Report of the Intergovernmental Panel on Climate Change. Cambridge University Press, Cambridge.

Keeling, C.D., Chin, J.F.S., Whorf, T.P., 1996. Increased activity of northern vegetation inferred from atmospheric CO2 measurements. Nature 382, 146–149. doi:10.1038/382146a0

Le Quere, C., Raupach, M.R., Canadell, J.G., Marland, G., et al., 2009. Trends in the sources and sinks of carbon dioxide. Nat. Geosci 2, 831–836.

Luo, Y., Hui, D., Zhang, D., 2006. Elevated CO2 stimulates net accumulations of carbon and nitrogen in land ecosystems: a meta-analysis. Ecology 87, 53–63. doi:10.1890/04-1724

Luo, Y., Su, B.O., Currie, W.S., Dukes, J.S., Finzi, A., Hartwig, U., Hungate, B., Mc Murtrie, R.E., Oren, R.A.M., Parton, W.J., Pataki, D.E., Shaw, M.R., Zak, D.R., Field, C.B., 2004. Progressive Nitrogen Limitation of Ecosystem Responses to Rising Atmospheric Carbon Dioxide. Bioscience 54, 731–739.

McGuire, A.D., Chapin III, F.S., Wirth, C., Apps, M., Bhatti, J., Callaghan, T., Christensen, T., Clein, J., Fukuda, M., Maximov, T., Onuchin, A., Shvidenko, A., Vaganov, E., 2007. Responses of High Latitude Ecosystems to Global Change: Potential Consequences for the Climate System, in: Canadell, J., Pataki, D., Pitelka, L. (Eds.), Terrestrial Ecosystems in a Changing World SE - 24, Global Change — The IGBP Series. Springer Berlin Heidelberg, pp. 297–310. doi:10.1007/978-3-540-32730-1_24

Melillo, J.M., Steudler, P.A., Aber, J.D., Newkirk, K., Lux, H., Bowles, F.P., Catricala, C., Magill, A., Ahrens, T., Morrisseau, S., 2002. Soil warming and carbon-cycle feedbacks to the climate system. Science 298, 2173–6. doi:10.1126/science.1074153

Nadelhoffer, K.J., Emmett, B.A., Gundersen, P., Kjonaas, O.J., Koopmans, C.J., Schleppi, P., Tietema, A., Wright, R.F., 1999. Nitrogen deposition makes a minor contribution to carbon sequestration in temperate forests. Nature 398, 145–148.

Reay, D.S., Dentener, F., Smith, P., Grace, J., Feely, R.A., 2008. Global nitrogen deposition and carbon sinks. Nat. Geosci 1, 430–437.

Reich, P.B., Tjoelker, M.G., Pregitzer, K.S., Wright, I.J., Oleksyn, J., Machado, J.-L., 2008. Scaling of respiration to nitrogen in leaves, stems and roots of higher land plants. Ecol. Lett. 11, 793–801. doi:10.1111/j.1461-0248.2008.01185.x

Scheffer, M., Bascompte, J., Brock, W.A., Brovkin, V., Carpenter, S.R., Dakos, V., Held, H., van Nes, E.H., Rietkerk, M., Sugihara, G., 2009. Early-warning signals for critical transitions. Nature 461, 53–59.

Schulze, E.-D., 2000. Carbon and nitrogen cycling in European forest ecosystems , Ecological studies. Springer, Berlin New York .

Schwalm, C.R., Williams, C.A., Schaefer, K., Anderson, R., Arain, M.A., Baker, I., Barr, A., Black, T.A., Chen, G., Chen, J.M., Ciais, P., Davis, K.J., Desai, A., Dietze, M., Dragoni, D., Fischer, M.L., Flanagan, L.B., Grant, R., Gu, L., Hollinger, D., Izaurralde, R.C., Kucharik, C., Lafleur, P., Law, B.E., Li, L., Li, Z., Liu, S., Lokupitiya, E., Luo, Y., Ma, S., Margolis, H., Matamala, R., McCaughey, H., Monson, R.K., Oechel, W.C., Peng, C., Poulter, B., Price, D.T., Riciutto, D.M., Riley, W., Sahoo, A.K., Sprintsin, M., Sun, J., Tian, H., Tonitto, C., Verbeeck, H., Verma, S.B., 2010. A model-data intercomparison of CO2 exchange across North America: Results from the North American Carbon Program site synthesis. J. Geophys. Res. 115, G00H05. doi:10.1029/2009JG001229

Shaver, G.R., 1992. Global change and the carbon balance of arctic ecosystems, Bioscience.

Sokolov, A.P., Kicklighter, D.W., Melillo, J.M., Felzer, B.S., Schlosser, C.A., Cronin, T.W., 2008. Consequences of Considering Carbon-Nitrogen Interactions on the Feedbacks between Climate and the Terrestrial Carbon Cycle. J. Clim. 21, 3776–3796.

Sutton, M.A., Vries, R.I.S.S.R.M. van O.W.I.M. de, 2008. Uncertainties in the relationship between atmospheric nitrogen deposition and forest carbon sequestration. Glob. Chang. Biol. 14, 2057–2063.

Thornton, P.E., Doney, S.C., Lindsay, K., Moore, J.K., Mahowald, N., Randerson, J.T., Fung, I., Lamarque, J.F., Feddema, J.J., Lee, Y.H., 2009. Carbon-nitrogen interactions regulate climate-carbon cycle feedbacks: results from an atmosphere-ocean general circulation model. Biogeosciences Discuss. 6, 3303–3354.

Thornton, P.E., Lamarque, J.-F., Rosenbloom, N.A., Mahowald, N.M., 2007a. Influence of carbon-nitrogen cycle coupling on land model response to CO2 fertilization and climate variability. Glob. Biogeochem. Cycles 21.

Thornton, P.E., Lamarque, J.-F., Rosenbloom, N.A., Mahowald, N.M., 2007b. Influence of carbon-nitrogen cycle coupling on land model response to CO 2 fertilization and climate variability. Global Biogeochem. Cycles 21, n/a–n/a. doi:10.1029/2006GB002868

Vitousek, P.M., Howarth, R.W., 1991. Nitrogen limitation on land and in the sea: How can it occur? Biogeochemistry 13, 87–115.

Von Randow, C., Zeri, M., Restrepo-Coupe, N., Muza, M.N., de Gonçalves, L.G.G., Costa, M.H., Araujo, A.C., Manzi, A.O., da Rocha, H.R., Saleska, S.R., Arain, M.A., Baker, I.T., Cestaro, B.P., Christoffersen, B., Ciais, P., Fisher, J.B., Galbraith, D., Guan, X., van den Hurk, B., Ichii, K., Imbuzeiro, H., Jain, A., Levine, N., Miguez-Macho, G., Poulter, B., Roberti, D.R., Sahoo, A., Schaefer, K., Shi, M., Tian, H., Verbeeck, H., Yang, Z.-L., 2013. Inter-annual variability of carbon and water fluxes in Amazonian forest, Cerrado and pasture sites, as simulated by terrestrial biosphere models. Agric. For. Meteorol. 182-183, 145–155. doi:10.1016/j.agrformet.2013.05.015

Zaehle, S., Friend, A.D., Friedlingstein, P., Dentener, F., Peylin, P., Schulz, M., 2010. Carbon and nitrogen cycle dynamics in the O-CN land surface model: 2. Role of the nitrogen cycle in the historical terrestrial carbon balance. Global Biogeochem. Cycles 24, n/a–n/a. doi:10.1029/2009GB003522

2. CHAPTER 2: Assessing Nitrogen Controls on Carbon, Water and Energy Exchanges in Vegetation Ecosystems using a Carbon and Nitrogen Coupled Ecosystem Model

Suo Huang[1], M. Altaf Arain[1, *], Paul Bartlett[2]

[1]School of Geography and Earth Sciences and McMaster Centre for Climate Change, McMaster University, Hamilton, Ontario, Canada

[2]Climate Processes Section, Environment Canada, Toronto, ON, M3H 5T4 Canada

* **Corresponding Author:** M. Altaf Arain, School of Geography and Earth Sciences, McMaster University, 1280 Main Street West, Hamilton, Ontario, L8S 4K1, Canada, Phone: 1-905-525-9140 Ext. 27941, Fax: 905-546-0463; Email: arainm@mcmaster.ca

Keywords: Canadian Land Surface Scheme (CLASS); Canadian Terrestrial Ecosystem Model (CTEM); Carbon (C); Nitrogen (N); Net Ecosystem Productivity (NEP); Sensible Heat (H); Latent Heat (LE); North American Carbon Program (NACP); Plant Functional Types (PFTs); Nitrogen Deposition (N_{dep})

2.1 Abstract

A carbon and nitrogen coupled dynamic vegetation model (CLASS-CTEM^{N+}) was used to assess the effects of nitrogen controls on simulated carbon, water and energy exchanges in a range of North American vegetation ecosystems. Standardized meteorological forcing data and eddy covariance flux measurements of carbon, water and energy from 32 FLUXNET sites covering seven biomes across North America were used for calibration and evaluation of the model. Two versions of the model, a carbon and nitrogen coupled (C-N) version and carbon-only (C) version, were employed. Simulated diurnal, daily, seasonal and annual values of gross ecosystem productivity (GEP), ecosystem respiration (Re), net ecosystem productivity (NEP), net radiation (Rn), sensible heat flux (H) and latent heat flux (LE), from both versions of the model were compared with measured eddy covariance fluxes at each site to evaluate the models' performance in simulating carbon, water and energy fluxes. Carbon pools and key nitrogen cycling variables from both versions of the model were also compared to investigate nitrogen controls on carbon, water and energy exchanges. A sensitivity analysis was performed to determine the relative influence of nitrogen deposition on the vegetation carbon exchanges in each biome or plant functional type (PFTs).

Generally, the inclusion of a N cycle with the C cycle in the model resulted in better accuracy scores for simulated C, water and energy fluxes when compared with observations. Model simulated N limitation effects vary among PFTs, but were strongest for boreal forests during the early-growing season, followed by temperate forests, and then non-forested sites (crops and grassland). The C-N version simulated annual mean NEP for evergreen needleleaf forests is 120 g C m^{-2} yr^{-1} compared to 100 g C m^{-2} yr^{-1} from observation and 410 g C m^{-2} yr^{-1} by the C version. Annual mean NEP for cold deciduous broadleaf forests is 330 g C m^{-2} yr^{-1} for the C-N version, compared to 140 g C m^{-2} yr^{-1} from observation and 520 g C m^{-2} yr^{-1} from the C version. Overall, the C-N version results explained 93.8%, 47.5%, 85.5%, 76.2% and 33.3% of the observed variance in GEP for evergreen needleleaf forest, cold deciduous broadleaf forest, dry deciduous broadleaf forest, crops and grassland, respectively; compared to explained variance of 80.1%, 42.6%, 60.4%, 78.2% and 29.3% by the C version. Dynamics of root nitrogen uptake simulated by the C-N version of the model are consistent with measurements and previous modeling studies for major biomes. The simulated daily mean root nitrogen uptake rate for all forests showed strong seasonal variability, ranging from no uptake in winter to a maximum of 38.8 mg N m^{-2} day^{-1} in the early growing season (April–June). For crops and grasslands, root nitrogen uptake rates were smaller (from 1.8 to 7.4 mg N m^{-2} day^{-1}) and had less seasonal variability than forests. Evaluation of nitrogen deposition impacts on GEP, NEP and biomass showed considerable variability between and within forest types due to non- linearity of N effects and spatial heterogeneity of C-N interactions.

Overall, the inclusion of the nitrogen cycle in the CLASS-CTEM^{N+} model improved the accuracy of its simulations, in particular for boreal forests. Inclusion of the nitrogen cycle in the model will help in its application at regional and global scales to evaluate nitrogen availability impacts on the carbon cycle in terrestrial ecosystems and to determine nitrogen cycle feedbacks on Earth's climate system.

2.2 Introduction

Terrestrial vegetation ecosystems play an important role in regulating Earth's climate. Rising levels of greenhouse gas (GHG) emissions, especially rapidly increasing atmospheric carbon dioxide (CO_2) levels (IPCC 2007; Le Quere et al. 2009; Dolman et al. 2010; Alexander et al. 2013) and enhanced deposition of reactive nitrogen (N) on land surfaces, have affected terrestrial vegetation ecosystems (Galloway et al., 2008, 2004; Gruber and Galloway, 2008) and the global climate (Arneth et al. 2011; Erisman et al. 2011; Zaehle et al. 2011). During the 2000-2007 period, terrestrial ecosystems have absorbed about 30% of anthropogenic CO_2 emissions (Le Quere et al., 2009). Increases in atmospheric N deposition in industrialized regions have contributed significantly to the terrestrial carbon (C) sink, particularly through enhancing vegetation growth in N limited areas (Sutton & Vries 2008; de Vries et al. 2009; Quinn Thomas et al. 2011; Fleischer et al. 2013), such as the boreal forest (Nissinen and Hari, 1998; Makipaa et al., 1999; Luyssaert et al., 2007; Ciais et al., 2008). There is large uncertainty in the exact contribution of N deposition (or N fertilization) on the historical and future C sink (Heimann and Reichstein, 2008; Reay et al., 2008; Scheffer et al., 2009). There is evidence that N-limitation may suppress maximum photosynthesis rates and hence C uptake, particularly in forests (Vitousek & Howarth 1991; Aber et al. 1998; Nadelhoffer et al. 1999; Schulze 2000; Hungate et al. 2003; IPCC 2007; Bonan 2008; Reich et al. 2008). Leaf N controls on photosynthesis may also affect stomatal conductance, and hence, evapotranspiration and the energy balance (Schulze 2000; Dickinson et al. 2002). Warming may increase the availability of mineral N to plants and has the potential to stimulate C storage in plants (Melillo et al., 2002). N limitation may also alter plant respiration due to changes in plant tissue N content (Reich et al., 2008). The impact of increased N availability in soils is even more uncertain, as some studies suggest that soil C may decrease with increased N availability, while others suggest no change or even increases in C storage (Reay et al., 2008). It is currently unclear how changes in N availability would affect C sequestration in vegetated ecosystems under enhanced atmospheric CO_2 concentrations and warmer temperatures (Reay et al., 2008; Sutton and Vries, 2008). Therefore, understanding of N cycling impacts on C, water and energy exchanges in terrestrial ecosystems is important to predict accurately, future climate changes and associated feedbacks, in particular those related to plant and soil nutrient status.

The significance of the N cycle has been recognized by the modeling community and components of the N cycle have been progressively incorporated into global climate models (Churkina et al., 2010; Dezi et al., 2010; Esser et al., 2011; Jain et al., 2009; Sokolov et al., 2008; Thornton et al., 2007; Xu and Prentice, 2008; Zaehle et al., 2010). Results of implementing N constraints on ecosystem functioning in land surface schemes used in global climate models (Bonan and Levis, 2010; Sokolov et al., 2008; Thornton et al., 2009, 2007; Xu and Prentice, 2008) suggest that the inclusion of the N cycle reduces the net C uptake of terrestrial vegetation. Coupling of C and N cycles also reportedly reduced the C cycle's sensitivity to changes in temperature and precipitation (Bonan and Levis, 2010; Thornton et al., 2007).

In our previous study, N controls on C and water exchanges were analyzed in a temperate conifer forest in Ontario, Canada from 2003 to 2007 using a newly developed C-N coupled model, CLASS-CTEM^{N+} (Huang et al., 2011). Key soil and plant N cycling algorithms including biological fixation, mineralization, nitrification, denitrification, leaching and N controls on plant photosynthesis capacity were incorporated into CLASS-CTEM^{N+}. Simulated values of soil-plant N contents and C and N fluxes were compared with available observation-based estimates for the study period (2003-2007). Model results showed that a proper representation of N controls on photosynthetic uptake and canopy conductance results in more plausible simulations of observed C and water fluxes. However, CLASS-CTEM^{N+} was not tested in other key biomes.

In this study, we compare simulated C, water and energy-fluxes, C pools and key N cycling variables, against observations from 32 FLUXNET sites across North America, spanning over 168 site-years and 7 biomes. The specific objectives of this study are to (1) evaluate the models' performance in simulating C, water and N dynamics in all major biomes or Plant Functional Types (PFTs) and (2) determine N controls on C and water exchanges in these biomes under different N deposition levels. The resulting model outputs and parameters will serve as a strong foundation for future regional and global scale and long-term modeling studies using the C-N coupled version of the model.

2.3 Methods

2.3.1 Model

The CLASS-CTEM^{N+} model is a process-based dynamic global vegetation model (DGVM) derived from two existing models: The Canadian Land Surface Scheme (CLASS) (Verseghy et al., 1993; Verseghy, 2000, 1991) and the Canadian Terrestrial Ecosystem Model (CTEM) (Arora and Boer, 2006, 2005a, 2005b, 2003), with a newly incorporated representation of soil-plant nitrogen (N) cycling algorithms (Arain et al., 2006; Huang et al., 2011; Yuan et al., 2008).

2.3.1.1 CLASS Model

The CLASS model was developed at Environment Canada for use in the Canadian Global Climate Model (CGCM) and the Canadian Regional Climate Model (CRCM) (Verseghy et al., 1993; Verseghy, 2000, 1991) . CLASS was originally designed with a composite canopy, composed of amalgamated properties of up to four vegetation classes (needleleaf trees, broadleaf trees, crops and grass) plus urban areas. The grid-cell is also divided into vegetated and bare soil fractions, each with and without snow cover, which are treated separately. Beginning with version 3.0, a full mosaic is able to represent different surfaces in distinct patches or tiles. There are three soil layers (with depths of 0.1, 0.25, and 3.75 m), a variable depth of snow layer where applicable, a single vegetation canopy layer (which intercepts both rain and snow), prognostic soil temperatures, liquid and frozen soil moisture contents, and soil surface properties, such as roughness length and surface albedo, which are functions of vegetation type, and soil moisture and texture, respectively. The radiation subroutine calculates the visible, near infrared (NIR), and longwave radiation absorbed by the canopy. The absorption of visible and NIR radiation is based on vegetation-dependent visible and NIR albedo and transmissivity, while net long-wave radiation absorbed by the canopy is based on the sky-view factor, which describes the degree of the canopy closure. The original canopy conductance parameterization used in CLASS was similar to that of the Jarvis model (Jarvis, 1976), where canopy resistance (r_c) is expressed as a function of minimum stomatal resistance and a series of environmental dependences whose effects are assumed to be multiplicative. Later, two leaf (sunlit and shaded) C and soil-plant N cycle modules were incorporated into what became known as C-CLASS and CN-CLASS, respectively (Arain et al., 2002; 2006).

2.3.1.2 CTEM Model

CTEM is a dynamic vegetation model developed at the Canadian Centre for Climate Modelling and Analysis (CCCma), Environment Canada. Version 1.2 of CTEM used here simulates the terrestrial ecosystem processes of photosynthesis, autotrophic and heterotrophic respiration, leaf phenology, allocation, biomass turnover, litterfall, and mortality, and prognostically determines the carbon in the model's three live (leaves, stem and root) and two dead (litter and soil carbon) pools. These processes are modelled for nine plant functional types (PFTs) that are linked directly to the four PFTs of CLASS (see Table 2.1): needleleaf trees are divided into their evergreen and deciduous sub-types, broadleaf trees are divided into evergreen and cold- and drought-deciduous sub-types, and grasses and crops are divided into C_3 and C_4 sub-types.

The photosynthesis sub-module of the CTEM is based on the biochemical model of Farquhar and Collatz (Farquhar et al. 1980; Collatz et al. 1991; Collatz et al. 1992). The coupling between photosynthesis and canopy conductance is based on vapour pressure deficit (Leuning et al., 1995) and when coupled to CTEM, the stomatal resistance calculated by the Jarvis type parameterization in CLASS is not used. Photosynthesis accounts for the differences in C_3 and C_4 pathways. The photosynthesis or gross ecosystem productivity (GEP) and autotrophic respiration (Ra) and heterotrophic respiration (Rh) sub-modules of CTEM, as described in Arora (2003), are used to calculate net primary productivity (NPP) and net ecosystem productivity (NEP). NPP is allocated to leaves, stem, and roots depending on water availability, light limitation and leaf phenological status. Prognostic leaf area index (LAI) is then determined from the leaf C and specific leaf area (SLA) (Dickinson et al., 1998).

The phenology sub-module of CTEM is based on a carbon-gain approach. Leaf onset is initiated when it is beneficial for the plant, in C terms, to produce new leaves. Leaf offset is initiated by unfavorable environmental conditions, including shorter day length, cooler temperatures, and low soil moisture (Arora and Boer, 2005a). The seasonal phenological cycle of leaves is prognostically calculated without any prescribed dates or use of satellite data. The root biomass declines exponentially with depth and the PFT-dependent exponent describing the root distribution depends on root biomass which makes the fraction of roots in each soil layer a dynamic function of vegetation growth (Arora and Boer, 2003). Mortality rates of leaves, wood, and fine and coarse roots are PFT-dependent and generate a flow of C into the model's single litter pool. Heterotrophic respiration from the litter and soil organic matter pools varies with soil temperature and soil moisture and tissue chemistry. A primary prognostic treatment of fire is also included in the model (Arora and Boer, 2005b). Allocation to, and respiratory losses from the three vegetation components (leaves, stem, and root) result in time-varying biomass values that are reflected in the structural vegetation attributes used in the energy and water balance calculations of the CLASS (Arora and Boer, 2005a).

Although it includes a parameterization for down-regulation of photosynthesis as CO_2 increases (Arora et al., 2009), CTEM does not include a coupling of terrestrial C and N cycles, and the effects of nutrient limitation on photosynthesis are not modeled explicitly. A representation of the soil-plant nitrogen cycle was introduced into the coupled CLASS-CTEM model recently, yielding the CLASS-CTEM^{N+} model version (Huang et al., 2011) which is described in the next section.

2.3.1.3 CLASS-CTEM^{N+}

The CLASS-CTEM^{N+} model used in this study was developed by incorporating plant and soil nitrogen cycling algorithms into the coupled CLASS (version 2.7) and CTEM models (version 1.2) (Huang et al., 2011). Soil N cycle processes in CLASS-CTEM^{N+} include immobilization, mineralization, nitrification, denitrification, volatilization, leaching, disturbance losses, and gaseous emissions of N_2O and NO. Plant N cycle processes include root N uptake, plant N allocation and N controls on photosynthetic capacity. The maximum carboxylation capacity of Rubisco (V_{cmax}) is determined nonlinearly from the modelled leaf Rubisco-nitrogen. Variations in plant C assimilation and stomatal conductance are linked with leaf N status through the Rubisco enzyme. The N uptake rate can be enhanced or limited by plant growth, depending on N demand and non-structural storage capacity. Thus, interactions between the C and N cycles in CLASS-CTEM^{N+} include (1) dependence of photosynthesis and plant respiration on leaf/plant tissue N, (2) limitation of decomposition by N availability, (3) the dependence of shoot and root C allocation on the N status in these tissues and (4) limitation of N uptake by fine root biomass. The calculation of foliar N concentrations and C:N ratios of plant tissues and soil pools allows N to impose constraints on productivity, respiration and C allocation. Apart from plant litterfall, the model has three other means of adding inorganic N to the soil–plant ecosystem: (i) bio-fixation; (ii) atmospheric deposition (wet and dry); and (iii) N fertilization (organic or inorganic). N losses are represented through leaching and disturbances (e.g. fire, harvest), as well as gaseous-N emissions. Nitrogen is cycled through plant tissues, litter, soil and the mineral pools at a daily time step. More details of CLASS-CTEM^{N+} soil-plant N processes are given in Arain et al. (2006) and Huang et al., (2011).

CLASS-CTEM^{N+} contains five C pools (leaves, stem, root, litter and soil organic carbon) and six N pools (leaves, stem, root, litter, soil ammonium (NH_4^+) and nitrate (NO_3^-)). Plant storage pools allow C and N acquired in one growing season to be retained and then distributed as new growth in subsequent years. CTEM has 9 PFTs as listed in Table 2.1, which also shows how CTEM's PFTs condense into 4 vegetation types for CLASS (Arora, 2002). In CLASS-CTEM^{N+}, while CTEM simulates vegetation attributes of all its PFTs separately (including LAI, vegetation height, the fraction of roots in each soil layer and canopy mass) these attributes are amalgamated before they are passed into CLASS (Table 2.1).

Energy and water exchanges estimated by CLASS usually operate at a half-hourly or shorter time step to provide boundary conditions (including soil moisture and temperature) for the biogeochemistry models of CLASS-CTEM^{N+}. Except photosynthesis, which operates at the time-step of CLASS; all other sub-modules of CTEM operate at a daily time step. The plant and soil N algorithms are adapted for a daily time step as well.

Table 2.1 CLASS-CTEM^{N+} PFTs and PFT-specific parameters updated in this study

CLASS PFTs Code [1]	**CTEM PFTs** [2]	**Vc,max** [3]	**α** [4]	**Rm,leaf** [5]	**R_{litter}** [6]	**R_{SOM}** [6]	**N/C ratio in leaves** [7]	**N/C ratio in stems** [7]	**N/C ratio in roots** [7]	**N/C ratio in litter** [7]	**N/C ratio in SOM** [7]
1	ENF	35	0.08	0.015	0.4453	0.0260	0.024	0.020	0.015	0.015	0.030
	DNF	40	0.08	0.017	0.5986	0.0260	0.024	0.020	0.015	0.015	0.030
2	DBE	51	0.08	0.020	0.6339	0.0208	0.030	0.025	0.020	0.020	0.030
	DBC	67	0.08	0.015	0.7576	0.0208	0.030	0.025	0.020	0.020	0.030
	DBD	40	0.08	0.015	0.6957	0.0208	0.030	0.025	0.020	0.020	0.030
3	CR3	55	0.08	0.015	0.6000	0.0350	0.040	-	0.018	0.018	0.030
	CR4	40	0.04	0.025	0.6000	0.0350	0.027	-	0.010	0.010	0.030
4	GR3	75	0.08	0.013	0.5260	0.0125	0.040	-	0.018	0.018	0.030
	GR4	15	0.04	0.025	0.5260	0.0125	0.027	-	0.010	0.010	0.030

[1] CLASS PFTs: Code 1: needleleaf tree; 2: broadleaf tree; 3: crops; 4:grass.

[2] CTEM PFTs: evergreen needleleaf forests (ENF), deciduous needleleaf forests (DNF); evergreen broadleaf forests (DBE); deciduous broadleaf-cold forests (DBC), deciduous broadleaf-dry forests (DBD), C3 crops (CR3), C4 crops (CR4), C3 grass (GR3) and C4 grass (GR4).

[3] Vc,max: maximum rate of carboxylation by the enzyme Rubisco, (μmol CO_2 m^{-2} s^{-1}) (Rogers, 2014).

[4] α: the quantum efficiency scalar.

[5] Leaf maintenance respiration co-efficient;

[6] litter and soil carbon respiration rate at 15 °C (Kg C/ Kg C) (Melton and Arora, 2014).

[7] N/C ratio in leaves, stems, roots, litter and soil organic matters (SOM), (Kg N/Kg C) (Huang et al., 2011; Meissner et al., 2003; Wania et al., 2012; White et al., 2000).

2.3.2 FLUXNET Sites and Data

In this study, we used 32 flux and meteorological datasets assembled, quality controlled and provided by the North American Carbon Program (NACP) for FLUXNET sites in North America (Schwalm et al., 2010). FLUXNET is a global network of eddy covariance tower based measurements of ecosystem carbon, water and energy exchange (Baldocchi, 2008; Baldocchi et al., 2001). At present, over 500 sites are operating on a long-term and continuous basis under FLUXNET. The 32 sites were suggested by a NACP site-level initiative for model calibration and evaluation depending on: (1) data quality and availability, and (2) representative PFTs, resulting in 168 data years ranging from 1995 to 2008. These data ranged from a minimum of 1 to a maximum of 13 years per site. Fig. 2.1 shows the location of all 32 sites with site details listed in Table 2.2.

FLUXNET sites were classified according to PFT and climate, based on the International Geosphere-Biosphere Programme (IGBP) land cover classification scheme (Loveland and Belward, 1997) and the Köppen-Geiger climate classification (Kottek et al., 2006). These 32 flux sites cover 8 of the 17 IGBP PFTs (ENF: evergreen needleleaf forest, DBF: deciduous broadleaf forest; MF: mixed forest; CS: closed shrubland; OS: open shrubland; WS: woody savanna; Gr: grassland; Wet: permanent wetland; Crop: cropland), representing a diverse range of vegetation types and climate zones. These sites are located between 33°N and 54°N with N deposition rates ranging from 0.15 to 2.18 g N m^{-1} yr^{-1} (Lamarque et al., 2010) (Fig. 2.1). The selected sites were further re-classified according to the PFT classification within CLASS-$CTEM^{N+}$ (Arora, 2002), resulting in 5 PFTs in the analysis: evergreen needleleaf (ENF, n=15), deciduous broadleaf-cold (DBC, n=4), deciduous broadleaf-drought (DBD, n=3), crops (CRO, n=4), and grasslands (GRA, n=6) (Table 2.2). Nearly all PFTs of CLASS-$CTEM^{N+}$ are represented in this study, except deciduous needleleaf forest (i.e., Larix), evergreen broadleaf forest (tropical broadleaf rainforests), C4 grasslands and C4 crops, which have been evaluated and reported in a separate study using data from the Large-scale Biosphere-Atmosphere Experiment in Amazonia (LBA) initiative (Huang et al., 2014).

For each site, the observed datasets include CO_2, water, and energy fluxes at half-hourly intervals along with meteorological and ancillary data, such as LAI, vegetation biomass partitions, soil properties and litterfall. Measured meteorological variables (longwave and shortwave radiation, air temperature, precipitation, wind speed, atmospheric pressure, specific humidity) were used as input to CLASS-$CTEM^{N+}$ from these 32 sites (Table 2.2). Model evaluations were then performed for simulated values of gross ecosystem productivity (GEP), ecosystem respiration (Re), net ecosystem productivity (NEP), net radiation (Rn), sensible heat (H) and latent heat (LE) fluxes at different timescales, ranging from half-hourly to annual values. Data such as LAI, photosynthetic variables, or soil carbon were not used for model initialization in order to allow for a less constrained validation of our model. Only climate data and vegetation distribution at each site were used to force the model.

2.3.3 Simulation Scheme

2.3.3.1 Initialization and Spin-up

It is known that initial values of slowly changing prognostic variables may strongly influence simulated surface fluxes, particularly the initial values for soil temperature, soil moisture, and carbon pools. In our study, the model was initialized following NACP protocol as follows: a) soil moisture in all layers was set to 0.95 of saturation (porosity); b) soil temperature in all layers and canopy temperatures were initialized to the overall, long-term average air temperature as defined by the gap-filled weather data; c) because reliable carbon and nitrogen pool observations are not available at all sites, soil carbon, living biomass, and N pools used empirical or generic values with spin-up, as described below and d) initial atmospheric CO_2 concentration values were assumed as steady-state.

We repeated the model spin-up for model physics and biogeochemistry to reach the equilibrium or steady-state following guidelines provided by the NACP. We replicated the driver dataset until the slow response prognostic variables, including soil temperature, soil moisture, and carbon pools (wood and slow soil C pools) met certain criteria. Steady state for soil moisture occurs when the seasonal cycle of monthly average values for each layer varies less than 5% between consecutive passes through the forcing dataset. Steady state for the carbon cycle occurs when growth balances decay and the annual NEP change reaches zero when averaged over the last five years of the spin-up. We assume steady state for soil temperature occurs when the soil moisture reaches steady state.

Two versions of the model, the carbon and nitrogen integrated (C-N) version and the carbon-only (C) version, were employed. Model predictions of diurnal, daily, seasonal and annual GEP, Re, NEP, Rn, H and LE, from both versions, were compared with eddy covariance flux measurements at each site. Both model versions used the same modeling protocol in terms of climatic drivers, CO_2 concentrations, spin-up and simulation phase. To be able to separate the effect of N dynamics for a direct comparison, all parameters shared between the C and C-N versions were set to equal values (Table 2.1).

2.3.3.2 Model Parameterization

The CLASS-CTEM^{N+} default parameters were adapted from previous studies, with CLASS (Arain et al., 2006; Verseghy et al., 1993; Verseghy, 2000, 1991) and CTEM (Arora, 2002; Arora and Boer, 2005a, 2003; Huang et al., 2011; Melton and Arora, 2013). For photosynthesis simulation, CLASS-CTEM^{N+} has two key user-estimated parameters that may depend on the location being simulated: α, and Vcmax. The quantum efficiency scalar α accounts for the reduction in CO_2 assimilation per unit of photosynthetically active radiation (PAR) absorbed when scaling up from the leaf to the canopy level and is highly influential on C flux and storage in CLASS-CTEM^{N+} (Huang et al. 2011). Previous modeling efforts were based on more conservative estimates, e.g. 0.5 in (Haxeltine and Prentice, 1996), to force the global carbon flux simulation. However this generally caused an overestimation of GEP in boreal forests and an underestimation in temperate forests (Jung et al., 2007; Morales et al., 2005). In our study, α was set to the value validated (Melton and Arora, 2014) for all PFTs for both the C-N and C versions of the model (Table 2.1). The calibrated allocation factors are dynamic and their values can change with time depending on water and light stress factors (Arora and Boer, 2005a). Maintenance respiration rates are different for different carbon pools (Amthor, 2000, 1984; Ryan et al., 1995). Therefore, different maintenance respiration rates for leaf, stem, and, root pools for each biome are introduced in the maintenance respiration equations. The parameters used in our study are summarized in Table 2.1.

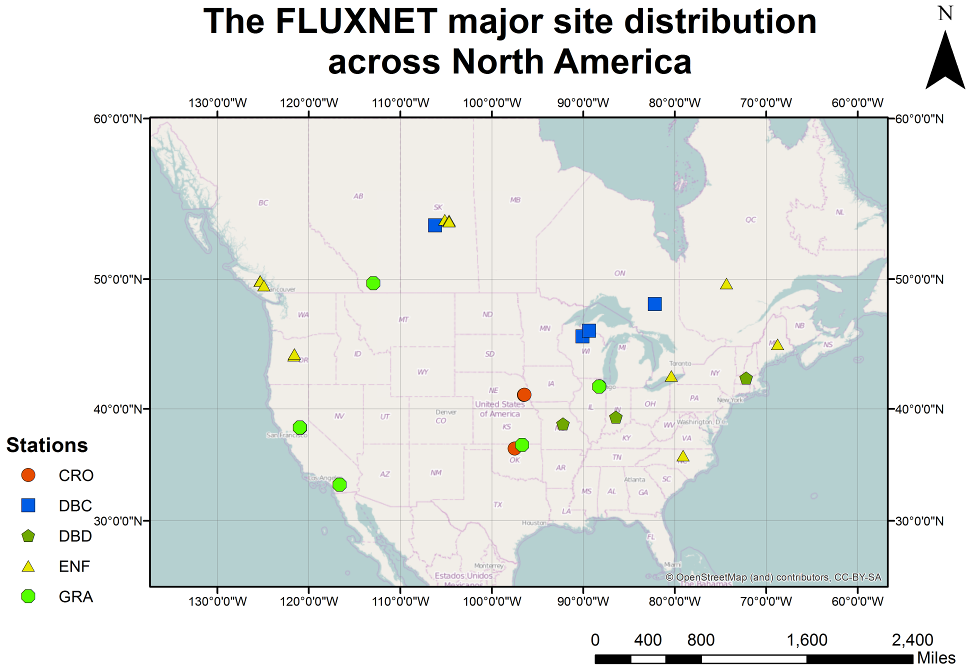

Figure 2.1 The FLUXNET major site distribution across North America

ENF: evergreen needleleaf forest, DBF: deciduous broadleaf forest; MF: mixed forest; CS: closed shrubland; OS: open shrubland; WS: woody savanna; Gr: grassland; Wet: permanent wetland; Crop: cropland (http://www.fluxdata.org)

Table 2.2 Summary of the 32 FLUXNET sites information used in this study

NO.	**Site Code**	**Full Name**	**Latitude**	**Longitude**	**Period of Record**[1]	**Type**[2]	**PFTs in Model** [3]
1	US-ARM	ARM – Southern Great Plains	36.61	-97.49	2000-2006	CRO	CRO
2	US-Ne1	Mead – Irrigated maize	41.17	-96.48	2001-2006	CRO	CRO
3	US-Ne3	Mead – Rainfed maize/soybean	41.18	-96.44	2001-2006	CRO	CRO
4	US-IB1	Fermi Lab – Maize/soybean rotation	41.86	-88.22	2005-2007	CRO	CRO
5	CA-Let	Lethbridge Grassland	49.71	-112.94	1997-2006	GRA	GRA
6	US-Var	Vaira Ranch	38.41	-120.95	2001-2007	GRA	GRA
7	US-Shd	Shidler	36.93	-96.68	1997-2001	GRA	GRA
8	US-IB2	Fermi Lab – Prairie	41.84	-88.24	2004-2007	GRA	GRA
9	CA-Oas	BERMS – Old Aspen	53.63	-106.20	1997-2006	DBF	DBC
10	US-Ha1	Harvard Forest – EMS Tower	42.54	-72.17	1991-2006	DBF	DBD
11	US-MMS	Morgan Monroe State Forest	39.32	-86.41	1999-2006	DBF	DBD
12	US-WCr	Willow Creek	45.81	-90.08	1998-2006	DBF	DBC
13	US-MOz	Missouri Ozark	38.74	-92.20	2004-2007	DBF	DBD
14	CA-Obs	BERMS – Old Black Spruce	53.99	-105.12	2000-2006	ENFB	ENF
15	CA-Ojp	BERMS – Old Jack Pine	53.92	-104.69	2000-2006	ENFB	ENF
16	CA-Qfo	Quebec – Mature Black Spruce	49.69	-74.34	2004-2006	ENFB	ENF
17	CA-Ca1	Campbell River – Mature Douglas-fir	49.87	-125.33	1998-2006	ENFT	ENF
18	US-Dk3	Duke Forest – Loblolly Pine	35.98	-79.09	1998-2005	ENFT	ENF
19	US-Ho1	Howland Forest – Main Tower	45.20	-68.74	1996-2004	ENFT	ENF
20	US-Me2	Metolius–Intermediate-aged Ponderosa Pine	44.45	-121.56	2002-2007	ENFT	ENF
21	CA-TP4	Turkey Point – Mature	42.71	-80.36	2002-2007	ENFT	ENF
22	US-Syv	Sylvania Wilderness Area	46.24	-89.35	2001-2006	MF	DBC
23	CA-Gro	Groundhog River Station	48.22	-82.16	2004-2006	MF	DBC
24	US-Ton	Tonzi Ranch	38.43	-120.97	2001-2007	WSA	GRA
25	US-SO2	Sky Oaks – Old	33.37	-116.62	1998-2006	SHR	GRA
26	CA-SJ1	BERMS – Jack Pine, 1994 harvest	53.91	-104.66	2002-2005	ENFB	ENF

Table 2.2 Summary of the 32 FLUXNET sites information used in this study (continued)

27	CA-SJ2	BERMS – Jack Pine, 2002 harvest	53.95	-104.65	2003-2006	ENFB	ENF
28	CA_SJ3	BERMS – Jack Pine, 1975 harvest	53.88	-104.65	2004-2005	ENFB	ENF
29	CA-Ca2	Campbell River – Douglas-fir clearcut	49.87	-125.29	2001-2006	ENFT	ENF
30	CA-Ca3	Campbell River – Douglas-fir juvenile	49.54	-124.90	2002-2006	ENFT	ENF
31	US-Me3	Metolius – Ponderosa Pine, young #2	44.32	-121.61	2004-2005	ENFT	ENF
32	US-Me5	Metolius – Ponderosa Pine, Young #1	44.44	-121.57	1999-2002	ENFT	ENF

[1] Start-end years in the gap-filled weather data and EC flux data. Partial years (from flux data record) have been extended to complete years of surface weather data to simplify model forcing.

[2] IGBP vegetation types: CRO = crop, GRA = grassland, ENFB = Evergreen needleleaf forest – boreal, ENFT = evergreen needle leaf forest – temperate, DBF = deciduous broadleaf forest, MF = mixed (deciduous/evergreen) forest, WSA = woody savanna, SHR = shrubland, TUN = tundra, WET = wetland.

[3] Plant Functional Types (PFTs) assigned in CLASS-CTEM^{N+}: evergreen needleleaf (ENF, model PFTs code=1, n=17), deciduous broadleaf-cold (DBC, model PFTs code = 4, n=4), deciduous broadleaf-drought (DBD, model PFTs code=5, n=4), C3 crops (CRO, model PFTs code= 6, n=4), and C3 grasslands (GRA, model PFTs code=8, n=4).

2.3.3.3 Model Evaluation Criteria

We used measured half-hourly, daily, seasonal and annual mean fluxes of C, water and energy cycles for model evaluation. Positive values of NEP [= GEP-Re] represent an uptake of C by the ecosystem, and negative values represent a loss of C to the atmosphere.

Model-data agreement was assessed by Root Mean Square Error (RMSE) and the Index of Agreement (d_t). RMSE measures the average distance of data points to the 1:1 line in units of the measured variable. d_t was determined following Willmott (1981):

$$\boldsymbol{d_t = 1 - \frac{\sum_{i=1}^{n}(P_i - O_i)^2}{\sum_{i=1}^{n}(|P_i - \bar{O}| + |O_i - \bar{O}|)^2}}$$

where P_i is predicted (simulated) and O_i is observed values, $\bar{O}$ is the observed average value, and n is the total number of data points. d_t is used to describe quantitatively the agreement between simulated and observed variables. It ranges from 0 to 1, where $d_t = 1.0$ corresponds to 'perfect agreement' between simulated and observed values; in turn, $d_t = 0$, indicates disagreement in general, and specifically that that the model simulations are no more accurate than the mean of the observed data. Unlike commonly used correlation parameters such as the coefficient of determination (r^2), d_t is sensitive to additive and proportional error.

Sensitivity tests of N deposition impacts on different PFTs were conducted by increasing the N deposition rate from the current prescribed rate of 0.75 g N m^{-2} yr^{-1} from the Canadian Acid Deposition Science Assessment, to 1.0, 1.25, 1.5 and 2.0 g N m^{-2} yr^{-1} (Environment Canada, 2005).

2.4 Results

In our previous study, the performance of the C-N version of the model was evaluated at an evergreen needleleaf forest (ENF) site (Turkey Point Flux station, CA-TP4) by comparing measured and modeled C, water, energy and N fluxes and pools (Huang et al., 2011). CLASS-CTEM^{N+} correctly reproduced the diurnal, daily, seasonal and annual cycles of GEP, Re, NEP, evapotranspiration (ET) and surface conductance (Gs) at this particular site (CA-TP4). Model results confirmed that a proper representation of N controls on photosynthetic uptake and canopy conductance could result in more plausible simulations of observed C and water fluxes. Our study also suggested that N limitations in spring and early summer were generally more important in controlling NEP in evergreen needleleaf forests. Discrepancies between simulated and measured annual variations of C exchanges occurred in years that experienced periods of extreme weather (e.g. low soil water content and warm spring/summer temperatures). However, in this study, the results from sites belonging to the same PFT were aggregated in order to perform a PFT-by-PFT comparison rather than a site-by-site analysis.

2.4.1 N controls on diurnal carbon, water and energy exchanges

Mean diurnal cycles of observed and simulated carbon (GEP), water (LE) and energy (Rn and H) fluxes are shown in Fig. 2.2 for both C-N and C versions of the models at 5 sample sites, one for each PFT category (US-ARM: cropland, CA-Oas: deciduous broadleaf-cold forest, US-MOz: deciduous broadleaf-dry forest, CA-TP4: evergreen needleleaf forest, US-Ton: grassland). These fluxes correspond to the average diurnal cycle over the growing season (1st April to 31st October) using data from all available years for each site (see Table 2.2 for site period of record details).

For GEP fluxes, the C-N coupled version of the model simulated amplitudes were better constrained than the C version results when compared to the ensemble observations at all sites (Fig. 2.2). The C-N version of the model simulated half-hourly GEP generally ranged from 0 to a maximum of 17.5 μmol CO_2 m^{-2} s^{-1}, compared to the observed range of 0 to 15.5 μmol CO_2 m^{-2} s^{-1}, while the corresponding C version of the model values ranged from 0 to a maximum of 24.5 μmol CO_2 m^{-2} s^{-1}. Overall, the C-N version of the model explained 82, 89, 87, 90, and 85% of the observed variance in GEP for the 5 sites (US-ARM: cropland, CA-Oas: deciduous broadleaf-cold forest, US-MOz: deciduous broadleaf-dry forest, CA-TP4: evergreen needleleaf forest, US-Ton: grassland) as compared to 75, 68, 66, 71, and 79% for the C version (Fig. 2.2).

For Rn, there is virtually no difference between results from the C-N and C versions at all sample sites. The model performed quite well for all sites when compared to observations (Fig. 2.2). At an evergreen needleleaf forest (CA-TP4) the model slightly overestimated the daily amplitude of Rn, likely related to the default albedo values (0.1) being too small for that specific site (0.12, reported by Restrepo and Arain, 2005).

H was slightly underestimated by both models during the growing seasons with a sharp decrease in simulated H in the afternoon, especially in broadleaf forests (CA-Oas and US-MOz) and the crop site (US-ARM)(Fig. 2.2). Overall, the C-N model version explained 77, 74, 78, 91 and 75% of the observed variation in H for crop, broadleaf-cold, broadleaf-dry, evergreen needleleaf forests, and grassland sites, respectively, showing marginally better accuracy compared to respective values of 73, 68, 76, 91 and 70% for the C version of the model.

Both the C and C-N versions' simulated LE showed a tendency of overestimation at all sample sites compared with the observation. This could suggest that the model is underestimating either a soil moisture or vapour pressure deficit constraint on stomatal conductance, or is overestimating evaporation from the soil. Bartlett et al. (2000; 2003) found that evaporation from the soil, which (prior to CLASS 3.0) was based on the estimated relative humidity at the soil surface

(Philip, 1957), was overestimated in CLASS version 2.6 over much of the range of observed soil moisture as the soil dried. Overall, results from the C-N version were in better agreement with observations and they explained 71, 93, 77, 94, and 68% of the variance when compared to observed LE for the 5 sites (US-ARM: cropland, CA-Oas: deciduous broadleaf-cold forest, US-MOz: deciduous broadleaf-dry forest, CA-TP4: evergreen needleleaf forest, US-Ton: grassland), while the C version of the model explained 64, 88, 75, 90, and 67% of annual variance over the 5 sites, respectively.

2.4.2 N controls on daily and seasonal carbon, water and energy exchanges

Figures 2.3 and 2.4 show a comparison of the measured and simulated (by the C-N and C version of the models) seasonal cycles of ensemble carbon (GEP, Re, NEP), water and energy (Rn, LE, H) fluxes averaged for each PFT's sites.

The steep rise in GEP in spring and the overestimated summer peak of GEP in ENF, DBC and GRA in the C version was eliminated with the inclusion of the N cycle, leaving modeled and observed seasonality in closer agreement. The C version simulated a fast build-up of photosynthesis at the start of the year, assuming no limitation due to N availability, resulting in high rates of GEP and subsequent high autotrophic respiration (R_a) early in the year. For evergreen needleleaf (ENF) and deciduous broadleaf-cold forests (DBC) the seasonality in GEP was generally reproduced by CLASS-CTEMN^{+} (Fig. 2.3), but leaf-out and the rise in GEP appears to begin early in DBC while senescence occurs late. The simulated GEP summer maximum was reduced in the C-N version due to N limitation for both forest types, which caused the model output to match better with observations. The C version of the model underestimated the summer peak for deciduous broadleaf-dry forests and crop sites, which was improved in the C-N version. Early crop growth may relate to a mismatch with sowing dates. Summertime Re is often overestimated, especially when GEP is overestimated. Values of Re were reduced for ENF, DBC and GRA in the C-N version, which improved the model fit although an overestimation in summer respiration remained in DBC and GRA. The small seasonality of observed Re for grasslands (GRA) was not reproduced well by CLASS-CTEM^{N+} and both GEP and Re were overestimated in the summer (Fig. 2.3). Both models missed an observed strong decline in GEP and Re during the summer in terms of timing and magnitude. The seasonal cycle was arguably better matched with observations by the C-N version for forests as the seasonal variation in GEP was somewhat less pronounced. For water and energy fluxes (Rn, LE and H), less discrepancy was observed between the two models' simulations (Fig. 2.4). The winter Rn is overestimated in ENF by both versions of the model, largely due to a result of a damped response of albedo to intercepted snow (Bartlett et al., 2006), while the summer Rn is overestimated by both model simulations in DBD. While we suspect that evaporation from the soil surface is overestimated, the large overestimation in both LE and GEP in

GRA suggests that a moisture stress limitation may not be captured by the model. An overestimation in the simulated soil moisture may contribute to enhanced evaporation from the soil, and to enhanced GEP and transpiration. In the C-N simulation in CRO (Fig. 2.3 and 2.4), GEP and LE are enhanced early in the growing season relative to the C model version, but then drop, possibly a result of the additional LE drying the soil and causing simulated moisture stress.

Ensemble mean seasonal values and standard deviations (SD), along with statistical quantities (RMSE and d_t), for simulated (C-N and C versions of the model) and observed C fluxes (GEP, Re and NEP, in g C m^{-2} d^{-1}) are evaluated for all sites (n=32) over different PFTs (ENF, DBC, DBD, CRO and GRA), shown in Table 2.3a; Similarly, ensemble seasonal water and energy fluxes (Rn, LE and H, in W m^{-2}) are shown in Table 2.3b. All simulated C fluxes of GEP, Re and NEP for evergreen needleleaf forests (ENF) showed a considerable improvement in the C-N version of the model with closer mean values and SD, a reduction in RMSE and an increase in d_t, when compared with the C version results (Table 2.3a). Results also indicated that more bias between the two model versions was reduced during the winter to early spring season (Table 2.3a), in agreement with our previous finding (Huang, et al., 2011). For example, seasonal RMSE values for GEP in ENF of 1.01, 2.47, 3.35, 1.97 g C m^{-2} day^{-1} by the C-N version were generally reduced, compared to RMSE of 2.37, 2.97, 3.08, 2.76 g C m^{-2} day^{-1} by the C version in DJF, MAM, JJA and SON, respectively, especially during the Dec-Jan-Feb months. For DBC, generally, both error and bias scores improved in the C-N version with lower RMSE and higher d_t (Table 2.3a). For example, the RMSE of seasonal mean GEP for DBC improved from 0.64 g C m^{-2} day^{-1} by the C version to 0.34 g C m^{-2} day^{-1} with the C-N version during the winter (DJF). Mixed results (e.g., RMSE of 3.07, 1.33, 3.56 g C m^{-2} day^{-1} for the C-N version, compared with RMSE of 3.46, 1.14, 3.93 g C m^{-2} day^{-1} for the C version for GEP, Re and NEP, respectively) were observed for DBC over the spring months (MAM). The C-N version also shows improvements in DBD during MAM (e.g., smaller RMSE values of 2.89, 2.32 g C m^{-2} day^{-1} for GEP and Re, respectively, compared with values of 2.94 and 2.47 g C m^{-2} day^{-1} by the C version). For CRO, modeled results were mixed. The SD and d_t were improved while the RMSE was sometimes larger in the C-N version (Table 2.3a). For GRA, incorporation of N constraints on C-cycle processes generally improved the simulated C fluxes over all the seasons, with smaller RMSE values; but the SD and d_t values were also mixed.

The simulated water and energy fluxes (Rn, LE and H) showed mixed results but minor differences between the C and C-N versions for seasonal ensemble statistics over all PFTs (Table 2.3b). The simulated Rn was overestimated in DBD by both model versions, especially during the summer (Figure 2.4), with seasonal RMSE values of 32.89, 62.00, 76.64, 52.81 in DJF, MAM, JJA and SON, respectively, by the C-N version compared with 33.53, 60.60, 71.23, 50.20 by the C version. This suggests that the default albedo parameters are in need of changes for this PFT but otherwise Rn simulations were very similar in the C and C-N versions of the model. Comparisons of observed and simulated LE and H are more mixed, with simulated values of both H and LE tending to be larger than the sum of the observed values. A lack of energy balance closure in the observed data may account for some of the apparent overestimation of these fluxes.

2.4.3 N controls on inter-annual variability

Comparisons of statistical quantities and scatter plots for observed and modeled annual C, water and energy fluxes (GEP, Re, NEP, Rn, H and LE) for each PFT are shown in Table 2.4 and Figures 2.5 and 2.6. The inclusion of C and N interactions caused different responses, depending on PFTs. Simulated GEP for ENF, DBD and GRA sites improved in the C-N version (Fig. 2.5a, b), with a considerable reduction in RMSE (e.g., RMSE for ENF of 0.35 by the C-N version compared to 0.61 kg C m^{-2} yr^{-1} by the C version) and an increase in the d_t values (e.g., d_t for ENF of 0.93 by the C-N version compared with 0.83 by the C version) (Table 2.4). For DBC sites, the C-N version simulated GEP was slightly improved (RMSE of 0.84 kg C m^{-2} yr^{-1} by the C-N version compared with 0.88 kg C m^{-2} yr^{-1} by the C version; and d_t value of 0.46 by C-N version compared with 0.34 by C version), but with more overestimation in SD than the C version. For CRO sites, the C version's modeled annual GEP showed better agreement with the observed mean, and a slightly smaller RMSE than the C-N version; while the C-N version showed better d_t values (0.73 compared with 0.17 by the C-N version and C version, respectively; Table 2.4).

Overall, inclusion of N dynamics in the model caused a reduction in annual GEP estimates of 0.32 ± 0.06 kg C m^{-2} yr^{-1} (Δ = C - C-N) over all the PFTs sites. GEP overestimation of 46% from the C version of the model was reduced to 18% in the C-N version, while the RMSE improved from 0.83 to 0.54 kg C m^{-2} yr^{-1} over all the PFTs sites (Fig. 2.5). For simulations of annual Re, the inclusion of the N cycle with the C-N version produced marginal improvements at ENF, DBD and GRA sites with better RMSE and d_t values than the C version results (Table 2.4). Re simulations by the C-N version for DBC and CRO sites, however, has not shown better agreement with the observations than the C version counterpart. Simulated annual values of NEP were in better agreement with observed values for the C-N version, for all PFTs (e.g., RMSE of 0.33, 0.42, 0.25, 0.43, 0.26 kg C m^{-2} yr^{-1} by the C-N version were improved when compared with 0.47, 0.58, 0.30, 0.34, 0.51 kg C m^{-2} yr^{-1} by the C version, for ENF, DBC, DBD, CRO and GRA, respectively; Table 2.4). The overall net C uptake during observation years was 0.17 ± 0.18 kg C m^{-2} yr^{-1}, while the models simulated a C sink of 0.23 ± 0.26 kg C m^{-2} yr^{-1} and 0.36 ± 0.25 kg C m^{-2} yr^{-1} in the C-N and C versions, respectively. DBD exhibited the largest net C uptake in the observation years with 0.27 ± 0.11 kg C m^{-2} yr^{-1}, compared with and 0.2 ± 0.25 kg C m^{-2} yr^{-1} for the C-N version and 0.26 ± 0.20 kg C m^{-2} yr^{-1} for the C version.

Both model versions simulated annual Rn and H were generally in good agreement with the observation (Fig. 2.6, Table 2.4). The error and bias in the C-N version simulated Rn and H in the ENF, DBC, CRO and GRA were marginally better than the C version. The C-N version simulated annual mean Rn for all PFTs was 75.43 W m^{-2}, compared to an observed value of 75.03 W m $^{-2}$, and a C version simulated value of 77.17 W m^{-2}. However, both models overestimated Rn and H in ENF. For simulated annual LE, an overestimation was observed at all PFTs with relatively higher error and bias scores (Fig. 2.6, Table 2.4). Meanwhile, the C-N version simulations for LE at all PFTs showed improvements in RMSE and d_t with respect to the C version. It is noteworthy that in every PFT, the sum of LE and H in the simulations is larger than the sum of the observed values. Failure to close the energy balance in eddy-covariance flux measurement studies has long been recognized as a problem, with underestimation of about 20% in the sum of H and LE relative to available energy (defined as (Rn – S) where S is the energy storage term), not uncommon (Wilson et al. 2002; Foken, 2008; Leuning et al. 2012). The inter-annual variability of observed water and energy fluxes was small, with an average standard deviation (SD) of 15.19, 11.03 and 11.80 W m^{-2} over all PFTs, for Rn, LE and H respectively. Both models were able to simulate inter-annual variability of water and energy fluxes within a reasonable range compared to observations, with simulated average SD of 17.04, 16.56 and 11.35 W m^{-2} by the C-N version; 16.33, 17.29 and 14.45 W m^{-2} by the C version, for Rn, LE and H, respectively (Table 2.4).

2.4.4 N controls on C stocks

Simulated total vegetation biomass and soil C pools were consistently reduced for all PFTs in the C-N version of the model as compared to the C version (Fig. 2.7). Both versions of the model showed an underestimation for vegetation biomass when compared with site-specific observations. For soil C pools, both model versions were in very good agreement with observations, and the simulated estimates only slightly differed. Among PFTS, the soil C pool for DBC was quite accurately reproduced by the C-N version, whereas the C version underestimated it (Fig. 2.7).

The simulated pattern of root N uptake by the C-N version of the model was able to capture the difference between forests (ENF, DBC, DBD) and herbaceous species (CRO, GRA). The simulated daily mean root N uptake rate for all forests showed strong seasonal variability, ranging from no uptake in winter to a maximum of 38.8 mg N m^{-2} day^{-1} in the early growing season (April to June) (Fig. 2.8). Root N uptake generally remained high from May through mid July, ranging from 15 to 38.8 mg N m^{-2} day^{-1}, then declined in late July and early August, and approached zero in the late autumn and winter months (Fig. 2.8). For crops and grasslands, the root N uptake rates were much smaller in scale and had a slight peak during the growing season.

2.4.5 Sensitivity analysis of N controls on C fluxes

The sensitivity of CLASS-CTEM^{N+} simulated vegetation biomass, GEP and NEP to changes in N deposition (Ndep) is shown in Fig. 2.9. As N deposition input was increased from an original prescribed value of 0.75 g N m^{-2} yr^{-1} to 1.0, 1.25, 1.5 and 2.0 g N m^{-2} yr^{-1}, the corresponding annual mean vegetation biomass showed change rate of 0.01, 0.03, -0.01, -0.11 and 0.03 Kg C m^{-2}, over 5 PFTs (ENF, DBC, DBD, CRO, GRA), respectively. Annual mean GEP changes by 0.05, 0.16, -0.02, 0.01 and 0.07 Kg C m^{-2} yr^{-1}; while annual mean NEP changes by 0.22, 0.22, -0.06, -0.17 and -0.01 Kg C m^{-2} yr^{-1}, over 5 PFTs, respectively. Nitrogen deposition changes yielded larger variations in simulated GEP and NEP fluxes compared to changes in vegetation biomass. The impact of N deposition was more pronounced on ENF and DBC to show greater response to additional N added.

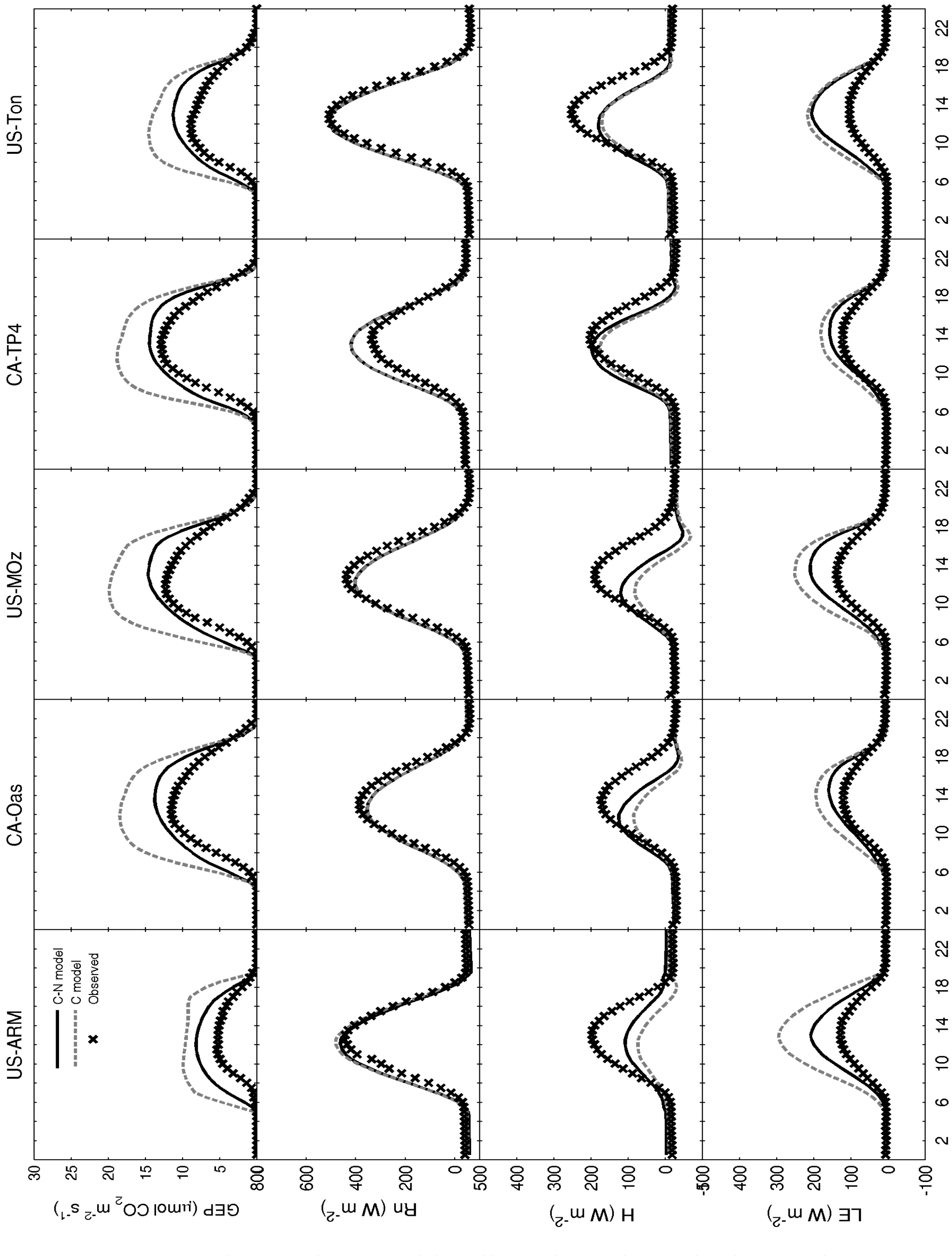

Figure 2.2 Comparison of ensemble diurnal cycles of observed (cross) and modeled (C-N version: solid line, C version: dash line) gross ecosystem productivity (GEP, μmol CO2 m^{-2} s^{-1}), net radiation (Rn, W m^{-2}), latent heat (LE, W m^{-2}) and sensible heat (H, W m−2) fluxes over the growing season at 5 sites representing each major plant functional type (US-ARM: cropland, CA-Oas: deciduous broadleaf-cold forest, US-MOz: deciduous broadleaf-dry forest, CA-TP4: evergreen needleleaf forest, US-Ton: grassland).

Table 2.3a Ensemble mean and standard deviations (SD) of seasonal[*] C fluxes (GEP, Re and NEP, in g C m^{-2} d^{-1}) from observations (Obs.) and models (C-N and C versions). Error metrics of RMSE and dt for both models were evaluated against observations from per plant functional type (evergreen needleleaf forests (ENF), deciduous broadleaf-cold forests (DBC), deciduous broadleaf-dry forests (DBD), crop lands (CRO) and grasslands (GRA)).

			ENF				**DBC**				**DBD**				**CRO**				**GRA**			
			DJF[*]	**MAM**	**JJA**	**SON**	**DJF**	**MAM**	**JJA**	**SON**	**DJF**	**MAM**	**JJA**	**SON**	**DJF**	**MAM**	**JJA**	**SON**	**DJF**	**MAM**	**JJA**	**SON**
GEP	**Mean**	**Obs.**	0.50	3.35	6.69	2.80	0.01	0.96	9.27	1.77	0.12	2.39	9.45	3.06	0.17	1.53	9.86	1.67	0.84	3.34	2.50	0.61
		C-N	0.83	2.75	6.24	2.91	0.27	2.84	9.85	5.07	1.34	1.05	8.38	4.86	0.31	4.35	9.55	2.86	1.12	3.07	5.23	2.82
		C	2.25	4.84	7.19	4.60	0.33	3.20	12.64	5.26	0.62	1.38	4.62	4.28	0.18	1.18	6.28	5.16	2.26	6.00	6.12	3.37
	SD	**Obs.**	0.29	0.51	0.19	0.58	0.03	0.78	0.68	0.70	0.11	0.94	0.43	0.74	0.19	0.68	2.50	1.42	0.40	0.35	0.66	0.42
		C-N	0.20	0.77	0.23	0.88	0.08	0.62	1.36	2.21	0.52	1.04	0.57	0.80	0.20	2.09	1.40	1.74	0.21	0.50	0.32	0.33
		C	0.29	0.37	0.19	0.49	0.11	0.97	0.62	0.91	0.18	1.07	0.57	0.35	0.33	0.42	0.27	0.25	0.33	0.25	0.54	0.71
	RMSE	**C-N**	1.01	2.47	3.35	1.97	0.34	3.07	5.51	5.70	2.08	2.89	5.50	3.19	0.66	6.22	9.71	4.68	1.14	2.76	4.35	2.88
		C	2.37	2.97	3.08	2.76	0.64	3.46	4.44	4.73	1.01	2.94	6.94	3.44	0.63	2.48	8.72	4.84	2.16	3.87	4.84	3.50
	d_t	**C-N**	0.72	0.82	0.77	0.85	0.32	0.65	0.45	0.60	0.43	0.69	0.29	0.71	0.49	0.37	0.64	0.49	0.61	0.69	0.52	0.47
		C	0.60	0.80	0.77	0.77	0.23	0.68	0.56	0.68	0.49	0.71	0.29	0.57	0.39	0.27	0.38	0.60	0.54	0.66	0.63	0.49
Re	**Mean**	**Obs.**	0.75	2.43	6.01	3.01	0.42	1.63	5.99	2.41	1.26	2.79	4.91	3.13	0.39	1.74	6.09	2.19	1.08	2.48	1.77	1.15
		C-N	0.89	1.99	5.59	2.97	0.13	0.84	8.67	4.55	0.67	1.66	7.38	3.75	0.21	2.89	7.79	3.31	1.20	2.38	3.69	2.23
		C	1.49	2.76	6.37	3.81	0.16	0.98	9.61	4.61	0.46	1.65	5.09	3.07	0.22	2.47	5.86	3.08	1.61	3.19	4.86	2.84
	SD	**Obs.**	0.33	0.41	0.31	0.47	0.08	0.42	0.53	0.59	0.36	0.24	0.15	0.24	0.28	0.38	0.93	0.77	0.51	0.16	0.40	0.20
		C-N	0.08	0.49	0.27	0.62	0.07	0.24	2.27	2.26	0.13	1.01	0.48	0.52	0.10	1.23	0.63	1.11	0.12	0.32	0.28	0.35
		C	0.06	0.34	0.32	0.54	0.10	0.33	1.84	1.23	0.18	1.19	0.51	0.66	0.16	0.57	0.35	0.38	0.16	0.19	0.33	0.23
	RMSE	**C-N**	0.97	1.34	2.83	1.80	0.46	1.33	8.18	5.15	1.30	2.32	3.79	2.22	0.75	2.82	4.72	2.26	1.55	1.78	3.01	1.81
		C	1.27	1.25	2.60	1.86	0.45	1.14	7.00	4.02	1.46	2.47	3.14	2.52	0.81	2.21	4.13	2.10	1.68	1.91	3.63	2.18
	d_t	**C-N**	0.67	0.88	0.75	0.85	0.27	0.66	0.34	0.52	0.26	0.64	0.43	0.58	0.21	0.54	0.65	0.79	0.54	0.72	0.55	0.58
		C	0.63	0.89	0.79	0.85	0.31	0.80	0.45	0.63	0.18	0.66	0.33	0.43	0.19	0.60	0.48	0.74	0.57	0.73	0.54	0.52
NEP	**Mean**	**Obs.**	-0.24	0.92	0.68	-0.22	-0.41	-0.67	3.29	-0.64	-1.14	-0.40	4.55	-0.07	-0.21	-0.21	3.77	-0.52	-0.24	0.86	0.73	-0.54
		C-N	-0.07	0.76	0.65	-0.06	-0.13	2.00	1.19	0.53	0.67	-0.61	0.99	1.11	0.11	1.47	1.76	-0.45	-0.07	0.69	1.54	0.60
		C	0.76	2.08	0.82	0.78	-0.16	2.23	3.03	0.65	0.16	-0.27	-0.47	1.21	-0.04	-1.29	0.42	2.08	0.66	2.81	1.26	0.53
	SD	**Obs.**	0.25	0.27	0.18	0.36	0.07	0.63	0.59	0.72	0.35	0.83	0.38	0.51	0.17	0.55	1.77	0.69	0.47	0.32	0.39	0.25
		C-N	0.12	0.42	0.37	0.55	0.07	0.44	1.15	1.49	0.39	0.67	0.54	0.56	0.19	1.46	1.09	1.69	0.09	0.24	0.38	0.23
		C	0.21	0.26	0.33	0.49	0.10	0.69	1.36	1.44	0.18	0.51	0.34	0.29	0.18	0.50	0.31	0.32	0.14	0.24	0.45	0.46
	RMSE	**C-N**	0.91	2.10	3.18	1.95	0.45	3.56	5.98	3.56	2.48	2.96	5.50	2.85	0.93	4.29	8.40	4.11	1.59	1.88	2.12	1.65
		C	1.64	2.61	3.27	2.41	0.44	3.93	6.19	3.41	1.68	2.64	6.06	2.94	0.84	2.94	6.89	3.55	2.02	2.76	2.68	2.04
	d_t	**C-N**	0.46	0.53	0.42	0.41	0.27	0.45	0.37	0.36	0.38	0.35	0.35	0.45	0.27	0.32	0.48	0.28	0.25	0.47	0.56	0.53
		C	0.50	0.57	0.45	0.42	0.31	0.47	0.35	0.39	0.30	0.38	0.25	0.32	0.23	0.33	0.35	0.45	0.36	0.50	0.63	0.54

Table 2.3b. Ensemble mean and standard deviations (SD) of seasonal water and energy fluxes (Rn, LE and H, in W m^{-2}) from observations (Obs.) and models (C-N and C versions). Error metrics of RMSE and d_t for both models were evaluated against observations from per plant functional type (evergreen needleleaf forests (ENF), deciduous broadleaf-cold forests (DBC), deciduous broadleaf-dry forests (DBD), crop lands (CRO) and grasslands (GRA)).

			ENF				**DBC**				**DBD**				**CRO**				**GRA**			
			DJF	**MAM**	**JJA**	**SON**	**DJF**	**MAM**	**JJA**	**SON**	**DJF**	**MAM**	**JJA**	**SON**	**DJF**	**MAM**	**JJA**	**SON**	**DJF**	**MAM**	**JJA**	**SON**
Rn	**Mean**	**Obs.**	10.63	99.24	138.73	43.15	7.25	94.30	132.05	31.41	13.63	62.99	85.25	31.09	20.40	71.28	103.39	40.98	24.12	116.11	156.14	61.75
		C-N	24.67	93.71	132.20	55.23	22.14	60.34	101.29	43.23	32.56	77.42	130.60	63.37	34.90	82.17	129.05	57.89	35.25	111.16	152.06	72.10
		C	24.83	96.10	134.34	55.48	22.08	60.45	109.62	44.36	33.30	78.92	126.40	61.29	34.15	78.46	133.98	65.94	36.18	116.97	161.19	72.24
	SD	**Obs.**	3.41	8.52	7.23	6.70	4.56	18.71	15.37	11.34	6.44	21.21	8.65	12.48	52.01	10.64	9.38	12.38	5.75	7.12	7.50	11.63
		C-N	4.23	9.63	7.50	8.31	3.57	9.80	8.67	10.96	4.16	9.49	7.29	8.85	7.19	9.52	8.64	9.08	4.09	9.99	7.09	6.22
		C	4.36	9.47	7.45	8.51	3.49	10.63	9.67	10.89	4.49	9.64	7.26	8.44	7.37	9.03	8.43	10.45	4.28	9.22	11.53	3.66
	RMSE	**C-N**	30.69	53.42	62.93	35.98	25.03	60.39	69.06	35.21	32.89	62.00	76.64	52.81	72.24	51.39	70.27	41.02	32.65	53.40	59.16	42.26
		C	31.55	54.09	62.97	36.66	25.02	60.47	66.49	35.26	33.53	60.60	71.23	50.20	73.57	48.57	67.56	47.82	32.89	54.38	47.01	39.07
	d_t	**C-N**	0.65	0.73	0.67	0.82	0.58	0.56	0.54	0.76	0.56	0.54	0.54	0.63	0.18	0.67	0.45	0.67	0.69	0.75	0.54	0.77
		C	0.63	0.73	0.67	0.82	0.58	0.56	0.57	0.77	0.55	0.59	0.58	0.64	0.15	0.69	0.48	0.66	0.71	0.75	0.60	0.80
LE	**Mean**	**Obs.**	9.52	35.69	65.11	27.68	1.74	16.66	79.15	20.66	4.93	19.78	49.32	18.16	10.22	32.31	62.07	24.20	16.22	45.20	35.48	13.66
		C-N	5.57	26.59	64.06	24.54	0.32	20.89	81.76	29.24	4.88	19.76	102.91	48.71	4.90	51.04	105.46	38.02	16.20	52.91	90.64	44.48
		C	9.93	35.11	66.28	30.21	0.34	22.90	106.48	35.12	4.39	24.93	75.71	46.29	4.93	36.81	109.60	58.97	21.14	72.21	93.02	41.70
	SD	**Obs.**	8.37	8.78	6.29	10.66	1.37	7.66	10.04	17.90	5.19	8.91	7.54	6.67	7.99	7.68	9.32	6.37	6.42	4.32	6.89	4.08
		C-N	2.84	11.91	5.58	11.02	0.18	14.59	10.22	17.38	3.20	16.38	8.91	14.88	3.47	19.24	12.15	15.96	3.53	8.21	3.78	6.40
		C	3.14	7.43	3.80	7.58	0.25	18.52	8.03	18.62	3.00	18.80	9.04	10.98	3.93	10.41	4.96	10.15	4.13	5.21	4.14	6.02
	RMSE	**C-N**	17.54	37.66	60.26	36.25	4.04	28.15	65.15	35.83	12.08	30.44	85.94	49.45	15.08	58.31	90.03	40.20	21.79	37.88	79.37	46.49
		C	18.87	37.68	57.93	36.78	4.05	32.03	74.51	40.84	11.33	35.80	59.46	45.84	15.54	37.52	76.21	56.35	25.35	47.76	67.60	40.44
	d_t	**C-N**	0.54	0.71	0.55	0.65	0.12	0.65	0.53	0.69	0.27	0.67	0.51	0.56	0.43	0.48	0.42	0.55	0.50	0.70	0.36	0.46
		C	0.62	0.70	0.49	0.64	0.12	0.65	0.54	0.68	0.34	0.71	0.60	0.56	0.39	0.62	0.39	0.54	0.51	0.67	0.54	0.53
H	**Mean**	**Obs.**	4.25	53.27	65.56	19.36	4.95	58.17	31.05	11.13	9.45	32.46	17.99	11.94	5.87	27.48	26.00	17.86	10.51	55.23	92.79	40.81
		C-N	19.10	67.13	68.14	30.70	21.82	39.45	19.53	13.99	27.68	57.66	27.69	14.66	30.00	31.13	23.59	19.87	19.05	58.25	61.42	27.62
		C	14.90	60.99	68.06	25.27	21.74	37.55	3.14	9.23	28.91	53.99	50.69	15.00	29.22	41.65	24.38	6.97	15.04	44.76	68.16	30.54
	SD	**Obs.**	5.98	4.66	4.16	4.01	6.17	17.29	11.08	10.72	5.20	6.10	6.33	4.71	5.53	5.49	8.82	7.69	7.10	6.44	7.51	6.98
		C-N	4.62	7.02	5.64	8.57	3.55	10.97	7.43	9.58	3.55	8.10	7.69	7.68	7.25	10.35	7.54	9.72	3.92	5.59	4.71	4.46
		C	4.54	5.74	5.27	7.95	3.47	10.36	6.44	11.08	3.64	8.01	6.22	6.63	7.48	6.48	5.26	6.68	2.73	7.31	2.41	8.10
	RMSE	**C-N**	37.49	56.90	62.02	40.18	28.72	60.74	54.92	39.00	33.05	53.28	58.37	36.45	34.51	38.97	51.22	30.77	32.36	45.52	52.28	36.33
		C	39.16	54.01	57.51	37.88	28.67	60.61	60.26	41.94	33.97	56.85	63.66	38.74	34.22	32.38	49.22	35.53	31.79	46.51	50.08	37.48
	d_t	**C-N**	0.56	0.56	0.53	0.63	0.48	0.42	0.41	0.38	0.53	0.43	0.25	0.35	0.46	0.45	0.43	0.50	0.55	0.60	0.60	0.67
		C	0.50	0.58	0.57	0.65	0.48	0.43	0.40	0.36	0.52	0.36	0.29	0.28	0.46	0.53	0.20	0.34	0.51	0.58	0.69	0.73

[*] Seasonal periods were defined as: DJF: Dec., Jan., Feb.; MAM: Mar., Apr., May.; JJA: Jun., Jul., Aug.; SON: Sep., Oct., Nov..

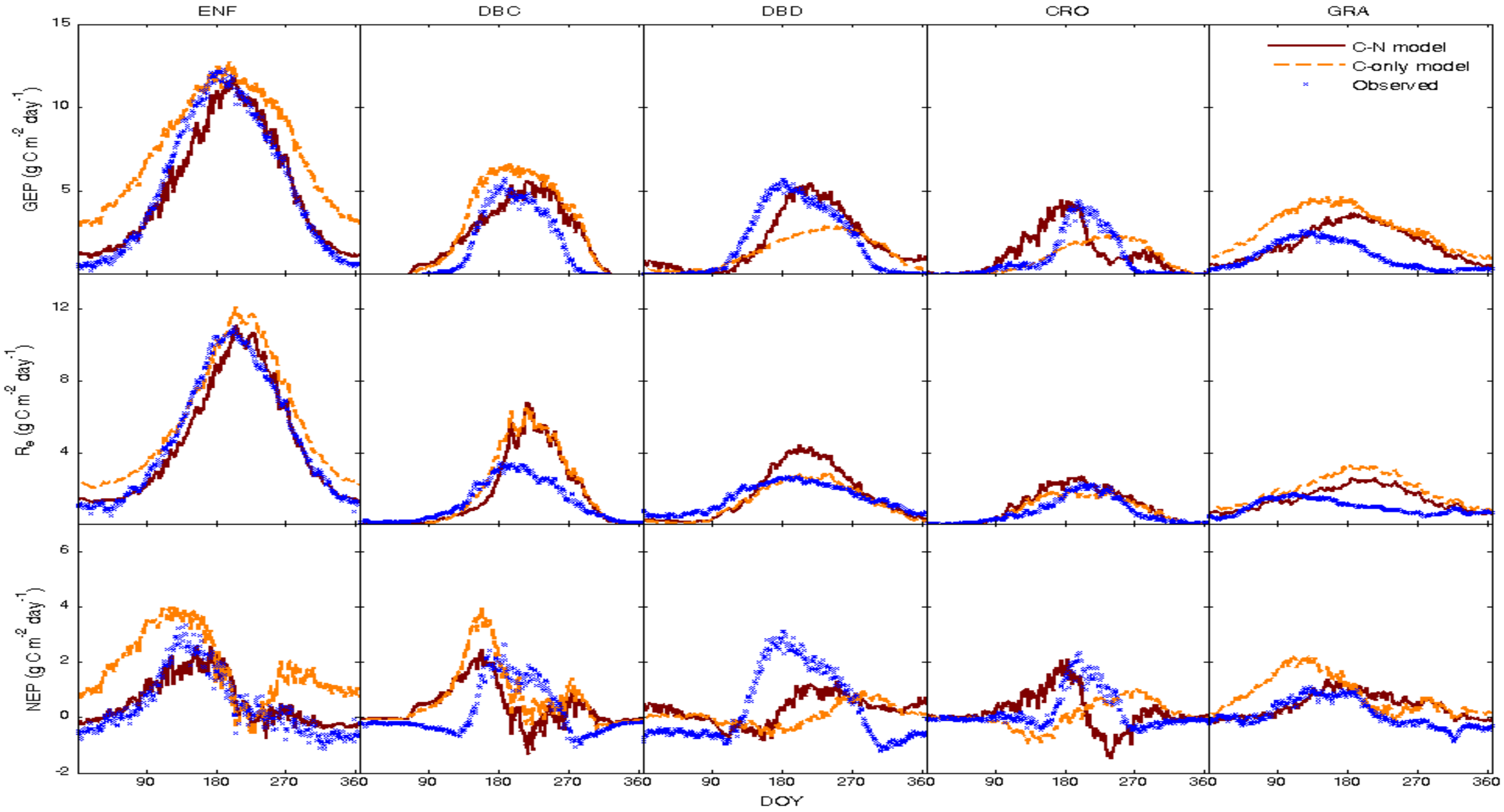

Figure 2.3 Comparison of observed (green cross) and modeled (C-N: maroon line, C: orange line) mean seasonal cycle of daily gross ecosystem productivity (GEP), ecosystem respiration (Re), and net ecosystem productivity (NEP) in g C m^{-2} d^{-1} for 5 sites (panels from left to right: evergreen needleleaf forests (ENF), deciduous broadleaf-cold forests (DBC), deciduous broadleaf-dry forests (DBD), crop lands (CRO) and grasslands (GRA)).

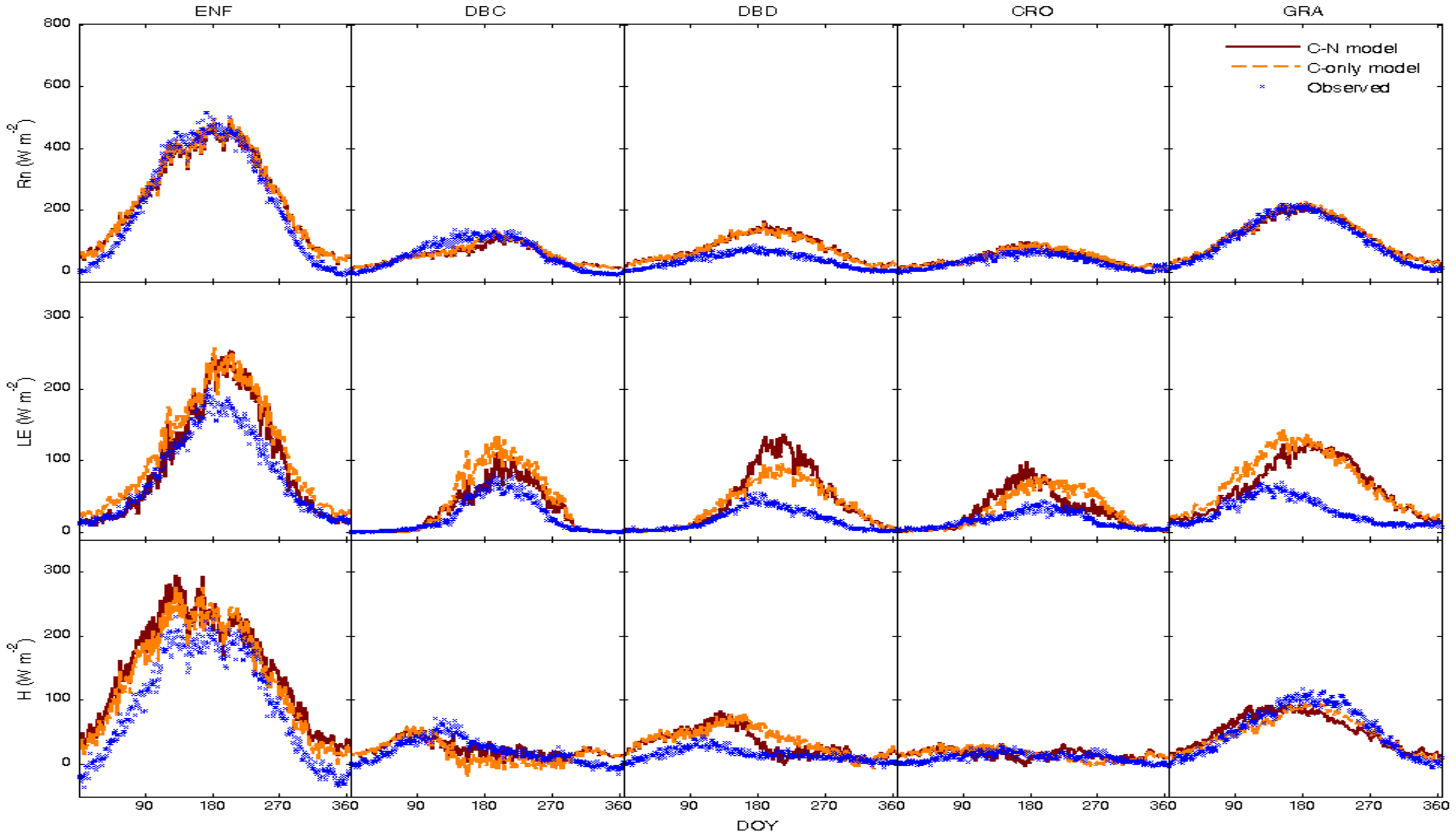

Figure 2.4 Comparison of observed (green cross) and modeled (C-N: maroon line, C: orange line) mean seasonal cycle of daily net radiation (Rn), latent heat (LE) and sensible heat (H) flux in W m^{-2} for 5 sites (panels from left to right: evergreen needleleaf forests (ENF), deciduous broadleaf-cold forests (DBC), deciduous broadleaf-dry forests (DBD), crop lands (CRO) and grasslands (GRA)).

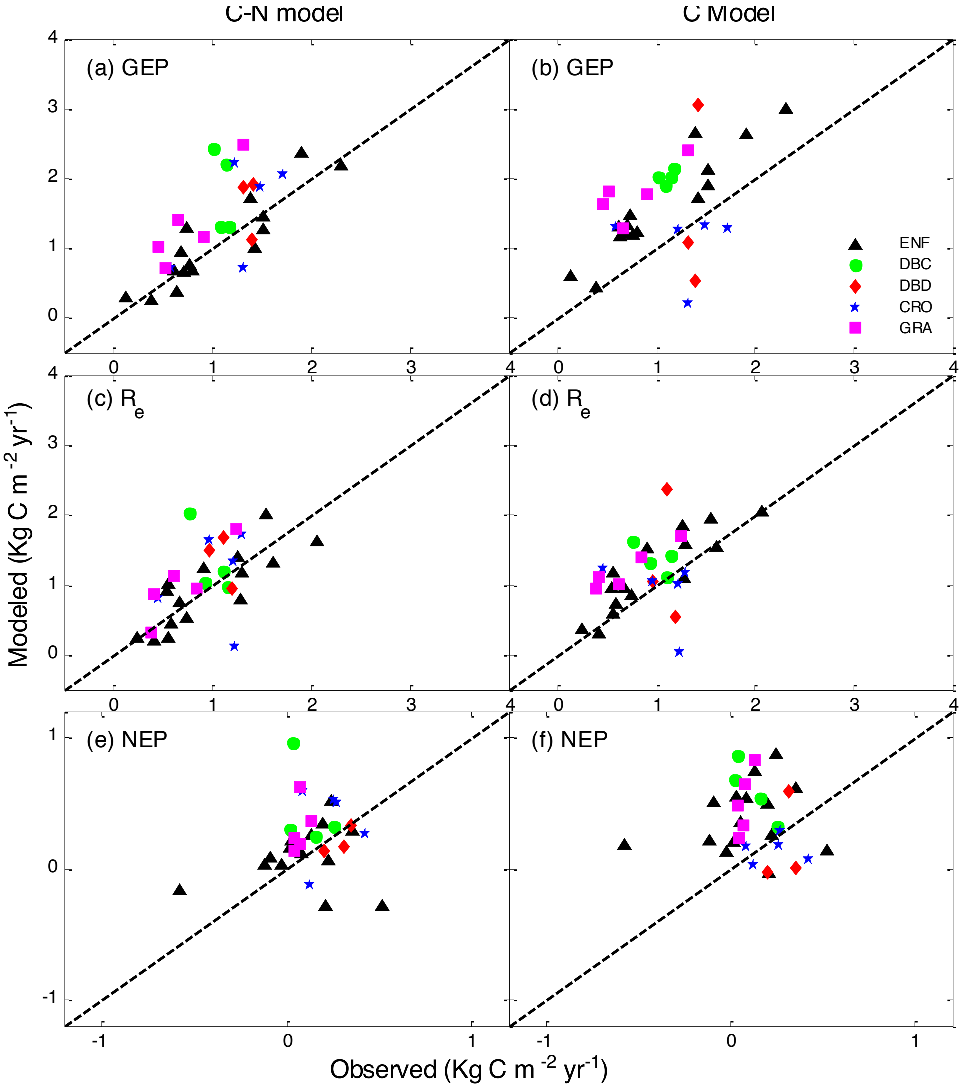

Figure 2.5 Annual mean observed versus modeled annual gross ecosystem productivity (GEP), ecosystem respiration (Re), and net ecosystem productivity (NEP) for each site (n=32), in (kg C m^{-2} yr^{-1}) for the C-N version (left) and the C version (right) of the model. Symbols in legend reflect plant functional type (PFT) classification.

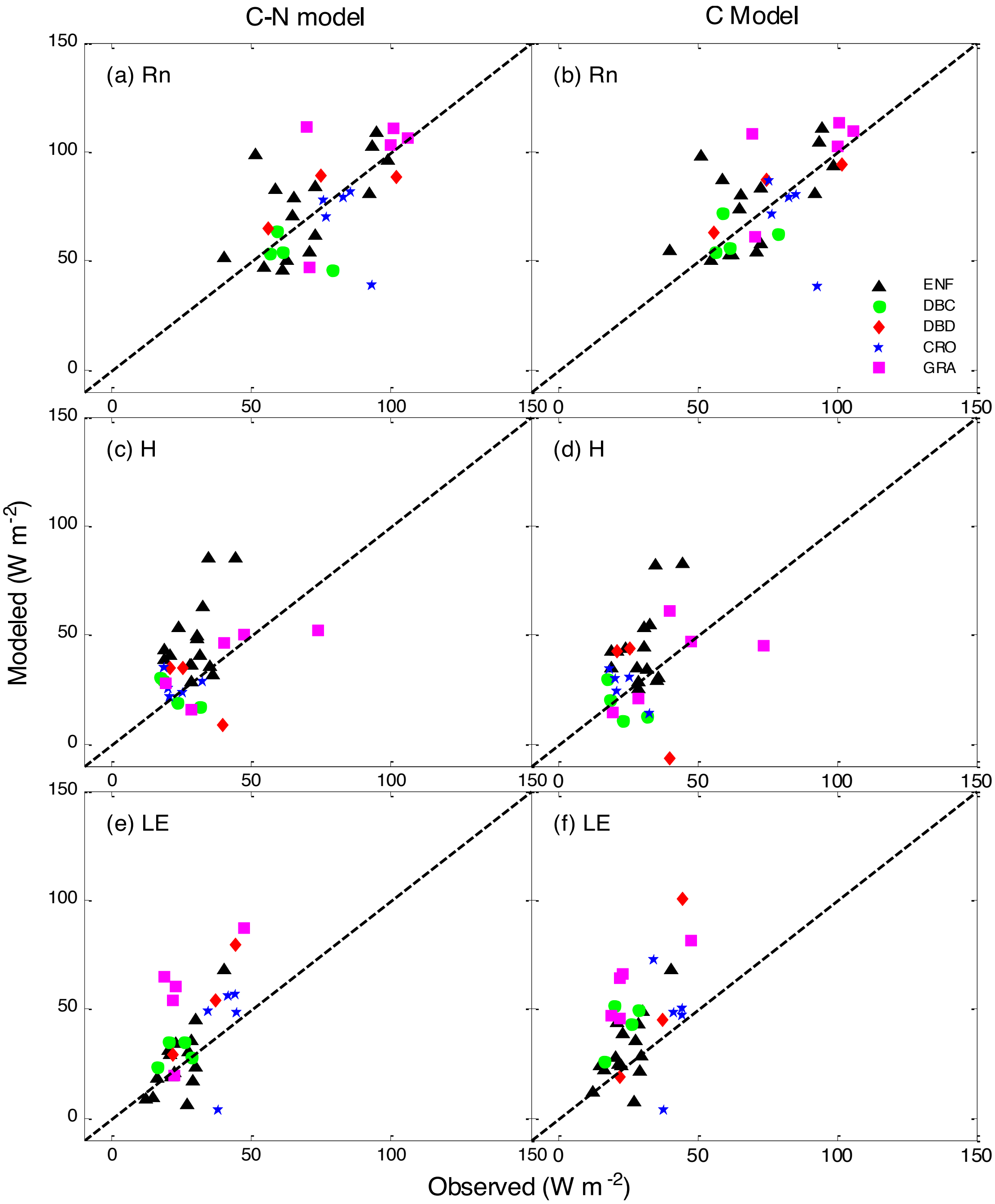

Figure 2.6 Annual mean observed versus modeled net radiation (Rn), latent heat (LE) and sensible heat (H) for each forest site (n=32), in (W m^{-2}) for the C-N version (left) and the C version (right) of the model. Symbols in the legend reflect plant functional type (PFT) classification.

Table 2.4 Mean and standard deviations (SD) of annual C fluxes (GEP, Re and NEP, in kg C m^{-2} yr^{-1}) and of water and energy fluxes (Rn, LE and H, in W m^{-2}) from observations (Obs) and models (C-N and C versions). Error metrics of RMSE and d_t for both models were evaluated against observations from per plant functional type (evergreen needleleaf forests (ENF), deciduous broadleaf-cold forests (DBC), deciduous broadleaf-dry forests (DBD), crop lands (CRO) and grasslands (GRA)), on the annual basis.

		Mean			**SD**			**RMSE**		**d_t**	
		Obs	**C-N**	**C**	**Obs**	**C-N**	**C**	**C-N**	**C**	**C-N**	**C**
GEP	**ENF**	1.21	1.16	1.72	0.64	0.66	0.72	0.35	0.61	0.93	0.83
	DBC	1.09	1.62	1.92	0.16	0.64	0.23	0.84	0.88	0.46	0.34
	DBD	1.37	1.42	0.99	0.13	0.50	0.79	0.55	0.91	0.23	0.37
	CRO	1.20	1.55	1.16	0.50	0.72	0.31	0.68	0.65	0.73	0.17
	GRA	0.66	1.11	1.62	0.29	0.48	0.45	0.61	1.08	0.56	0.42
Re	**ENF**	1.11	1.04	1.32	0.56	0.54	0.56	0.38	0.39	0.87	0.88
	DBC	0.95	1.29	1.40	0.16	0.66	0.39	0.84	0.66	0.32	0.38
	DBD	1.11	1.23	0.94	0.16	0.34	0.60	0.46	0.70	0.18	0.24
	CRO	0.95	1.29	1.06	0.36	0.53	0.31	0.61	0.59	0.60	0.09
	GRA	0.59	0.87	1.14	0.27	0.43	0.31	0.43	0.62	0.69	0.51
NEP	**ENF**	0.10	0.12	0.41	0.29	0.23	0.27	0.33	0.47	0.54	0.44
	DBC	0.14	0.33	0.52	0.17	0.25	0.31	0.42	0.58	0.27	0.34
	DBD	0.27	0.20	0.26	0.11	0.25	0.20	0.25	0.30	0.50	0.46
	CRO	0.26	0.26	0.11	0.20	0.37	0.15	0.43	0.34	0.42	0.26
	GRA	0.07	0.25	0.48	0.12	0.18	0.30	0.26	0.51	0.47	0.47
Rn	**ENF**	70.90	76.29	77.52	18.45	20.45	19.92	20.28	21.01	0.71	0.68
	DBC	61.00	56.64	59.01	9.04	10.41	11.00	11.63	11.99	0.60	0.56
	DBD	72.89	75.84	74.83	21.02	13.26	13.96	18.36	17.30	0.70	0.75
	CRO	82.78	75.88	78.00	7.12	11.97	13.65	19.07	20.52	0.24	0.09
	GRA	87.56	92.48	96.47	20.33	29.12	23.14	27.19	23.59	0.69	0.71
LE	**ENF**	32.53	30.12	35.32	21.96	16.66	15.83	16.19	17.35	0.81	0.77
	DBC	26.14	32.96	41.10	7.36	9.27	11.73	12.68	21.05	0.51	0.45
	DBD	33.49	43.99	37.77	10.13	19.86	27.20	17.83	21.71	0.69	0.65
	CRO	45.76	49.75	52.49	6.98	14.43	18.38	15.91	24.17	0.38	0.22
	GRA	26.24	50.96	56.92	8.71	22.59	13.30	32.81	33.62	0.49	0.42
H	**ENF**	33.91	46.17	42.21	13.37	18.13	17.33	26.32	23.93	0.33	0.32
	DBC	24.09	23.68	17.91	6.23	9.34	10.35	12.43	13.96	0.33	0.42
	DBD	28.57	31.85	37.07	8.28	10.75	16.95	17.05	24.66	0.11	0.02
	CRO	25.76	26.14	25.51	6.69	4.73	8.27	8.20	14.74	0.39	0.04
	GRA	47.33	41.52	39.56	24.44	13.81	19.34	18.81	22.26	0.74	0.71

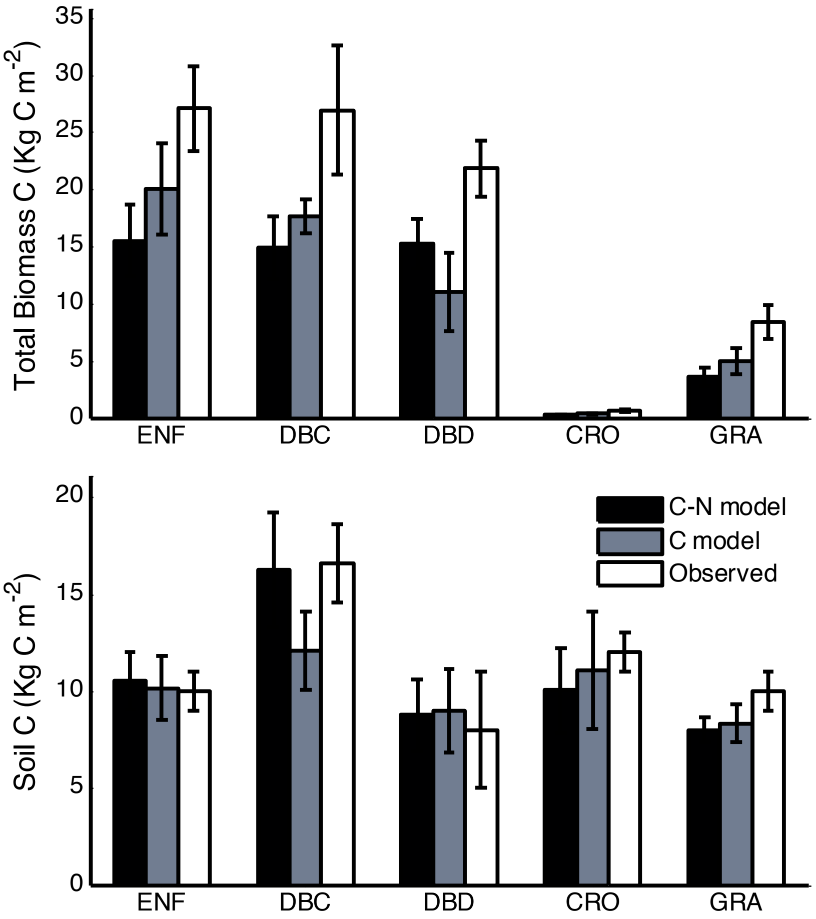

Figure 2.7 Mean biomass and soil C pools in kg C m^{-2} for C-N and C versions of the model for each PFT compared to observations. Whiskers represent 1 standard deviation. PFT abbreviations are: evergreen needleleaf forests (ENF), deciduous broadleaf-cold forests (DBC), deciduous broadleaf-dry forests (DBD), crops (CRO) and grasslands (GRA).

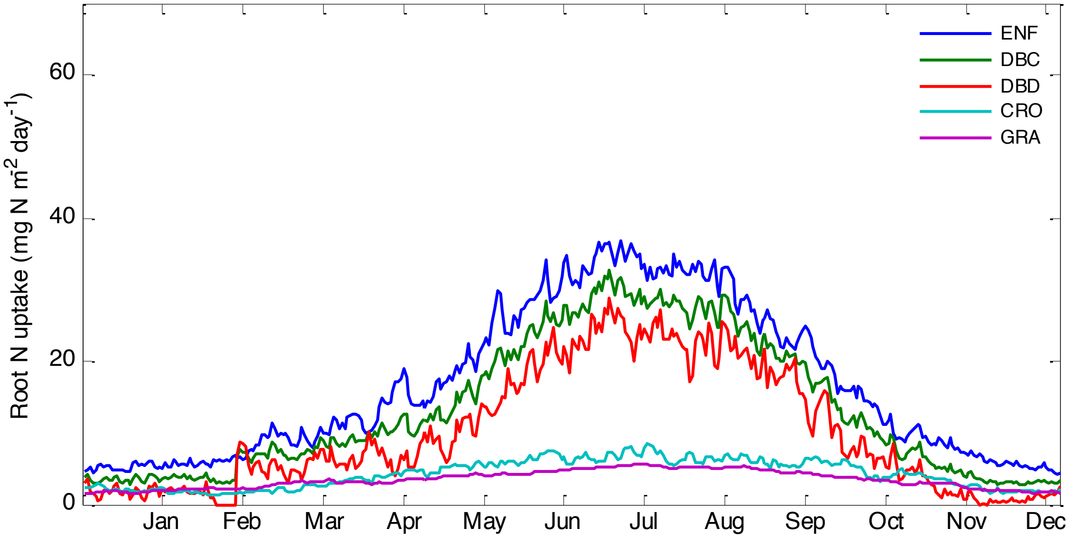

Figure 2.8 Simulated daily mean values of root N uptake (mg N m^{-2} day^{-1}) for each PFT.

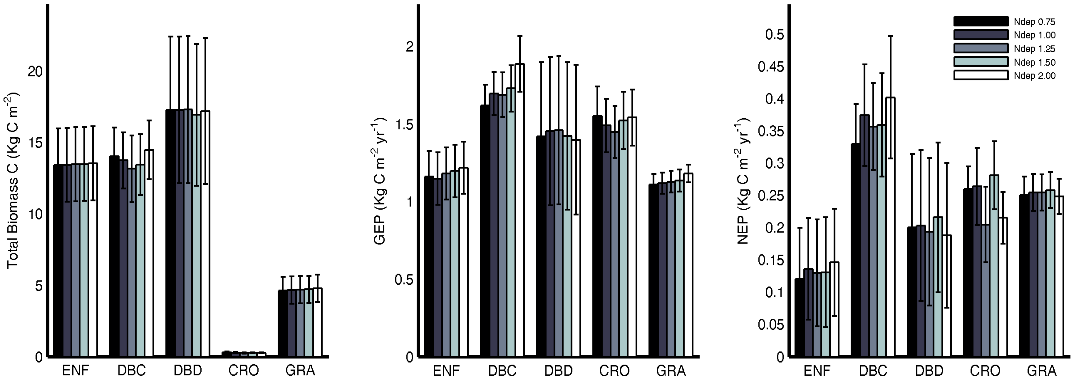

Figure 2.9 Sensitivity of N deposition contributions to simulated annual gross ecosystem productivity (GEP, Kg C m^{-2} yr^{-1}), net ecosystem productivity (NEP, Kg C m^{-2} yr^{-1}) and total vegetation biomass (Kg C m^{-2}). Legend represent imposed N deposition levels (increasing from 0.75 to 2.0 g N m^{-2} yr^{-1}); bars represent PFT classification.

2.5 Discussion

The inclusion of N cycle dynamics in CLASS-CTEM^{N+} has introduced key features of biogeochemical cycling in terrestrial ecosystems such as N limitation on photosynthesis and ecosystem respiration, realistic values of foliar N, and dynamic N/C ratios in plant tissues. N limitation in the model is represented as the difference between N uptake and N demand for plant productivity given other limiting conditions such as temperature and water availability, whereby N uptake is a function of N availability and plant uptake capacity (Huang et al., 2011). The version of CLASS-CTEM^{N+} (CLASS 2.7 and CTEM 1.2) used here (v1.2) differs from the previously published version (v1.0) for PFT parameterization (Table 2.1; Huang et al., 2011). Areas where improvements were made include (i) N/C ratios for leaves and roots for each PFT (Wania et al., 2012; White et al., 2000); (ii) photosynthesis parameters including the maximum photosynthetic rate, Vcmax, (Rogers, 2014); and (iii) leaf maintenance and respiration parameters (Melton and Arora, 2014).

Studies in the literature suggest that model parameters vary across different PFTs (Ruimy et al., 1994; Turner et al., 2003). In our study, some of the parameters used also slightly differ across the PFTs as shown in Table 2.1, however, our PFTs specific parameters for photosynthesis formulation had similar values among croplands and multiple forest types including evergreen broadleaf, evergreen needleleaf, deciduous broadleaf, and mixed; they only differ for savannas and grasslands. Our values are in agreement with those used in the literature (Groenendijk et al., 2011; Schwalm et al., 2006; Yuan et al., 2007). Kuppel et al. (2012) in their study suggest that multi-site parameterizations are able to reproduce site-level photosynthesis and respiration roughly as well as single-site parameterizations. Therefore, our investigation to ascertain whether these parameter differences in PFTs are significant in reproducing ecosystem C, water and energy fluxes and changes in C pools, as well as N dynamics was necessary and informative for the modeling community.

We evaluated the performance of our C-N and C versions of the models at different time scales (diurnal, daily, seasonal and annual) at 32 sites and across many of the major plant functional types. The statistics comparison of our model output at each time scale showed how well our model reproduced observed variability for each PFT. Boreal and temperate forests are large C sinks (Pan et al., 2011), therefore accurate model simulations for these ecosystem are very critical for determining the global C balance. Previous studies in the literature have shown improvements in model predictions, in particular for nitrogen limited ecosystems such as boreal evergreen needleleaf forests (ENF) when N cycling was included in the models (Fleischer et al., 2013; Jarvis and Linder, 2000; Zhu and Zhuang, 2013). Our model findings corroborate these results; inclusion of a nitrogen cycle improved the simulation of observed patterns of annual and seasonal GEP compared to the C-only counterpart. Nitrogen dynamics caused smaller changes in ecosystem productivity for other PFTs, such as the temperate forest ecosystems (DBD) for which the C-N version achieves marginal improvements in C, water and energy flux simulations compared to its C-only counterpart. These temperate PFTs have lesser degrees of nitrogen limitation for the C cycle than boreal PFTs (e.g., ENF), and ignoring nitrogen dynamics in the model had little impact on model performance. This indicates either N limitation of temperate forests is small or negligible, or that any existing N limitation is compensated by other processes or parameter settings in the model.

Inclusion of nitrogen dynamics in CLASS-CTEM^{N+} induced changes to simulated ecosystem respiration, as well as C pool sizes. Both of these are interlinked due to the dependence of Re on C respired in biomass (Ra) and soil (Rh), as well as their stoichiometric composition (Fleischer et al., 2013; Janssens et al., 2011). Overall a reduction in Re and in the size of C pools was noted in simulations by the C-N version of the model, improving their agreement with observations. These reductions are attributable to combined nitrogen controls on photosynthetic productivity and respiration, causing reductions in biomass and soil C pools. C pool reductions only partly explain reductions in Re. Dynamic N/C ratios of plant tissue for a given PFT in the C-N version of the model and dependence of Ra on them may be another reason to cause reduction in biomass C pools. In the C-N version of the model, nitrogen limitation causes lower N/C ratios and higher respiration rates. These ratios and leaf N content are fixed for each PFT in the C-only version of the model, and Ra is thus entirely based on the size of the biomass C pool and largely modified by temperature. The lower biomass pool sizes in the C-N version might thus be compensated by higher N/C ratios of the plant compartments deriving similar Ra rates and vice versa. A slightly small but persistent overestimation in Re remained however in both versions (C-N and C-only) of the model, especially for boreal and temperate deciduous forests (DBD and DBC), which calls for further investigation of Re related parameterizations (Janssens et al., 2011). Our C-N version showed only small improvements in the prediction accuracy of water and energy fluxes, as model errors are inferred to be due to misrepresentation of water-related mechanisms, as identified in earlier CLASS (Bartlett et al. 2000; Bartlett et al. 2003) and CLASS-CTEM^{N+} studies (Arora, 2001; Kothavala et al., 2005; F. Yuan et al., 2008).

Sensitivity analysis of CLASS-CTEM^{N+} simulated GEP, NEP and vegetation biomass responses to N deposition changes (imposed with Ndep values ranging from 0.75 to 2.0 g N m^{-2} yr^{-1}) indicated the efficiency of the model in converting deposited N into biomass, known as nitrogen use efficiency (NUE). Simulated NUE for different PFTs ranged from 0.37 to 24 ± 15 kg C kg N^{-1} (Fig. 2.9). Our results indicated a lower response of C sequestration to N addition compared to a previously reported mean value of 41 kg C kgN^{-1} based on various studies in temperate and boreal forests (Butterbach-Bahl et al., 2011; De Vries et al., 2009). Another meta-analysis of nitrogen addition experiments indicated a very comparable response of ~25 ± 9 kg C kgN^{-1}, however included soil C and was not exclusively applied to forests (Liu and Greaver, 2009). NUE differed among forest types, whereby coniferous forests exhibited higher efficiencies in total ecosystem C sequestration rates per unit nitrogen addition than deciduous broadleaf forests, potentially due to higher efficiency in utilizing it for growth (Liu and Greaver, 2009), based on starting from a stronger deficit. Thus our results suggest that nitrogen is the main limiting factor of growth for boreal conifer forests as argued by Jarvis and Linder (2000). However, due to a lack of field experiments or observational data for validation, we are not able to define a validated N deposition threshold for a model algorithm to induce negative effects on NUE. We cannot conclude whether any PFTs in our study are truly N saturated or show no positive effects on growth due to nitrogen addition. Past bottom-up studies suggest that a persistent C sink is expected for temperate or boreal forests (Pan et al., 2011). Meanwhile, NUE is also found to depend on forest age and historical N loads (Fleischer et al., 2013). Maximum NUE may decline with increasing current and historical nitrogen load and such saturation effects of NUE are more apparent for historical nitrogen loads than for current deposition rates (Fleischer et al., 2013). This highlights that NUE is site-specific and its response is non-linear. Moreover, relative contributions of nitrogen deposition to C sink strengths at local scales do not reflect the large variation over the global or regional averages, especially in temperate regions (Jain et al., 2009). As a result, NUE and the resulting C sink strengths can vary largely on different spatial scales. Inevitably, to simulate NUE in different forest ages and at different spatial scales is a challenge and is the logical next step for ecosystem modeling studies, including ours. Such assessments, on site, regional and global scales, need to focus on meaningful separation of ecosystems into PFTs or species-groups taking into account forest ages, in order to quantify accurately nitrogen deposition effects on C budgets. On the other hand, quantified uncertainty and bias of simulated fluxes and biomass are essential for ecosystem model evaluations. Because of lack of observed flux data in certain regions and the potential for introducing bias due to data gap filling (Schwalm et al., 2010), accurate estimation of long-term sources and sinks of C and its sensitivity of nitrogen deposition is challenging and calls for more efforts from both the modeling and field observation communities.

In summary, model outputs and parameters of our study serve as a strong foundation for future regional and global scale modeling studies using the C-N coupled version of the CLASS-CTEM^{N+} model. This study also identified some remaining challenges for the application of CLASS-CTEM^{N+} at a global scale such as C and nitrogen dynamics in tropical ecosystems which are not yet fully understood (Galbraith et al., 2013; Mercado et al., 2009; Restrepo-Coupe et al., 2013; van der Molen et al., 2011).

2.6 Conclusion

In this study, a C and nitrogen coupled dynamic vegetation model (CLASS-CTEM^{N+}) was parameterized over a range of North American vegetation ecosystems, representing five Plant Functional Types (PFTs). Eddy covariance flux measurements from 32 FLUXNET sites were used to evaluate and assess the simulation of carbon, water and energy exchanges and carbon pools and their sensitivity to nitrogen deposition. Two versions of the model (C-N and C-only) were compared at different temporal scales (diurnal cycles and daily, monthly, seasonal and annual mean values). A sensitivity analysis was also performed to determine the relative contribution of nitrogen deposition on the forest C exchanges in each PFT. The model successfully captured both the C and N dynamics for major biomes and a wide range of climate conditions. The C-N version of the model showed improvements in the prediction of C dynamics, in particular for boreal evergreen needleleaf forests (ENF), followed by deciduous broadleaf-cold (DBC) and temperate deciduous broadleaf – drought forests (DBD). Overall, the inclusion of the nitrogen cycle in the CLASS-CTEM^{N+} model improved its prediction accuracy, in particular for boreal forests. This multi-site parameterization and C-N analysis will serve as a strong foundation for future regional and global scale modeling studies using the C-N coupled version of our model.

Acknowledgement

Funding for this study was provided by the Natural Sciences and Engineering Research Council (NSERC) of Canada Discovery and Strategic grants and Ontario Ministry of Environment (MOE). Canadian Foundation of Innovation (CFI) and Ontario Innovation Trust (OIT) provided funds for computational facilities in our lab. We thank all the scientists involved in flux data collection under global FLUXNET and researcher involved in North American Carbon Program for providing model forcing and observed flux data. We acknowledge work of many scientists from Environment Canada, who have contributed to the development of CLASS and CTEM models over the past many years. We acknowledge SHARCNET for providing computational faculties to make these simulations. We are thankful to Sergey Mashchenko at SHARCNET for his generous help and support.

2.7 References

Aber, J., McDowell, W., Nadelhoffer, K., Alison, M., Berntson, G., Kamakea, M., McNulty, S., Currie, W., Rustad, L., Fernandez, I., 1998. Nitrogen Saturation in Temperate Forest Ecosystems. Bioscience 48, 921–934.

Alexander, L. V., Allen, S.K., Bindoff, N.L., Bréon, F.-M., Church, J.A., 2013. Working Group I Contribution to the IPCC Fifth Assessment Report Climate Change 2013: The Physical Science Basis Summary for Policymakers. URL http://www.climatechange2013.org/ (accessed 6.2.14).

Amthor, J., 2000. The McCree–de Wit–Penning de Vries–Thornley Respiration Paradigms: 30 Years Later. Ann. Bot. 86, 1–20. doi:10.1006/anbo.2000.1175

Amthor, J.S., 1984. The role of maintenance respiration in plant growth. Plant, Cell Environ. 7, 561–569. doi:10.1111/1365-3040.ep11591833

Arain, M.A., Black, T.A., Barr, A.G., Jarvis, P.G., Massheder, J.M., Verseghy, D.L., Nesic, Z., 2002. Effects of seasonal and interannual climate variability on net ecosystem productivity of boreal deciduous and conifer forests. Can. J. For. Res. Can. Rech. For. 32, 878–891.

Arain, M.A., Yuan, F.M., Black, T.A., 2006. Soil-plant nitrogen cycling modulated carbon exchanges in a western temperate conifer forest in Canada. Agric. For. Meteorol. 140, 171–192.

Arneth, A., Harrison, S.P., Zaehle, S., Tsigaridis, K., Menon, S., Bartlein, P.J., Feichter, J., Korhola, A., Kulmala, M., O'Donnell, D., Schurgers, G., Sorvari, S., Vesala, T., 2011. Terrestrial biogeochemical feedbacks in the climate system. Nat. Geosci 3, 525–532.

Arora, V., 2002. Modeling vegetation as a dynamic component in soil-vegetation-atmosphere transfer schemes and hydrological models. Rev. Geophys. 40, 1006. doi:10.1029/2001RG000103

Arora, V.K., 2001. Assessment of simulated water balance for continental-scale river basins in an AMIP 2 simulation. J. Geophys. Res. 106, 14827. doi:10.1029/2000JD900698

Arora, V.K., Boer, G.J., 2003. A representation of variable root distribution in dynamic vegetation models. Earth Interact. 7, 6–19.

Arora, V.K., Boer, G.J., 2005a. A parameterization of leaf phenology for the terrestrial ecosystem component of climate models. Glob. Chang. Biol. 11, 39–59.

Arora, V.K., Boer, G.J., 2005b. Fire as an interactive component of dynamic vegetation models. J. Geophys. Res. 110.

Arora, V.K., Boer, G.J., 2006. Simulating competition and coexistence between plant functional types in a dynamic vegetation model. Earth Interact. 10.

Arora, V.K., Boer, G.J., Christian, J.R., Curry, C.L., Denman, K.L., Zahariev, K., Flato, G.M., Scinocca, J.F., Merryfield, W.J., Lee, W.G., 2009. The Effect of Terrestrial Photosynthesis Down Regulation on the Twentieth-Century Carbon Budget Simulated with the CCCma Earth System Model. J. Clim. 22, 6066–6088. doi:doi:10.1175/2009JCLI3037.1

Baldocchi, D., 2008. "Breathing" of the terrestrial biosphere: lessons learned from a global network of carbon dioxide flux measurement systems. Aust. J. Bot. 56, 1. doi:10.1071/BT07151

Baldocchi, D., Falge, E., Gu, L., Olson, R., Hollinger, D., Running, S., Anthoni, P., Bernhofer, C., Davis, K., Evans, R., Fuentes, J., Goldstein, A., Katul, G., Law, B., Lee, X., Malhi, Y., Meyers, T., Munger, W., Oechel, W., Paw, K.T., Pilegaard, K., Schmid, H.P., Valentini, R., Verma, S., Vesala, T., Wilson, K., Wofsy, S., 2001. FLUXNET: A New Tool to Study the Temporal and Spatial Variability of Ecosystem–Scale Carbon Dioxide, Water Vapor, and Energy Flux Densities. Bull. Am. Meteorol. Soc. 82, 2415–2434. doi:10.1175/1520-0477(2001)082<2415:FANTTS>2.3.CO;2

Bartlett, P.A., MacKay, M.D., Verseghy, D.L. 2006. Modified snow algorithms in the Canadian Land Surface Scheme: Model runs and sensitivity analysis at three boreal forest stands. Atmosphere-Ocean 44, 207-222.

Bartlett, P.A., Harry McCaughey, J., Lafleur, P.M., Verseghy, D.L., 2003. Modelling evapotranspiration at three boreal forest stands using the CLASS: tests of parameterizations for canopy conductance and soil evaporation. Int. J. Climatol. 23, 427–451. doi:10.1002/joc.884

Bartlett, P.A., McCaughey, J.H., Lafleur, P.M., Verseghy, D.L., 2000. Performance of the Canadian land surface scheme at temperate aspen‑birch and mixed forests, and a boreal young jack pine forest: Tests involving canopy conductance parameterizations. Atmosphere-Ocean 38, 113–140. doi:10.1080/07055900.2000.9649642

Bonan, G.B., 2008. Forests and Climate Change: Forcings, Feedbacks, and the Climate Benefits of Forests. Science (80-.). 320, 1444–1449. doi:10.1126/science.1155121

Bonan, G.B., Levis, S., 2010. Quantifying carbon-nitrogen feedbacks in the Community Land Model (CLM4). Geophys. Res. Lett. 37, 1–6. doi:10.1029/2010GL042430

Butterbach-Bahl, K., Gundersen, P., Ambus, P., Augustin, J., Beier, C., Boeckx, P., Dannenmann, M., Gimeno, B.S., Ibrom, A., Kiese, R., Kitzler, B., Rees, R.M., Smith, K.A., Stevens, C., Vesala, T., Zechmeister-Boltenstern, S., 2011. Nitrogen processes in terrestrial ecosystems, in The European Nitrogen Assessment. Cambridge University Press, Cambridge. doi:10.1017/CBO9780511976988

Churkina, G., Zaehle, S., Hughes, J., Viovy, N., Chen, Y., Jung, M., Heumann, B.W., Ramankutty, N., Heimann, M., Jones, C., 2010. Interactions between nitrogen deposition, land cover conversion, and climate change determine the contemporary carbon balance of Europe. Biogeosciences 7, 2749–2764. doi:10.5194/bg-7-2749-2010

Ciais, P., Schelhaas, M.J., Zaehle, S., Piao, S.L., Cescatti, A., Liski, J., Luyssaert, S., Le-Maire, G., Schulze, E.D., Bouriaud, O., Freibauer, A., Valentini, R., Nabuurs, G.J., 2008. Carbon accumulation in European forests. Nat. Geosci 1, 425–429.

Collatz, G., Ribas-Carbo, M., Berry, J., 1992. Coupled Photosynthesis-Stomatal Conductance Model for Leaves of C 4 Plants. Aust. J. Plant Physiol. 19, 519. doi:10.1071/PP9920519

Collatz, G.J., Ball, J.T., Grivet, C., Berry, J.A., 1991. Physiological and environmental regulation of stomatal conductance, photosynthesis and transpiration: a model that includes a laminar boundary layer. Agric. For. Meteorol. 54, 107–136. doi:10.1016/0168-1923(91)90002-8

De Vries, W., Solberg, S., Dobbertin, M.D., Sterba, H., Laubhann, D., van Oijen, M., Evans, C., Gundersen, P., Kros, J., Wamelink, G.W.W., Reinds, G.J., Sutton, M.A., 2009. The impact of nitrogen deposition on carbon sequestration by European forests and heathlands. For. Ecol. Manage. 258, 1814-1823. doi:10.1016/j.foreco.2009.02.034.

Dezi, S., MEDLYN, B.E., TONON, G., MAGNANI, F., 2010. The effect of nitrogen deposition on forest carbon sequestration: a model-based analysis. Glob. Chang. Biol. 16, 1470–1486. doi:10.1111/j.1365-2486.2009.02102.x

Dickinson, R.E., Berry, J.A., Bonan, G.B., Collatz, G.J., Field, C.B., Fung, I.Y., Goulden, M., Hoffmann, W.A., Jackson, R.B., Myneni, R., Sellers, P.J., Shaikh, M., 2002. Nitrogen Controls on Climate Model Evapotranspiration. J. Clim. 15, 278–295.

Dickinson, R.E., Shaikh, M., Bryant, R., Graumlich, L., 1998. Interactive Canopies for a Climate Model. J. Clim. 11, 2823–2836. doi:10.1175/1520-0442(1998)011<2823:ICFACM>2.0.CO;2

Dolman, A.J., van der Werf, G.R., van der Molen, M.K., Ganssen, G., Erisman, J.-W., Strengers, B., 2010. A carbon cycle science update since IPCC AR-4. Ambio 39, 402–12.

Environment Canada, 2005. 2004 Canadian acid deposition science assessment: summary of key results.

Erisman, J.W., Galloway, J., Seitzinger, S., Bleeker, A., Butterbach-Bahl, K., 2011. Reactive nitrogen in the environment and its effect on climate change. Curr. Opin. Environ. Sustain. 3, 281–290. doi:10.1016/j.cosust.2011.08.012

Esser, G., KATTGE, J., SAKALLI, A., 2011. Feedback of carbon and nitrogen cycles enhances carbon sequestration in the terrestrial biosphere. Glob. Chang. Biol. 17, 819–842. doi:10.1111/j.1365-2486.2010.02261.x

Farquhar, G.D., von Caemmerer, S., Berry, J.A., 1980. A biochemical model of photosynthetic CO2 assimilation in leaves of C 3 species. Planta 149, 78–90. doi:10.1007/BF00386231

Fleischer, K., Rebel, K.T., van der Molen, M.K., Erisman, J.W., Wassen, M.J., van Loon, E.E., Montagnani, L., Gough, C.M., Herbst, M., Janssens, I.A., Gianelle, D., Dolman, A.J., 2013. The contribution of nitrogen deposition to the photosynthetic capacity of forests. Global Biogeochem. Cycles 27, 187–199. doi:10.1002/gbc.20026

Foken, T., 2008. The energy balance closure problem. Ecological Applications 18, 1351-1367.

Galbraith, D., Malhi, Y., Affum-Baffoe, K., Castanho, A.D.A., Doughty, C.E., Fisher, R.A., Lewis, S.L., Peh, K.S.-H., Phillips, O.L., Quesada, C.A., Sonké, B., Lloyd, J., 2013. Residence times of woody biomass in tropical forests. Plant Ecol. Divers. 6, 139–157. doi:10.1080/17550874.2013.770578

Galloway, J.N., Dentener, F.J., Capone, D.G., Boyer, E.W., Howarth, R.W., Seitzinger, S.P., Asner, G.P., Cleveland, C.C., Green, P.A., Holland, E.A., Karl, D.M., Michaels, A.F., Porter, J.H., Townsend, A.R., Vöosmarty, C.J., 2004. Nitrogen Cycles: Past, Present, and Future. Biogeochemistry 70, 153–226.

Galloway, J.N., Townsend, A.R., Erisman, J.W., Bekunda, M., Cai, Z., Freney, J.R., Martinelli, L.A., Seitzinger, S.P., Sutton, M.A., 2008. Transformation of the Nitrogen Cycle: Recent Trends, Questions, and Potential Solutions. Science (80-.). 320, 889–892. doi:10.1126/science.1136674

Groenendijk, M., Dolman, A.J., van der Molen, M.K., Leuning, R., Arneth, A., Delpierre, N., Gash, J.H.C., Lindroth, A., Richardson, A.D., Verbeeck, H., Wohlfahrt, G., 2011. Assessing parameter variability in a photosynthesis model within and between plant functional types using global Fluxnet eddy covariance data. Agric. For. Meteorol. 151, 22–38. doi:10.1016/j.agrformet.2010.08.013

Gruber, N., Galloway, J.N., 2008. An Earth-system perspective of the global nitrogen cycle. Nature 451, 293–296.

Haxeltine, A., Prentice, I.C., 1996. A general model for the light-use efficiency of primary production. Funct. Ecol. 10, 551–561.

Heimann, M., Reichstein, M., 2008. Terrestrial ecosystem carbon dynamics and climate feedbacks. Nature 451, 289–292.

Huang, S., Arain, M.A., Arora, V.K., Yuan, F., Brodeur, J., Peichl, M., 2011. Analysis of nitrogen controls on carbon and water exchanges in a conifer forest using the CLASS-CTEMN+ model. Ecol. Modell. 222, 3743–3760. doi:10.1016/j.ecolmodel.2011.09.008

Huang, S., Arain, M.A., Bartlett, P., Verseghy, D., Arora, V., 2014. Modelling Carbon, Water and Energy Exchanges Over Amazonian Tropical Forests Using the Carbon-Nitrogen Coupled CLASS-CTEM^{N+} Model, in submitting to Agricultural and Forest Meteorology.

Hungate, B.A., Dukes, J.S., Shaw, M.R., Luo, Y., Field, C.B., 2003. ATMOSPHERIC SCIENCE: Nitrogen and Climate Change. Science (80-.). 302, 1512–1513. doi:10.1126/science.1091390

IPCC, 2007. Climate Change 2007: The Physical Science Basis, Contribution of Working Group I to the Fourth Assessment Report of the Intergovernmental Panel on Climate Change. Cambridge University Press, Cambridge.

Jain, A., Yang, X., Kheshgi, H., McGuire, A.D., Post, W., Kicklighter, D., 2009. Nitrogen attenuation of terrestrial carbon cycle response to global environmental factors. Global Biogeochem. Cycles 23, n/a–n/a. doi:10.1029/2009GB003519

Janssens, I.A., Dieleman, W., Luyssaert, S., Subke, J.A., Reichstein, M., Ceulemans, R., Ciais, P., Dolman, A.J., Grace, J., Matteucci, G., Papale, D., Piao, S.L., Schulze, E.D., Tang, J., Law, B.E., 2011. Reduction of forest soil respiration in response to nitrogen deposition. Nat. Geosci 3, 315–322.

Jarvis, P., Linder, S., 2000. Constraints to growth of boreal forests. Nature 405, 904–5. doi:10.1038/35016154

Jarvis, P.G., 1976. The Interpretation of the Variations in Leaf Water Potential and Stomatal Conductance Found in Canopies in the Field. Philos. Trans. R. Soc. B Biol. Sci. 273, 593–610. doi:10.1098/rstb.1976.0035

Jung, M., Le Maire, G., Zaehle, S., Luyssaert, S., Vetter, M., Churkina, G., Ciais, P., Viovy, N., Reichstein, M., 2007. Assessing the ability of three land ecosystem models to simulate gross carbon uptake of forests from boreal to Mediterranean climate in Europe. Biogeosciences 4, 647–656. doi:10.5194/bg-4-647-2007

Kothavala, Z., Arain, M.A., Black, T.A., Verseghy, D., 2005. The simulation of energy, water vapor and carbon dioxide fluxes over common crops by the Canadian Land Surface Scheme (CLASS). Agric. For. Meteorol. 133, 89–108. doi:10.1016/j.agrformet.2005.08.007

Kottek, M., Grieser, J., Beck, C., Rudolf, B., Rubel, F., 2006. World Map of the Köppen-Geiger climate classification updated. Meteorol. Zeitschrift 15, 259–263. doi:10.1127/0941-2948/2006/0130

Kuppel, S., Peylin, P., Chevallier, F., Bacour, C., Maignan, F., Richardson, A.D., 2012. Constraining a global ecosystem model with multi-site eddy-covariance data. Biogeosciences 9, 3757–3776. doi:10.5194/bg-9-3757-2012

Lamarque, J.-F., Bond, T.C., Eyring, V., Granier, C., Heil, A., Klimont, Z., Lee, D., Liousse, C., Mieville, A., Owen, B., Schultz, M.G., Shindell, D., Smith, S.J., Stehfest, E., Van Aardenne, J., Cooper, O.R., Kainuma, M., Mahowald, N., McConnell, J.R., Naik, V., Riahi, K., van Vuuren, D.P., 2010. Historical (1850–2000) gridded anthropogenic and biomass burning emissions of reactive gases and aerosols: methodology and application. Atmos. Chem. Phys. 10, 7017–7039. doi:10.5194/acp-10-7017-2010

Le Quere, C., Raupach, M.R., Canadell, J.G., Marland, G., et al., 2009. Trends in the sources and sinks of carbon dioxide. Nat. Geosci 2, 831–836.

Leuning, R., van Gorsel, E., Massman, W.J., Isaac, P.R., 2012. Reflections on the surface energy imbalance problem. Agric. For. Meteorol. 156, 65–74. doi:10.1016/j.agrformet.2011.12.002

Leuning, R., Kelliher, F.M., Pury, D.G.G., Schulze, E.-D., 1995. Leaf nitrogen, photosynthesis, conductance and transpiration: scaling from leaves to canopies. Plant, Cell Environ. 18, 1183–1200.

Liu, L., Greaver, T.L., 2009. A review of nitrogen enrichment effects on three biogenic GHGs: the CO2 sink may be largely offset by stimulated N2O and CH4 emission. Ecol. Lett. 12, 1103–17. doi:10.1111/j.1461-0248.2009.01351.x

Loveland, T.R., Belward, A.S., 1997. The international geosphere biosphere programme data and information system global land cover data set (DIScover). Acta Astronaut. 41, 681–689.

Luyssaert, S., Inglima, I., Jung, M., Richardson, A.D., Reichstein, M., Papale, D., Piao, S.L., Schulze, E.-D., Wingate, L., Matteucci, G., Aragao, L., Aubinet, M., Beer, C., Bernhofer, C., Black, K.G., Bonal, D., Bonnefond, J.M., Chambers, J., Ciais, P., Cook, B., Davis, K.J., Dolman, A.J., Gielen, B., Goulden, M., Grace, J., Grrnier, A., Gelle, A., Griffis, T., Grunwald, T., Guidolotti, G., Hanson, P.J., Harding, R., Hollinger, D.Y., Hutyra, L.R., Kolari, P., Kruijt, B., Kutsch, W., Lagergren, F., Laurila, T., Law, B.E., Le Maire, G., Lindroth, A., Loustau, D., Malhi, Y., Mateus, J., Migliavacca, M., Misson, L., Montagnani, L., Moncrieff, J., Moors, E., Munger, J.W., Nikinmaa, E., Ollinger, S. V., Pita, G., Rebmann, C., Roupsard, O., Saigusa, N., Sanz, M.J., Seufert, G., Sierra, C., Smith, M.-L., Tang, J., Valentini, R., Vesala, T., Janssens, I.A., 2007. CO2 balance of boreal, temperate, and tropical forests derived from a global database. Glob. Chang. Biol. 13, 2509–2537. doi:10.1111/j.1365-2486.2007.01439.x

Makipaa, R., Karjalainen, T., Pussinen, A., Kellomaki, S., 1999. Effects of climate change and nitrogen deposition on the carbon sequestration of a forest ecosystem in the boreal zone. Can. J. For. Res. 29, 1490–1501.

Meissner, K.J., Weaver, A.J., Matthews, H.D., Cox, P.M., 2003. The role of land surface dynamics in glacial inception: a study with the UVic Earth System Model. Clim. Dyn. 21, 515–537. doi:10.1007/s00382-003-0352-2

Melillo, J.M., Steudler, P.A., Aber, J.D., Newkirk, K., Lux, H., Bowles, F.P., Catricala, C., Magill, A., Ahrens, T., Morrisseau, S., 2002. Soil warming and carbon-cycle feedbacks to the climate system. Science 298, 2173–6. doi:10.1126/science.1074153

Melton, J.R., Arora, V.K., 2013. Sub-grid scale representation of vegetation in global land surface schemes: implications for estimation of the terrestrial carbon sink. Biogeosciences Discuss. 10, 16003–16041. doi:10.5194/bgd-10-16003-2013

Melton, J.R., Arora, V.K., 2014. Sub-grid scale representation of vegetation in global land surface schemes: implications for estimation of the terrestrial carbon sink. Biogeosciences 11, 1021–1036. doi:10.5194/bg-11-1021-2014

Mercado, L.M., Lloyd, J., Dolman, A.J., Sitch, S., Patiño, S., 2009. Modelling basin-wide variations in Amazon forest productivity – Part 1: Model calibration, evaluation and upscaling functions for canopy photosynthesis. Biogeosciences 6, 1247–1272. doi:10.5194/bg-6-1247-2009

Morales, P., Sykes, M.T., Prentice, I.C., Smith, P., Smith, B., Bugmann, H., Zierl, B., Friedlingstein, P., Viovy, N., Sabate, S., Sanchez, A., Pla, E., Gracia, C.A., Sitch, S., Arneth, A., Ogee, J., 2005. Comparing and evaluating process-based ecosystem model predictions of carbon and water fluxes in major European forest biomes. Glob. Chang. Biol. 11, 2211–2233. doi:10.1111/j.1365-2486.2005.01036.x

Nadelhoffer, K.J., Emmett, B.A., Gundersen, P., Kjonaas, O.J., Koopmans, C.J., Schleppi, P., Tietema, A., Wright, R.F., 1999. Nitrogen deposition makes a minor contribution to carbon sequestration in temperate forests. Nature 398, 145–148.

Nissinen, A., Hari, P., 1998. Effects of nitrogen deposition on tree growth and soil nutrients in boreal Scots pine stands. Environ. Pollut. 102, 61–68.

Pan, Y., Birdsey, R.A., Fang, J., Houghton, R., Kauppi, P.E., Kurz, W.A., Phillips, O.L., Shvidenko, A., Lewis, S.L., Canadell, J.G., Ciais, P., Jackson, R.B., Pacala, S.W., McGuire, A.D., Piao, S., Rautiainen, A., Sitch, S., Hayes, D., 2011. A large and persistent carbon sink in the world's forests. Science 333, 988–93. doi:10.1126/science.1201609

Philip, J.R. 1957. Evaporation and moisture and heat fields in the soil. Journal of Meteorology 14, 354–366.

Quinn Thomas, R., Canham, C.D., Weathers, K.C., Goodale, C.L., 2011. Increased tree carbon storage in response to nitrogen deposition in the US. Nat. Geosci 3, 13–17.

Reay, D.S., Dentener, F., Smith, P., Grace, J., Feely, R.A., 2008. Global nitrogen deposition and carbon sinks. Nat. Geosci 1, 430–437.

Reich, P.B., Tjoelker, M.G., Pregitzer, K.S., Wright, I.J., Oleksyn, J., Machado, J.-L., 2008. Scaling of respiration to nitrogen in leaves, stems and roots of higher land plants. Ecol. Lett. 11, 793–801. doi:10.1111/j.1461-0248.2008.01185.x

Restrepo-Coupe, N., Arain, M.A., 2005. Energy and water exchanges from a temperate pine plantation forest. Hydrological Processes 19, 27–49.

Restrepo-Coupe, N., da Rocha, H.R., Hutyra, L.R., da Araujo, A.C., Borma, L.S., Christoffersen, B., Cabral, O.M.R., de Camargo, P.B., Cardoso, F.L., da Costa, A.C.L., Fitzjarrald, D.R., Goulden, M.L., Kruijt, B., Maia, J.M.F., Malhi, Y.S., Manzi, A.O., Miller, S.D., Nobre, A.D., von Randow, C., Sá, L.D.A., Sakai, R.K., Tota, J., Wofsy, S.C., Zanchi, F.B., Saleska, S.R., 2013. What drives the seasonality of photosynthesis across the Amazon basin? A cross-site analysis of eddy flux tower measurements from the Brasil flux network. Agric. For. Meteorol. 182-183, 128–144. doi:10.1016/j.agrformet.2013.04.031

Rogers, A., 2014. The use and misuse of V(c,max) in Earth System Models. Photosynth. Res. 119, 15–29. doi:10.1007/s11120-013-9818-1

Ruimy, A., Saugier, B., Dedieu, G., 1994. Methodology for the estimation of terrestrial net primary production from remotely sensed data. J. Geophys. Res. 99, 5263. doi:10.1029/93JD03221

Ryan, M.G., Gower, S.T., Hubbard, R.M., Waring, R.H., Gholz, H.L., Cropper, W.P., Running, S.W., 1995. Woody tissue maintenance respiration of four conifers in contrasting climates. Oecologia 101, 133–140. doi:10.1007/BF00317276

Scheffer, M., Bascompte, J., Brock, W.A., Brovkin, V., Carpenter, S.R., Dakos, V., Held, H., van Nes, E.H., Rietkerk, M., Sugihara, G., 2009. Early-warning signals for critical transitions. Nature 461, 53–59.

Schulze, E.-D., 2000. Carbon and nitrogen cycling in European forest ecosystems , Ecological studies. Springer, Berlin New York .

Schwalm, C.R., Black, T.A., Arniro, B.D., Arain, M.A., Barr, A.G., Bourque, C.P.A., Dunn, A.L., Flanagan, L.B., Giasson, M.A., Lafleur, P.M., Margolis, H.A., McCaughey, J.H., Orchansky, A.L., Wofsy, S.C., 2006. Photosynthetic light use efficiency of three biomes across an east-west continental-scale transect in Canada. Agric. For. Meteorol. 140, 269–286.

Schwalm, C.R., Williams, C.A., Schaefer, K., Anderson, R., Arain, M.A., Baker, I., Barr, A., Black, T.A., Chen, G., Chen, J.M., Ciais, P., Davis, K.J., Desai, A., Dietze, M., Dragoni, D., Fischer, M.L., Flanagan, L.B., Grant, R., Gu, L., Hollinger, D., Izaurralde, R.C., Kucharik, C., Lafleur, P., Law, B.E., Li, L., Li, Z., Liu, S., Lokupitiya, E., Luo, Y., Ma, S., Margolis, H., Matamala, R., McCaughey, H., Monson, R.K., Oechel, W.C., Peng, C., Poulter, B., Price, D.T., Riciutto, D.M., Riley, W., Sahoo, A.K., Sprintsin, M., Sun, J., Tian, H., Tonitto, C., Verbeeck, H., Verma, S.B., 2010. A model-data intercomparison of CO2 exchange across North America: Results from the North American Carbon Program site synthesis. J. Geophys. Res. 115, G00H05. doi:10.1029/2009JG001229

Sokolov, A.P., Kicklighter, D.W., Melillo, J.M., Felzer, B.S., Schlosser, C.A., Cronin, T.W., 2008. Consequences of Considering Carbon-Nitrogen Interactions on the Feedbacks between Climate and the Terrestrial Carbon Cycle. J. Clim. 21, 3776–3796.

Sutton, M.A., Vries, R.I.S.S.R.M. van O.W.I.M. de, 2008. Uncertainties in the relationship between atmospheric nitrogen deposition and forest carbon sequestration. Glob. Chang. Biol. 14, 2057–2063.

Thornton, P.E., Doney, S.C., Lindsay, K., Moore, J.K., Mahowald, N., Randerson, J.T., Fung, I., Lamarque, J.F., Feddema, J.J., Lee, Y.H., 2009. Carbon-nitrogen interactions regulate climate-carbon cycle feedbacks: results from an atmosphere-ocean general circulation model. Biogeosciences Discuss. 6, 3303–3354.

Thornton, P.E., Lamarque, J.-F., Rosenbloom, N.A., Mahowald, N.M., 2007. Influence of carbon-nitrogen cycle coupling on land model response to CO 2 fertilization and climate variability. Global Biogeochem. Cycles 21, n/a–n/a. doi:10.1029/2006GB002868

Turner, D.P., Urbanski, S., Bremer, D., Wofsy, S.C., MEYERS, T., GOWER, S.T., GREGORY, M., 2003. A cross-biome comparison of daily light use efficiency for gross primary production. Glob. Chang. Biol. 9, 383–395. doi:10.1046/j.1365-2486.2003.00573.x

Van der Molen, M.K., van den Hurk, B.J.J.M., Hazeleger, W., 2011. A dampened land use change climate response towards the tropics. Clim. Dyn. 37, 2035–2043. doi:10.1007/s00382-011-1018-0

Verseghy, D.L., 1991. CLASS--A Canadian Land Surface Scheme for GCMS: I. Soil Model Int. J. Climatol. 11, 111–133.

Verseghy, D.L., 2000. The Canadian land surface scheme (CLASS): Its history and future. Atmosphere-Ocean 38, 1–13. doi:10.1080/07055900.2000.9649637

Verseghy, D.L., Lazare, M., 1993. CLASS-Canadian land surface scheme for GCMS, II. Vegetation model and coupled runs. Int. J. Climatol. 13, 347–370.

Vitousek, P.M., Howarth, R.W., 1991. Nitrogen limitation on land and in the sea: How can it occur? Biogeochemistry 13, 87–115.

Wania, R., Meissner, K.J., Eby, M., Arora, V.K., Ross, I., Weaver, A.J., 2012. Carbon-nitrogen feedbacks in the UVic ESCM. Geosci. Model Dev. 5, 1137–1160. doi:10.5194/gmd-5-1137-2012

White, M.A., Thornton, P.E., Running, S.W., Nemani, R.R., 2000. Parameterization and Sensitivity Analysis of the BIOME–BGC Terrestrial Ecosystem Model: Net Primary Production Controls. Earth Interact. 4, 1–85. doi:10.1175/1087-3562(2000)004<0003:PASAOT>2.0.CO;2

Willmott, C.J., 1981. On the validation of models. Phys. Geogr. 2, 184–194. doi:10.1080/02723646.1981.10642213

Wilson, K., Goldstein, A., Falge, E., Aubinet, M., Baldocchi, D., Berbigier, P., Bernhofer, C., Ceulemans, R., Dolman, H., Field, C., Grelle, A., Ibrom, A., Law, B.E., Kowalski, A., Meyers, T., Moncrieff, J., Monson, R., Oechel, W., Tenhunen, J., Valentini, R., Verma, S. 2002. Energy balance closure at Fluxnet sites. Agric. For. Meteorol. 113, 223-243.

Xu, R., Prentice, I.C., 2008. Terrestrial nitrogen cycle simulation with a dynamic global vegetation model. Glob. Chang. Biol. 14, 1745–1764.

Yuan, F., McCaughey, H., Wofsy, S.C., 2008. Modeling analysis of primary controls on net ecosystem productivity of seven boreal and temperate coniferous forests across a continental transect. Glob. Chang. Biol. 14, 1765–1784.

Yuan, W., Liu, S., Zhou, G., Zhou, G., Tieszen, L.L., Baldocchi, D., Bernhofer, C., Gholz, H., Goldstein, A.H., Goulden, M.L., Hollinger, D.Y., Hu, Y., Law, B.E., Stoy, P.C., Vesala, T., Wofsy, S.C., 2007. Deriving a light use efficiency model from eddy covariance flux data for predicting daily gross primary production across biomes. Agric. For. Meteorol. 143, 189–207. doi:10.1016/j.agrformet.2006.12.001

Zaehle, S., Ciais, P., Friend, A.D., Prieur, V., 2011. Carbon benefits of anthropogenic reactive nitrogen offset by nitrous oxide emissions. Nat. Geosci 4, 601–605.

Zaehle, S., Friend, A.D., Friedlingstein, P., Dentener, F., Peylin, P., Schulz, M., 2010. Carbon and nitrogen cycle dynamics in the O-CN land surface model: 2. Role of the nitrogen cycle in the historical terrestrial carbon balance. Global Biogeochem. Cycles 24, n/a–n/a. doi:10.1029/2009GB003522

Zhu, Q., Zhuang, Q., 2013. Modeling the effects of organic nitrogen uptake by plants on the carbon cycling of boreal forest and tundra ecosystems. Biogeosciences 10, 7943–7955. doi:10.5194/bg-10-7943-2013

3. CHAPTER 3: Modelling Carbon, Water and Energy Exchanges Over Amazonian Tropical Forests Using the Carbon-Nitrogen Coupled CLASS-CTEM^{N+} Model

Suo Huang[1], M. Altaf Arain[1, *], Paul Bartlett[2]

[1]School of Geography and Earth Sciences and McMaster Centre for Climate Change,
McMaster University, Hamilton, Ontario, Canada

[2]Climate Processes Section, Environment Canada, Toronto, ON, M3H 5T4 Canada

* **Corresponding Author:** M. Altaf Arain, School of Geography and Earth Sciences, McMaster University, 1280 Main Street West, Hamilton, Ontario, L8S 4K1, Canada, Phone: 1-905-525-9140 Ext. 27941, Fax: 905-546-0463; Email: arainm@mcmaster.ca

Keywords: Canadian Land Surface Scheme; Canadian Terrestrial Ecosystem Model; Carbon; Nitrogen; Net ecosystem productivity; Plant Functional Types; Amazon; Large Scale Biosphere-Atmosphere Experiment in Amazonia; Canadian Lands Surface Scheme; Canadian Terrestrial Ecosystem Model

3.0 Abstract

In this study, nitrogen (N) coupled dynamic ecosystem model, CLASS-CTEM^{N+} (C-N version) was used to simulate carbon (C), water and energy fluxes and carbon pools at 7 flux tower sites across the Amazonian basin. Standardized meteorological forcing data, eddy covariance fluxes, and site characteristics from the Large Scale Biosphere-Atmosphere Experiment in Amazonia (LBA) project, spanning 26 site-years over 3 major tropical plant functional types (PFTs), were used. Simulated values of gross ecosystem productivity (GEP), ecosystem respiration (Re), net ecosystem productivity (NEP), sensible heat flux (H) and latent heat flux (LE) were also compared with simulations made by the carbon-only version (C version) of the model.

The parameterization with tropical PFTs in the model showed improvement in model's capabilities to simulate carbon, water and energy fluxes and C stocks in Amazonia ecosystems from daily, monthly to annual scales when compared with observations, in particular for tropical evergreen broadleaf forest sites. The inclusion of the N cycle in the model caused observed annual and seasonal GEP to be successfully reproduced and slightly improved by the C-N coupled model when compared to C-only version of the model. Simulated daily mean NEP values showed that all forest sites were net sink of carbon, while pasture and agriculture sites were either neutral or net source of carbon. The C-N coupled model simulated annual NEP for all 5 tropical forest sites was 0.210 Kg C m^{-2} yr^{-1} compared to 0.126 Kg C m^{-2} yr^{-1} from observation and 0.188 Kg C m^{-2} yr^{-1} by C-only version of the model. Annual NEP for the agricultural site was 0.0 Kg C m^{-2} yr^{-1} by C-N coupled model, compared to 0.170 Kg C m^{-2} yr^{-1} from observation and -0.01 Kg C m^{-2} yr^{-1} of C-only version of the model. At the pasture site, annual NEP simulated by C-N coupled model was -0.04 Kg C m^{-2} yr^{-1} compared to 0.28 Kg C m^{-2} yr^{-1} from observation and -0.02 Kg C m^{-2} yr^{-1}from C-only model. Our model indicated a small nitrogen availability deficit for C uptake in tropical forests.

This study gives us confidence that CLASS-CTEM^{N+} can predict carbon, water and energy fluxes and carbon stocks quite well at typical Amazonia ecosystems. The consideration of C-N interactions with tropical PFTs is necessary for CLASS-CTEM^{N+}'s further application at regional and global scales for long-term evaluating of the responses and feedbacks between future climate change and terrestrial ecosystems. Our results also highlighted the importance of long-term observed data sets to study the impact of nitrogen cycling on changes in the vegetation and soil carbon biomass in tropical ecosystems.

3.1 Introduction

The Amazonian forests cover an area of over 4 million km^2 and comprise half of the earth's undisturbed tropical evergreen forests. They play a key role in the global carbon cycle, contributing about 10%-30% of the global biomass and terrestrial ecosystem productivity (Andreae, 2002; Beer et al., 2011; Costa and Foley, 2000; de Gonçalves et al., 2013; Foley et al., 2007; Houghton et al., 2001; Malhi and Grace, 2000).

Amazonian tropical forests are undergoing drastic alterations due to recent changes in climate such as increased air temperature and atmospheric CO_2, shift in precipitation intensity and duration and human activities, such as deforestation (Asner et al., 2005; Foley et al., 2007; Morton et al., 2005) and increased nitrogen (N) deposition rates (Holland et al. 1997; Nadelhoffer et al. 1999; Davidson et al. 2004; Churkina et al. 2007; Thornton et al. 2007). These impacts will lead to a massive release of carbon from the soils and vegetation ecosystem in the Amazon region. Some studies suggested that the increased atmospheric CO_2 might have led to an increase in carbon uptake by about 3 Pg C yr^{-1} in undisturbed areas of Amazonian forests (Houghton et al., 2001; Saleska et al., 2003). Because of the large spatial coverage, changes in carbon, water and energy cycles in Amazonian forests over the short- and long-term would have an important feedback effect on regional and potentially global climate system (Laurance, 2001; Ramankutty et al., 2007). Therefore, Amazonian forests future has become a matter of worldwide concern, which has drawn attention of researches across the world to observe, model and understand the functioning of these forests and determine how these forests may respond to future climate change.

Dynamic Global Vegetation Models (DGVM) or Land Surface Models (LSM), are used to simulate the complex and detailed biogeochemical and biogeophysical processes. These models are essential tools to investigate the interactions and feedbacks between vegetation ecosystems in the Amazon region and climate changes. Several studies using LSM have predicted a decline in topical forest water and carbon fluxes during the dry season (Botta, 2002; Tian et al., 1998). Some other similar ecosystem modeling studies suggested that due to climate variability, the Amazon basin is a net source of carbon during the drier and warmer El Nino years and net sink of carbon during the wetter and cooler La Nina years (Asner et al., 2000; Baker et al., 2008; Foley et al., 2002; Potter et al., 2001; Tian et al., 1998). However, due to the complexity of the soil and vegetation properties, it is difficult to accurately parameterize and evaluate these DGVM and LSM in the Amazon region. Well-tested models are essential to improve the confidence in the global carbon, water and energy balance simulations. Because of the availability of very limited observed flux data in the Amazon region, there has been a lack of efforts regarding the model parameterization or intercomparison in the Amazon region (Henderson-Sellers et al., 1995).

An international scientific endeavor headed by Brazil had led to the establishment of a Large Scale Biosphere-Atmosphere Experiment in Amazonia (LBA) (Avissar, 2002a), with a primary goal to understand the interactions between the atmosphere and terrestrial ecosystems in the Amazon region (Avissar, 2002b). Observed flux and meteorological data from the LBA initiative have provided a unique data source to evaluate the performance of the LSM and DGVM (Christoffersen et al., 2014; de Gonçalves et al., 2013; von Randow et al., 2013).

In this study, we used a newly developed C and N coupled model, CLASS-CTEM^{N+} (Huang et al., 2011), derived from Canadian Land Surface Scheme, CLASS (Verseghy et al., 1993; Verseghy, 1991; 2000) and the Canadian Terrestrial Ecosystem Model, CTEM (Arora and Boer, 2006; 2005a; 2003) to simulate carbon, water and energy fluxes at 7 LBA flux tower sites in the Amazon region. These sites include 5 forests, one agricultural and one grassland or pasture site. This exercise is important because, in the past, performance of CLASS-CTEM^{N+} has not been evaluated for vegetation ecosystem in the tropical regions. The specific objectives of this study are (1) to evaluate the model performance by comparing simulated carbon, water and energy fluxes and carbon stocks with eddy covariance flux and biometric measurements from forest, crop and grassland sites in the Amazon region, and (2) to determine nitrogen (N) induced impacts on carbon and water exchanges in tropical forest ecosystems. Our study helps to reduce the uncertainty about the responses of the vegetation ecosystems in the Amazon region to climate variability and N cycle feedbacks.

3.2 Methods

3.2.1 Model

The CLASS-CTEM^{N+} model is a process-based dynamic global vegetation model (DGVM) derived from two existing models: The Canadian Land Surface Scheme (CLASS) (Verseghy et al., 1993; Verseghy, 2000, 1991) and the Canadian Terrestrial Ecosystem Model (CTEM) (Arora and Boer, 2006, 2005a, 2005b, 2003), with a newly incorporated representation of soil-plant nitrogen (N) cycling algorithms (Arain et al., 2006; Huang et al., 2011; Yuan et al., 2008).

3.2.1.1 CLASS Model

The CLASS model was originally developed at Environment Canada for use in the Canadian Global Climate Model (CGCM) and the Canadian Regional Climate Model (CRCM) (Verseghy et al., 1993; Verseghy, 2000, 1991) . CLASS was originally designed with a composite canopy, composed of amalgamated properties of up to four vegetation classes (needleleaf trees, broadleaf trees, crops and grass) plus urban areas. The grid-cell is also divided into vegetated and bare soil fractions, each with and without snow cover, which are treated separately. Beginning with version 3.0, a full mosaic is able to represent different surfaces in distinct patches or tiles. There are three soil layers (with depths of 0.1, 0.25, and 3.75 m), a variable depth of snow layer where applicable, a single vegetation canopy layer (which intercepts both rain and snow), prognostic soil temperatures, liquid and frozen soil moisture contents, and soil surface properties (e.g. surface roughness heights and surface albedo) which are functions of soil moisture and the soil and vegetation types. The radiation subroutine calculates the visible, near infrared (NIR), and longwave radiation absorbed by the canopy. The absorption of visible and NIR radiation is based on vegetation-dependent visible and NIR albedo and transmissivity, while net long-wave radiation absorbed by the canopy is based on the sky-view factor, which describes the degree of the canopy closure. The original canopy conductance parameterization used in CLASS was similar to that of the Jarvis model (Jarvis, 1976), where canopy resistance (r_c) is expressed as a function of minimum stomatal resistance and a series of environmental dependences whose effects are assumed to be multiplicative. Later, two leaf (sunlit and shaded) C and soil-plant N cycle modules were incorporated into CLASS and those versions of the model are known as C-CLASS and CN-CLASS, respectively (Arain et al., 2006; 2002).

3.2.1.2 CTEM Model

CTEM is a dynamic vegetation model developed at the Canadian Centre for Climate Modelling and Analysis (CCCma), Environment Canada. Version 1.2 of CTEM used here simulates the terrestrial ecosystem processes of photosynthesis, autotrophic and heterotrophic respiration, leaf phenology, allocation, biomass turnover, litterfall, and mortality, and prognostically determines the carbon in model's three live (leaves, stem and root) and two dead (litter and soil carbon) components. These processes are modelled for nine plant functional types (PFTs) that are linked directly to the four PFTs of CLASS (see Table 3.1): needleleaf trees are divided into their evergreen and deciduous sub-types, broadleaf trees are divided into evergreen and cold- and drought-deciduous sub-types, and grasses and crops are divided into C_3 and C_4 sub-types. The photosynthesis sub-module of the CTEM is based on the biochemical model of Farquhar and Collatz (Farquhar et al. 1980; Collatz et al. 1991; Collatz et al. 1992) with the 'big-leaf' option. The coupling between photosynthesis and canopy conductance is based on vapour pressure deficit (Leuning et al., 1995) and when coupled to CTEM, the stomatal resistance calculated by the Jarvis type parameterization in CLASS is not used. Photosynthesis accounts for the differences in C_3 and C_4 pathways. The photosynthesis or gross ecosystem productivity (GEP) and autotrophic respiration (Ra) and heterotrophic respiration (Rh) sub-modules of the CTEM, as described in Arora (2003), are used to calculate net primary productivity (NPP) and net ecosystem productivity (NEP). NPP is allocated to leaves, stem, and roots depend on water availability, light limitation and leaf phenological status. Prognostic leaf area index (LAI) is then determined from the leaf C and specific leaf area (SLA) (Dickinson et al., 1998). The root biomass declines exponentially with depth and the PFT-dependent exponent describing the root distribution depends on root biomass which makes fraction of roots in each soil layer a dynamic function of vegetation growth (Arora and Boer, 2003). The phenology sub-module of CTEM is based a carbon-gain approach. Leaf onset is initiated when it is beneficial for the plant, in C terms, to produce new leaves. Leaf offset is initiated by unfavorable environmental conditions, including shorter day length, cooler temperatures, and low soil moisture (Arora and Boer, 2005a). The seasonal phenological cycle of leaves is prognostically calculated without any prescribed dates or use of satellite data. Mortality rates of leaves, wood, and fine and coarse roots are PFT-dependent and generate a flow of C into the model's single litter pool. Heterotrophic respiration from the litter and soil organic matter pools varies with soil temperature and soil moisture and tissue chemistry. A primary prognostic treatment of fire is also included in the model (Arora and Boer, 2005b). Allocation to, and respiratory losses from the three vegetation components (leaves, stem, and root) result in time-varying biomasses that are reflected in the structural vegetation attributes used in the energy and water balance calculations of the CLASS (Arora and Boer, 2005a). While CTEM simulates vegetation attributes of all its PFTs separately (including LAI, vegetation height, fraction of roots in each layer and canopy mass) these attributes are weighted in proportion of their fractional coverage as per Table 3.1 before being passed to CLASS. Other than photosynthesis (which is modelled at a half-hour time step), all CTEM related processes are modelled at a daily time step.

Although it includes a parameterization for down-regulation of photosynthesis as CO_2 increases (Arora et al., 2009), CTEM does not include a coupling of terrestrial C and N cycles, and the effects of nutrient limitation on photosynthesis are not modeled explicitly. A representation of the soil-plant nitrogen cycle was introduced into the coupled CLASS-CTEM model recently, yielding the CLASS-CTEM^{N+} model version (Huang et al., 2011) which is described in the next section.

3.2.1.3 CLASS-CTEM^{N+} Model

The CLASS-CTEM^{N+} model used in this study was developed by incorporating plant and plant nitrogen cycling algorithms into the coupled CLASS (version 2.7) and CTEM models (version 1.2) (Huang et al., 2011). Soil N cycle processes in CLASS-CTEM^{N+} include immobilization, mineralization, nitrification, denitrification, volatilization, leaching, disturbance losses, and gaseous emissions of N_2O and NO. Plant N cycle processes include root N uptake, plant N allocation and N controls on photosynthetic capacity. The maximum carboxylation capacity of Rubisco (V_{cmax}) is determined nonlinearly from the modelled leaf Rubisco-nitrogen. Variations in plant C assimilation and stomatal conductance are linked with leaf N status through the Rubisco enzyme. The N uptake rate can be enhanced or limited by plant growth, depending on N demand and non-structural storage capacity. Thus, interactions between the C and N cycles in CLASS-CTEM^{N+} include (1) dependence of photosynthesis and plant respiration on leaf/plant tissue N, (2) limitation of decomposition by N availability, (3) the dependence of shoot and root C allocation on the N status in these tissues and (4) limitation of N uptake by fine root biomass. The calculation of foliar N concentrations and C:N ratios of plant tissues and soil compartments allows N to impose constraints on productivity, respiration and C allocation. Apart from plant litterfall, the model has three other means of adding inorganic N to the soil–plant ecosystem: (i) bio-fixation; (ii) atmospheric deposition (wet and dry); and (iii) N fertilization (organic or inorganic). N losses are represented through leaching and disturbances (e.g. fire, harvest), as well as gaseous-N emissions. Nitrogen is cycled through plant tissues, litter, soil and the mineral pools at a daily time step. More details of CLASS-CTEM^{N+} soil-plant N processes are given in (Arain et al., 2006) and (Huang et al., 2011).

CLASS-CTEM^{N+} contains five C pools (leaves, stem, root, litter and soil organic carbon) and six N pools (leaves, stem, root, litter, soil ammonium (NH_4^+) and nitrate (NO_3^-)). Plant storage pools allow C and N acquired in one growing season to be retained and then distributed as new growth in subsequent years. Allocation to, and the respiratory and litter losses from the three vegetation components (leaves, stem, and root) result in time-varying biomass values that are reflected in the structural vegetation attributes used in the energy and water balance calculations of CLASS (Arora and Boer, 2005a). CTEM has 9 PFTs as listed in Table 3.1, which also shows how CTEM's PFTs condense into 4 vegetation types for CLASS (Arora, 2002). In CLASS-CTEM^{N+}, while CTEM simulates vegetation attributes of all its PFTs separately (including LAI, vegetation height, the fraction of roots in each soil layer and canopy mass) these attributes are lumped as per PFT before they are passed onto CLASS (Table 3.1).

Energy and water exchanges estimated by CLASS operate at a half-hourly or shorter time step to provide boundary conditions (including soil moisture and temperature) for the biogeochemistry models of CLASS-CTEM^{N+}. Except photosynthesis, which operates at the time-step of CLASS; all other sub-modules of CTEM operate at a daily time step. The plant and soil N algorithms are adapted for a daily time step as well.

3.2.2 Measured Data Sites

In this study, we used flux and meteorological data from the Large Scale Biosphere–Atmosphere Experiment in Amazonia (LBA) project (Avissar, 2002a, 2002b; de Gonçalves et al., 2013). Seven flux tower sites (Table 3.2), including five forests (known as RJA, K34, K67, K83, BAN (forest-savanna)), one pasture-agricultural (known as K77) and one pasture (known as FNS), were selected representing a variety of vegetation classes and soil types in the Amazon region, located in the geographic zone ranging from 10° N to 25° S and 30° to 85° W.

The pasture-agricultural K77 site was originally a pasture site from September 2000 until November 2001, but was converted to a rice site in February 2002 (Sakai et al., 2004). We simplified to simulate this site as a C4 crop (Jan. 2001–Dec. 2005), despite the previous pasture history. The forest-savanna BAN site is a semi-deciduous site and it resembles the features of evergreen forests (de Gonçalves et al., 2013). Hence, we treat this site as a tropical evergreen site similar to other modeling studies (Poulter et al., 2010). International Geosphere-Biosphere Programme (IGBP) land cover classification scheme (Loveland et al., 2000) was used to re-classify these vegetation types into CLASS-CTEM^{N+}'s PFTs classification, resulting with five evergreen broadleaf forests (CTEM PFTs=3), one C4 grassland (CTEM PFTs=9) and one C4 cropland in this study (Table 3.2).

The site-specific multi-year meteorological data from each site were used to drive the model time series at hourly intervals. These data were provided by the LBA-Model Inter comparison Project (website http://www.climatemodeling.org/lba-mip/). Some of these sites also have ancillary data, such as Leaf Area Index (LAI), vegetation biomass partitions, soil properties, soil carbon stocks, litterfall rates, or maximum photosynthetic capacity. These ancillary data were not used for model parameterization or initialization of our model, but they were used for the model evaluation.

Table 3.1 CLASS-CTEM^{N+} PFTs and PFT-specific parameters updated in this study.

CLASS PFTs Code [1]	**CTEM PFTs** [2]	**Vc,max** [3]	**α** [4]	**Rm,leaf** [5]	R_{litter} [6]	R_{SOM} [6]	**N/C ratio in leaves** [7]	**N/C ratio in stems** [7]	**N/C ratio in roots** [7]	**N/C ratio in litter** [7]	**N/C ratio in SOM** [7]
1	ENF	35	0.08	0.015	0.4453	0.0260	0.024	0.020	0.015	0.015	0.030
	DNF	40	0.08	0.017	0.5986	0.0260	0.024	0.020	0.015	0.015	0.030
2	DBE	51	0.08	0.020	0.6339	0.0208	0.030	0.025	0.020	0.020	0.030
	DBC	67	0.08	0.015	0.7576	0.0208	0.030	0.025	0.020	0.020	0.030
	DBD	40	0.08	0.015	0.6957	0.0208	0.030	0.025	0.020	0.020	0.030
3	CR3	55	0.08	0.015	0.6000	0.0350	0.040	-	0.018	0.018	0.030
	CR4	40	0.04	0.025	0.6000	0.0350	0.027	-	0.010	0.010	0.030
4	GR3	75	0.08	0.013	0.5260	0.0125	0.040	-	0.018	0.018	0.030
	GR4	15	0.04	0.025	0.5260	0.0125	0.027	-	0.010	0.010	0.030

[1] CLASS PFTs: Code 1: needleleaf tree; 2: broadleaf tree; 3: crops; 4:grass.

[2] CTEM PFTs: evergreen needleleaf forests (ENF), deciduous needleleaf forests (DNF); evergreen broadleaf forests (DBE); deciduous broadleaf-cold forests (DBC), deciduous broadleaf-dry forests (DBD), C3 crops (CR3), C4 crops (CR4), C3 grass (GR3) and C4 grass (GR4).

[3] Vc,max: maximum rate of carboxylation by the enzyme Rubisco, (μmol CO_2 m^{-2} s^{-1}) (Rogers, 2014).

[4] α: the quantum efficiency scalar.

[5] Leaf maintenance respiration co-efficient;

[6] litter and soil carbon respiration rate at 15 °C (Kg C/ Kg C) (Melton and Arora, 2014).

[7] N/C ratio in leaves, stems, roots, litter and soil organic matters (SOM), (Kg N/Kg C) (Huang et al., 2011; Meissner et al., 2003; Wania et al., 2012; White et al., 2000).

Table 3.2 Characteristics of the study sites

Short Code	Site Name	Lon (degree)	Lat (degree)	Elev. (m)	Tower Height	Canopy Height	Biome Type	**CTEM PFTs** [a]	Sand[c] %	Silt[c] %	Clay[c] %	Data Years
BAN	Javaes River-Bananal Island	-50.16	-09.82	120	40	16	Forest-Savanna	3	24	39	37	2004-2006
K34	Manaus Km34	-60.21	-02.61	130	50	35	Tropical rainforest	3	20	12	68	2000-2005
K67	Santarém Km67	-54.96	-02.86	130	63	35	Tropical rainforest	3	2	8	90	2002-2004
K77	Santarém Km77	-54.89	-03.02	130	18	0~0.6	Pasture-Agriculture	7	18	2	80	2001-2005
K83	Santarém Km83	-54.97	-03.02	130	64	35	Tropical rainforest	3	18	2	80	2001-2003
RJA	Reserva Jarú	-61.93	-10.08	191	60	30	Tropical rainforest	3	80	10	10	2000-2002
FNS	Fazenda Nossa Senhora	-62.36	-10.76	306	8.5	0.2~0.5	Pasture	9	85	12	3	1999-2001

[a] 9 of the CTEM PFTs classifications (Arora and Boer, 2005a); also refer to Table 3.1.

[b] Principle Investigators and data references for these tower sites are as follows:
BAN: da Rocha, H. (USP, Brazil) (Borma et al., 2009)
K34: Manzi, A., Nobre, A. (INPA, Brazil) (Araújo, 2002)
K67: Wofsy, S. (Harvard University, USA), Saleska, S. (UofA, USA), Camargo, A. CENA/USP, Brazil). (Hutyra et al., 2007; Saleska et al., 2007)
K83: Goulden M. (UC Irvine, USA), Miller, S. (SUNY, Albany, USA), da Rocha, H. (USP, Brazil). (da Rocha et al. 2004; Goulden et al. 2006; Miller et al. 2007)
K77: Fitzjarrald, D. (SUNY, Albany , USA) (Sakai et al., 2004)
RJA: Manzi, A. (INPA, Brasil), Cardoso, F. (UFR, Brazil.) (Kruijt et al., 2004; von Randow et al., 2004)
FNS: Waterloo, M.(Vrije Universiteit Amsterdam, The Netherlands), Manzi, A. (INPA, Brazil) (von Randow et al., 2004)

[c] Soil Texture references:
BAN: da Rocha, H. personal comunication (email Feb 4, 2009)
K34: (Chambers et al., 2001)
K67: (Williams et al., 2002) (Average of sites 1, 3, 4)
K77: Same as K83
K83: (Keller et al., 2005)
RJA: (Andreae, 2002)
FNS: same as RJA

3.2.3 Model Initialization and Parameterization

The model initialization details following LBA-MIP protocol are as follows: (a) Soil moisture in all layers was set to 0.95 of saturation (porosity); (b) Soil temperature in all layers was set to the mean of the annual air temperature; (c) Because reliable carbon and nitrogen pools observations are not available at all sites, initial values of soil carbon, live biomass and nitrogen pools were estimated by model spin-up as described below; (d) Initial CO_2 value was assumed at 375 ppm as a steady-state solution, (e) photosynthesis, carbon allocation, maintenance respiration, and carbon turnover rates were assigned from the empirical values used in CTEM (Melton and Arora, 2014). The model was spun-up to reach the equilibrium or steady state using the following procedure recommended by the LBA-MIP initiative. It includes the following steps: (a) Replicated the driving dataset to achieve 15 year simulations at each site; (b) Replicated the driver dataset until the slow response prognostic variables, including soil temperature, soil moisture, and some carbon pools (i.e. primarily wood and slow soil pools), reached a certain criteria. Steady state for soil moisture occurred when the seasonal cycle of monthly average values for each layer varied less than 1% between consecutive years. Steady state for the carbon cycle occurred when growth balances decay and the annual NEP~0 when averaged over the last five years of the spin-up. We assumed that steady state for soil temperature occurs when the soil moisture reaches steady state.

In the model, carbon allocation factors are dynamic and their values can change with time depending on water and light stress factors (Arora and Boer, 2005a). Maintenance respiration rates were used for different carbon pools such as leaf, stem and root following Amthor (2000; 1984) and Ryan et al. (1995). Details of model parameters used in this study are summarized in Table 3.1.

3.2.4 Model Evaluation and Analysis Criteria

Simulated daily, monthly and annual values of gross ecosystem productivity (GEP), ecosystem respiration (Re), net ecosystem productivity (NEP), sensible heat flux (H) and latent heat flux (LE) from C-N coupled and C-only versions of the model were compared with observed fluxes at each site. Positive values of NEP [= GEP-Re] represent an uptake of C by the ecosystem, and negative values represent a loss of C to the atmosphere. Both model versions used the same modeling protocol in terms of climatic drivers, CO_2 concentrations, spin-up and simulation phase. To be able to separate the effect of N dynamics for a direct comparison, all parameters shared between the C and C-N versions were set to equal values (Table 3.1). Simulated vegetation biomass and soil C pools were also compared with observation-based estimates from the literature.

Statistical measures such as Root Mean Square Error (RMSE) and Model Efficiency Index (EI) were used to evaluate the model performance. RMSE measures the average distance of data points from fitted 1:1 line. EI was determined following Nash and Sutcliffe (1970) as:

$$EI = 1 - \frac{\sum_{i=1}^{N}(O_i - P_i)^2}{\sum_{i=1}^{N}(O_i - \overline{O})^2}$$

where P_i is predicted and O_i is observed values, $\overline{O}$ is the observed average value, and N is the total number of data points. EI is widely used to quantitatively describe the accuracy of model outputs. It ranges from −1 to 1, where EI = 1 corresponds to a perfect match between simulated and observed values; EI = 0, indicates that the model predictions are as accurate as the mean of the observed data and EI < 0 indicates that simulated values are not a good fit to observation.

3.3 Results

3.3.1 Annual Carbon, Water and Energy Exchanges

We evaluated the model performance for C, water and energy exchanges by comparing simulated annual values for both C-N and C-only versions with observations at each site (Fig. 3.1 and 3.2). Simulated annual GEP values were in good agreement with measurements, as indicated by RMSE and EI values (Table 3.3). For tropical evergreen forest sites, K34 and K83, the C-N coupled model showed improvements in GEP with a reduction in RMSE as compared to C-only model with RMSE ranging from 0.86 to 0.56 for K34 and K83, respectively using C-N model and 0.45 to 0.31 kg C m^{-2} yr^{-1}, using C-only model, Table 3.3). For other sites, simulated GEP from both C-N and C-only models were comparable, although the C-only version achieved marginally better accuracy. For tropical evergreen forest sites (K34, K67, K83, RJA), simulated GEP varied between 0.7 and 1.6 kg C m^{-2} yr^{-1} compared to measured values ranging from 0.6 to 1.3 kg C m^{-2} yr^{-1} (Fig. 3.1a,b). Simulated GEP for the agricultural (K77), pasture (FNS) and forest-savanna (BAN) sites were lower than the forest sites, because herbaceous ecosystems are less productive than forest ecosystems. The measured annual GEP for the pasture sites (FNS) is about 3 times higher than the pasture-agricultural site, K77. One explanation for the large difference in productivity between these two pasture sites is that the soil in the Eastern Amazon, the region where K77 is located, is believed to be drier with lower soil nutrients than the soils in the Western Amazon, the region where FNS is located (Asner et al., 1999). Moreover, literature studies suggest that pasture growth is more prone to be limited by nutrient availability, such as phosphorus, calcium and potassium (de Moraes et al., 1996). Thus, the productivity of the K77 site is lower largely due to water and nutrient stresses (Sakai et al., 2004). Overall, N inclusion in the model caused a minor reduction in annual mean GEP estimates (Δ = C-CN = 0.03 kg C m^{-2} yr^{-1}) in the tropical forest sites (K34, K67 K83, RJA); while, a slight increase was observed in the C-N simulated annual mean GEP in crops and pasture sites (Δ = C-C-N = -0.17 kg C m^{-2} yr^{-1}) (K77, FNS, BAN) (Table 3.3). N dynamics of the C-N model caused some changes in GEP from all sites, which caused C-N model outputs to better match observations (Table 3.3; Fig. 3.1a, b).

Similar to GEP, both models simulated annual Re were in agreement with observations (Table 3.3; Fig. 3.1c, d). C-N simulated Re predictions for K34, K77 and FNS were similarly reduced in both RMSE and bias, although improvements were smaller. The error and bias at other sites (K67, K83, RJA and BAN) in simulated Re were comparable for both model versions. Both C-N and C models estimated Re for the pasture sites (FNS) and forest-savanna site (BAN) are about half of the Re for tropical evergreen sites and is about 5 times for the pasture-agriculture site (K77), which are consistent with the measurement data (Table 3.3). Again, the inclusion of the N cycle had not shown pronounced improvement to any of the PFTs.

The CLASS-CTEM^{N+} annual NEP estimates for all sites by both model versions varied between -0.04 and 0.35 kg C m^{-2} yr^{-1}, which falls within the range of observational NEP values reported for the same site (Table 3.3; Fig. 3.1e, f). Both the C-N and C modeled NEP indicated a small overestimation for forest sites and a slight underestimation for agriculture and pasture sites. While the exact cause of these mismatches is still unknown; we speculate this could also be due to uncertainty associated with measured input variable. The C-N coupled model showed small improvement over all sites. For example, the bias in the predictions of mean NEP simulated by the C-N model for BAN site reduced from 7% underestimation to 2% underestimation, while RMSE was also slightly reduced from 0.65 to 0.34 kg C m^{-2} yr^{-1}. Overall observed average NEP during all study years was 0.15 ± 0.05 kg C m^{-2} yr^{-1}, while simulated NEP was 0.14 ± 0.02 kg C m^{-2} yr^{-1} and 0.13 ± 0.03 kg C m^{-2} yr^{-1} by the C-N and C-only versions of the model, respectively (Fig. 3.1e, f). For the individual sites, both models generally reproduced NEP, however they slightly varied in magnitudes, which resulted in comparable error and bias scores (Table 3.3). BAN site had the largest observed mean annual NEP value of 0.39 ± 0.04 kg C m^{-2} yr^{-1}, compared to 0.19 ± 0.04 kg C m^{-2} yr^{-1} for C-N coupled model and 0.01 ± 0.07 kg C m^{-2} yr^{-1} for C-only model, respectively (Table 3.4). K34 site exhibited the largest mean annual NEP of 0.35 ± 0.04 kg C m^{-2} yr^{-1} from both models, when compared to 0.05 ± 0.06 kg C m^{-2} yr^{-1} from observation (Table 3.4).

The C-N coupled model simulated annual mean Rn value at all sites was 132.76 W m^{-2}, compared to 122.08 W m^{-2} from observations and 132.59 W m^{-2} from C-only model (Table 3.4). Similarly, simulated mean annual H values were 29.15 W m^{-2} and 28.24 W m^{-2} from C-N and C-only models, respectively, compared to 24.03 W m^{-2} from observation, indicating a good agreement between C-N coupled model and observation. Both models underestimated LE with mean annual values of 40.86 W m^{-2} and 36.71 W m^{-2} from C-N and C-only versions of the model, respectively, compared to 71.98 W m^{-2} from measurement. These results indicated that, overall, the C-N coupled and C-only models simulated Rn, LE and H values were statistically comparable with observation for each site (Table 3.3, Fig. 3.2). Both models were able to simulate inter-annual variability within a reasonable range, as shown by standard deviation (SD) with C-N coupled model indicating slight improvements.

3.3.2 Seasonal Carbon, Water and Energy Exchanges

Fig. 3.3 shows the comparison between the monthly mean values of measured and simulated seasonal cycles of carbon (GEP, Re, NEP), water and energy (Rn, LE, H) fluxes over one year (2002) for each site, except FNS and BAN, where data shown is for 2001 and 2006). Three sites representing each PFT class are also shown (such as C4 pasture site FNS in Fig. 3.4; tropical evergreen forest site K67 in Fig. 3.5 and C4 agricultural crop site K77 in Fig. 3.6).

Seasonal trends in carbon, water and energy fluxes were generally reproduced well by the model (Fig. 3.3). Small discrepancy in simulated seasonal carbon fluxes between the C-N coupled and C-only versions when compared to observation was due to the inclusion of the N cycle in the model (Fig. 3.3). Often simulated peaks in monthly values were not matched with observation, and both models missed an observed strong decline in GEP and Re during the summer in terms of timing and magnitude.

The seasonal cycle is arguably better matched between the C-N version of the model and observation at forest sites. Also, seasonal dynamics at forest sites (K34, K67, K83, RJA) were more stable all over the year than agricultural or pasture sites (K77, FNS, BAN). The agriculture and pasture sites simulated a fast built-up of photosynthesis at the start of the growing season, followed by persistent high values till the end of the growing season, resulting in high GEP and subsequent Re (Fig 3.3). The simulated steep rise in GEP in spring and the overestimated summer peak of GEP in the C version was reduced with the inclusion of the N cycle in the C-N version due to N limitation for both forest types, leaving modeled and observed seasonality in close agreement (Fig. 3.3). Both model versions were able to capture the seasonal variability in the Re for each of the vegetation biomes as well (Fig. 3.3). There are no clear differences between the two model versions simulations. For both model versions simulated water and energy fluxes (Rn, LE and H), variations between sites were apparent, with the similar pattern as of simulated C fluxes. Less discrepancy was observed between simulated water and energy fluxes by the C-N and C-only models, compared to observation (Fig. 3.3).

3.3.3 Daily Carbon, Water and Energy Exchanges

Daily mean values, standard deviations (SD), RMSE and EI of C fluxes (GEP, Re and NEP, in g C m^{-2} d^{-1}) and water and energy fluxes (Rn, LE and H, in W m^{-2}) simulated by the C-N coupled and C-only models were compared with observations at all sites (n=7), as indicated in Table 3.4. Incorporation of N constraints on C-cycle processes showed small but significant improvements in simulated daily GEP fluxes for the forest sites (K34, K67, K83 and RJA) (Table 3.4). The C-N coupled model simulated GEP values for these sites were in better agreement with observations than the C-only model as shown by the higher EI and lower RMSE values (Table. 3.4). Improvements due to inclusion of N controls in simulated GEP for agricultural or pasture sites (K77, BAN, FNS) were not clearly observed. Also for simulated daily Re values, the inclusion of the N cycle produced a small improvement for all sites, reducing RMSE and overestimation for each site (Table 3.4), although the simulated respiration rates are slightly overestimated by both models. Simulated Re from C-N coupled model for K67 site, for example, showed large improvement with a considerable reduction in RMSE (1.23 compared to 2.00 g C m^{-2} day^{-1} for C-only model) and an increase in EI (-1.34 compared to -3.50 for C-only model). For all sites, both error and bias scores improved with the N cycle inclusion with lower RMSE and higher EI. Simulated NEP results were comparable with the observations, although the C-only version achieved marginally better accuracy scores (Table 3.4). Overall, improvements in NEP due to inclusion of N dynamics were not clearly observed. Similarly, water and energy values (Rn, LE and H) simulated by the C-N model were in better agreement with observation as compared to the C-only model, as indicated by smaller RSME and higher EI values for the C-N version of the model compared to the C-only versions, although improvements were small.

To analyze the disparity between models and observations more closely, we plotted scattered plots of simulated daily C, water and energy fluxes against observations for site K34 site (2000-2005) as an example (Fig. 3.7). Simulated GEP, Re, NEP, Rn, LE and H values were in better agreement with observations from both models, with C-N coupled model indicating better agreement (Fig. 3.7). Simulated daily NEP ranged from 1.51± 1.73 g C m^{-2} day^{-1} from the C-N coupled model, and 1.33 ± 1.73 g C m^{-2} day^{-1} from C-only model, compared to 0.98 ± 1.78 g C m^{-2} day^{-1} from the observations. Variations in simulated Re from both models were slightly bigger, while the error and bias for predictions of Re is comparable in both models. Overall, inclusion of N dynamics in the model caused a small but meaningful reduction in errors with simulated C, water and energy fluxes against observation, compared to the C-only model.

3.3.4 Carbon Stocks

3.3.4.1 Total Vegetation Biomass

Simulated annual total vegetation biomass from both versions of the model was compared with reported observed values in the literature (Fisher et al., 1994; Trumbore et al., 1995; Saleska et al., 2003; Telles et al., 2003; Miller et al., 2004; Malhi et al., 2009) for each site (Table 3.5). Overall, model simulated biomass values from both versions ranges from 1.12 kg C m^{-2} yr^{-1} for the pasture-agricultural site (K77) to 20.58 kg C m^{-2} yr^{-1} for the tropical forest site (RJA), were comparable to the available measured values at K34, K67 and K83 sites (Table 3.5). Model estimated vegetation biomass at BAN sites were 18.73 kg C m^{-2} yr^{-1} by C-N model and 18.01 kg C m^{-2} yr^{-1} by C model, respectively. These simulated biomass values fall within the range of observed values (16.6 ± 3.6 to 21.8 ± 0.2 kg C m^{-2} yr^{-1}) at other forest sites, such as K34, K67 and K83 (Table 3.5). The simulated annual biomass value at the RJA site in 2002 was 20.58 kg C m^{-2} yr^{-1} by C-N coupled model and 20.14 kg C m^{-2} yr^{-1} by C-only model. The CLASS-CTEM^{N+} C-N version simulated biomass for the agricultural site (K77) was 1.12 kg C m^{-2} yr^{-1} compared to a slightly higher estimate of 1.68 kg C m^{-2} yr^{-1} by the C-only model. For the pasture site (FNS), the C-N coupled model simulated values were slightly lower than the C-only model values (Table 3.5). As expected, the agricultural and pasture sites (K77 and FNS) stored much less biomass than the forest sites as simulated by the model (Table 3.5). Measured data were not available for RJA, BAN, FNS and K77 sites, we could not draw any conclusions as to whether the model is overestimating or underestimating vegetation biomass at these sites. These variations in the vegetation biomass for the tropical evergreen sites are mainly due to the fact that the soil characteristics vary among sites. The sites with clay soil have higher biomass than the sites with silt or sandy soils. For example, the topical evergreen forest site K67 is hypothesized to be experiencing mortality (Malhi et al., 2009; Saleska et al., 2003) over the time and therefore has lower total biomass compared to other LBA forest sites (Table 3.5).

3.3.4.2 Soil carbon

Simulated annual soil organic carbon (SOC) in the top 1.0 m soil layer for each site from both models are summarized in Table 3.5. Corresponding observed values are also given in Table 3.5. For sites, where observed SOC data is available (K34, K67, K83, FNS), both C-N and C-only versions of the model simulated SOC are in close agreement with the measurements (Table 3.5). Simulated SOC varied among sites, ranging from 8.1 kg C m^{-2} at K83 site to 13.1 kg C m^{-2} at K34 sites (Table 3.5). C-N coupled model simulated SOC value for the K34 site was only 3.2% higher than the observed value of 12.7 kg C m^{-2}, and was marginally better than simulated estimates of 12.9 kg C m^{-2} by the C-only model. Both models estimated similar values of 12.8 kg C m^{-2} for K67 site, which as slightly higher than the observed value of 12.1 kg C m^{-2}. Simulated SOC values for the RJA and BAN forest sites were within the range of observed values from K83 site, which are somewhat similar in stands characteristics (observed data for RJA and BAN site not available). Estimated SOC for the pasture site (FNS) (12.6 kg C m^{-2} by C-N coupled model and 12.6 kg C m^{-2} by C-only version of the model, respectively) were slightly higher than that of the observed range of 10.0 to 12.0 kg C m^{-2} at this site (Table 3.5). The C-N coupled and C-only models estimated SOC (8.2 and 8.1 kg C m^{-2}, respectively) for the agricultural site (K77) was the lowest as compared to other study sites. The pasture-agricultural site (K77) simulated SOC is lower than the other sites (Table 3.5), which can be related to the observed difference in soil types and textures (Andreae, 2002; Keller et al., 2005) that determines the amount of carbon stored in the soil.

Table 3.3 Mean and standard deviations (SD) of annual C fluxes (GEP, Re and NEP, in kg C m^{-2} yr^{-1}) and of water and energy fluxes (Rn, LE and H, in W m^{-2}) from observations (Obs) and models (C-N coupled and C-only versions). RMSE and EI for both models are also given.

		Mean			**SD**			**RMSE**		**EI**	
		Obs	**C-N**	**C**	**Obs**	**C-N**	**C**	**CN**	**C**	**CN**	**C**
GEP	**K34**	0.84	1.23	1.47	0.13	0.03	0.15	0.56	0.86	0.25	-0.57
	K67	1.17	1.02	1.08	0.02	0.08	0.09	0.28	0.21	0.16	0.20
	K83	1.01	1.18	0.75	0.02	0.04	0.11	0.31	0.45	-0.32	-2.11
	RJA	1.21	1.00	1.22	0.04	0.04	0.02	0.37	0.10	0.47	0.69
	K77	0.30	0.74	0.68	0.09	0.03	0.03	0.59	0.52	-0.87	-0.44
	FNS	0.85	1.12	0.77	0.09	0.03	0.15	0.47	0.17	-0.13	0.28
	BAN	0.98	1.21	1.11	0.10	0.08	0.09	0.42	0.28	-0.55	0.06
Re	**K34**	0.79	0.73	0.80	0.24	0.05	0.05	0.30	0.30	0.65	0.67
	K67	1.18	0.91	1.00	0.03	0.03	0.04	0.47	0.31	-3.19	-3.08
	K83	1.00	0.77	0.79	0.07	0.01	0.04	0.41	0.36	-5.67	-4.68
	RJA	1.02	0.86	0.87	0.09	0.01	0.02	0.32	0.30	-3.82	-2.98
	K77	0.12	0.10	0.09	0.02	0.01	0.01	0.04	0.05	-2.32	-3.56
	FNS	0.60	0.55	0.51	0.04	0.02	0.03	0.10	0.17	-1.12	-3.87
	BAN	0.64	0.47	0.54	0.03	0.02	0.01	0.29	0.18	-3.07	-2.73
NEP	**K34**	0.05	0.35	0.35	0.06	0.04	0.05	0.37	0.37	-3.19	-3.08
	K67	-0.01	0.14	0.16	0.05	0.02	0.02	0.25	0.30	-2.67	-4.68
	K83	0.01	0.25	0.30	0.05	0.01	0.02	0.42	0.52	-3.02	-2.98
	RJA	0.19	0.12	0.12	0.05	0.00	0.00	0.14	0.15	-2.32	-2.56
	K77	0.17	0.00	-0.01	0.08	0.02	0.03	0.25	0.26	-3.12	-3.87
	FNS	0.28	-0.04	-0.02	0.03	0.00	0.01	0.56	0.52	-0.03	0.11
	BAN	0.39	0.19	0.01	0.04	0.02	0.07	0.34	0.65	0.15	0.10
Rn	**K34**	126.52	134.16	134.15	16.68	5.01	5.00	19.04	19.03	-0.50	0.00
	K67	119.88	131.08	130.93	8.75	10.69	10.68	32.18	32.01	-1.90	-1.30
	K83	107.90	132.15	132.12	21.56	1.90	1.88	50.39	50.35	-1.07	-0.91
	RJA	139.75	146.89	146.87	11.09	5.11	5.14	26.01	26.04	0.15	-0.02
	K77	110.67	131.68	131.73	17.75	6.56	6.68	32.41	32.37	-1.06	-2.39
	FNS	115.57	121.00	121.09	4.72	2.20	2.27	10.51	10.74	-0.10	-0.45
	BAN	134.10	132.42	131.00	2.26	1.58	2.61	3.20	5.58	0.24	-0.12
LE	**K34**	61.74	32.36	32.37	10.48	2.31	2.31	38.63	38.63	0.05	0.35
	K67	79.62	28.70	28.70	6.26	2.43	2.43	88.40	88.39	-0.47	-0.76
	K83	89.31	33.96	33.93	25.39	2.08	2.07	102.60	102.65	-1.48	-6.41
	RJA	62.92	21.56	21.65	15.78	1.90	1.94	75.55	75.41	-1.65	-1.26
	K77	71.93	45.25	45.23	4.02	4.27	4.22	35.58	35.59	-0.35	-0.22
	FNS	43.07	36.66	36.76	14.40	1.41	1.72	21.55	21.05	-0.81	-0.46
	BAN	95.27	87.54	58.35	16.65	0.38	1.49	26.85	67.45	-1.01	-0.91
H	**K34**	25.23	30.54	28.50	5.38	1.53	1.42	8.86	7.21	-1.57	-1.75
	K67	19.73	21.64	20.16	1.25	2.03	1.89	3.52	1.27	-0.56	-0.20
	K83	23.05	25.85	24.13	2.04	0.16	0.14	5.60	3.37	0.31	-0.36
	RJA	20.37	25.07	23.79	0.29	0.66	0.63	8.15	5.94	0.76	0.21
	K77	22.68	29.02	28.40	3.76	1.60	1.57	8.82	8.14	-0.51	-1.37
	FNS	27.53	39.11	37.16	9.18	0.95	0.97	24.25	21.56	-0.16	-0.19
	BAN	29.61	32.84	35.57	2.94	1.52	0.75	8.28	11.43	0.10	-2.96

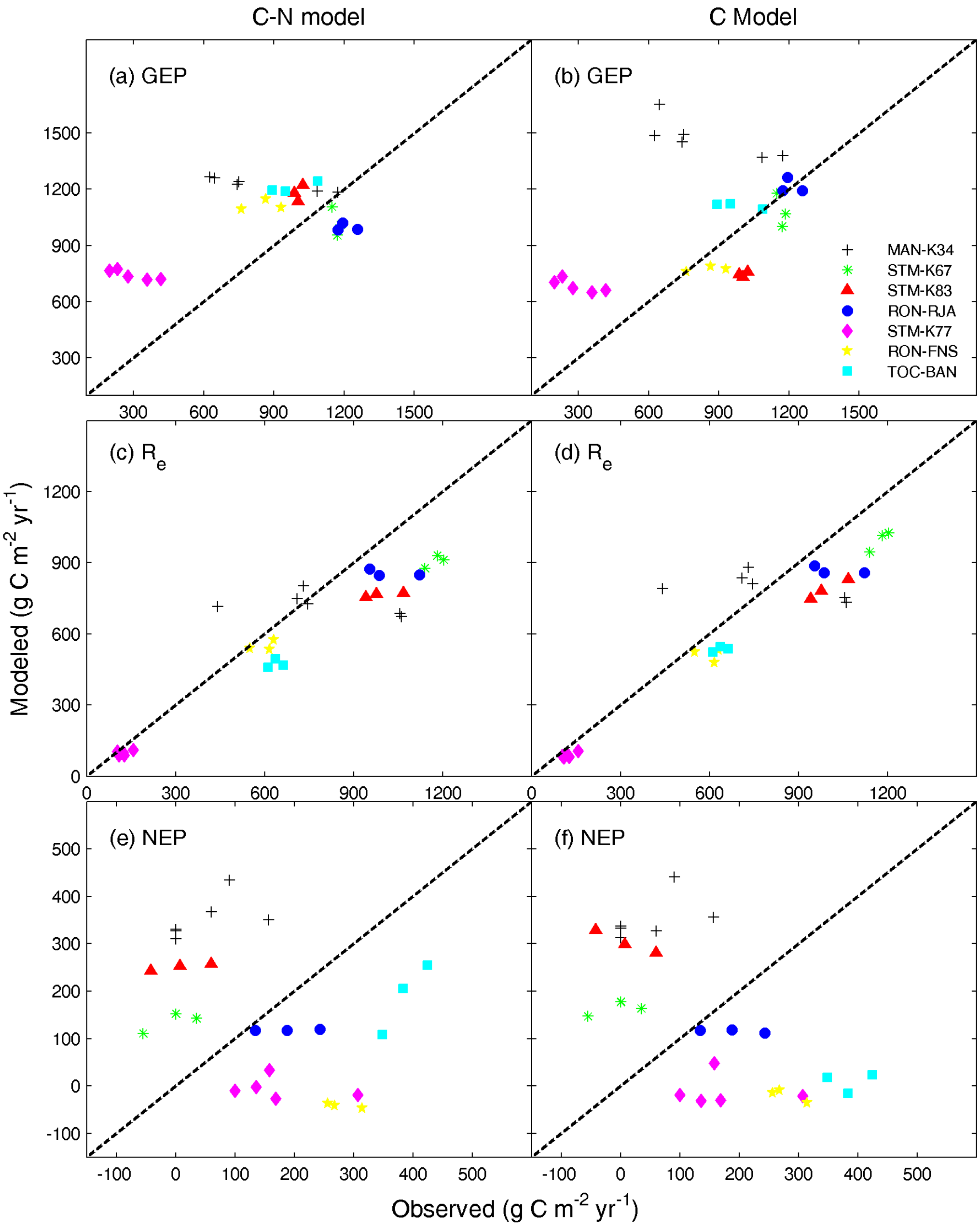

Figure 3.1 Simulated annual values of gross ecosystem productivity (GEP), ecosystem respiration (Re), and net ecosystem productivity (NEP) from the C-N coupled model (left panels) and the C-only model (right panels) versus observations.

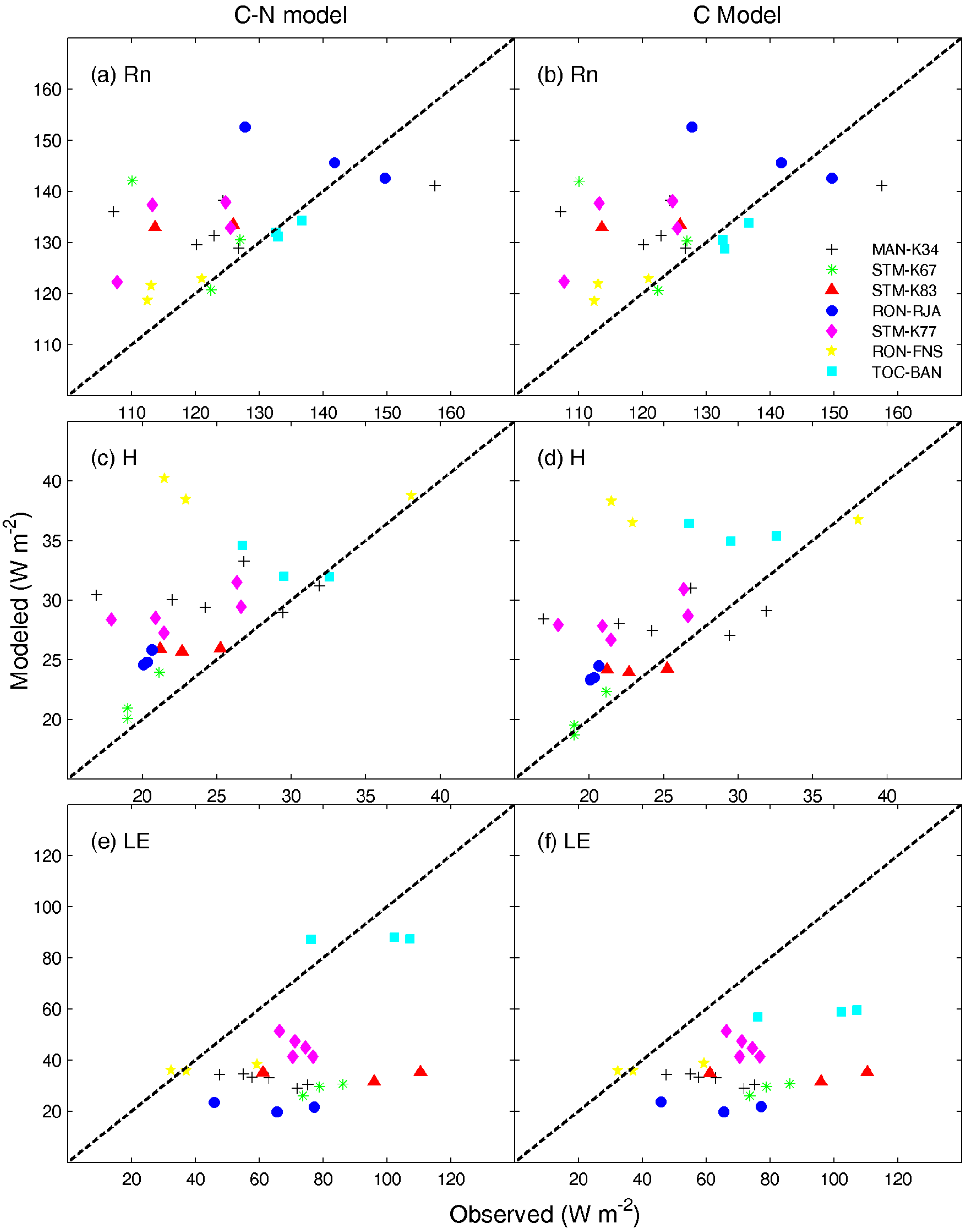

Figure 3.2 Simulated annual values of net radiation (Rn), latent heat (LE) and sensible heat (H) from the C-N coupled model (left panels) and the C-only model (right panels) versus observations.

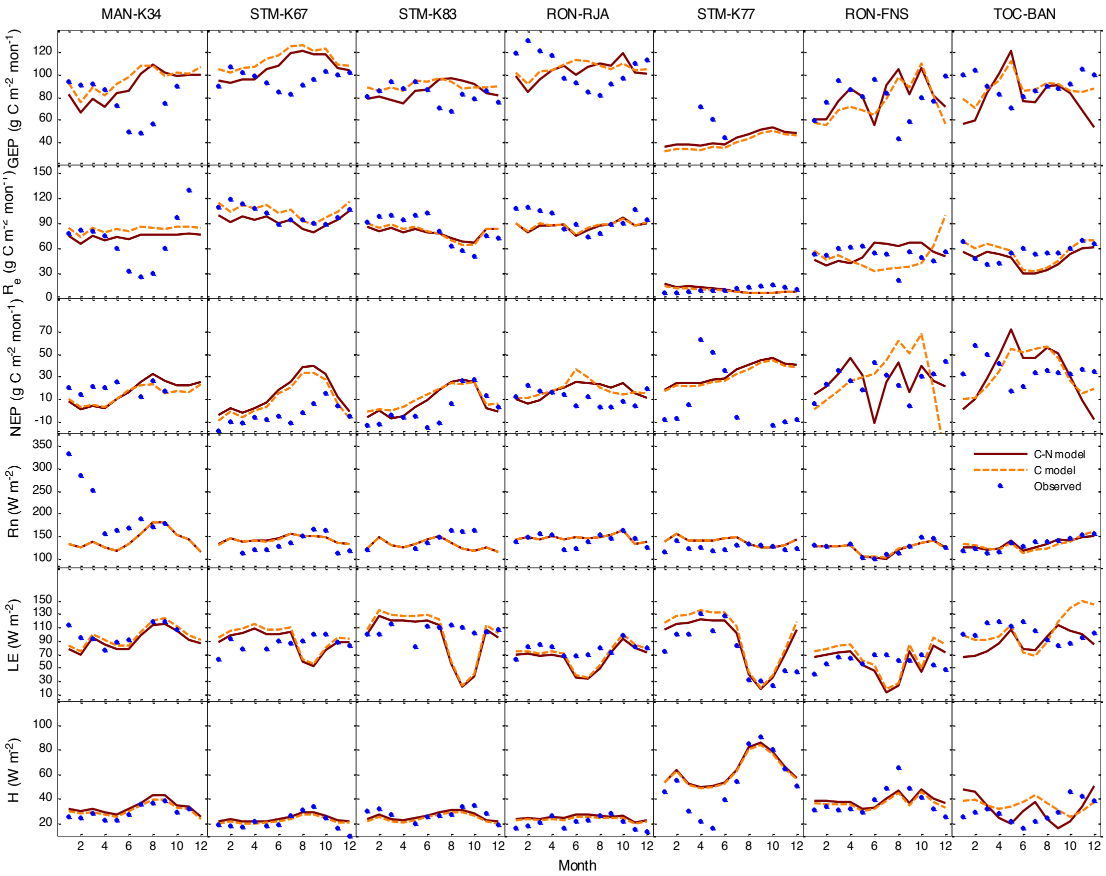

Figure 3.3 Monthly values of gross ecosystem productivity (GEP), ecosystem respiration (Re), net ecosystem productivity (NEP), net radiation (Rn), latent heat (LE) and sensible heat (H) from C-N coupled and C-only model and observations for year 2002 for each site, except FNS and BAN sites, where shown data is 2001 and 2004 respectively.

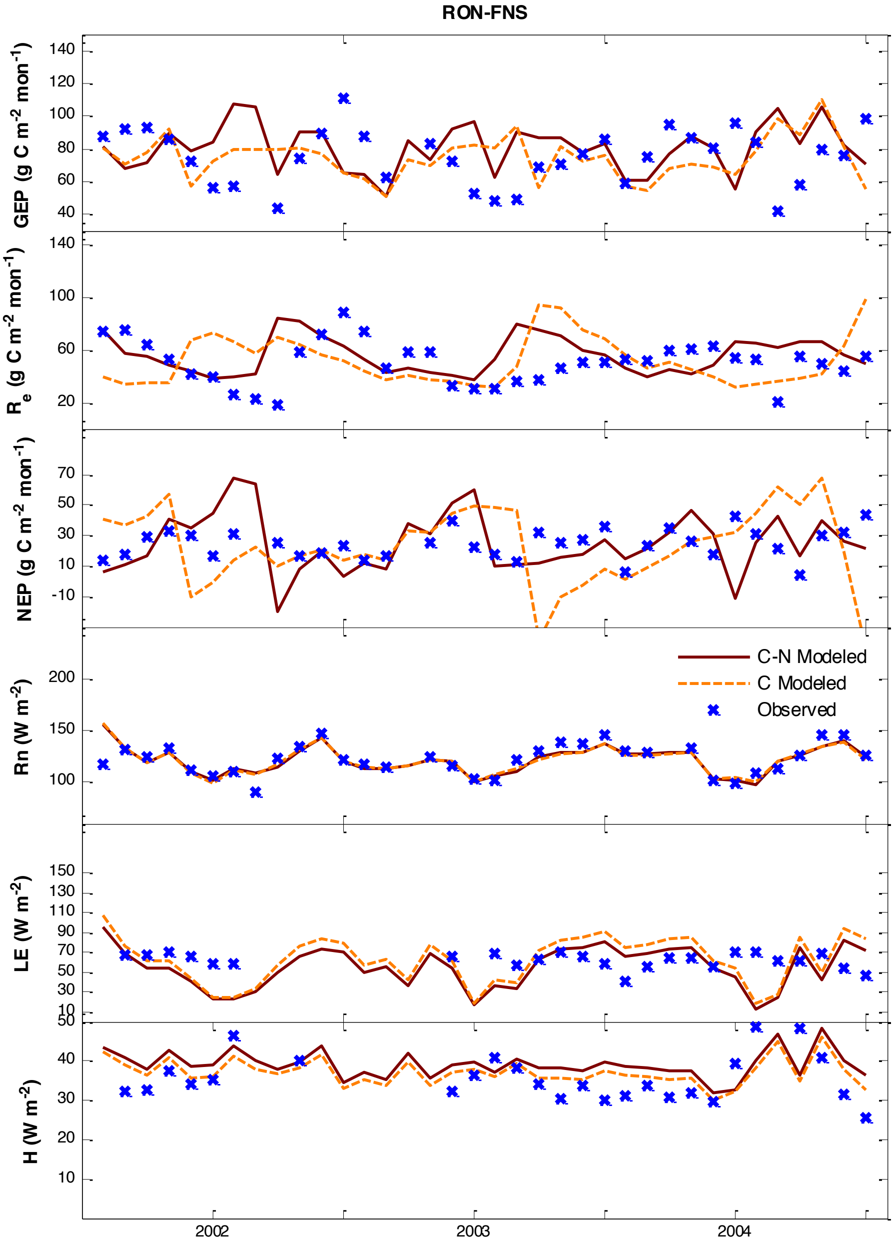

Figure 3.4 Monthly values of gross ecosystem productivity (GEP), ecosystem respiration (Re), net ecosystem productivity (NEP), net radiation (Rn), latent heat (LE) and sensible heat (H) fluxes from C-N coupled and C-only model and observations at FNS site from 1999 to 2001.

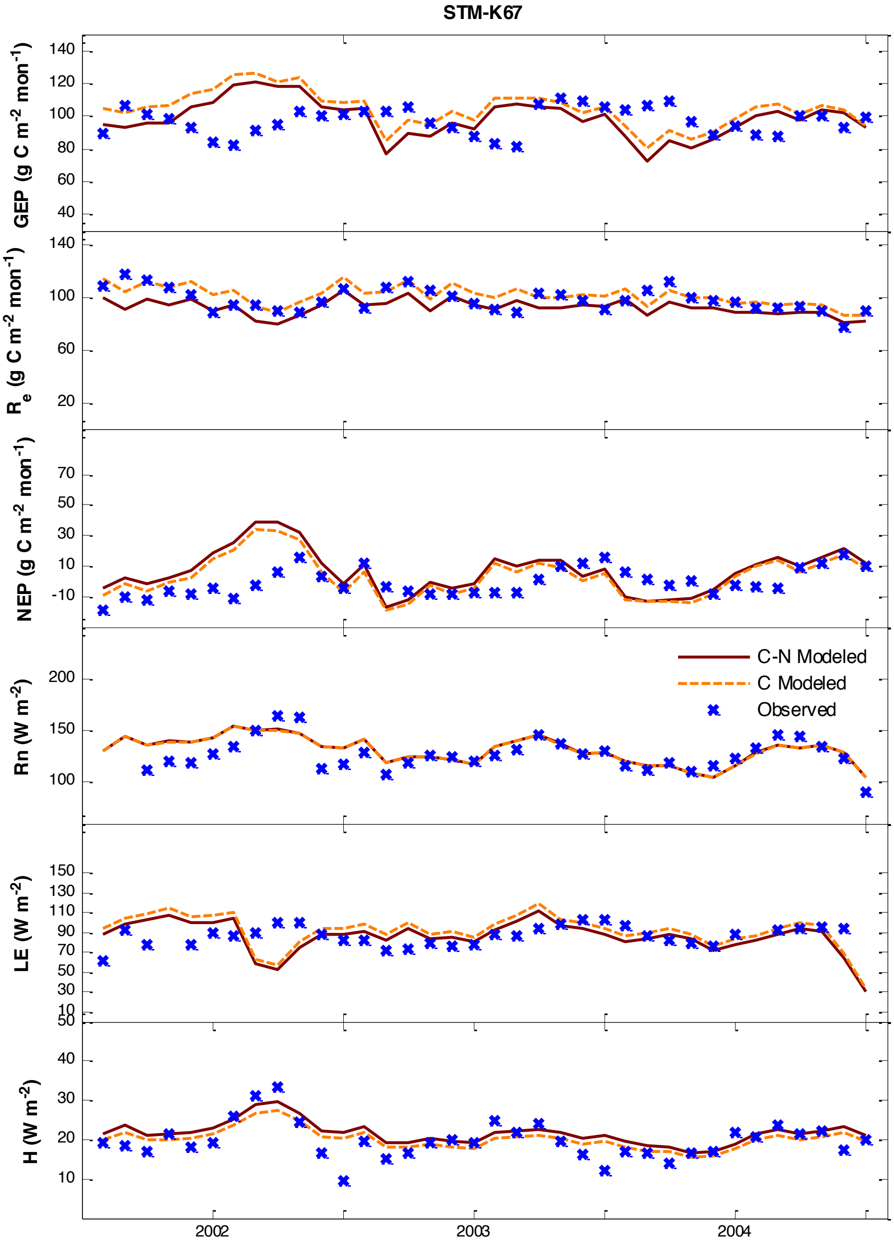

Figure 3.5 Monthly values of gross ecosystem productivity (GEP), ecosystem respiration (Re), net ecosystem productivity (NEP), net radiation (Rn), latent heat (LE) and sensible heat (H) fluxes from C-N coupled and C-only model and observations at K67 site from 2002 to 2004.

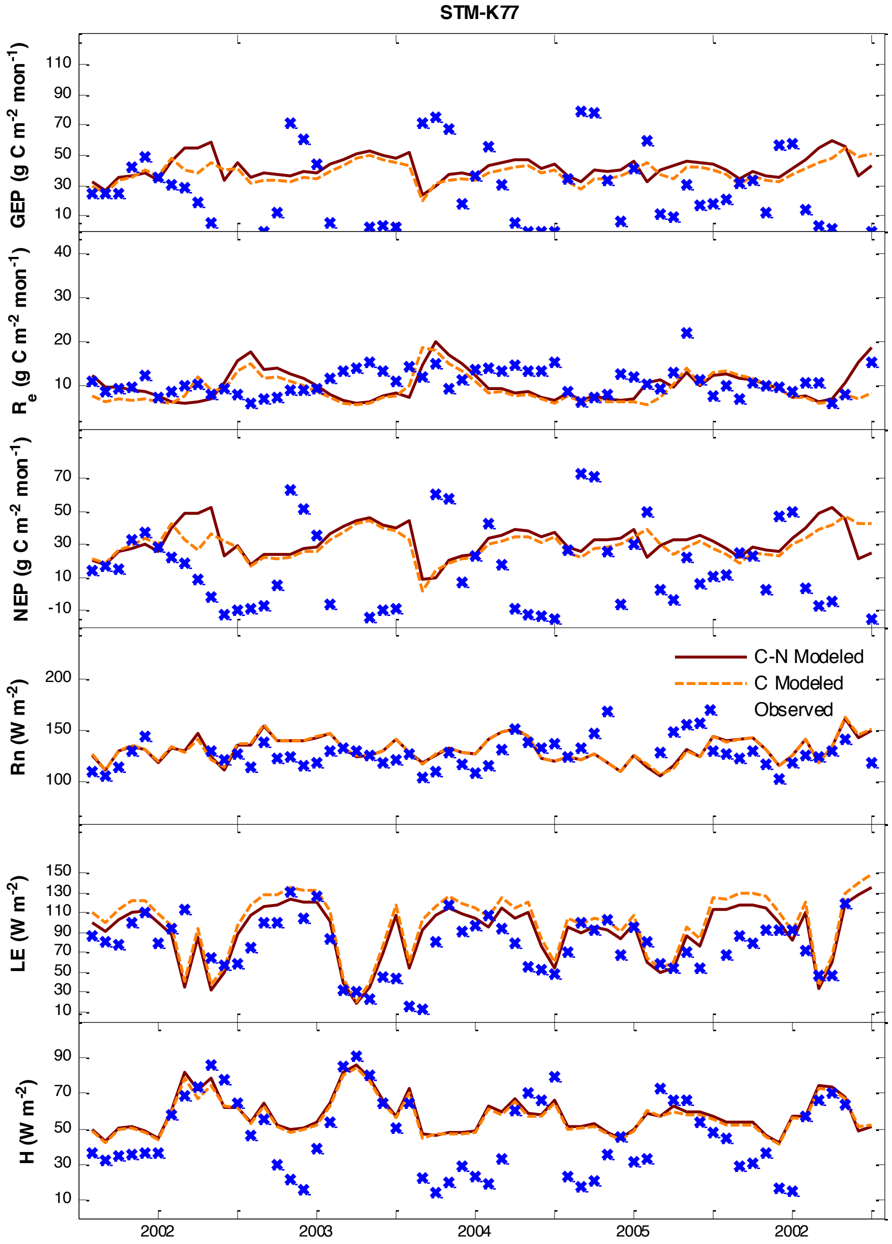

Figure 3.6 Monthly values of gross ecosystem productivity (GEP), ecosystem respiration (Re), net ecosystem productivity (NEP), net radiation (Rn), latent heat (LE) and sensible heat (H) fluxes from C-N coupled and C-only model and observations at K77 site from 2001 to 2005.

Table 3.4 Mean and standard deviations (SD) of daily C fluxes (GEP, Re and NEP, in kg C m^{-2} yr^{-1}) and of water and energy fluxes (Rn, LE and H, in W m^{-2}) from observations (Obs) and models (C-N coupled and C-only versions). RMSE and EI for both models are also given.

		Mean			**SD**			**RMSE**		**EI**	
		Obs	**C-N**	**C**	**Obs**	**C-N**	**C**	**CN**	**C**	**CN**	**C**
GEP	**K34**	7.15	8.77	9.34	2.01	1.88	1.92	3.11	3.39	-1.52	-2.04
	K67	8.11	9.73	10.30	1.21	1.88	1.88	2.67	3.05	-1.15	-1.85
	K83	7.02	8.42	8.88	1.46	1.47	0.84	2.65	2.54	-2.11	-7.79
	RJA	8.35	10.28	10.61	2.24	2.03	1.69	3.75	3.63	-2.40	-3.57
	K77	2.24	4.12	3.80	2.26	1.21	1.01	3.27	2.98	-6.54	-8.42
	FNS	6.26	7.96	7.37	1.93	2.60	2.14	3.54	3.07	-0.83	-1.00
	BAN	7.43	7.67	8.82	1.54	2.27	1.37	3.16	2.63	-0.91	-2.73
Re	**K34**	6.44	7.26	8.01	1.80	0.60	0.67	2.18	2.59	-11.07	-12.91
	K67	8.16	9.06	9.96	0.85	0.81	0.94	1.23	2.00	-1.34	-3.50
	K83	6.94	7.67	7.88	1.54	0.68	0.96	1.55	1.56	-4.19	-1.68
	RJA	7.06	8.57	8.68	1.47	1.01	1.01	2.34	2.41	-4.37	-4.67
	K77	1.08	0.98	0.88	1.11	0.38	0.35	1.10	1.11	-7.55	-8.95
	FNS	4.10	5.50	5.11	1.74	1.44	1.92	2.64	2.96	-2.34	-1.36
	BAN	4.43	4.74	5.35	1.15	1.31	1.51	1.54	1.90	-0.38	-0.56
NEP	**K34**	0.98	1.51	1.33	1.78	1.73	1.73	2.26	2.34	-0.45	-0.38
	K67	-0.03	0.67	0.34	1.31	2.02	1.98	2.14	1.99	-0.14	-0.04
	K83	0.07	0.75	1.00	1.70	1.61	1.13	2.21	2.03	-0.83	-2.16
	RJA	1.29	1.71	1.93	1.96	1.83	1.78	2.71	2.57	-1.25	-1.14
	K77	1.40	3.14	2.92	2.34	1.35	1.15	3.27	3.06	-5.28	-7.27
	FNS	2.18	2.46	2.26	1.93	2.83	3.06	3.03	3.56	-0.18	-0.28
	BAN	2.94	2.93	3.46	1.62	2.87	2.16	3.45	2.86	-0.38	-0.68
Rn	**K34**	141.98	134.16	134.15	58.46	38.45	38.44	65.86	65.86	-1.76	-1.76
	K67	127.01	131.08	130.93	33.43	31.15	31.13	24.22	24.20	0.40	0.40
	K83	129.12	132.15	132.12	33.64	29.42	29.41	39.35	39.34	-0.68	-0.69
	RJA	143.79	146.89	146.87	38.55	35.81	35.81	50.93	50.94	-1.03	-1.03
	K77	126.74	131.68	131.73	31.20	33.03	33.00	32.35	32.48	0.10	0.09
	FNS	123.16	121.00	121.09	34.08	29.86	29.90	32.87	32.84	-0.17	-0.17
	BAN	133.14	132.42	131.00	39.61	33.42	34.57	45.60	46.96	-0.86	-0.84
LE	**K34**	3.05	3.40	3.62	1.17	1.16	1.23	1.46	1.57	-0.53	-0.55
	K67	3.06	3.01	3.21	0.80	1.20	1.28	1.14	1.21	0.04	0.04
	K83	3.77	3.56	3.80	0.72	1.50	1.60	1.82	1.88	-0.23	-0.15
	RJA	2.71	2.26	2.42	0.85	1.22	1.30	1.49	1.50	-0.57	-0.42
	K77	2.69	3.17	3.48	1.31	1.80	1.97	1.69	1.92	0.07	0.01
	FNS	2.17	1.92	2.19	0.68	1.10	1.25	1.35	1.46	-0.46	-0.34
	BAN	3.47	3.06	3.67	0.90	0.98	1.42	1.39	1.64	-0.95	-0.26
H	**K34**	1.01	1.07	1.00	0.53	0.32	0.30	0.59	0.58	-2.15	-2.46
	K67	0.69	0.76	0.71	0.37	0.18	0.17	0.30	0.29	-1.62	-1.91
	K83	0.93	0.90	0.84	0.40	0.21	0.20	0.41	0.41	-3.18	-3.73
	RJA	0.81	0.88	0.83	0.50	0.21	0.20	0.53	0.52	-5.80	-6.36
	K77	1.62	2.03	1.99	0.91	0.59	0.57	0.83	0.81	-0.96	-1.00
	FNS	1.27	1.37	1.30	0.50	0.35	0.33	0.54	0.52	-1.39	-1.43
	BAN	1.06	1.15	1.24	0.50	0.50	0.36	0.72	0.66	-1.14	-2.58

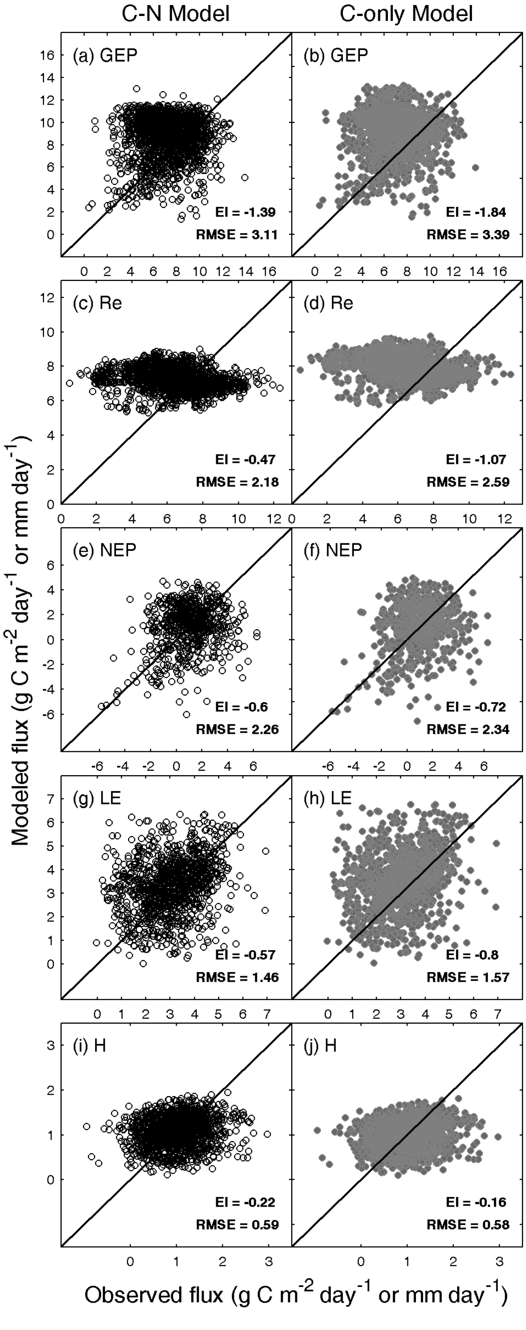

Figure 3.7 Daily mean values of gross ecosystem productivity (GEP), ecosystem respiration (Re), net ecosystem productivity (NEP), net radiation (Rn), latent heat (LE) and sensible heat (H) fluxes from C-N coupled model (a, c, e, g) and C-only model (b, d, f, h) versus observed values, at K34 site from 2000 to 2005. Solid line indicates 1:1 relationship.

Table 3.5 Simulated total vegetation biomass (Kg C m^{-2} yr^{-1}) and soil organic carbon (Kg C m^{-2}; 0-1 m) from C-N and C-only version of the model for each site and observed values.

	Vegetation Biomass			**Soil Carbon**		
	Obs	**C-N**	**C**	**Obs**	**C-N**	**C**
K34	20.3 ± 5.6[a]	18.77	19.34	12.7[a]	13.1	12.9
K67	16.6 ± 3.6[b]	10.62	10.50	12.1[a]	12.8	12.8
K83	19.9-21.8 ± 0.2[a,c]	18.49	18.88	7.8±1.1~11.2±1.3[d]	11.7	12.4
RJA	-	20.58	20.14	-	11.3	10.9
K77	-	1.12	1.68	-	8.2	8.1
FNS	-	1.96	2.37	10.0-12.0[e]; 10.0-10.8[f]	12.6	12.14
BAN	-	18.73	18.01	-	10.3	10.2

[a] (Malhi et al., 2009)
[b] (Saleska et al., 2003)
[c] (Miller et al., 2004)
[d] (Telles et al., 2003)
[e] (Fisher et al., 1994)
[f] (Trumbore et al., 1995)

3.4 Discussion

Our model results indicated that all Amazonia forest sites (K34, K67, K89, RJA and BAN) used in this study are a net sink of carbon (with positive NEP values), while the savanna-pasture site (FNS) is a minor net source of carbon (NEP = -0.04 kg C m^{-2} yr^{-1} by C-N and NEP = -0.02 kg C m^{-2} yr^{-1} by C versions, respectively) and the pasture-agricultural site (K77) is carbon neutral (NEP = 0.00 kg C m^{-2} yr^{-1}) to minor source of carbon (NEP = -0.01 kg C m^{-2} yr^{-1}). Based on the measured data, K67 site has a negative annual mean NEP compared to other tropical evergreen forest sites, which suggest that this site has released carbon during the study years (2002-2004, Table 3.2), and hence acted as a carbon source. The exceptional NEP at the K67 site than other tropical evergreen forest sites might be due to a shift in carbon allocation to wood production, largely because that this site is undergoing a transition after some mortality in 1990s (Malhi et al., 2009; Pyle et al., 2008; Saleska et al., 2003). Re-growing younger trees could have absorbed more carbon during the early stages of their life cycle (Delucia et al., 2007; Figueira et al., 2008). This is also indicated from the model estimated NEP for this site with smaller positive NEP values compared to other LBA forest sites. Another explanation for the simulated positive values than the measured negative NEP, might due to the model underestimated soil respiration (Table 3.3, Fig. 3.1). The pasture and savanna (FNS and BAN) and the pasture-agricultural (K77) sites have higher NEP (Table 3.3) mainly because of relatively higher GEP and lower Re. Moreover, the savanna and the pasture sites experience the long dry season and plants growing in such environmental conditions have larger efficiency to store carbon as they have less plant material to sustain compared to forests (Zhang et al., 2009). Also, the transition from dry to wet climate leads to an increase in plant respiration which may cause a decrease in forest NEP.

In our earlier studies at temperate and boreal forest sites, model results indicated that inclusion of nitrogen has exerted strong controls on productivity and respiration in the mid to high latitude PFTs, causing reduction in the biomass and soil C pools. However, in this study in tropical forests, our model results indicated a minor response to nitrogen limitation. An opposite response to nitrogen limitation was observed in tropical savanna, pasture and crop sites. This indicates that the sensitivity of tropical PFTs to nitrogen limitation is small or negligible and therefore ignoring nitrogen dynamics in simulations of ecosystem processes may not significantly affect model results or other processes compensate prevalent nitrogen limitation in tropical PFTs. Some studies corroborate that tropical biomes are phosphorus (P) limited (Harrington et al., 2001) and they do not respond strongly to nitrogen deposition (Lewis et al., 2009; Reay et al., 2008) and nitrogen is not the main limiting factor of growth (Cleveland et al., 2011). Our model, indicating a small nitrogen availability deficit for C uptake in tropical forests, whereby the N-cycle extension caused observed annual and seasonal GEP to be successfully reproduced and slightly improved by the C-N coupled model when compared to C-only version of the model.

Due to large uncertainties and limitations in both modeling and observation studies such as structural uncertainty, parameter uncertainty, input uncertainty and initial condition uncertainty in models (Martin Jung et al., 2007; Larocque et al., 2008; Liu et al., 2008; Wramneby et al., 2008) and uncertainty associated with the measurements such as flux partitioning uncertainty and gap-filling uncertainty (Wilson et al., 2002; Hollinger and Richardson, 2005; Ryan and Law, 2005; Suseela et al., 2012), it is difficult to accurately evaluate model results and therefore the impact of nitrogen limitation on carbon sink or source strength in tropical ecosystems. The representation of nitrogen limitation widely differs in global ecosystem models (R. Q. Thomas et al., 2013) and is a potential large determinant of divergences in predictions among them (Xia et al., 2013). Moreover, many aspects, such as the effects of direct and diffuse light, soil moisture and drought effect on GEP in tropical forests, are not fully understood. The large variation in nitrogen limitation responses within and between PFTs also dependent on forest age and historical nitrogen loads, which are site-specific and non-linear over time. It calls for a careful evaluation of nitrogen effects in tropical forests (Hietz et al., 2011). In our study, we didn't account for any disturbances (e.g. fire, insect outbreaks) due to limited input datasets. Global datasets on burned area should be a priority for future analysis on fire disturbances and emissions. Datasets on stand mortality and other forms of disturbance, including insect outbreaks, intense droughts, harvesting and hurricanes (Chambers et al., 2007) are also needed for modeling studies. These data would allow in detailed model intercomparison studies. Development of these datasets and model-data comparisons focused on these processes must be a high priority for the ecological research community (Masek et al., 2008). So far, modeling of carbon, water and energy dynamics with a comprehensive understanding of the nutrients cycling interactions in tropical forests remain a challenge for ecosystem modeler (Mercado et al., 2009; Restrepo-Coupe et al., 2013; van der Molen et al., 2011). Our study using CLASS-CTEM^{N+} model is one forward step in this direction.

This is first evaluation of CLASS-CTEM^{N+} model that includes plant and soil N over the Amazon region. This analysis quantifies strengths and weaknesses of the CLASS-CTEM^{N+} and helps to determine N-induced impacts on carbon and water exchanges in tropical ecosystems. Overall our study results showed reasonable accuracy when compared with observed eddy covariance flux and eco-physiological observations. Our results, in general, showed similar behavior when compared to other C-N coupled models in literature (Thomas et al., 2013; El-Masri et al., 2013; Mercado et al., 2009; Weber et al., 2009). This study also highlights the importance of the observed data to improve model performance in the Amazon region. Our results suggest that several improvements are needed to enhance the model capability for better performance in tropical biomes such as (1) adding more biome to represent heterogeneity in tropical PFTs (e.g. woody savanna); (2) adjusting temperature thresholds of GEP and respiration as suggested by Davidson and Janssens (2006) and Mahecha et al. (2010); (3) improving the representation of dynamic LAI simulation; (4) optimizing the litter production schemes and C allocation parameters for tropical forests to better capture the seasonal variability in C dynamics; and (5) developing parameterization or process algorithms to capture tropical forest's physiological response to extreme weather conditions (e.g., drought and high temperature). Adopting these steps in future studies would allow for a more thorough assessment of model uncertainties and development of more robust model to study carbon–climate feedbacks, in particular the responses of the vegetation ecosystems to climate variability and nutrient cycle feedbacks (Friedlingstein et al., 2006).

3.5 Conclusion

We used the CLASS-CTEM^{N+} model (both C-N and C-only versions) to simulate the carbon, water and energy dynamics for 7 Amazonia flux sites representing three different biome types (tropical forest, C4 pasture-agriculture, and savanna-pasture). We compared model results with flux measurements made by the Large Scale

Biosphere–Atmosphere Experiment in Amazonia (LBA) project. Our model results revealed reliable performance of simulated carbon, water and energy fluxes and carbon stocks by CLASS-CTEM^{N+} against measurements. Simulated daily mean NEP values showed that all forest sites were net sink of carbon, while pasture and agriculture sites were either neutral or net source of carbon. The inclusion of the nitrogen cycle in the model showed small but significant improvement in model capabilities to simulate carbon, water and energy fluxes in forest ecosystems, in particular for tropical evergreen broadleaf forests, while it had little impact on simulated fluxes for pasture and agricultural sites. This study gives us confidence that CLASS-CTEM^{N+} can predict carbon, water and energy fluxes and carbon stocks quite well in tropical ecosystems. This is fundamental for CLASS-CTEM^{N+}'s further application at regional and global scales for evaluating the impacts future climate change on terrestrial ecosystems and their feedbacks on Earth's climate system, thus, to provide reliable global carbon emissions estimates. Our results also highlighted the importance of long-term observed data sets to study changes in the vegetation and soil carbon biomass and impact of nitrogen cycling on these processes in tropical biomes.

Acknowledgements

Funding for this study was provided by the Natural Sciences and Engineering Research Council (NSERC) of Canada Discovery and Strategic grants and Ontario Ministry of Environment (MOE). Canadian Foundation of Innovation (CFI) and Ontario Innovation Trust (OIT) provided funds for computational facilities in our lab. Support from Environment Canada is acknowledged for CLASS and CTEM models. The data used in this study were provided by the Large Scale Biosphere-Atmosphere Experiment in Amazonia (LBA), an international research initiative lead by Brazil. We thank the scientists who collected tower observations during field campaigns under the LBA project, funded by NASA, the Brazilian Ministry of Science and Technology and European Agencies. We also thank the LBA-Data-Model-Intercomparison project funded by NASA's Terrestrial Ecology Program, which prepared the model input datasets that made this work possible. We acknowledge the work of many scientists from Environment Canada, who have contributed to the development of CLASS and CTEM models over the past many years. We acknowledge SHARCNET for providing computational faculties to make these simulations. We are thankful to Sergey Mashchenko at SHARCNET for his generous help and support.

3.6 Reference

Amthor, J., 2000. The McCree–de Wit–Penning de Vries–Thornley Respiration Paradigms: 30 Years Later. Ann. Bot. 86, 1–20. doi:10.1006/anbo.2000.1175

Amthor, J.S., 1984. The role of maintenance respiration in plant growth. Plant, Cell Environ. 7, 561–569. doi:10.1111/1365-3040.ep11591833

Andreae, M.O., 2002. Biogeochemical cycling of carbon, water, energy, trace gases, and aerosols in Amazonia: The LBA-EUSTACH experiments. J. Geophys. Res. 107, 8066. doi:10.1029/2001JD000524

Arain, M.A., Black, T.A., Barr, A.G., Jarvis, P.G., Massheder, J.M., Verseghy, D.L., Nesic, Z., 2002. Effects of seasonal and interannual climate variability on net ecosystem productivity of boreal deciduous and conifer forests. Can. J. For. Res. Can. Rech. For. 32, 878–891.

Arain, M.A., Yuan, F.M., Black, T.A., 2006. Soil-plant nitrogen cycling modulated carbon exchanges in a western temperate conifer forest in Canada. Agric. For. Meteorol. 140, 171–192.

Araújo, A.C., 2002. Comparative measurements of carbon dioxide fluxes from two nearby towers in a central Amazonian rainforest: The Manaus LBA site. J. Geophys. Res. 107, 8090. doi:10.1029/2001JD000676

Arora, V., 2002. Modeling vegetation as a dynamic component in soil-vegetation-atmosphere transfer schemes and hydrological models. Rev. Geophys. 40, 1006. doi:10.1029/2001RG000103

Arora, V.K., Boer, G.J., 2003. A representation of variable root distribution in dynamic vegetation models. Earth Interact. 7, 6–19.

Arora, V.K., Boer, G.J., 2005a. A parameterization of leaf phenology for the terrestrial ecosystem component of climate models. Glob. Chang. Biol. 11, 39–59.

Arora, V.K., Boer, G.J., 2005b. Fire as an interactive component of dynamic vegetation models. J. Geophys. Res. 110.

Arora, V.K., Boer, G.J., 2006. Simulating competition and coexistence between plant functional types in a dynamic vegetation model. Earth Interact. 10.

Arora, V.K., Boer, G.J., Christian, J.R., Curry, C.L., Denman, K.L., Zahariev, K., Flato, G.M., Scinocca, J.F., Merryfield, W.J., Lee, W.G., 2009. The Effect of Terrestrial Photosynthesis Down Regulation on the Twentieth-Century Carbon Budget Simulated with the CCCma Earth System Model. J. Clim. 22, 6066–6088. doi:doi:10.1175/2009JCLI3037.1

Asner, G.P., Knapp, D.E., Broadbent, E.N., Oliveira, P.J.C., Keller, M., Silva, J.N., 2005. Selective logging in the Brazilian Amazon. Science 310, 480–2. doi:10.1126/science.1118051

Asner, G.P., Townsend, A.R., Braswell, B.H., 2000. Satellite observation of El Niño effects on Amazon Forest phenology and productivity. Geophys. Res. Lett. 27, 981–984. doi:10.1029/1999GL011113

Asner, G.P., Townsend, A.R., Bustamante, M.M.C., 1999. Spectrometry of pasture condition and biogeochemistry in the central Amazon. Geophys. Res. Lett. 26, 2769–2772. doi:10.1029/1999GL900546

Avissar, R., 2002a. Preface to special issue on the Large-Scale Biosphere-Atmosphere Experiment in Amazonia (LBA). J. Geophys. Res. 107, 8034. doi:10.1029/2002JD002507

Avissar, R., 2002b. The Large-Scale Biosphere-Atmosphere Experiment in Amazonia (LBA): Insights and future research needs. J. Geophys. Res. 107, 8086. doi:10.1029/2002JD002704

Baker, I.T., Prihodko, L., Denning, A.S., Goulden, M., Miller, S., da Rocha, H.R., 2008. Seasonal drought stress in the Amazon: Reconciling models and observations. J. Geophys. Res. 113, G00B01. doi:10.1029/2007JG000644

Ball, J.T., Woodrow, I.E., Berry, J.A., 1987. A model predicting stomatal conductance and its contribution to the control of photosynthesis under different environmental conditions, Progress in Photosynthesis Research. Martinus-Nijhoff, Dordrecht, The Netherlands.

Beer, C., Reichstein, M., Tomelleri, E., Ciais, P., Jung, M., Carvalhais, N., Rodenbeck, C., Arain, M.A., Baldocchi, D., Bonan, G.B., Bondeau, A., Cescatti, A., Lasslop, G., Lindroth, A., Lomas, M., Luyssaert, S., Margolis, H., Oleson, K.W., Roupsard, O., Veenendaal, E., Viovy, N., Williams, C., Woodward, F.I., Papale, D., 2011. Terrestrial Gross Carbon Dioxide Uptake: Global Distribution and Covariation with Climate. Science (80-.). 329, 834–838. doi:10.1126/science.1184984

Borma, L.S., da Rocha, H.R., Cabral, O.M., von Randow, C., Collicchio, E., Kurzatkowski, D., Brugger, P.J., Freitas, H., Tannus, R., Oliveira, L., Rennó, C.D., Artaxo, P., 2009. Atmosphere and hydrological controls of the evapotranspiration over a floodplain forest in the Bananal Island region, Amazonia. J. Geophys. Res. 114, G01003. doi:10.1029/2007JG000641

Botta, A., 2002. Long-term variations of climate and carbon fluxes over the Amazon basin. Geophys. Res. Lett. 29, 1319. doi:10.1029/2001GL013607

Chambers, J.Q., Fisher, J.I., Zeng, H., Chapman, E.L., Baker, D.B., Hurtt, G.C., 2007. Hurricane Katrina's carbon footprint on U.S. Gulf Coast forests. Science 318, 1107. doi:10.1126/science.1148913

Chambers, J.Q., Santos, J. dos, Ribeiro, R.J., Higuchi, N., 2001. Tree damage, allometric relationships, and above-ground net primary production in central Amazon forest. For. Ecol. Manage. 152, 73–84. doi:10.1016/S0378-1127(00)00591-0

Christoffersen, B.O., Restrepo-Coupe, N., Arain, M.A., Baker, I.T., Cestaro, B.P., Ciais, P., Fisher, J.B., Galbraith, D., Guan, X., Gulden, L., van den Hurk, B., Ichii, K., Imbuzeiro, H., Jain, A., Levine, N., Miguez-Macho, G., Poulter, B., Roberti, D.R., Sakaguchi, K., Sahoo, A., Schaefer, K., Shi, M., Verbeeck, H., Yang, Z.-L., Araújo, A.C., Kruijt, B., Manzi, A.O., da Rocha, H.R., von Randow, C., Muza, M.N., Borak, J., Costa, M.H., Gonçalves de Gonçalves, L.G., Zeng, X., Saleska, S.R., 2014. Mechanisms of water supply and vegetation demand govern the seasonality and magnitude of evapotranspiration in Amazonia and Cerrado. Agric. For. Meteorol. 191, 33–50. doi:10.1016/j.agrformet.2014.02.008

Churkina, G., Trusilova, K., Vetter, M., Dentener, F., 2007. Contributions of nitrogen deposition and forest regrowth to terrestrial carbon uptake. Carbon Balance Manag. 2, 5. doi:10.1186/1750-0680-2-5

Cleveland, C.C., Townsend, A.R., Taylor, P., Alvarez-Clare, S., Bustamante, M.M.C., Chuyong, G., Dobrowski, S.Z., Grierson, P., Harms, K.E., Houlton, B.Z., Marklein, A., Parton, W., Porder, S., Reed, S.C., Sierra, C.A., Silver, W.L., Tanner, E.V.J., Wieder, W.R., 2011. Relationships among net primary productivity, nutrients and climate in tropical rain forest: a pan-tropical analysis. Ecol. Lett. 14, 939–47. doi:10.1111/j.1461-0248.2011.01658.x

Collatz, G., Ribas-Carbo, M., Berry, J., 1992. Coupled Photosynthesis-Stomatal Conductance Model for Leaves of C 4 Plants. Aust. J. Plant Physiol. 19, 519. doi:10.1071/PP9920519

Collatz, G.J., Ball, J.T., Grivet, C., Berry, J.A., 1991. Physiological and environmental regulation of stomatal conductance, photosynthesis and transpiration: a model that includes a laminar boundary layer. Agric. For. Meteorol. 54, 107–136. doi:10.1016/0168-1923(91)90002-8

Costa, M.H., Foley, J.A., 2000. Combined Effects of Deforestation and Doubled Atmospheric CO 2 Concentrations on the Climate of Amazonia. J. Clim. 13, 18–34. doi:10.1175/1520-0442(2000)013<0018:CEODAD>2.0.CO;2

Da Rocha, H.R., Goulden, M.L., Miller, S.D., Menton, M.C., Pinto, L.D.V.O., de Freitas, H.C., e Silva Figueira, A.M., 2004. Seasonality of water and heat fluxes over a tropical forest in Eastern Amazonia. Ecol. Appl. 14, 22–32. doi:10.1890/02-6001

Davidson, E.A., Janssens, I.A., 2006. Temperature sensitivity of soil carbon decomposition and feedbacks to climate change. Nature 440, 165–173.

Davidson, E.A., Reis de Carvalho, C.J., Vieira, I.C.G., Figueiredo, R. de O., Moutinho, P., Yoko Ishida, F., Primo dos Santos, M.T., Benito Guerrero, J., Kalif, K., Tuma Sabá, R., 2004. Nitrogen and Phosphorus limitation of biomass growth in a tropical secondary forest. Ecol. Appl. 14, 150–163. doi:10.1890/01-6006

De Gonçalves, L.G.G., Borak, J.S., Costa, M.H., Saleska, S.R., Baker, I., Restrepo-Coupe, N., Muza, M.N., Poulter, B., Verbeeck, H., Fisher, J.B., Arain, M.A., Arkin, P., Cestaro, B.P., Christoffersen, B., Galbraith, D., Guan, X., van den Hurk, B.J.J.M., Ichii, K., Imbuzeiro, H.M.A., Jain, A.K., Levine, N., Lu, C., Miguez-Macho, G., Roberti, D.R., Sahoo, A., Sakaguchi, K., Schaefer, K., Shi, M., Shuttleworth, W.J., Tian, H., Yang, Z.-L., Zeng, X., 2013. Overview of the Large-Scale Biosphere–Atmosphere Experiment in Amazonia Data Model Intercomparison Project (LBA-DMIP). Agric. For. Meteorol. 182-183, 111–127. doi:10.1016/j.agrformet.2013.04.030

De Moraes, J.F.L., Volkoff, B., Cerri, C.C., Bernoux, M., 1996. Soil properties under Amazon forest and changes due to pasture installation in Rondônia, Brazil. Geoderma 70, 63–81. doi:10.1016/0016-7061(95)00072-0

Delucia, E.H., Drake, J.E., Thomas, R.B., Gonzalez-Meler, M., 2007. Forest carbon use efficiency: is respiration a constant fraction of gross primary production? Glob. Chang. Biol. 13, 1157–1167. doi:10.1111/j.1365-2486.2007.01365.x

Dickinson, R.E., Shaikh, M., Bryant, R., Graumlich, L., 1998. Interactive Canopies for a Climate Model. J. Clim. 11, 2823–2836. doi:10.1175/1520-0442(1998)011<2823:ICFACM>2.0.CO;2

El-Masri, B., Barman, R., Meiyappan, P., Song, Y., Liang, M., Jain, A.K., 2013. Carbon dynamics in the Amazonian Basin: Integration of eddy covariance and ecophysiological data with a land surface model. Agric. For. Meteorol. 182, 156–167.

Farquhar, G.D., von Caemmerer, S., Berry, J.A., 1980. A biochemical model of photosynthetic CO2 assimilation in leaves of C 3 species. Planta 149, 78–90. doi:10.1007/BF00386231

Figueira, A.M. e S., Miller, S.D., de Sousa, C.A.D., Menton, M.C., Maia, A.R., da Rocha, H.R., Goulden, M.L., 2008. Effects of selective logging on tropical forest tree growth. J. Geophys. Res. 113, G00B05. doi:10.1029/2007JG000577

Fisher, M.J., Rao, I.M., Ayarza, M.A., Lascano, C.E., Sanz, J.I., Thomas, R.J., Vera, R.R., 1994. Carbon storage by introduced deep-rooted grasses in the South American savannas. Nature 371, 236–238. doi:10.1038/371236a0

Foley, J.A., Asner, G.P., Costa, M.H., Coe, M.T., DeFries, R., Gibbs, H.K., Howard, E.A., Olson, S., Patz, J., Ramankutty, N., Snyder, P., 2007. Amazonia revealed: forest degradation and loss of ecosystem goods and services in the Amazon Basin. Front. Ecol. Environ. 5, 25–32. doi:10.1890/1540-9295(2007)5[25:ARFDAL]2.0.CO;2

Foley, J.A., Botta, A., Coe, M.T., Costa, M.H., 2002. El Niño-Southern oscillation and the climate, ecosystems and rivers of Amazonia. Global Biogeochem. Cycles 16, 79–1–79–20. doi:10.1029/2002GB001872

Friedlingstein, P., Cox, P., Betts, R., 2006. Climate-carbon cycle feedback analysis: Results from the C4MIP model intercomparison. J. ….

Goulden, M.L., Miller, S.D., da Rocha, H.R., 2006. Nocturnal cold air drainage and pooling in a tropical forest. J. Geophys. Res. 111, D08S04. doi:10.1029/2005JD006037

Harrington, R.A., Fownes, J.H., Vitousek, P.M., 2001. Production and Resource Use Efficiencies in N- and P-Limited Tropical Forests: A Comparison of Responses to Long-term Fertilization. Ecosystems 4, 646–657. doi:10.1007/s10021-001-0034-z

Henderson-Sellers, A., Pitman, A.J., Love, P.K., Irannejad, P., Chen, T.H., 1995. The Project for Intercomparison of Land Surface Parameterization Schemes (PILPS): Phases 2 and 3. Bull. Am. Meteorol. Soc. 76, 489–503. doi:10.1175/1520-0477(1995)076<0489:TPFIOL>2.0.CO;2

Hietz, P., Turner, B.L., Wanek, W., Richter, A., Nock, C.A., Wright, S.J., 2011. Long-term change in the nitrogen cycle of tropical forests. Science 334, 664–6. doi:10.1126/science.1211979

Holland, E., Braswell, B., Lamarque, J.F., Townsend, A., Sulzman, J., J.-F, M., uuml, ller, 1997. Variations in the predicted spatial distribution of atmospheric nitrogen deposition and their impact on carbon uptake by terrestrial ecosystems. J. Geophys. Res.

Hollinger, D.Y., Richardson, A.D., 2005. Uncertainty in eddy covariance measurements and its application to physiological models. Tree Physiol. 25, 873–885. doi:10.1093/treephys/25.7.873

Houghton, J.T., Ding, Y., Griggs, D.J., Noguer, M., der Linden, P.J., Dai, X., Maskell, K., Johnson, C.A., 2001. 2001, Climate change 2001: The scientific basis: Contribution of Working Group I to the third assessment report of the Intergovernmental Panel on Climate Change.

Huang, S., Arain, M.A., Arora, V.K., Yuan, F., Brodeur, J., Peichl, M., 2011. Analysis of nitrogen controls on carbon and water exchanges in a conifer forest using the CLASS-CTEMN+ model. Ecol. Modell. 222, 3743–3760. doi:10.1016/j.ecolmodel.2011.09.008

Hutyra, L.R., Munger, J.W., Saleska, S.R., Gottlieb, E., Daube, B.C., Dunn, A.L., Amaral, D.F., de Camargo, P.B., Wofsy, S.C., 2007. Seasonal controls on the exchange of carbon and water in an Amazonian rain forest. J. Geophys. Res. 112, G03008. doi:10.1029/2006JG000365

Jarvis, P.G., 1976. The Interpretation of the Variations in Leaf Water Potential and Stomatal Conductance Found in Canopies in the Field. Philos. Trans. R. Soc. B Biol. Sci. 273, 593–610. doi:10.1098/rstb.1976.0035

Jung, M., Vetter, M., Herold, M., Churkina, G., Reichstein, M., Zaehle, S., Ciais, P., Viovy, N., Bondeau, A., Chen, Y., Trusilova, K., Feser, F., Heimann, M., 2007. Uncertainties of modeling gross primary productivity over Europe: A systematic study on the effects of using different drivers and terrestrial biosphere models. Global Biogeochem. Cycles 21, n/a–n/a. doi:10.1029/2006GB002915

Keller, M., Varner, R., Dias, J.D., Silva, H., Crill, P., de Oliveira, R.C., Asner, G.P., 2005. Soil–Atmosphere Exchange of Nitrous Oxide, Nitric Oxide, Methane, and Carbon Dioxide in Logged and Undisturbed Forest in the Tapajos National Forest, Brazil. Earth Interact. 9, 1–28. doi:10.1175/EI125.1

Kruijt, B., Elbers, J.A., von Randow, C., Araújo, A.C., Oliveira, P.J., Culf, A., Manzi, A.O., Nobre, A.D., Kabat, P., Moors, E.J., 2004. The robustness of eddy correlation fluxes for Amazon rain forest conditions. Ecol. Appl. 14, 101–113. doi:10.1890/02-6004

Larocque, G.R., Bhatti, J.S., Boutin, R., Chertov, O., 2008. Uncertainty analysis in carbon cycle models of forest ecosystems: Research needs and development of a theoretical framework to estimate error propagation. Ecol. Modell. 219, 400–412.

Laurance, W.F., 2001. ENVIRONMENT: The Future of the Brazilian Amazon. Science (80-.). 291, 438–439. doi:10.1126/science.291.5503.438

Leuning, R., Kelliher, F.M., Pury, D.G.G., Schulze, E.-D., 1995. Leaf nitrogen, photosynthesis, conductance and transpiration: scaling from leaves to canopies. Plant, Cell Environ. 18, 1183–1200.

Lewis, S.L., Lopez-Gonzalez, G., Sonke, B., Affum-Baffoe, K., Baker, T.R., Ojo, L.O., Phillips, O.L., Reitsma, J.M., White, L., Comiskey, J.A., K, M.-N.D., Ewango, C.E.N., Feldpausch, T.R., Hamilton, A.C., Gloor, M., Hart, T., Hladik, A., Lloyd, J., Lovett, J.C., Makana, J.-R., Malhi, Y., Mbago, F.M., Ndangalasi, H.J., Peacock, J., Peh, K.S.H., Sheil, D., Sunderland, T., Swaine, M.D., Taplin, J., Taylor, D., Thomas, S.C., Votere, R., Woll, H., 2009. Increasing carbon storage in intact African tropical forests. Nature 457, 1003–1006.

Liu, S., Anderson, P., Zhou, G., Kauffman, B., Hughes, F., Schimel, D., Watson, V., Tosi, J., 2008. Resolving model parameter values from carbon and nitrogen stock measurements in a wide range of tropical mature forests using nonlinear inversion and regression trees. Ecol. Modell. In Press, .

Loveland, T.R., Reed, B.C., Brown, J.F., Ohlen, D.O., Zhu, Z., Yang, L., Merchant, J.W., 2000. Development of a global land cover characteristics database and IGBP DISCover from 1 km AVHRR data. Int. J. Remote Sens. 21, 1303–1330. doi:10.1080/014311600210191

Luyssaert, S., Inglima, I., Jung, M., Richardson, A.D., Reichstein, M., Papale, D., Piao, S.L., Schulze, E.-D., Wingate, L., Matteucci, G., Aragao, L., Aubinet, M., Beer, C., Bernhofer, C., Black, K.G., Bonal, D., Bonnefond, J.M., Chambers, J., Ciais, P., Cook, B., Davis, K.J., Dolman, A.J., Gielen, B., Goulden, M., Grace, J., Grrnier, A., Gelle, A., Griffis, T., Grunwald, T., Guidolotti, G., Hanson, P.J., Harding, R., Hollinger, D.Y., Hutyra, L.R., Kolari, P., Kruijt, B., Kutsch, W., Lagergren, F., Laurila, T., Law, B.E., Le Maire, G., Lindroth, A., Loustau, D., Malhi, Y., Mateus, J., Migliavacca, M., Misson, L., Montagnani, L., Moncrieff, J., Moors, E., Munger, J.W., Nikinmaa, E., Ollinger, S. V., Pita, G., Rebmann, C., Roupsard, O., Saigusa, N., Sanz, M.J., Seufert, G., Sierra, C., Smith, M.-L., Tang, J., Valentini, R., Vesala, T., Janssens, I.A., 2007. CO2 balance of boreal, temperate, and tropical forests derived from a global database. Glob. Chang. Biol. 13, 2509–2537. doi:10.1111/j.1365-2486.2007.01439.x

Mahecha, M.D., Reichstein, M., Carvalhais, N., Lasslop, G., Lange, H., Seneviratne, S.I., Vargas, R., Ammann, C., Arain, M.A., Cescatti, A., Janssens, I. a, Migliavacca, M., Montagnani, L., Richardson, A.D., 2010. Global convergence in the temperature sensitivity of respiration at ecosystem level. Science 329, 838–40. doi:10.1126/science.1189587

Malhi, Y., Aragao, L.E.O.C., Metaclfe, D.B., Paiva, R., QUESADA, C.A., ALMEIDA, S., ANDERSON, L., BRANDO, P., CHAMBERS, J.Q., da COSTA, A.C.L., HUTYRA, L.R., OLIVEIRA, P., PATIÑO, S., PYLE, E.H., ROBERTSON, A.L., TEIXEIRA, L.M., 2009. Comprehensive assessment of carbon productivity, allocation and storage in three Amazonian forests. Glob. Chang. Biol. 15, 1255–1274. doi:10.1111/j.1365-2486.2008.01780.x

Malhi, Y., Grace, J., 2000. Tropical forests and atmospheric carbon dioxide. Trends Ecol. Evol. 15, 332–337. doi:10.1016/S0169-5347(00)01906-6

Masek, J.G., Huang, C., Wolfe, R., Cohen, W., Hall, F., Kutler, J., Nelson, P., 2008. North American forest disturbance mapped from a decadal Landsat record. Remote Sens. Environ. 112, 2914–2926. doi:10.1016/j.rse.2008.02.010

Meissner, K.J., Weaver, A.J., Matthews, H.D., Cox, P.M., 2003. The role of land surface dynamics in glacial inception: a study with the UVic Earth System Model. Clim. Dyn. 21, 515–537. doi:10.1007/s00382-003-0352-2

Melton, J.R., Arora, V.K., 2014. Sub-grid scale representation of vegetation in global land surface schemes: implications for estimation of the terrestrial carbon sink. Biogeosciences 11, 1021–1036. doi:10.5194/bg-11-1021-2014

Mercado, L.M., Lloyd, J., Dolman, A.J., Sitch, S., Patiño, S., 2009. Modelling basin-wide variations in Amazon forest productivity – Part 1: Model calibration, evaluation and upscaling functions for canopy photosynthesis. Biogeosciences 6, 1247–1272. doi:10.5194/bg-6-1247-2009

Miller, S.D., Goulden, M.L., da Rocha, H.R., 2007. The effect of canopy gaps on subcanopy ventilation and scalar fluxes in a tropical forest. Agric. For. Meteorol. 142, 25–34. doi:10.1016/j.agrformet.2006.10.008

Miller, S.D., Goulden, M.L., Menton, M.C., da Rocha, H.R., de Freitas, H.C., Figueira, A.M. e S., Dias de Sousa, C.A., 2004. Biometric and micrometeorological measurements of tropical forest carbon balance. Ecol. Appl. 14, 114–126. doi:10.1890/02-6005

Morton, D.C., DeFries, R.S., Shimabukuro, Y.E., Anderson, L.O., Del Bon Espírito-Santo, F., Hansen, M., Carroll, M., 2005. Rapid Assessment of Annual

Deforestation in the Brazilian Amazon Using MODIS Data. Earth Interact. 9, 1–22. doi:10.1175/EI139.1

Nadelhoffer, K.J., Emmett, B.A., Gundersen, P., Kjonaas, O.J., Koopmans, C.J., Schleppi, P., Tietema, A., Wright, R.F., 1999. Nitrogen deposition makes a minor contribution to carbon sequestration in temperate forests. Nature 398, 145–148.

Potter, C., Klooster, S., de Carvalho, C.R., Genovese, V.B., Torregrosa, A., Dungan, J., Bobo, M., Coughlan, J., 2001. Modeling seasonal and interannual variability in ecosystem carbon cycling for the Brazilian Amazon region. J. Geophys. Res. 106, 10423. doi:10.1029/2000JD900563

Poulter, B., Hattermann, F., Hawkin, E., Zaehle, S., Sitch, S., Restrepo-Coupe, N., Heyder, U., Cramer, W., 2010. Robust dynamics of Amazon dieback to climate change with perturbed ecosystem model parameters. Glob. Chang. Biol. doi:10.1111/j.1365-2486.2009.02157.x

Pyle, E.H., Santoni, G.W., Nascimento, H.E.M., Hutyra, L.R., Vieira, S., Curran, D.J., van Haren, J., Saleska, S.R., Chow, V.Y., Carmago, P.B., Laurance, W.F., Wofsy, S.C., 2008. Dynamics of carbon, biomass, and structure in two Amazonian forests. J. Geophys. Res. 113, G00B08. doi:10.1029/2007JG000592

Ramankutty, N., GIBBS, H.K., ACHARD, F., DEFRIES, R., FOLEY, J.A., HOUGHTON, R.A., 2007. Challenges to estimating carbon emissions from tropical deforestation. Glob. Chang. Biol. 13, 51–66. doi:10.1111/j.1365-2486.2006.01272.x

Reay, D.S., Dentener, F., Smith, P., Grace, J., Feely, R.A., 2008. Global nitrogen deposition and carbon sinks. Nat. Geosci 1, 430–437.

Restrepo-Coupe, N., da Rocha, H.R., Hutyra, L.R., da Araujo, A.C., Borma, L.S., Christoffersen, B., Cabral, O.M.R., de Camargo, P.B., Cardoso, F.L., da Costa, A.C.L., Fitzjarrald, D.R., Goulden, M.L., Kruijt, B., Maia, J.M.F., Malhi, Y.S., Manzi, A.O., Miller, S.D., Nobre, A.D., von Randow, C., Sá, L.D.A., Sakai, R.K., Tota, J., Wofsy, S.C., Zanchi, F.B., Saleska, S.R., 2013. What drives the seasonality of photosynthesis across the Amazon basin? A cross-site analysis of eddy flux tower measurements from the Brasil flux network. Agric. For. Meteorol. 182-183, 128–144. doi:10.1016/j.agrformet.2013.04.031

Rogers, A., 2014. The use and misuse of V(c,max) in Earth System Models. Photosynth. Res. 119, 15–29. doi:10.1007/s11120-013-9818-1

Ryan, M.G., Gower, S.T., Hubbard, R.M., Waring, R.H., Gholz, H.L., Cropper, W.P., Running, S.W., 1995. Woody tissue maintenance respiration of four conifers in contrasting climates. Oecologia 101, 133–140. doi:10.1007/BF00317276

Ryan, M.G., Law, B.E., 2005. Interpreting, measuring, and modeling soil respiration. Biogeochemistry 73, 3–27. doi:10.1007/s10533-004-5167-7

Sakai, R.K., Fitzjarrald, D.R., Moraes, O.L.L., Staebler, R.M., Acevedo, O.C., Czikowsky, M.J., Silva, R. da, Brait, E., Miranda, V., 2004. Land-use change effects on local energy, water, and carbon balances in an Amazonian agricultural field. Glob. Chang. Biol. 10, 895–907. doi:10.1111/j.1529-8817.2003.00773.x

Saleska, S.R., Didan, K., Huete, A.R., da Rocha, H.R., 2007. Amazon forests green-up during 2005 drought. Science 318, 612. doi:10.1126/science.1146663

Saleska, S.R., Miller, S.D., Matross, D.M., Goulden, M.L., Wofsy, S.C., da Rocha, H.R., de Camargo, P.B., Crill, P., Daube, B.C., de Freitas, H.C., Hutyra, L., Keller, M., Kirchhoff, V., Menton, M., Munger, J.W., Pyle, E.H., Rice, A.H., Silva, H., 2003. Carbon in Amazon forests: unexpected seasonal fluxes and disturbance-induced losses. Science 302, 1554–7. doi:10.1126/science.1091165

Suseela, V., Conant, R.T., Wallenstein, M.D., Dukes, J.S., 2012. Effects of soil moisture on the temperature sensitivity of heterotrophic respiration vary seasonally in an old-field climate change experiment. Glob. Chang. Biol. 18, 336–348. doi:10.1111/j.1365-2486.2011.02516.x

Telles, E. de C.C., de Camargo, P.B., Martinelli, L.A., Trumbore, S.E., da Costa, E.S., Santos, J., Higuchi, N., Oliveira, R.C., 2003. Influence of soil texture on carbon dynamics and storage potential in tropical forest soils of Amazonia. Global Biogeochem. Cycles 17, n/a–n/a. doi:10.1029/2002GB001953

Thomas, R.Q., Bonan, G.B., Goodale, C.L., 2013. Insights into mechanisms governing forest carbon response to nitrogen deposition: a model–data comparison using observed responses to nitrogen addition. Biogeosciences 10, 3869–3887. doi:10.5194/bg-10-3869-2013

Thornton, P.E., Lamarque, J.-F., Rosenbloom, N.A., Mahowald, N.M., 2007. Influence of carbon-nitrogen cycle coupling on land model response to CO2 fertilization and climate variability. Glob. Biogeochem. Cycles 21.

Tian, H., Melillo, J.M., Kicklighter, D.W., McGuire, A.D., Helfrich, J.V.K.., Moore, B., Vorosmarty, C.J., 1998. Effect of interannual climate variability on carbon storage in Amazonian ecosystems 396, 664–667. doi:10.1038/25328

Trumbore, S.E., Davidson, E.A., Barbosa de Camargo, P., Nepstad, D.C., Martinelli, L.A., 1995. Belowground cycling of carbon in forests and pastures of eastern Amazonia. Global Biogeochem. Cycles 9, 515–528. doi:10.1029/95GB02148

Van der Molen, M.K., van den Hurk, B.J.J.M., Hazeleger, W., 2011. A dampened land use change climate response towards the tropics. Clim. Dyn. 37, 2035–2043. doi:10.1007/s00382-011-1018-0

Verseghy, D.L., 1991. CLASS--A Canadian Land Surface Scheme for GCMS: I. Soil Model Int. J. Climatol. 11, 111–133.

Verseghy, D.L., 2000. The Canadian land surface scheme (CLASS): Its history and future. Atmosphere-Ocean 38, 1–13. doi:10.1080/07055900.2000.9649637

Verseghy, D.L., Lazare, M., 1993. CLASS-Canadian land surface scheme for GCMS, II. Vegetation model and coupled runs. Int. J. Climatol. 13, 347–370.

Von Randow, C., Manzi, A.O., Kruijt, B., de Oliveira, P.J., Zanchi, F.B., Silva, R.L., Hodnett, M.G., Gash, J.H.C., Elbers, J.A., Waterloo, M.J., Cardoso, F.L., Kabat, P., 2004. Comparative measurements and seasonal variations in energy and carbon exchange over forest and pasture in South West Amazonia. Theor. Appl. Climatol. 78. doi:10.1007/s00704-004-0041-z

Von Randow, C., Zeri, M., Restrepo-Coupe, N., Muza, M.N., de Gonçalves, L.G.G., Costa, M.H., Araujo, A.C., Manzi, A.O., da Rocha, H.R., Saleska, S.R., Arain, M.A., Baker, I.T., Cestaro, B.P., Christoffersen, B., Ciais, P., Fisher, J.B., Galbraith, D., Guan, X., van den Hurk, B., Ichii, K., Imbuzeiro, H., Jain, A., Levine, N., Miguez-Macho, G., Poulter, B., Roberti, D.R., Sahoo, A., Schaefer, K., Shi, M., Tian, H., Verbeeck, H., Yang, Z.-L., 2013. Inter-annual variability of carbon and water fluxes in Amazonian forest, Cerrado and pasture sites, as simulated by terrestrial biosphere models. Agric. For. Meteorol. 182-183, 145–155. doi:10.1016/j.agrformet.2013.05.015

Wania, R., Meissner, K.J., Eby, M., Arora, V.K., Ross, I., Weaver, A.J., 2012. Carbon-nitrogen feedbacks in the UVic ESCM. Geosci. Model Dev. 5, 1137–1160. doi:10.5194/gmd-5-1137-2012

Weber, U., Jung, M., Reichstein, M., Beer, C., Braakhekke, M.C., Lehsten, V., Ghent, D., Kaduk, J., Viovy, N., Ciais, P., Gobron, N., Rödenbeck, C., 2009. The interannual variability of Africa's ecosystem productivity: a multi-model analysis. Biogeosciences 6, 285–295. doi:10.5194/bg-6-285-2009

White, M.A., Thornton, P.E., Running, S.W., Nemani, R.R., 2000. Parameterization and Sensitivity Analysis of the BIOME–BGC Terrestrial Ecosystem Model: Net Primary Production Controls. Earth Interact. 4, 1–85. doi:10.1175/1087-3562(2000)004<0003:PASAOT>2.0.CO;2

Williams, M., Shimabukuro, Y.E., Herbert, D.A., Pardi Lacruz, S., Renno, C., Rastetter, E.B., 2002. Heterogeneity of Soils and Vegetation in an Eastern Amazonian Rain Forest: Implications for Scaling Up Biomass and Production. Ecosystems 5, 692–704. doi:10.1007/s10021-002-0165-x

Wilson, K., Goldstein, A., Falge, E., Aubinet, M., Baldocchi, D., Berbigier, P., Bernhofer, C., Ceulemans, R., Dolman, H., Field, C., Grelle, A., Ibrom, A., Law, B.., Kowalski, A., Meyers, T., Moncrieff, J., Monson, R., Oechel, W., Tenhunen, J., Valentini, R., Verma, S., 2002. Energy balance closure at FLUXNET sites. Agric. For. Meteorol. 113, 223–243. doi:10.1016/S0168-1923(02)00109-0

Wramneby, A., Smith, B., Zaehle, S., Sykes, M.T., 2008. Parameter uncertainties in the modelling of vegetation dynamics--Effects on tree community structure and ecosystem functioning in European forest biomes. Ecol. Modell. 216, 277–290.

Xia, J., Luo, Y., Wang, Y.-P., Hararuk, O., 2013. Traceable components of terrestrial carbon storage capacity in biogeochemical models. Glob. Chang. Biol. 19, 2104–16. doi:10.1111/gcb.12172

Yuan, F., McCaughey, H., Wofsy, S.C., 2008. Modeling analysis of primary controls on net ecosystem productivity of seven boreal and temperate coniferous forests across a continental transect. Glob. Chang. Biol. 14, 1765–1784.

Zhang, Y., Xu, M., Chen, H., Adams, J., 2009. Global pattern of NPP to GPP ratio derived from MODIS data: effects of ecosystem type, geographical location and climate. Glob. Ecol. Biogeogr. 18, 280–290. doi:10.1111/j.1466-8238.2008.00442.x

4. CHAPTER 4: An Analysis of Global Terrestrial Carbon, Water and Energy Dynamics Using Carbon-Nitrogen Coupled CLASS-CTEM^{N+} Model

Suo Huang[1], M. Altaf Arain[1, *], Vivek Arora[2], Paul Bartlett[3], Diana Verseghy[3]

[1]School of Geography and Earth Sciences and McMaster Centre for Climate Change, McMaster University, Hamilton, Ontario, Canada

[2]Canadian Centre for Climate Modelling and Analysis, Environment Canada, Victoria, BC, Canada.

[3]Climate Processes Section, Environment Canada, Toronto, ON, M3H 5T4 Canada

* **Corresponding Author:** M. Altaf Arain, School of Geography and Earth Sciences, McMaster University, 1280 Main Street West, Hamilton, Ontario, L8S 4K1, Canada, Phone: 1-905-525-9140 Ext. 27941, Fax: 905-546-0463; Email: arainm@mcmaster.ca

4.0 Abstract

A dynamic vegetation model CLASS-CTEM^{N+} with coupled Carbon-Nitrogen (C-N) cycles was used to simulate terrestrial carbon, water and energy dynamics at the global scale at 0.5-degree spatial resolution from 1901 to 2010. Forcing and initializing data sets developed by the North American Carbon Program (NACP)-Multi-Scale Synthesis and Terrestrial Model Intercomparison Project (MsTMIP) were used. Simulations were also performed using the carbon-only (C) version of the model. Comparison of coupled carbon-nitrogen (C-N) and C-only (C) versions of the model helped to assess the impact of carbon-nitrogen interactions on the spatio-temporal patterns of terrestrial carbon behavior. This model has been assessed against observation-based flux data from the global FLUXNET for a range of eddy covariance (EC) tower sites.

At the global scale, the simulated values of C, water and energy fluxes and C pools compared well with the observation-based estimates. C-N coupled model simulated global total mean annual estimates of Gross Ecosystem Production (GEP, 122.7 Pg C yr^{-1}), Ecosystem Respiration (Re, 119.1 Pg C yr^{-1}), Net Ecosystem Productivity (NEP, 3.64 Pg C yr^{-1}), Net Primary Productivity (NPP, 62.7 Pg C yr^{-1}), Latent Heat (LE, 146.2 ZJ yr^{-1}), Sensible Heat Flux (H, 194.0 ZJ yr^{-1}), Soil Organic Carbon (SOC, 1230.0 Pg C) and Total Vegetation Biomass (Tvg, 608.0 Pg C) over 1980-2010 period are similar to estimates reported in other studies. Simulated GEP values from C-N coupled and C-only models were 122.7 and 128.2 Pg C yr^{-1}, respectively, compared to 113.0 to 131.0 Pg C yr^{-1} from observations over the 1980-2010 period. However, on regional scales, the C-N coupled and C-only models showed larger differences, especially in high latitude regions during summer months, where N is limiting. Analysis of the long-term annual variations over the 1901-2010 period also showed different responses of two models to evolving climate, CO_2 and N deposition. For the 1970-2010 period, the C-N coupled model indicated a strong N constraint on the rate of increase of GEP and NPP compared to the C-only model.

The results indicated that compared to the C-only model, the C-N interactions in the C-N coupled model influenced the spatial distribution of carbon uptake and loss, with greater carbon uptake occurring at high latitudes in response to climate change and smaller carbon uptake occurring in the southern ecosystems and tropical forests in response to climate, CO_2 and N forcings. This study helped to identify and diagnose the impact of N controls on the simulated spatio-temporal patterns of terrestrial C sinks and sources; and to evaluate and quantify the variability of simulated N effects on different plant functional types.

4.1 INTRODUCTION

Terrestrial ecosystems play an important role in regulating Earth's climate through their biogeophysical and biogeochemical responses and feedbacks that affect the carbon (C), water and energy exchanges between the land surface and the atmosphere. Terrestrial ecosystems currently remove approximately 25 percent of annual anthropogenic fossil fuel carbon dioxide (CO_2) emissions (Keeling et al., 1996). However, recent changes in climate due to increased atmospheric CO_2 concentration, mostly caused by fossil fuel burning, land use changes (LUC), fertilizer application and enhanced atmospheric nitrogen (N) deposition are altering the carbon dynamics of the terrestrial ecosystems (Nadelhoffer et al., 1999; McGuire et al., 2001; Holland et al., 2005; Denman 2007; Reay et al., 2008).

There is growing evidence that N availability constraints and interactions with C cycle is an important factor that affects the response of terrestrial ecosystems to climate and CO_2 forcings (Canadell et al. 2007; Gerber et al. 2010; Zaehle et al. 2010; Bonan & Levis 2010; Hungate et al. 2003; Luo et al. 2004). Observations from Free-Air Concentration Enrichment (FACE) experiments suggest that terrestrial ecosystems grown under elevated CO_2 require more N to support enhanced plant growth than is required at ambient CO_2 (Luo et al., 2006). Warmer and wetter soils have the potential to increase the amount of inorganic N in soil through enhanced mineralization associated with decomposition. The improved N availability in soil may lead to enhanced soil microbial activity, which generally increases plant-available N in addition to meeting the N needs of soil organisms. The enhanced mineralization of soil N associated with accelerated decomposition in warmer soils has the potential to enhance the uptake of CO_2 by vegetation more than the loss of CO_2 from the decomposition due to warmer temperatures (McGuire et al., 2007; Shaver, 1992).

There has been a large increase in atmospheric N deposition in some regions that have been typically N limited, causing an increase in C uptake in these areas (Holland et al. 1997; Nadelhoffer et al. 1999; Davidson et al. 2004; Churkina et al. 2007; Thornton et al. 2007). The processes that directly or indirectly affect the response of terrestrial C storage to increased CO_2 concentration operate on a wide range of time scales. The impact of elevated CO_2 on C and N dynamics derived from short-time-scale experiments i.e., less than 5 years, may therefore not be adequate to evaluate the long-term impacts.

Process-based terrestrial ecosystem models (TEMs) or dynamic global vegetation models (DGVMs), with their associated land surface schemes, are capable of projecting changes in C exchanges in terrestrial ecosystems over multiple time scales. Some of these models have also been implemented in the Earth System Models (ESMs) used to simulate future climate changes. Several recent studies using TEMs and DGVMs highlight the importance of integrating N dynamics in regulating the response of terrestrial C cycle to increasing atmospheric CO_2 and climate change (Sokolov et al., 2008; Thornton et al., 2009, 2007a). Thornton et al. (2007) showed that N availability strongly constrains the CO_2 fertilization effect on plant productivity under increasing atmospheric CO_2. In their simulations that did not consider C-N interactions, they found that global warming always reduces terrestrial C storage. However, when C-N interactions were included, they found that their simulated terrestrial C storage actually increased with moderate increase in temperature. It has been shown that the consideration of N dynamics in C cycle studies, may change the sign of the carbon-climate feedback (Sokolov et al., 2008; Thornton et al., 2009). Despite the close coupling of C and N cycles and the significance of N dynamics in terrestrial C cycle, only few terrestrial ecosystem models have incorporated the N dynamics (Sokolov et al., 2008; Jain et al., 2009; Bonan and Levis, 2010; Zaehle et al., 2010; Zaehle and Dalmonech, 2011). These models are unable to account for N feedback on terrestrial C uptakes.

Here, we use a C-N coupled dynamic vegetation model, CLASS-CTEM^{N+} (Huang et al., 2011) to investigate the global dynamics of C, water and energy fluxes and C pools over the 1901-2010 at 0.5 degree resolution. The main goal of this study was to analyze the interactions of the terrestrial C and N cycles at regional and global scales and to explore the impact of N cycle feedbacks on spatial and temporal variability of primary carbon pools and fluxes. The specific objectives of this study are (1) to assess the performance of CLASS-CTEM^{N+} in simulating regional and global spatiotemporal patterns of C, water and energy budgets; (2) to identify and diagnose the impact of N controls on the simulated spatiotemporal patterns of terrestrial C sinks and sources; and (3) to evaluate and quantify the effect of C-N interactions on different plant functional types (PFTs). To achieve these objectives, two versions of the model, a C and N coupled (C-N) version and a carbon-only (C) version, were employed. Section 2 of this paper describes the data and the methods used; section 3 describes the results and the specific findings, and uncertainties; limitations of the study are discussed in section 4, and finally conclusions are presented in section 5.

4.2 METHODS

4.2.1 Model

The CLASS-CTEM^{N+} model is a DGVM derived from two different existing models: Canadian Land Surface Scheme (CLASS) (Verseghy 1991; Verseghy et al. 1993; Versegey 2000) and the Canadian Terrestrial Ecosystem Model (CTEM) (Arora & Boer 2003; Arora & Boer 2005a and b; Arora & Boer 2006), with a newly incorporated representation of soil-plant nitrogen (N) cycling algorithms (Arain et al. 2006; Yuan et al. 2008; Huang et al. 2011).

4.2.1.1 CLASS Model

The CLASS was originally developed by the Meteorological Service of Canada, Environment Canada for implementation in the Canadian global and regional climate models (Verseghy et al., 1993; Verseghy, 2009, 2000, 1991). CLASS was originally designed with a composite canopy, composed of amalgamated properties of up to four vegetation classes (needleleaf trees, broadleaf trees, crops and grass) plus urban areas. The grid-cell is also divided into vegetated and bare soil fractions, each with and without snow cover, which are treated separately. Beginning with version 3.0, a full mosaic is able to represent different surfaces in distinct patches or tiles. There are three soil layers (with depths of 0.1, 0.25, and 3.75 m), a variable depth of snow layer where applicable, a single vegetation canopy layer (which intercepts both rain and snow), prognostic soil temperatures, liquid and frozen soil moisture contents, and soil surface properties (e.g. surface roughness heights and surface albedo) which are functions of soil moisture and the soil and vegetation types. The radiation subroutine calculates the visible, near infrared (NIR), and long-wave radiation absorbed by the canopy. The absorption of visible and NIR radiation is based on vegetation-dependent visible and NIR albedo and transmissivity, while net long-wave radiation absorbed by the canopy is based on sky-view factor, which describes the degree of the canopy closure. The original canopy conductance parameterization used in CLASS was similar to that of the Jarvis model (Jarvis, 1976), where canopy resistance (r_c) is expressed as a function of minimum stomatal resistance and a series of environmental dependences whose effects are assumed to be multiplicative. Later, two leaf (sunlit and shaded) C and soil-plant N cycle modules were incorporated into CLASS and those versions of the model are known as C-CLASS and CN-CLASS, respectively (Arain et al., 2006; 2002).

4.2.1.2 CTEM Model

The CTEM is a dynamic vegetation model developed at the Canadian Centre for Climate Modelling and Analysis (CCCMa), Environment Canada in Victoria, British Columbia, Canada under a joint university-government effort as part of the Canadian Global Coupled Climate-Carbon Model (CGC3M) network for coupling with the CGCM. CTEM includes most of the terrestrial ecosystem processes including photosynthesis, plant and soil respiration, plant phenology, allocation, biomass turnover, litterfall, mortality, fire and competition between nine plant functional types (PFTs). The photosynthesis sub-module of the CTEM is based on the biochemical model of Farquhar and Collatz (Farquhar et al. 1980; Collatz et al. 1991; Collatz et al. 1992). The model has an option of 'big-leaf' or 'sunlit/shaded-leaf' photosynthesis with coupling between photosynthesis and canopy conductance (Leuning et al., 1995). Radiation interception includes explicit treatment of sunlit and shaded parts of leaves separately, while accounting for the differences in C_3 and C_4 pathways, as well as an analytical solution for vertical canopy gradients of specific leaf area. The photosynthesis or gross ecosystem productivity (GEP) and autotrophic respiration (Ra) and heterotrophic respiration (Rh) sub-modules of the CTEM, as described in Arora (2003), are used to calculate net primary productivity (NPP) and net ecosystem productivity (NEP). NPP is allocated to leaves, stem, and roots depend on water availability, light limitation and leaf phenological status. Prognostic leaf area index (LAI) is then determined from the leaf C and a vertical gradient of specific leaf area (SLA) (Dickinson et al., 1998). Root distribution follows the exponential decline with depth (Arora and Boer, 2003). The phenology sub-module of CTEM is based on 9 plant functional types (PFTs), using a carbon-gain approach. Leaf onset is initiated when it is beneficial for the plant, in C terms, to produce new leaves. Leaf offset is initiated by unfavorable environmental conditions, including shorter day length, cooler temperatures, and low soil moisture (Arora and Boer, 2005a). The whole seasonal phenological cycle is prognostically calculated without any prescribed dates or use of satellite data. Mortality rates of leaves, wood, and fine and coarse roots are PFTs dependent and generate a flow of C into leaf, coarse woody debris, and fine root litter pools. C flow in litter and soil organic matter pools and Rh vary with soil temperature and soil moisture and tissue chemistry. Altogether there are three living vegetation pools (leaves, stem, and root) and two dead carbon pools (litter and soil organic carbon). Soil C reservoir contains two pools: fast or short-lived soil organic matter (FOM) and stable soil organic matter (SOM), with turnover times ranging from days to centuries. A primary prognostic treatment of fire is also included in the model (Arora and Boer, 2005b). CTEM did not include N cycle, and the effects of nutrient limitation on photosynthesis were not modeled explicitly. Recently, a representation of the soil-plant nitrogen cycle was introduced into the coupled CLASS-CTEM model, which is known as the CLASS-CTEM^{N+} as described below (Huang et al., 2011).

4.2.1.3 CLASS-CTEM^{N+} Model

The CLASS-CTEM^{N+} model used in this study is fully prognostic with respect to the principal processes of the terrestrial C, water and energy cycles (Huang et al., 2011). The CLASS-CTEM^{N+} includes a prognostic representation of leaf N concentration, which determines the rate of photosynthesis. This implies that in the case of N deficiency, leaf N concentrations will decrease and reduce photosynthesis rates and hence GEP. Plant N cycle processes are incorporated into the model through root N uptake, plant N allocation and N controls on photosynthetic capacity. The maximum carboxylation capacity of Rubisco (V_{cmax}) is determined nonlinearly from the modeled leaf Rubisco-nitrogen, so called V_{cmaxN}. Variations in plant C assimilation and stomatal conductance are linked with leaf N status through the Rubisco enzyme. The N uptake rate can be enhanced or limited by plant growth, depending on N demand and non-structural storage capacity. The calculation of Ra is also affected by the N content status of the leaf, stem and root on which Ra depend. In the C-only version of the model the N content of plant tissues was derived allometrically. Apart from plant litterfall, the model has three other means of adding inorganic N to the soil–plant ecosystem: (i) bio-fixation; (ii) atmospheric deposition (wet and dry); and (iii) N fertilization (organic or inorganic); and N losses through leaching and disturbances (e.g. fire, harvest), as well as gaseous-N emissions. N also influences litter decomposition processes, leading to faster decomposition under higher soil mineral N concentrations. Soil N-cycle processes in CLASS-CTEM^{N+} includes immobilization, mineralization, nitrification, denitrification, volatilization, leaching, disturbance losses, and gaseous emissions of nitrogen dioxide (N_2O) and nitrous oxide (NO).

Overall, the CLASS-CTEM^{N+} contains five C pools (leaves, stem, root, litter and soil organic carbon) and seven N pools (leaves, stem, root, litter, soil ammonium (NH_4^+) and nitrate (NO_3^-)). Plant storage pools allow C and N acquired in one growing season to be retained and then distributed as new growth in subsequent years. Allocation to, and respiratory losses and litter from the three vegetation components (leaves, stem, and root) result in time-varying biomasses that are reflected in the structural vegetation attributes used in the energy and water balance calculations of the CLASS (Arora and Boer, 2005a). CTEM has 9 PFTs as listed in Table 4.1 (Arora and Boer, 2003). In CLASS-CTEM^{N+}, while CTEM simulates vegetation attributes of all its PFTs separately (including LAI, vegetation height, fraction of roots in each layer and canopy mass) these attributes are lumped as per Table 4.1 before they are passed into CLASS. Additionally, vegetation and soil hydrology parameterizations were modified to improve evapotranspiration partitioning and to reduce photosynthetic uptake bias in rainforest areas in the Amazon region.

Energy and water exchanges estimated by CLASS operate at half-hourly (or hourly) time step to provide boundary conditions (including soil moisture and temperature) for biogeochemistry models of CLASS-CTEM^{N+}. Except photosynthesis, which operates at half-hourly (or hourly) time step, all other sub-modules of CTEM operate at a daily time step. The plant and soil N algorithms are adapted at daily time step as well.

4.2.2 Data

Model input data including climate forcing (downward shortwave and longwave radiation, air temperature, specific humidity, wind speed, atmospheric pressure and precipitation), soil and geophysical initial conditions, nitrogen inputs, land cover classification were obtained for 110 years (1901–2010) at 0.5° × 0.5° grid resolution from the observation-constrained CRU-NCEP v4 dataset (Viovy et al. 2012) processed by the North American Carbon Program (NACP) - Multi-Scale Synthesis and Terrestrial Model Intercomparison Project (MsTMIP) (Huntzinger et al., 2013; Wei et al., 2013). The CRU-NCEP dataset is a combination of two existing datasets: the Climatic Research Unit Time Series, version 2.1 (CRU TS 2.1) at 0.5° × 0.5° spatial resolution and monthly climatology covering the period 1901- 2006 (Mitchell and Jones, 2005) and the National Centers for Environmental Prediction (NCEP) / National Center for Atmospheric Research (NCAR) reanalysis data at 2.5° × 2.5° spatial and 6-hour temporal resolution beginning in 1948 and available in near real time (Kanamitsu et al., 2002). All CLASS-CTEM^{N+} simulations were performed at the hourly time step and 0.5° × 0.5° spatial resolution, by disaggregating CRU-NCEP data from its original 6 hourly values. Shortwave radiation was diurnally interpolated based on day of year and latitude with the maximum value occurring at solar noon. Longwave radiation was uniformly distributed over the 6-hour period. Surface temperature, wind speed, surface pressure, and specific humidity were linearly interpolated. The total 6 hourly precipitation amount was used to determine the wet periods and the total 6-hourly amount was then distributed at hourly time steps for that period. For CO_2 concentration, a latitude-dependent seasonal cycle derived from the GlobalView dataset (GLOBALVIEW-CO2, 2013) superimposed on a curve fitted to the global average CO_2 was used (Marland et al., 2008). CO_2 concentrations had a preindustrial inter-hemispheric gradient of 0 ppm.

Terrestrial land grid cells in this study were adapted according to the global land water masks used by the TransCom project (Gurney et al., 2004; Le Quere et al., 2009b). For soil texture, we used the International Geosphere-Biosphere Programme (IGBP) percent sand and clay maps for the global simulation (Global Soil Data Task Group, 2000) with soil texture within each grid cell kept the same for both C-N and C version of the model. The global land use and vegetation types were adapted from the Synergetic Land Cover Product (SYNMAP) data set (Jung et al., 2006). The 48 SYNMAP land cover types were reclassified into the respective CLASS-CTEM^{N+} 9 PFTs classes (Table 4.1). Fraction of each dominant PFT class was generated at 0.5° × 0.5° resolution, with PFT with more than 50% fractional area considered as a dominant PFT across the globe. Grasslands were further separated into C3, C4, and mixtures of C3/C4 vegetation types following (Winslow et al., 2003); fractions of C3 and C4 crop types were estimated using the gridded data-base of (Monfreda et al., 2008), which is based on the Food and Agriculture Organization of the United Nations (FAO) crop statistics.

Nitrogen deposition (NH_4^+ and NO_3^-) occurs in both dry and wet forms. The gridded annual N deposition data from 1860 to 2050 was based on Dentener's global atmospheric N deposition maps in the years of 1860, 1993 and 2050 (Dentener et al., 2006) and N emission data from EDGAR-HYDE 1.3 (van Aardenne et al., 2001). Dentener's global atmospheric N deposition maps were re-gridded from the original 5◦ × 3.75◦ map to the CLASS-CTEM^{N+}'s grid resolution of 0.5◦ × 0.5◦ and linearly interpolated between time slices in order to obtain annual deposition rates from 1860 to 1999. Deposition rates for the year 1860 were used for the 1800 to 1859 period. The annual variation of N deposition rate from 1890 to 1990 was controlled by EDGAR-HYDE 1.3 N emission data, which provides information on annual totals of NH_3 and NO_x emissions from 10 anthropogenic sources within $1^o \times 1^o$ degree grid cells for each decade. The temporal trends of NH_x-N and NO_y-N deposition were assumed to be consistent with those of NH_3 and NO_x emissions, respectively. N deposition was assumed to increase linearly over the rest of time period (1990-2050) by a factor of 3.6 since the pre-industrial period and was projected to double again between 1990 and 2050 (Galloway et al., 2004). The main areas of N deposition since the early 1990s are the Eastern United States, Central Europe, South Asia, Southeast Asia and Southeastern Brazil, which are likely to intensify and spread in the future (Galloway et al., 2004).

4.2.3 Simulation Scheme

In this study, simulations were performed at the global scale at 0.5° × 0.5° spatial resolution using two versions of the model: (1) Carbon-Nitrogen integrated (C-N) version; and (2) Carbon-only (C) version. The two versions varied in their treatment of plant and soil N processes. Both versions of the model were run using similar (1) climate forcing (2) land us and vegetation cover initialization; (3) time-varying atmospheric CO_2 concentration and (4) time varying N deposition rates, used in C-N version of the model only.

At the start of spin-up, all prognostic soil (for three layers) and canopy temperatures were initialized to the average air temperature for the first 30 years of input weather data for NACP-MsTMIP protocol. Soil moisture for each of the three layers was initialized to 95% of saturation. Biogeochemical pools and all other prognostic variables were initialized with the empirical values evaluated from our previous studies (Arain et al., 2006; Arora and Boer, 2005a; Arora and Boer, 2006; Huang et al., 2011).

Both models were spun for more than 300 years to reach steady state, repeatedly using randomized forcing, atmospheric CO_2, and N deposition data from 1901 to 1930 (30 years). Steady state criteria as suggested by NACP protocols and used for our model were: (1) annual net ecosystem productivity (NEP) summed over all terrestrial grids and averaged over the first 30 years of the simulation balanced the annual gross ecosystem production (GEP) minus ecosystem respiration (Re) summed over all terrestrial pixels to within 1.0%; (2) at the end of a consecutive 30 year block of repeated initialization data, soil temperature in each soil layer should have the same repeating pattern as for the previous 30 year period, within 0.5 °C for each time step; (3) at the end of a consecutive 30 year of repeated initializing data, soil moisture, as measured by percent of saturation, should have the same repeating pattern as for the previous 30 year period within 1% for each time step and each soil layer. After reaching steady state, the global simulations started in 1901 and ended in 2010.

To evaluate our results, simulated C (gross ecosystem productivity (GEP), ecosystem respiration (Re), net ecosystem productivity (NEP, which equals the negative value of net ecosystem productivity (NEP)), water and energy (evapotranspiration (ET), latent heat (LE), sensible heat (H), surface runoff (runoff)) fluxes, and C stocks (soil organic carbon (SOC), total vegetation biomass (Tvg), leaf area index (LAI)) were compared with values reported in the literature (e.g., Beer et al. 2011; Tarnocai et al. 2009; Ruesch & Holly 2008; FAO/IIASA/ISRIC/ISSCAS/JRC 2012), data derived from the

FLUXNET network of eddy covariance (EC) towers using multiple ensembles and up-scaling approaches (e.g., Jung et al. 2009; 2010), and data from remote sensing studies (e.g., Zhao et al. 2006). The performance statistical measures derived from the model-data intercomparison were used (Hoffman et al., 2007; Randerson et al., 2009). Several time scales were used for these comparisons such as: (1) global total annual means from 1980 to 2010, (2) global spatial pattern of monthly mean values, (3) mean values for major geographic regions: (4) long-term annual variation and anomalies and (6) variations of seasonal amplitude and phase.

4.3 RESULTS

4.3.1 Global Mean Annual Values

Simulated global total mean annual values of C, water and energy fluxes and C stocks over the vegetated land surface over the last 30 years (1980-2010) from both versions of the model are summarized in Table 4.2. Corresponding observation-based estimates are also shown.

The C-N coupled model estimated global total mean annual terrestrial GEP of 122.7 Pg C yr^{-1}, for the 1980 to 2010 period, compared to the 128.2 Pg C yr^{-1} simulated by the C-only version of the model (Table 4.2). These estimates of GEP are consistent with the Intergovernmental Panel on Climate Change (IPCC) AR4 estimate of 120 Pg C yr^{-1} (Denman et al., 2007) and are also comparable to recent estimates of 123 ± 8 Pg C yr^{-1} based on FLUXNET data (Beer et al., 2011), 119 ± 6 Pg C yr^{-1} from upscaled FLUXNET observations (Jung et al., 2011) and 125 Pg C yr^{-1} from a Remote Sensing study (Zhao et al., 2006). Also, our global total mean annual GEP estimate was within the range of 92-140 Pg C yr^{-1} as simulated by over 20 terrestrial biogeochemistry models participating in the MsTMIP intercomparison project (Huntzinger et al., 2013). Simulated global total mean annual Re (1980-2010) from C-only and C-N coupled versions of the model was 122.4 Pg C yr^{-1} and 119.1 Pg C yr^{-1}, respectively, as compared to the likely range of 100–110 Pg C yr^{-1} inferred from independent Re estimates (Lasslop et al., 2010) and those derived from upscaled FLUXNET data (Jung et al., 2011) (Table 4.2). Simulated global mean annual NPP values (calculated as the difference between simulated GEP and Ra) over 1980-2010 were 62.7 Pg C yr^{-1}, and 67.4 Pg C yr^{-1} by C-N and C-only versions of the model, respectively. These values are consistent with the observed NPP range of 56.6 to 62.6 Pg C yr^{-1} from the flux estimates (Table 4.2). The global mean annual NEP estimated by the C-N version of the model was 3.64 Pg C yr^{-1} (positive values of NEP [= GEP-Re] represent an uptake of C by the ecosystem, and negative values represent a loss of C to the atmosphere), slightly smaller than the carbon-only version model simulated 5.82 Pg C yr^{-1}. Both of these values were comparable to the values of 0.3±0.9, 1.0±0.6 and 0.9±0.6 Pg C yr^{-1}, estimated by IPCC AR4 of land carbon sink for 1980s, 1990s and 2000-2005, respectively, (IPCC, 2007b), and slightly smaller than the lower end of the 17 ± 5 Pg C yr^{-1} of NEP derived by up-scaling of EC measurements (Jung et al., 2011). It indicates that the model estimated a smaller C sink on the global long-term scale. Given that the uncertainties in spatio-temporal variability of C fluxes are substantial in both approaches, the magnitude of the NEP disparity here remains an open question as to whether the model delivered an underestimation.

Simulated global mean annual total for SOC was 1230 Pg C by the C-N version of the model, while compared with the C-only version simulated a SOC of 1328 Pg C (Table

4.2). The simulated SOC is reasonably within the range of current SOC estimates of about 891 to 1657 Pg C in the literature (Post et al., 1982; Schlesinger, 1977; Tarnocai et al., 2009; FAO/IIASA/ISRIC/ISSCAS/JRC, 2012). By contrast, the size of the Tvg, which comprised aboveground and belowground plant biomass in the model, appears to be slightly overestimated, with simulated values of 608 and 629 Pg C by the C-N and C-only version of the model, respectively, compared to an observed value of 446 Pg C (Ruesch and Holly, 2008). Overall, the C-N coupled model simulated lower photosynthesis and respiratory fluxes than simulated by C-only version of the model.

Simulated global mean ET predicted by the C-N coupled version of the model is 66.7×10^3 km^3 yr^{-1} (equivalent to 590.3 mm yr^{-1} with total vegetated areas of 113×10^6 km^2) for the 1980–2010 period, compared to 71.0×10^3 km^3 by the C-only version of the model. Simulated ET agrees with the reported values of 65.5×10^3 km^3 yr^{-1} (Oki and Kanae, 2006), 58–85 × 10^3 km^3 yr^{-1} (Dirmeyer et al., 2006) and 574 mm yr^{-1} for the 1985-2010 period (Shi et al., 2013) and $65\pm3\times10^3$ km^3 yr^{-1} (Jung et al., 2010) using FLUXNET data (Table 4.2). Many studies in the literature reported their results as LE rather evapotranspiration. In order to compare our results with these studies, we also have reported simulated evapotranspiration in energy units. Simulated global mean annual LE was 146.2 × 10^{21} J yr^{-1} (equivalent to 41.0 W m^{-2}) by the C-N version of the model and it is in agreement with independent global estimates (Table 4.2), for example, 38.5 W m^{-2} (Trenberth et al., 2009), 37–59 W m^{-2} (Jiménez et al., 2011). The simulated LE value by the C-only version of the model was 167.4 × 10^{21} J yr^{-1} or 46.98 W m^{-2}. Simulated global mean H was 194 × 10^{21} J yr^{-1} (or 54.43 W m^{-2}) by the C-N version of the model, and 162 × 10^{21} J yr^{-1} (or 45.46 W m^{-2}) by the C-only version over the 1980-2010 period. These values are slightly higher than the observed value 164 ± 15 × 10^{21} J yr^{-1} (Jung et al., 2011) and 27 W m^{-2} (Trenberth et al., 2009). However, our simulated H values were within 18 to 57 W m^{-2} range reported by another study (Jiménez et al., 2011). The C-N coupled model simulated global mean annual runoff during 1980-2010 period was 310 mm yr^{-1} (equivalent to 35.0×10^{12} m^3 yr^{-1}), which is well within the current range of estimates in literature such as 35.2×10^{12} m^3 yr^{-1} (Chahine, 1992) and 45.1×10^{12} m^3 yr^{-1} by (Labat et al., 2004). The C-only version of the model simulated global mean annual runoff was 277 mm yr^{-1} (25.7×10^{12} m^3 yr^{-1}) is lower than the values reported in literature.

4.3.2 Spatial Patterns

4.3.2.1 Spatial Distribution of Carbon Fluxes

The CLASS-CTEM^{N+} simulated global distribution of monthly mean values of GEP, Re, NPP and NEP, with corresponding spatial differences between the C-N coupled and C-only version of the model are shown in Fig. 4.1a–h. Simulated annual mean GEP by both versions of the model showed high spatial heterogeneity; the CLASS-CTEM^{N+} simulated global GEP distribution patterns largely resembled those found in other studies (Beer et al., 2011; Jung et al., 2011), with the highest C assimilation in tropical ecosystems, followed by temperate and boreal forests. High-latitude regions with short growing seasons and dry regions had the lowest GEP. The major regions, where GEP from two versions of the model significantly differed, sometime >25%, included the northern high latitude and west coast of North America, northern Europe, southeast Asia, southern parts of South America (e.g. the Pampas region in Argentina), the southern part of Africa, and southeast coast of Australia (Fig. 4.1b). In each of those regions, the C version of the model yielded higher GEP, especially some boreal regions in North America and Eurasia, which exhibited a large difference in GEP from the two versions of the model. In contrast, there was a smaller difference in the magnitude of GEP from the two versions of the model in the tropics, followed by temperate regions (Fig. 4.1b). Similar to the spatial distribution of GEP, the simulated monthly mean Re was largest in the tropical regions of South American and East Asia with smaller Re values found in high latitude and dry regions (Fig. 4.1c). This is similar to the global Re pattern reported in the recent EC up-scaling study (Jung et al., 2011). The largest difference in mean Re values from the two versions of the model was in North America and Eurasia (Fig. 4.1d), where GEP also differed between two models.

Simulated global mean NEP and NPP from the C-N and C versions of the model are shown in Fig. 4.1e, f and Fig. 4.1g, h, respectively. Monthly mean NEP values simulated by the C-N and C version of the model were generally consistent with observations (Jung et al., 2011) with larger values of NEP or C uptake simulated by the model in eastern North America and Western Europe. These regions also showed the largest seasonal cycle of NEP (See further discussion in section 3.3.2). Both models simulated a similar spatial distribution of NPP, with high NPP values occurring in forested areas, especially in the tropical and subtropical forest areas with warm climate and sufficient precipitation and radiation. Low NPP values were associated with areas under cold climate with low precipitation and/or low radiation. The NPP distribution pattern simulated by our model is also similar to other studies (Cramer et al., 1999; Goetz et al., 2000; Krinner et al., 2005). The model estimated high values of NPP in the lower latitude temperate forest regions (e.g. Pacific Northwest region of North America) are almost the same as that of tropical rain forests (Fig. 4.1g). Some observations support the contention that the mean NPP of these temperate ecosystems is as large as in the tropics (Hudiburg et al., 2009; Huston and Wolverton, 2009).

Overall, our model results demonstrate that the impact of N limitation on the terrestrial net C flux distribution during the 1980-2010 varies spatially over the globe (C-N minus C version) (Fig. 4.1). The inclusion of N dynamics in the C-N version simulations significantly reduces the terrestrial C uptake compared with that of the C-only counterpart in some regions where N might not always be sufficiently available for plant growth (Fig. 4.1 and 4.6) (Thomas et al., 2013). In general, this N limitation is clearly indicated in mid to high latitude regions of decreased C uptake from terrestrial ecosystems in C-N version relative to C version (i.e., negative values of C-N minus C version, Fig. 4.1), particularly in boreal forests, tundra and some temperate forest regions, where N is a primary limiting nutrient (Hobbie et al., 2002). In large parts of the boreal zone that experienced the strongest warming over the last decades (IPCC, 2007a), the response of these regions to N limitation seems less pronounced than the temperate evergreen deciduous and evergreen forest regions (Fig. 4.1). This might be because ecosystem productivity in high latitudes is also limited by shorter growing seasons with relatively less N is required for plant growth. While moist tropical forest regions are highly productive, our modeling results did not indicate clear N limitation effects in these regions. This is consistent with studies that suggest that phosphorus (P) instead of N takes the major function in limiting ecosystem production in tropical forests (Harrington et al., 2001), and there is no indirect N mineralization feedback effect in tropical forests (Arneth et al., 2011; Jain et al., 2009; Thornton et al., 2007a; Wania et al., 2012). In spite of this, there are some spots in tropical and mid-to-low-latitudes, which show more C release to the atmosphere in C-N simulations than in the C version (Fig. 4.1), because in some regions the rate of release of plant-available N from soils reduces over time and carbon emissions from heterotrophic respiration rates of C become larger than the climate-driven C sequestration rates in vegetation. This is supported by some other studies that have documented a N limitation on productivity in tropical shrub lands (Gallardo and Schlesinger, 1992; Yates et al., 1982).

4.3.2.2 Spatial Distribution of Water and Energy Fluxes

Fig. 4.2a and 4.2b shows the spatial distributions of monthly mean ET simulated by the C-N version of the model and the difference between the C-N and C-only versions over the 1980-2010 periods. The C-N model simulated ET captured similar spatial patterns compared to observation-based FLUXNET estimates (Jung et al., 2010), with the largest values ranging from 100 to 150 mm mon^{-1} in tropical forest areas (Amazon, Africa). However, our model showed relatively smaller ET in South Asia. Since the C-N model did not improve prediction accuracy of simulated water and energy fluxes, model errors are inferred to be due to misrepresentation of water-related mechanisms, identified earlier for CLASS-CTEM^{N+} (Arora, 2001; Kothavala et al., 2005; Yuan et al., 2007). Overall, there was a smaller difference in the ET distribution across the globe by two versions of the model than that of carbon fluxes (Fig. 4.2b), indicating less influence of simulated N in water flux than photosynthesis. Meanwhile, The scattered higher value of ET from the C-N version of the model as compared to the C version in the tropics was also largely due to moisture-supply limitation (Shi et al., 2013). The spatial distribution of the mean monthly transpiration rate (Tr) showed a similar pattern to ET in general, with the highest value ranging from 80 to 100 mm mon^{-1} in tropical forest areas, except some lower values in parts of the Amazon (Fig. 4.2b); the patterns are similar compared to observation-based ET data (Jung et al., 2010). However, there are some notable differences between the modeled and observed ET over Europe, China, southeastern North America and southeastern Africa (Shi et al., 2013). The simulated differences in Tr between the two versions of the model were less obvious as well. The simulated global total surface runoff is shown in Fig 4.2e. In general, tropical areas showed the highest simulated surface runoff of around 150 mm mon^{-1} (Fig. 4.2e), with some exceptions in extra-tropical regions such as in Chile, Mexico and South Africa, where both broad-leaved and needle-leaved PFTs occur. C-N model simulated runoff in temperate forest regions in North America was about 50 to 70 mm mon^{-1} and it decreased northwards with values ranging from 10 to 20 mm mon^{-1}. Similar low runoff values were also simulated for the Eurasian boreal zone. There was no apparent difference in the spatial distribution of runoff between the two versions of the model. Simulated global spatial distribution of H shows the largest values in subtropical dry regions (such as sub-Saharan Africa, South Asia, part of South America and Australia) where available energy is preferentially partitioned to H rather than LE (Fig. 4.2g). There were some notable differences in simulated H between the C-N version of the model and the C version over dry regions, such as Eurasia, southeastern Australia, southwestern coastal areas of South America and southeastern Africa (Fig. 4.2h). In the absence of reliable observation-based estimates of global Tr, LE, H and runoff, the evaluation of modeled global distribution of water and energy fluxes remains difficult.

4.3.2.3 Spatial Distribution of C pools and stocks

Fig. 4.3 (a, c and e) shows the spatial distribution of simulated SOC, Tvg and LAI by the C-N version of the model. The corresponding spatial differences between the C-N and C version of the model are also shown in Fig. 4.3 (b, d and f). Compared to the global data set of 0.5-degree grid SOC (FAO/IIASA/ISRIC/ISSCAS/JRC, 2012), the C-N version of the model simulated spatial distribution of SOC generally showed the same pattern, but higher in North America and the northern parts of Europe, and lower in Siberia. The negative biases in Siberia are mainly located in areas with high wetland fractions, which are characteristic for the high SOC contents (Matthews and Fung, 1987). Because CLASS-CTEM^{N+} does not simulate the organic soils of wetlands in the current versions, the underestimate of SOC in these regions was expected. Overall, the simulated differences in SOC between the C-N and C version of the model showed larger differences in northern latitudes (Fig. 4.3b), such as North America and northern Eurasia, where forests growth is more subject to N limitation (Thomas et al., 2013); moreover, these areas have high SOC storage in the soil (FAO/IIASA/ISRIC/ISSCAS/JRC, 2012). Regions with large (in some areas > 30%) differences in simulated Tvg between two versions of the model include Southeast Asia, parts of South America, the southeast and west coast of North America, and northern Europe (Fig. 4.3d). In each of those regions, the C-only version of the model provided higher vegetation biomass (indicated as negative values for C-N minus C in Fig. 4.3d). The C-N version provided higher vegetation biomass in southeast North America, South Africa and Amazon region of South America only. Some regions showed contrasting patterns between vegetation biomass and soil carbon storage, such as in the southeast US, the Chilean coast, the Baltic region in Europe, and western Russia, although the differences were relatively small. The C-N model simulated global map of LAI compared well to Remote Sensing derived global LAI distributions (Chen et al., 2012), with generally high values in regions with predominantly woody vegetation and lower values in semiarid and tundra regions (Fig. 4.3e, f). In the Eurasian forest belt, the percentage of herbaceous vegetation is underestimated. Since satellite LAI estimates are subject to fairly large uncertainties for dense canopies (Carlson and Ripley, 1997), this model underestimated LAI bias might, at least in part, be due to problems associated with the satellite data set.

In summary, the global spatial distribution of mean monthly GEP, Re, NEP, NPP, ET, H and Runoff generally showed large fluxes occurring in the equatorial tropics followed by monsoonal subtropical regions (e.g., south and east Asia), and humid temperate regions in eastern North America, and western and central Europe (Fig 4.1-4.3). Small C, water and energy fluxes occur in cold and dry environments as expected. The similarity in the spatial pattern of GEP, Re, and ET originated from their intimate coupling: GEP provides substrate for ecosystem respiration and thus is the main controlling factor of Re as shown by various studies (e.g., Lasslop et al., 2010); GEP and ET are closely linked through stomatal conductance for transpiration from the canopy and the dependence of intercepted precipitation on LAI.

These results indicated that the inclusion of N cycle caused general reductions in GEP simulations, better matching observations. N dynamics in CLASS-CTEM^{N+} have further induced changes in simulated ecosystem respiration, as well as C pool sizes, both interlinked due to the dependence of Re on C respired in biomass (Ra) and soil (Rh), as well as their stoichiometric composition. Spatial differences in simulated vegetation and soil C values from both versions of the model, yielded substantially different estimates of the global land C sink. These results demonstrated that the simulated N interactions have an important impact on the model's representation of global C sinks and sources.

4.3.2.4 Regional Patterns of Fluxes and C Stocks

Both C-N and C model simulated regional GEP values are summarized in Table 4.3. C-N model simulated values showed that tropical forests assimilated 45% of the global terrestrial GEP and have the highest GEP per unit area (Table 4.3). Temperate forests accounted for 23% of the global GEP and were the second most important biome in terms of photosynthetic C uptake. The large areas of the tropical savannahs (about twice the surface area of tropical forests) explained their high contribution to global GEP (11%), followed by temperate grasslands (7.5%), croplands (5.1%), boreal forests (5%) and tundra (2%). Overall, the C version of the model generally simulated larger regional totals of GEP as compared to the C-N version, but the C-N version of the model was in better agreement with reported values in the literature (Table 4.3) (Saugier et al., 2001). The reason for both models slightly overestimating GEP in the boreal and temperate forest might be their location in high latitude regions, where the growing season is short and N availability is limited (Hobbie et al., 2002). By contrast, in tropical forests, where the forests have a longer growing season, and are less N limited (Davidson et al., 2004; R Quinn Thomas et al., 2013), simulated GEP values were in better agreement with observations (Table 4.3). Similar good agreement is obtained in tropical savannahs and grasslands, where the C-N version of the model indicated a GEP of 14.9 Pg C yr^{-1}, compared with the C version simulated value of 14.4 Pg C yr^{-1}.

Similarly, compared to regional estimates of observed forest biomass, CLASS-CTEM^{N+} generally overestimates the magnitude of vegetation biomass in the high and mid latitudes (e.g., Canada and Continental United States). This can be seen in Table 4.4, which displays a regional breakdown of simulated forest biomass compared to observed estimates (Dixon et al., 1994). Similar patterns were shown Fig. 4.1 and described in the section 3.2.1. The slight underestimation of vegetation biomass in the low latitude regions (such as Asia, Africa and Americas) might largely due to the overestimated Re values in the model. In these regions, model simulations depend critically on the parameterization of the temperature sensitivity of respiration (Jones et al., 2003). Recent results suggest that this temperature sensitivity could be overestimated in the ecosystem models (Frank et al., 2010; Mahecha et al., 2010). Overall, there were minor differences between the C-N and C version of the model, as compared to the differences in Re in high and mid latitudes. A possible explanation for this is related to nutrient dynamics and N limitations in these regions. The availability of N provides an important constraint on forest growth and biomass storage in the C-N version of the model, but other nutrient cycles have so far been ignored. Of particular concern is the phosphorus cycle since phosphorus is generally believed to be more limiting than N to tree growth in lowland tropical moist forests (Townsend et al., 2011).

4.3.3 Temporal Patterns

4.3.3.1 Long-term Annual Variations

Environmental forcings, such as, climate variability, CO$_2$ fertilization, nitrogen limitation, current land management, and the recovery from historical land use and disturbance are integrated and critical to the terrestrial carbon cycle. Flux measurements and observations already implicitly included the influence of these forcing factors (Jung et al., 2009). To distinguish the different responses between the C-N and the C-only version simulations in this study, we used the combined multi-forcing factors to drive both model simulations for comparing with flux measurements and other independent observations. Time series of both model versions simulated annual values of major C fluxes (GEP, Re, NPP and NEP) (Fig. 4.4), water and energy fluxes (ET, Tr, Runoff and H) (Fig. 4.5) over the 1910–2010 period showed different responses to the evolving environmental driving factors. The imposed forcings included climate, CO_2 concentrations and N deposition (Ndep), as data described in sections 2.2 and 2.3. Considering that both versions were imposed with the same environmental forcing, we hypothesize that the differences between the two versions are induced by the N cycle inclusion in the C-N version, and the increased N deposition input is presumed to be the cause of the disparity in model results.

4.3.3.1.1 Annual Variations of C fluxes and C pools

Both C-N coupled and C-only versions simulated 100-year annual GEP showed strong nonlinear responses for the imposed environmental forcing variations (Fig. 4.4a). The C-N version simulated annual GEP time series displayed an overall positive trend (increase rate of 0.17 Pg C yr^{-1}) from 1910 to 2010. The C version simulated a slightly slower annual GEP increase slightly of 0.10 Pg C yr^{-1} during 1910 to 1970, compared to the C-N version increase rate of 0.07 Pg C yr^{-1} during the same period; but the C version simulated global total annual GEP increased much faster i.e. 0.61 Pg C yr^{-1}, compared to the C-N version (increase rate of 0.53 Pg C yr^{-1}) during the 1970 to 2010 period, characterized by an industrial boom and high CO_2 emissions (IPCC 2007b). Similar to GEP, both versions simulated global total annual Re showed the same variations to the imposed forcings (Fig. 4.4b). Before 1970, both models simulated an overall minor increase of Re by 0.06 and 0.03 Pg C yr^{-1}, for C-N and C versions, respectively; during the 1970-2010period, however, the C-only model simulated Re showed a significant increasing trend (increase rate of 0.45 Pg C yr^{-1}), compared to the C-N version increased of 0.28 Pg C yr^{-1}. Here, the interannual variability of Re is larger than the interannual variability of GEP, probably because photosynthesis is not strongly limited by climatic conditions. Both C-N and C versions simulated global total annual NEP showed slightly increase through the 100 years (the C-N simulated annual mean NEP of 1.69 Pg C yr^{-1}, the C version simulated annual mean NEP of 2.19 Pg C yr^{-1}), with a minor increase rate of 0.07 Pg C yr^{-1} and 0.11 Pg C yr^{-1}, for C-N and C versions, respectively (Fig. 4.4c). The simulated global mean annual NEP variability shares several features with climate anomalies associated with El Nino–Southern Oscillation, which has been shown to correlate with interannual variations of global land carbon uptake estimated by atmospheric inversions (Gurney et al., 2008; Williams and Hanan, 2010). The absolute magnitude of the NEP interannual variability is considerably lower in the model results compared to the changes produced by Thornton et al. (2007), indicating that the current CLASS-CTEM^{N+} version may underestimate the interannual variability. Nevertheless, our results are close to changes simulated by another modeling study (Sokolov et al., 2008). Comparative annual mean NPP values (57.1 Pg C yr^{-1} by the C-N version, 61.9 Pg C yr^{-}1 by the C version) were observed for 100-year period for both model versions. With similar trends as GEP and Re, NPP showed with an overall increase rate of 0.13 Pg C yr^{-1} for C-N version and 0.18 Pg C yr^{-1} for the C version during the 100-year period (Fig. 4.4d). The interannual variability of global annual mean NPP is dominated by interannual variations of GEP and Re (Fig. 4.4a, b), which is roughly consistent with findings in some regional to continental studies (Ciais et al., 2005; Vetter et al., 2008; Weber et al., 2009), and suggests that in CLASS-CTEM^{N+}, the amount of C loss to the atmosphere as a result of the temperature-driven enhancements in respiration were partially compensated by a climate-enhanced productivity of plants.

4.3.3.1.2 Annual Variations of Water and Energy Fluxes

Time series of both versions (C-N and C) simulated global total annual mean values of water and energy fluxes (ET, Tr, Runoff and H) are shown in Fig. 4.5. On average, simulated global annual mean ET values from both the C-N coupled and C-only versions of the model showed similar dynamic long-term annual variability over 1910 to 2010 (Fig. 4.5a). The C-N model results suggest that global annual ET decreased by 0.66 mm yr^{-1} ($P < 0.005$) during 1910-1970, followed by an increase on average of 0.88 mm yr^{-1} ($P < 0.005$) from 1970 to 2010, compared with a similar trend by the C version simultaneously (decreased by 0.50 mm yr^{-1} ($P < 0.005$) during 1910-1970, and increased by 0.87 mm yr^{-1} ($P < 0.005$) during 1970-2010). A slight difference was observed between the C-N and C versions (Fig. 4.5a). Simulated annual variability of ET in our study is consistent with observation-based ET estimates in the literature (Jung et al., 2010; Piao et al., 2009; Shi et al., 2013; Zhao and Running, 2011). Jung et al. (2010) also have reported that ET shows a rising trend over the 1970-2010 period. The largest decline seems to have occurred in regions in which ET is limited by moisture. One study has found that the strong spatial consistency of the patterns in the independently estimated ET and soil-moisture trends suggests that decreasing soil moisture supply in the Southern Hemisphere is the main mechanism contributing to the decreasing ET trend after 1998 (Jung et al., 2010). Similar to ET, the simulated Tr associated with all environmental driving factors during the 1970-2010 periods showed the same story with a decrease during earlier decades (0.17 mm yr^{-1} of decrease by C-N version and 0.03 mm yr^{-1} of decrease by C version) followed by an increase after 1970s (0.56 mm yr^{-1} of decrease by C-N version compared with 0.50 mm yr^{-1} of decrease by C version), with relative small disparity between the two model versions simulations (Fig. 4.5b). This result is consistent with other studies which showed that a N limitation generates a small decrease in transpiration (Leuning et al., 1995; Matimati et al., 2014; Shimshi, 1970). Our simulated annual mean runoff due to the combined effects of climate, atmospheric CO_2, and N deposition reveal a positive trend of 0.17 mm yr^{-1} ($R=0.31$, $P=0.002$) for both versions of the model (Fig. 4.5c), which is close to the observation-based trend of 0.18 mm yr^{-1} (Piao et al., 2007). A decrease was observed after 1960 for the simulated H (Fig. 4.5d). The C version simulated H showed a decrease of 0.2 MJ m^{-2} yr^{-1} during the 1760-2010 period, compared to a slightly conservative decrease rate (0.16 MJ m^{-2} yr^{-1}) produced by the C-N version of the model (Fig. 4.5d). This is in line with a quantitative comparison of the FLUXNET upscaled mean annual LE and H against catchment water balances by land surface model simulations, which shows strong consistency (R^2 of 0.92 for catchment water balances and 0.91 for ensemble of land surface models (Jiménez et al., 2011; Jung et al., 2010). Generally, there is no clear disparity between the two versions simulated annual trends of water and energy fluxes (ET, Tr, H, Runoff) under the combined forcing (Fig. 4.5). This may indicate that the simulated N limitation effect is more obvious on C fluxes rather than hydrological processes in the model (Leuning et al., 1995).

4.3.3.2 Seasonal variations in global mean fluxes and C stocks

The seasonal disparities of simulated global monthly mean values of GEP, Re, NPP and NEP between the two versions of the model (C-N and C-only) for 1980-2010 are shown in Fig. 4.6. For simulated global patterns of seasonal mean GEP disparities between the two model versions (Fig. 4.6), larger differences were displayed in the northern hemisphere during the growing season (summer (Jun. ~ Aug.) and autumn (Sept. ~ Nov.) months), especially in some boreal and temperate forest regions in North America and Eurasia (Fig. 4.6). These regions also showed the largest amplitude of the regional GEP seasonality (discussed in the section 3.3.3, Fig. 4.9). The spatial patterns of the seasonal disparity of simulated global monthly mean Re and NPP values are roughly consistent with the disparity patterns of GEP (Fig. 4.6), which tends to be large in regions where the growing season is short and N availability is limited (Hobbie et al., 2002), such as northern North America and Europe boreal and temperate forests, during the summer and autumn months (Fig. 4.6). In middle to low latitude regions, however, where the forests have a longer growing season and are less N limited (Davidson et al., 2004), fewer simulated seasonal disparities of GEP, Re and NPP were found between the two model versions. In contrast to the global pattern of seasonal GEP disparity, the mean seasonal NEP difference between the two model versions was less obvious, with generally smaller values simulated by C-N model, in particular during the spring and winter seasons in North America and Europe (Fig. 4.6).

Our analysis of the mean seasonal pattern of water and energy fluxes showed minor differences of ET, Tr and Runoff between the two versions of the model (Fig. 4.7), except for some of the disparities that exist in the savannas regions of central and South Africa, with scattered smaller simulated ET, Tr and Runoff values by the C-only model. On a larger scale, the C-N version of the model simulated smaller values of ET, Tr and Runoff in temperate North America and Eurasia during the summer season, and in tropical Africa and South Australia (southern hemisphere) during the summer months (Fig. 4.7). It shows the impact of regional N controls when the C-N coupled model was applied in these regions. The seasonal variation in H, however, was much more evident than ET. The largest disparity in H between the two versions of the model occurred between summer and autumn months, and especially in Asia and semi-arid regions of Africa. The positive anomalies in H were found in spring, summer and autumn, while negative anomalies in H during the first and last 3 months of the year, indicating that the C-N version simulated H exceeded that of the C-only model simulations during these periods (Fig. 4.7)

The seasonal patterns in C stocks showed the largest difference in SOC between the two models, while there was less disparity between the C-N and C versions for simulated Tvg and LAI. For SOC, there was a large disparity between two model versions for most of boreal regions in the northern hemisphere (Fig. 4.8); these regions are more subject to the N limitation (Hobbie et al., 2002) than the mid-to-low latitudinal areas (Davidson et al., 2004; R Quinn Thomas et al., 2013) with substantially smaller SOC seasonal disparities between the two versions during all four seasons. This is also consistent with the simulated seasonal disparity patterns between the two versions for global C fluxes.

4.3.3.3 Seasonal variation in regional mean fluxes and C stocks

Because of variation in climate and vegetation distribution across these regions, the CLASS-CTEM^{N+} simulated seasonal cycle of C, water and energy fluxes varied greatly on a regional basis. In order to evaluate these differences, we aggregated the 30 years (from 1980 to 2010) monthly mean seasonal values of GEP, NEP, ET, H and Runoff over regions dominated by individual PFTs as classified in the CLASS-CTEM^{N+} and as shown in Fig. 4.9.

We found that in the tropical regions, there was relatively small variation in the seasonal GEP cycle (Fig. 4.9a). There were lower simulated midsummer GEP values in tropical zones, especially in South America, and Africa. GEP in these regions slightly increased earlier in the spring and later declined in the autumn (Fig. 4.9a). Dynamic seasonality is seen in other non-tropical PFTs with an increase in the spring and midsummer, followed by a sharp decline over the autumn and winter months (Fig. 4.9a). Temperate regions of North America and Europe show high amplitudes of GEP over the year with approximately a factor of 2 changes from low values in winter to high values in summer. Similar variations in boreal regions of North America and Europe with a modest factor of 1 changed from winter to summer (Fig. 4.9a). Overall, the Eurasian temperate PFT had much lower amplitudes of seasonal GEP variations than the North America and European temperate biomes but they showed a longer growing season than the North America and Europe boreal biomes. Similar trends and patterns were also observed with some temperate regions in eastern North America and Eurasia exhibiting a similarly high or even larger maximum GEP during northern hemisphere summer months (June, July) compared to rates in the tropics (Jung et al., 2011).

The aggregated regional PFTs seasonal cycle of NEP showed large variations among different PFTs (Fig. 4.9b). For Boreal forests (North American and Eurasia), NEP values increased during the growing season with peak values up to 0.3 Pg C month^{-1} observed during the summer months. Negative NEP values were found in these boreal forest regions during the spring and winter months (Fig. 4.9b), indicating these areas as the carbon sources during these non-growing season periods. For temperate forests, e.g., the Eurasia temperate, NEP increased at the start of the growing season but sharply decrease during the summer months, indicating a suppressed carbon uptake, which possibly due to the increased respirations during the summer months. Australia PFTs demonstrated a seasonal dynamics with higher NEP values during September till December and with lower NEP values during January to May. In the tropical and Eurasia temperate areas, NEP showed minor seasonal variations for tropical PFTs (Fig. 4.9b), indicating that the ecosystems in these areas served as minor carbon sink through the year.

The seasonal pattern of CLASS-CTEM^{N+} simulated monthly ET is evident in Figure 4.9c. The temperate forest regions (Northern temperate, Europe and Eurasia temperate) showed the largest amplitude of the mean seasonal cycle of ET ranging from 0 to 1.02 (10^3 km^3 H_2O month^{-1}). In contrast, the boreal and tropics PFTs showed with substantially smaller seasonal dynamics (Fig. 4.9c). The maximum average monthly ET was observed in South American tropics (0.91 10^3 km^3 H_2O month^{-1}), while the mean minimum monthly ET is in Australia (0.12 10^3 km^3 H_2O month^{-1}), which was quite similar to the GEP seasonal variation pattern. Our modeled ET patterns are also comparable with other studies (Jung et al., 2011; Shi et al., 2013).

The main features of the seasonal variations of H generally followed latitudinal radiation trends with the higher H values found during the summer months in the Northern hemisphere, compared to the minor or lower values during the summer months in the southern hemisphere (Fig. 4.9d). Our analyses showed the largest amplitude of the mean monthly H in Eurasian temperate biomes, with value as high as a factor of 3 larger other biomes. We found minimum monthly H values in South American temperate and South American tropical biomes, primarily during the growing season (May–July), where these regions have the largest vegetation density and coverage with most of the available energy being portioned as LE, rather H (Findell et al., 2011; Jung et al., 2011). Seasonality of H in Australia was also notably different than other regions. This is possibly due to dry regional characteristics of the inner part of Australia, where the dominant vegetation cover type are grasslands, open shrub lands or bare ground (Lehmann et al., 2008; Mitchell et al., 2009).

Large seasonal variation in mean monthly Runoff was seen in high and mid latitudes of Eurasia in temperate and boreal biomes and tropics of South America. The largest monthly Runoff values were simulated for the South American tropical regions with relatively small seasonal variation over the year. The low monthly Runoff generally appeared in the southern hemisphere (South American temperate areas, Southern Africa and Australia) with the lowest values during the northern hemisphere summer months. This is in general agreement with the global precipitation spatiotemporal pattern (Piao et al., 2007).

Table 4.1 CLASS-CTEM^{N+} PFTs and PFT-specific parameters updated in this study.

CLASS PFTs Code [1]	**CTEM PFTs [2]**	**Vc,max [3]**	**α [4]**	**Rm,leaf [5]**	**R_{litter} [6]**	**R_{SOM} [6]**	**N/C ratio in leaves [7]**	**N/C ratio in stems [7]**	**N/C ratio in roots [7]**	**N/C ratio in litter [7]**	**N/C ratio in SOM [7]**
1	ENF	35	0.08	0.015	0.4453	0.0260	0.024	0.020	0.015	0.015	0.030
	DNF	40	0.08	0.017	0.5986	0.0260	0.024	0.020	0.015	0.015	0.030
2	DBE	51	0.08	0.020	0.6339	0.0208	0.030	0.025	0.020	0.020	0.030
	DBC	67	0.08	0.015	0.7576	0.0208	0.030	0.025	0.020	0.020	0.030
	DBD	40	0.08	0.015	0.6957	0.0208	0.030	0.025	0.020	0.020	0.030
3	CR3	55	0.08	0.015	0.6000	0.0350	0.040	-	0.018	0.018	0.030
	CR4	40	0.04	0.025	0.6000	0.0350	0.027	-	0.010	0.010	0.030
4	GR3	75	0.08	0.013	0.5260	0.0125	0.040	-	0.018	0.018	0.030
	GR4	15	0.04	0.025	0.5260	0.0125	0.027	-	0.010	0.010	0.030

[1] CLASS PFTs: Code 1: needleleaf tree; 2: broadleaf tree; 3: crops; 4:grass.

[2] CTEM PFTs: evergreen needleleaf forests (ENF), deciduous needleleaf forests (DNF); evergreen broadleaf forests (DBE); deciduous broadleaf-cold forests (DBC), deciduous broadleaf-dry forests (DBD), C3 crops (CR3), C4 crops (CR4), C3 grass (GR3) and C4 grass (GR4).

[3] Vc,max: maximum rate of carboxylation by the enzyme Rubisco, (μmol CO_2 m^{-2} s^{-1}) (Rogers, 2014).

[4] α: the quantum efficiency scalar.

[5] Leaf maintenance respiration co-efficient;

[6] litter and soil carbon respiration rate at 15 °C (Kg C/ Kg C) (Melton and Arora, 2014).

[7] N/C ratio in leaves, stems, roots, litter and soil organic matters (SOM), (Kg N/Kg C) (Huang et al., 2011; Meissner et al., 2003; Wania et al., 2012; White et al., 2000).

Table 4.2 Comparison of simulated and observed global total mean annual (1980-2010)[a] carbon, water and energy fluxes and C stocks across vegetated land surface (112.5×10^6 km^2)[b]

	C-N Model	C Model	Observations	Reference for Obs.
Gross Ecosystem Productivity (GEP, Pg C yr^{-1})	122.7	128.2	120	(Denman, 2007)
			123±8	(Beer et al., 2011)
			119±6	(Jung et al., 2011)
			125	(Zhao et al., 2006)
Terrestrial Ecosystem Respiration (Re, Pg C yr^{-1})	119.1	122.4	96.4±6	(Jung et al., 2011)
			98±7	(Lasslop et al., 2010)
Net Ecosystem Productivity (NEP, Pg C yr^{-1})	3.64	5.82	17.1±4.7	(Jung et al., 2011)
			-0.6~1.6	(IPCC, 2007b)
Net Primary Productivity (NPP, Pg C yr^{-1})	62.7	67.4	59.9	(Ajtay et al., 1979)
			62.6	(Saugier et al., 2001)
			56.6	(Running et al., 2004)
Soil Organic Carbon Storage (SOC, Pg C)	1230	1328	1255 (891, 1657)	HWSD[c]
			1024	NCSCD[d]
			1400-1600	(Schlesinger, 1977)
			1395	(Post et al., 1982)
Total Vegetation Biomass (Tvg, Pg C)	608	629	446	(Ruesch and Holly, 2008)
Evapotranspiration (ET)	66.7×10^3 (km^3 yr^{-1})	71.0×10^3 (km^3 yr^{-1})	65.5×10^3 (km^3 yr^{-1})	(Oki and Kanae, 2006)
			574 (mm yr^{-1})	(Shi et al., 2013)
			$65\pm3\times10^3$ (km^3 yr^{-1})	(Jung et al., 2010)
Latent Heat (LE)	146.2 (ZJ yr^{-1})	167.4 (ZJ yr^{-1})	158±7 (ZJ yr^{-1})	(Jung et al., 2011)
			66×10^3 (km^3 yr^{-1})	(Oki and Kanae, 2006)
			38.5 (W m^{-2})	(Trenberth et al., 2009)
			58-85×10^3(km^3 yr^{-1})	(Dirmeyer et al., 2006)
			37-59 (W m^{-2})	(Jiménez et al., 2011)
Sensible Heat (H)	194 (ZJ yr^{-1})	162 (ZJ yr^{-1})	164±15 (ZJ yr^{-1})	(Jung et al., 2011)
			27 (W m^{-2})	(Trenberth et al., 2009)
			18-57 (W m^{-2})	(Jiménez et al., 2011)
Runoff (km^3 yr^{-1})	35.0×10^3	25.7×10^3	35.2×10^3	(Chahine, 1992)
			45.1×10^3	(Labat et al., 2004)

[a] Values are 30-year average at the end of the 110 years simulation after spin-up run (section 2.3).
[b] Vegetated land mask: refer to section 2.2.
[c] HWSD: harmonized world soil database (FAO/IIASA/ISRIC/ISSCAS/JRC, 2012)
[d] NCSCD: Northern Circumpolar Soil Carbon Database (Tarnocai et al., 2009)

Table 4.3 Comparison of regional Gross Ecosystem Productivity (GEP in Pg C yr^{-1}) simulated by the C-N coupled and C-only versions of the model and observations.

Region	C-N model [a]	C model [a]	Observed [b]
Tropical forests	62.8	62.1	73.9
Temperate forests	31.3	33.9	29.8
Boreal forests	6.6	8.3	5.2
Tropical savannahs and grasslands	14.9	14.4	16.2
Temperate grasslands and shrub-lands	8.5	12.2	14
Tundra	2.6	3.3	1.0
Croplands	6.8	7.3	8.2

[a] Modeled respective GEP separately for each Plant Functional Type (PFT), then multiplied by the PFT area defined by (Prentice, 2007).

[b] The observed GEP values are estimated fro year 2000 using Net Primary Productivity, NPP under the assumption that NPP/GEP = 0.5 (Saugier et al., 2001).

Table 4.4 Comparison of regional total vegetation biomass stocks (Tvg, Pg C) in forests simulated by CLASS-$CTEM^{N+}$ (C-N coupled and C-only versions) and observations.

Region	C-N model	C model	Observed [b]
	High latitudes [a]		
Russia	53	62	74
Canada	27	33	12
Alaska	1.2	1.5	2
	Mid latitude [a]		
Continental United States	22	26	15
Europe	7	16	9
China	15	22	17
Australia	16	24	18
	Low latitude [a]		
Asia	36	38	41-54
Africa	43	55	52
Americas	97	103	119

[a] High latitudes are between 50°N and 75°N; Middle latitudes are between 25° and 50° (north and south) and low latitudes are between 25°S and 25°N.

[b] Adapted forest biomass estimates reported by (Dixon et al., 1994).

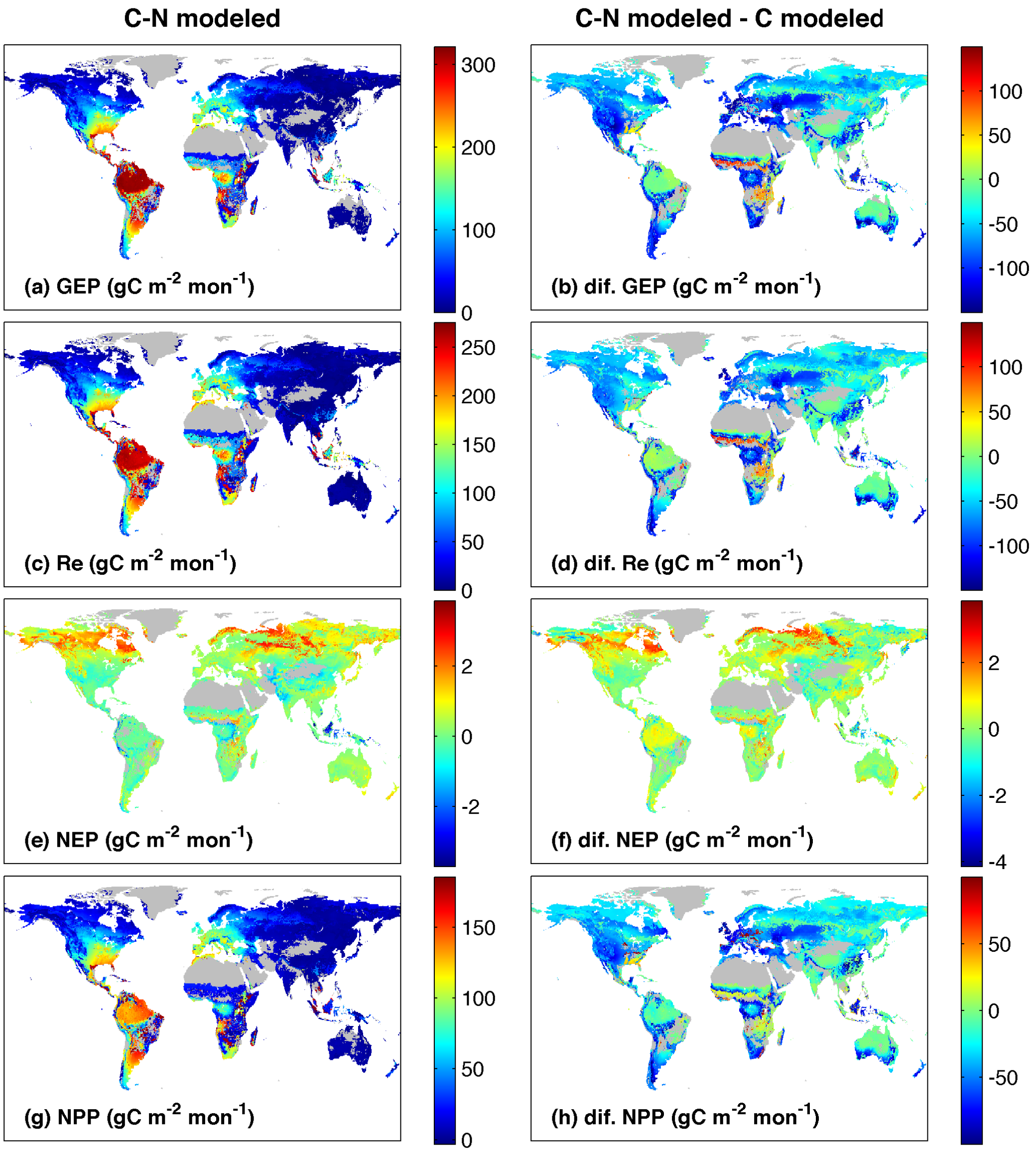

Figure 4.1 Simulated mean monthly carbon fluxes of (a) gross ecosystem productivity (GEP), (c) ecosystem respiration (Re), (e) net ecosystem productivity (NEP) and (g) net primary productivity (NPP) at 0.5 × 0.5 degree resolution from 1980-2010. The difference between the C-N coupled and C-only versions of the model are shown in the right hand column, characterized as “dif” in legend Positive values indicate that the values from the C-N version of the model are larger; negative values indicate that the C-only version values were larger.

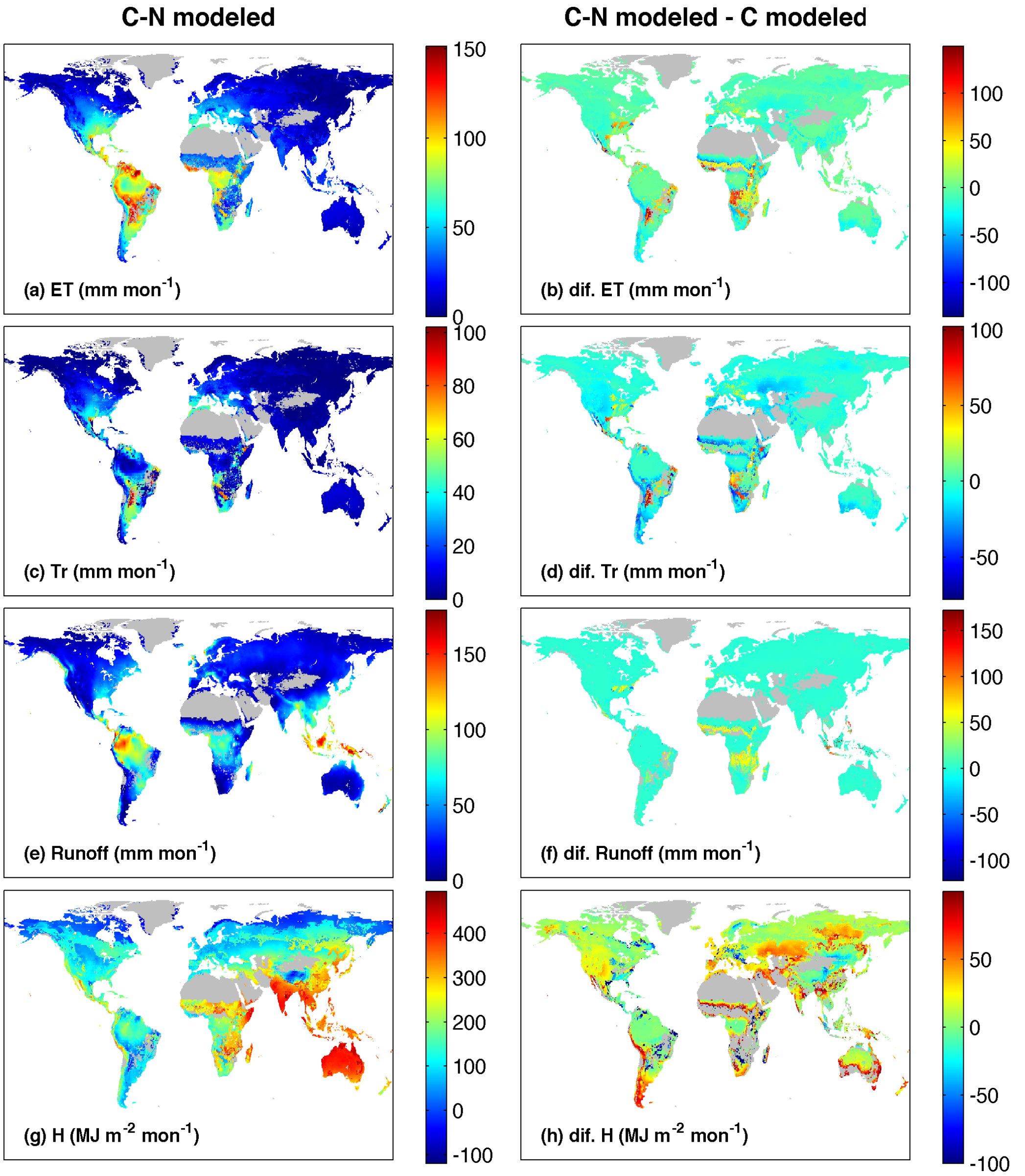

Figure 4.2 Simulated mean monthly values of water and energy fluxes: (a) evapotranspiration, ET, (c) transpiration, Tr, (e) surface runoff, Runoff and (g) sensible heat flux, H at 0.5 × 0.5 degree spatial resolution from 1980-2010. The difference between the C-N coupled and C-only versions of the model are also shown in the right hand columns, characterized as "dif" in legend. Positive values indicate that the values from the C-N coupled model are larger; negative values indicate that the C-only model simulated values are larger.

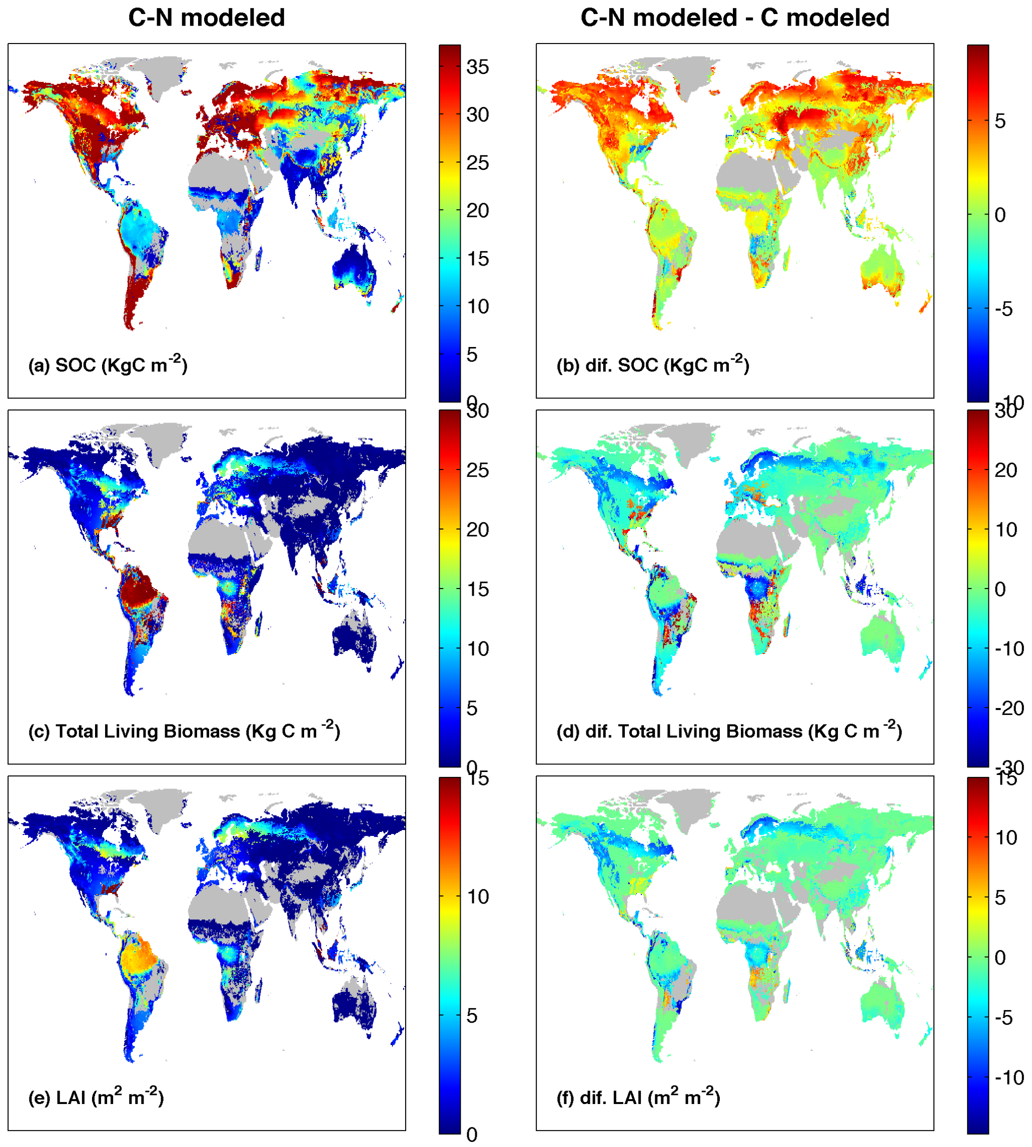

Figure 4.3 Simulated mean monthly values of water and energy fluxes: (a) soil organic carbon, SOC, (c) total vegetation biomass, Tvg and (e) leaf area index, LAI at 0.5 × 0.5 degree spatial resolution from 1980-2010. The difference between the C-N couple and C-only version of the model are shown in the right hand column, characterized as “dif” in legend. Positive values indicate that the values from the C-N coupled model are larger; negative values indicate that the C-only model simulated values are larger.

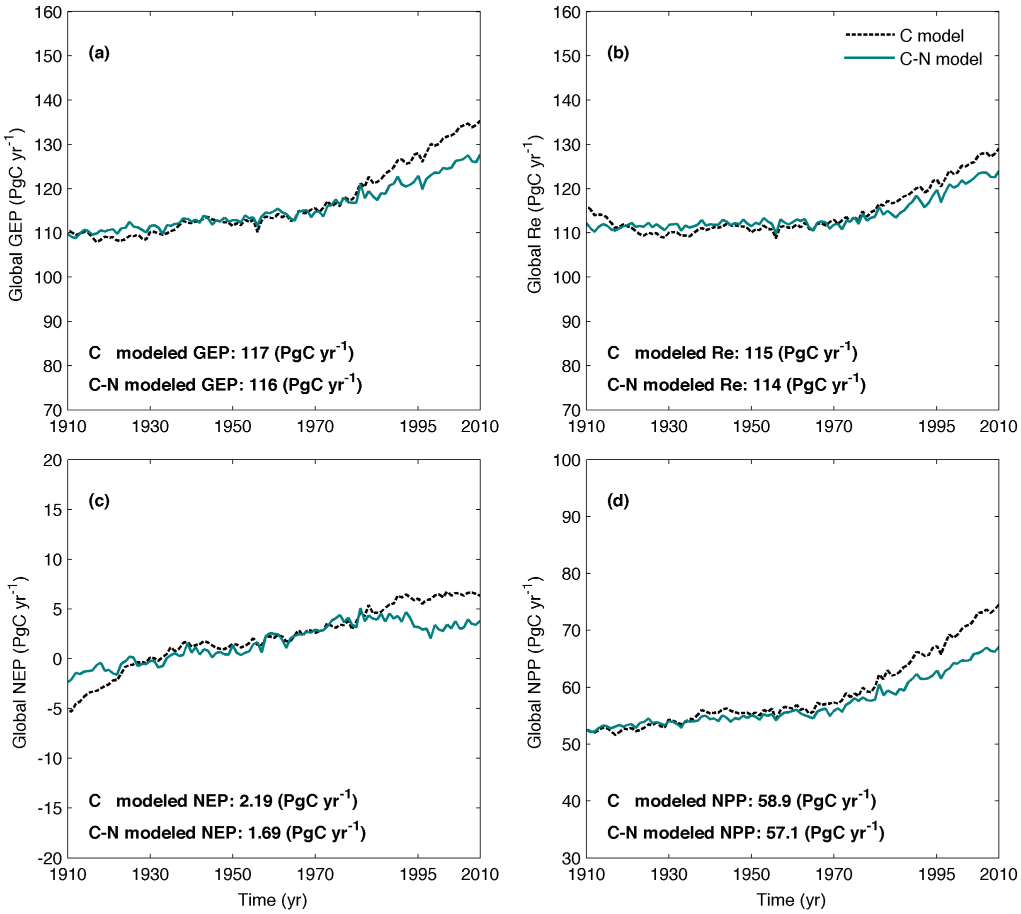

Figure 4.4 Simulated time series of (a) global mean gross ecosystem productivity (GEP), (b) ecosystem respiration (Re), (c) net primary productivity (NPP), and (d) net ecosystem productivity (NEP) from 1910-2010. Green solid line represents C-N coupled version, while black dashed line is for C-only version of the model. Global total annual mean estimates are also given for both models.

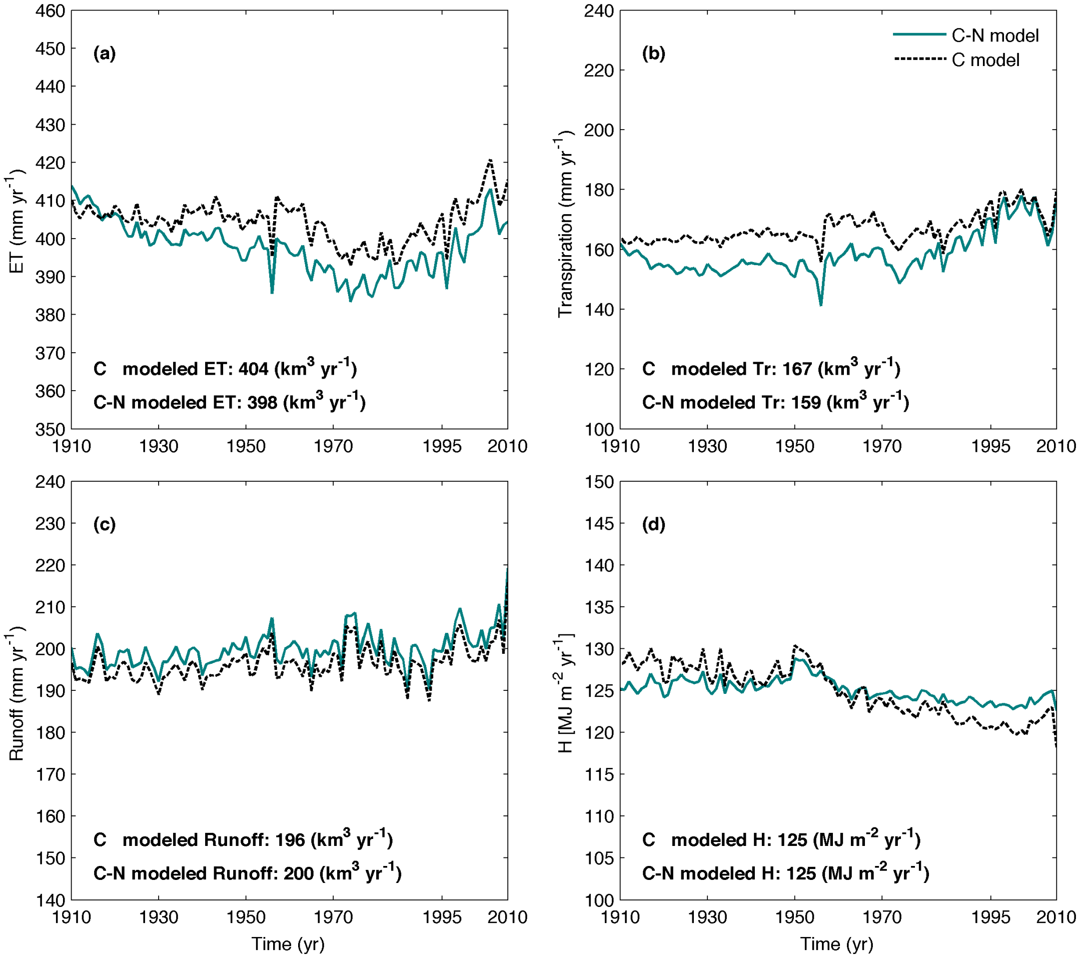

Figure 4.5 Simulated anomalies in global annual mean (a) evapotranspiration (ET), (b) Transpiration (Tr), (c) surface runoff (Runoff) and (d) sensible heat flux (H) from 1910-2010. Red solid line represents C-N coupled version and black dashed line is for C-only version of the model. Global total annual mean estimates are also given for both models.

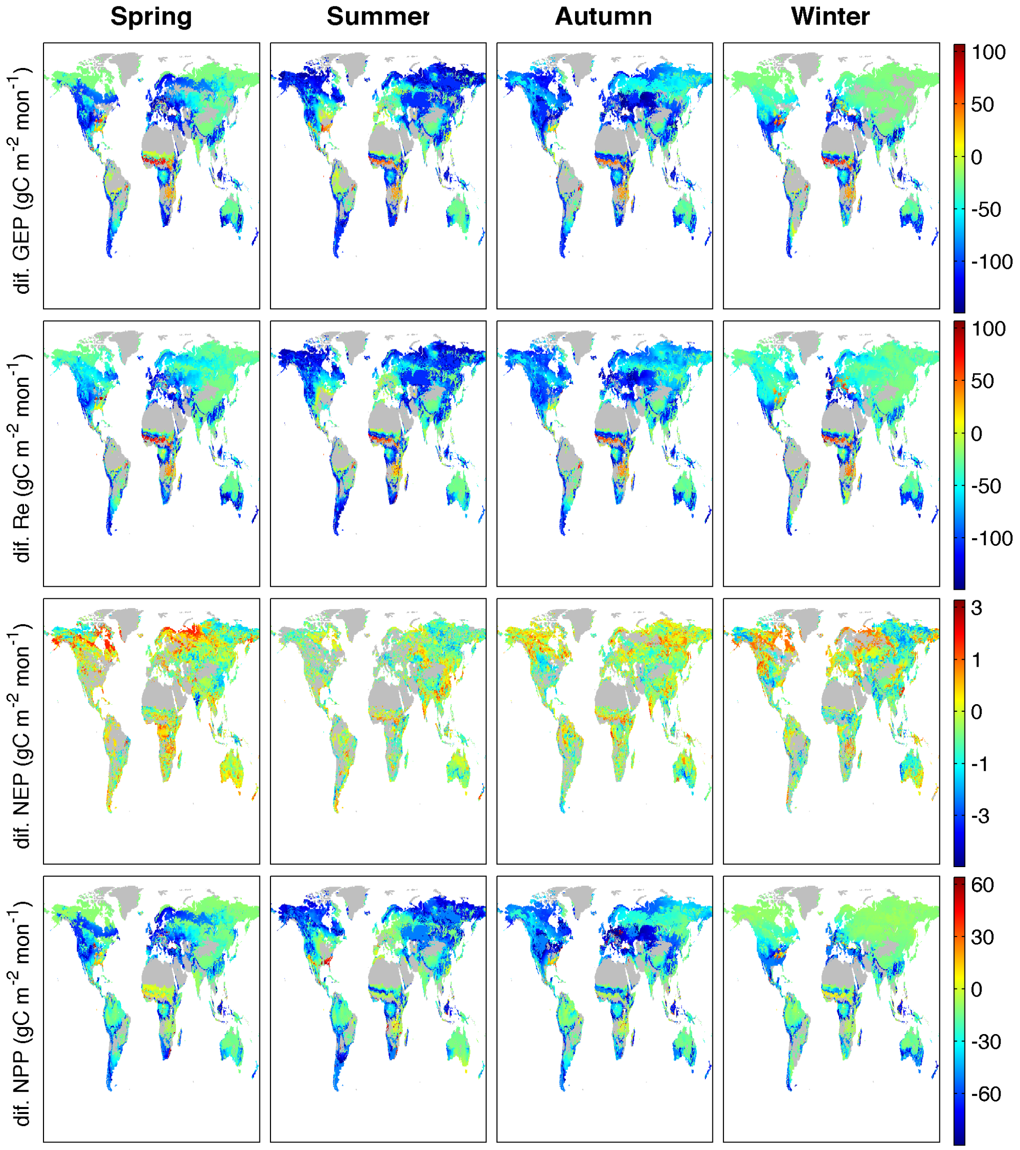

Figure 4.6 Difference between the C-N coupled and C-only model simulated monthly mean values of gross ecosystem productivity (GEP), ecosystem respiration (Re), net primary productivity (NPP) and net ecosystem productivity (NEP) for each season from 1980-2010. Positive values indicate the C-N model outputs are larger than C-only model results. Spring comprised March, April and May, while autumn comprised September, October and November.

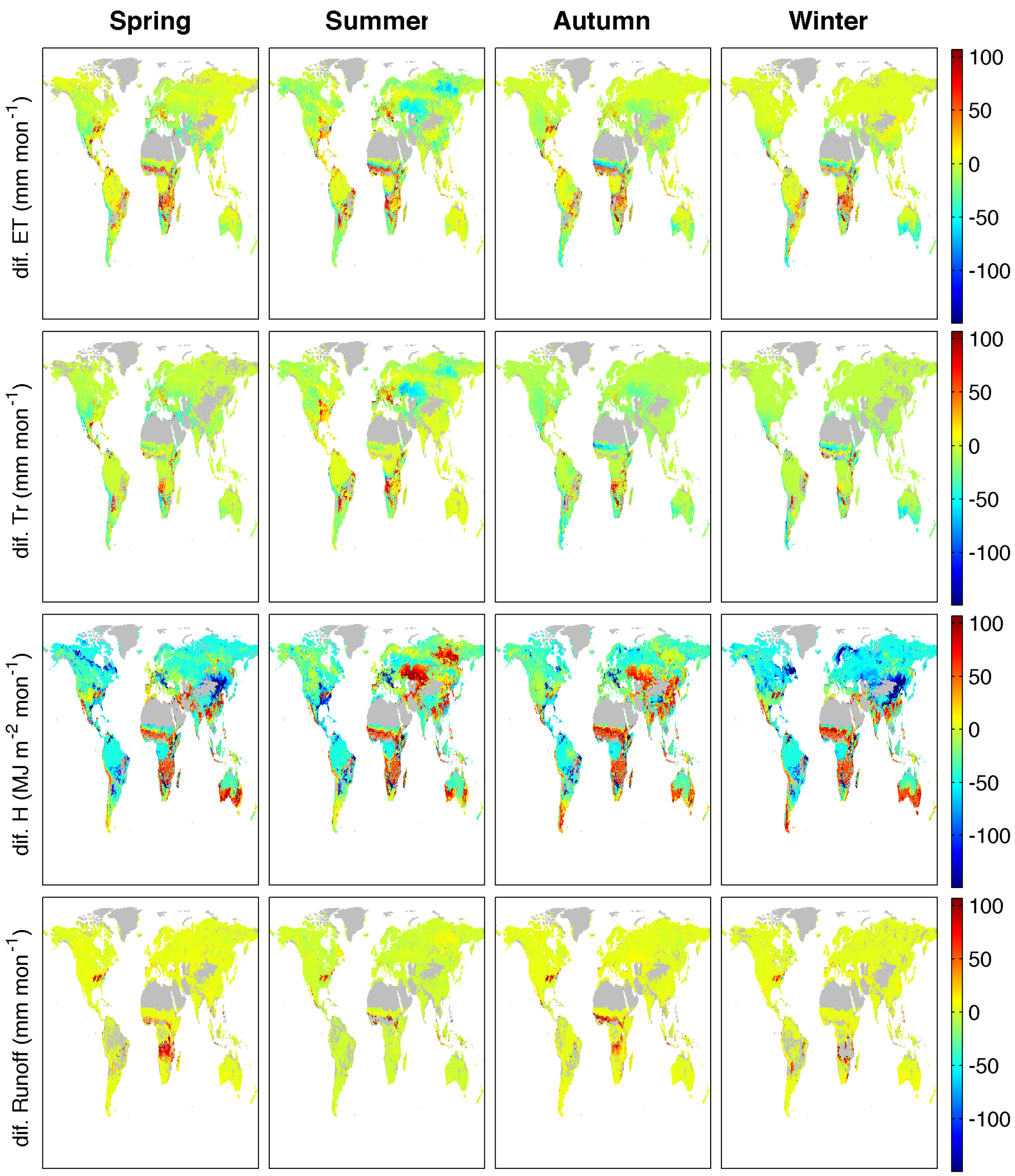

Figure 4.7 Difference between the C-N coupled and C-only model simulated monthly mean values of evapotranspiration (ET), Transpiration (Tr), sensible heat flux (H), and surface runoff (Runoff) for each season from 1980-2010. Positive values indicate the C-N model outputs are larger than C-only model results. Spring comprised March, April and May, while autumn comprised September, October and November.

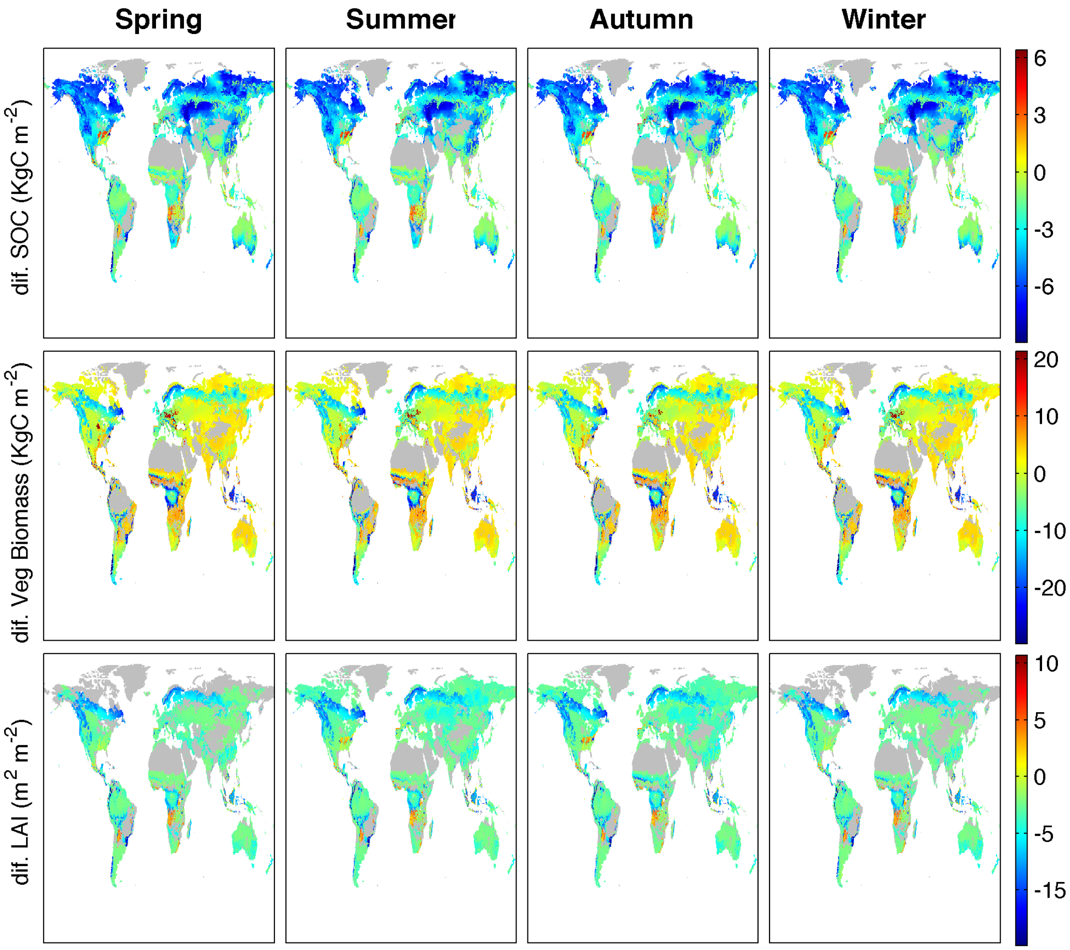

Figure 4.8 Difference between the C-N coupled and C-only model simulated monthly mean values of soil organic carbon (SOC), total live vegetation biomass (Tvg) and leaf area index (LAI) for each season from 1980-2010. Positive values indicate the C-N model outputs are larger than C-only model results. Spring comprised March, April and May, while autumn comprised September, October and November.

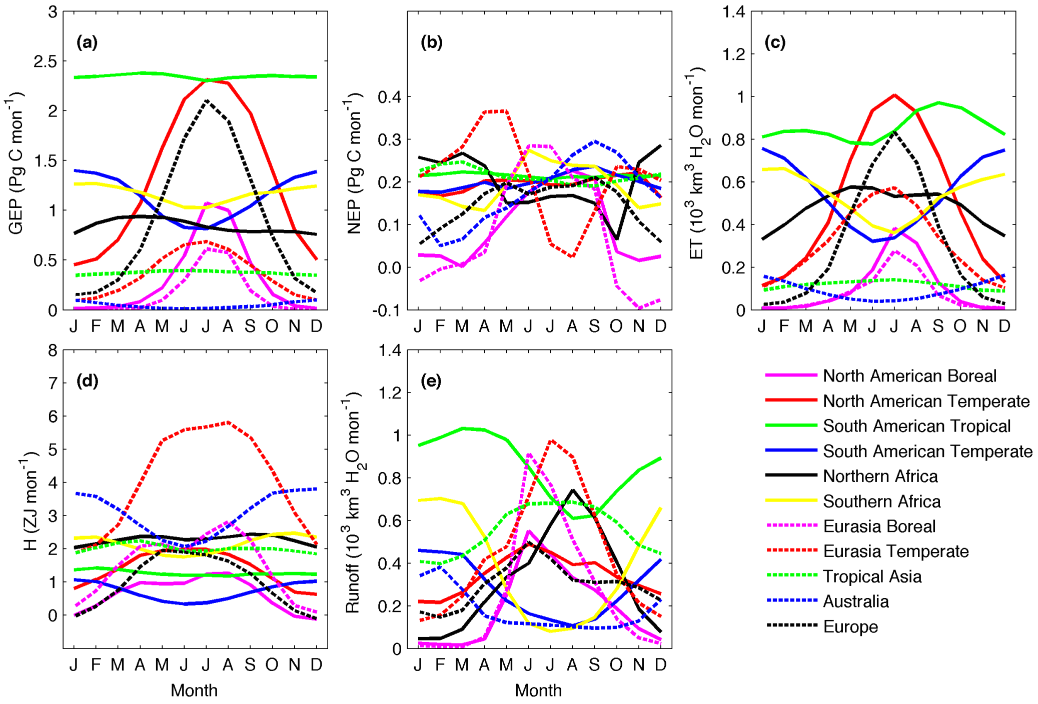

Figure 4.9 Simulated seasonal variation (monthly ensemble) of (a) gross ecosystem productivity (GEP), (b) net ecosystem productivity (NEP), (c) evapotranspiration (ET), (d) sensible heat flux (H) and (e) surface runoff (Runoff) from 1980-2010 periods for various geographic regions across the world.

4.4 DISCUSSION

This is the first time that the CLASS-CTEM^{N+} model (v. 2.1, CLASS2.7 with CTEM 1.2) have been tested and applied at all PFTs at the global scale. Model improvements from our previously published version (v. 1.0) (Huang et al., 2011) include (i) incorporating Rubisco-N related enzyme controls on photosynthesis; (ii) dynamic simulation of N_2O fluxes and (iii) development of generalized parameters for each PFT for model application at regional and global scale. Earlier, we have thoroughly evaluated our model at the site-level using observed data from the North American Carbon Program (NACP) (Schwalm et al., 2010) and Large Scale Biosphere-Atmosphere Experiment in Amazonia (LBA) (Avissar, 2002a) projects as well as .global FLUXNET (Baldocchi et al., 2001) datasets. In this study, we evaluated the performance of the CLASS-CTEM^{N+} model by simulating C, water and energy fluxes and C pools (i.e. GEP, Re, NEP, NPP, H, LE, ET, Tr, Runoff, Tvg, SOC, LAI) on different temporal and spatial scales across the world. In particular, we focused on N impacts on the global C sinks and sources, analyzed C, water and energy flux distribution patterns across the globe and their intra-annual and inter-annual variability over the past 110 years (1901-2010).

Our reported global average C uptake value of 3.64~5.82 Pg C yr^{-1} during 1980-2010 is within the range of reported NEP values (0.6 to 17.1 Pg C yr^{-1}) in literature (Churkina et al., 2007; Holland et al., 1997; Townsend et al., 1996; IPCC 2007b; Jung et al., 2011). The C-N version of our model estimated annual average NEP increases (0.05 Pg C yr^{-1}) in the global mean C sink in terrestrial ecosystems over 1970-2010 period, as compared to rate of increase of 0.12 Pg C yr^{-1} simulated by the C-only version of the model (Fig. 4.4c). This suggests that the C-only version of model overestimated the C uptake during the past 40-years than the C-N coupled results. Although annual variations in C exchanges are driven largely by the environmental forcing (Shi et al., 2013), however, the differences between simulated annual C fluxes by two versions of our model after the 1970s, when industrial activity and associated rates of increase in atmospheric CO_2 concentration were highest, suggest that N availability may also have impacted terrestrial C fluxes over this period (Fig. 4.4). There have been changes in global temperature and precipitation patterns in recent decades with an increasing warming trend and accelerated rate of CO_2 release to the atmosphere (Denman, 2007). Warm conditions have also enhanced N mineralization associated with enhanced microbial decomposition, inducing an indirect N fertilization effect that stimulates plant N uptake and C uptake by plants (Felzer et al., 2011). Enhanced atmospheric CO_2 concentrations have also lead to higher plant growth and productivity in recent decades (Ciais et al., 2008; Mycroft et al., 2008; Dolman et al., 2010). Some studies have suggested that the limiting effect of N availability under increasing CO_2 and the indirect N fertilization effect driven by climate change approximately cancelled each other around the 1970s (Churkina et al., 2007; Jain et al., 2009; Luo et al., 2006; Thornton et al., 2007; Zaehle and Dalmonech, 2011). Thus, a small reduction in simulated C fluxes by our C-N version of the model after 1970 may be attributed to N limitations on photosynthetic productivity. Our model results are supported by the finding of Nadelhoffer (Nadelhoffer et al., 1999), who used ^{15}N-tracers in 9 forests to show that the effect of increased N deposition on temperate forests C sequestration was about 0.25 Pg C yr^{-1}. Our results are in general agreement with previous global estimates of C-N integrated ecosystem models, which infer an additional 0.2 to 0.6 Pg C yr^{-1} in C uptake globally due to N deposition (Zaehle and Dalmonech, 2011) and a field up-scaling study (0.4 to 0.7 Pg C yr^{-1}) conducted by Liu and Greaver (2009).

The consideration of N dynamics in our C-N version of the model resulted in a 0-30% increase in C uptake in different biomes, with a greater C sink in the northern high latitudes (boreal forests), a smaller C sink in the south temperate latitudes primarily located in the southeastern United States, and the tropical region being C neutral (Fig. 4.1e). Because boreal and temperate forests are currently responsible for a large part of the global net C sink (Pan et al., 2011), interaction between C and N cycles in these ecosystems is crucial for determining the global C balance. There are studies suggesting that the current N deposition loads are generally low in boreal regions and below critical thresholds of N saturation (e.g. 8 kg N ha^{-1} yr^{-1}) (Fleischer et al., 2013). However, it is unlikely that the contribution of N deposition on the C sink in the boreal region is to increase in the future (Lamarque et al., 2013) and it would be modified strongly by climate feedbacks (Jarvis and Linder, 2000; Wårlind et al., 2014). Also, the effect of warming on soil N mineralization and subsequent N availability will also play a critical role in determining the factor controlling N limitation of C uptake and growth in boreal forest ecosystems (Janssens et al., 2011). Meanwhile, boreal forests are reported be only half as effective in sequestering C due to N deposition as compared to tropical and temperate forests due to a combination of smaller nitrogen use efficiency (NUE), lower N deposition rates and higher C sink strengths (Jain et al., 2009; Fleischer et al., 2013). Thus, it is unclear whether the future N deposition and accumulated historical N loads will be enough to support the forest growth for a while.

As reported in the literature, the majority of the N deposition occurs in the forests in Northern Hemisphere temperate zones (Beier et al., 2008; Nadelhoffer et al., 1999; Quinn Thomas et al., 2011; Reay et al., 2008). As a result, nearly all of global C sink due to N deposition occurs in this region, particularly in the eastern United States, Europe, China and India (Jain et al., 2009). In some temperate regions, such as China and India, studies have indicated that N deposition is expected to rise significantly due to their rapid industrialization and these regions are expected to experience enormous changes driven by N deposition (Lamarque et al., 2013; Liu et al., 2013). Increased N availability driven by atmospheric N deposition could stimulate the accumulation of additional C in temperate ecosystems (Nadelhoffer et al., 1999), because of the high N/C ratios and the large C storage capacity of forests in these regions (Holland et al., 1997). Nonetheless, the temperate forests have on an area basis the largest capacity to store C due to N deposition, but their small occupancy limits this impact on the global scale. Therefore, overall the future of the temperate C sink and the relative contribution of N deposition to this sink remain uncertain.

A dramatic contribution of N deposition to carbon sequestration in tropical forests is unexpected as these biomes are believed to be P-limited (Harrington et al., 2001) and they do not respond strongly to N deposition (Luyssaert et al., 2007; Muller-Landau, 2009; Hietz et al., 2011; Fleischer et al., 2013). However the relatively large amounts of N deposition deposited over global tropical forests for which little data is currently available calls for a careful evaluation of the N deposition effects in these forests (Hietz et al., 2011).

It is important to recognize the limitations and uncertainties that are inherent in C cycle modeling studies. Our model simulations do not explicitly take into account some other environmental factors that may influence the terrestrial ecosystem C cycle, such as disturbances (e.g., deforestation, fire, flooding, pests), ecosystem age, land use and land cover changes (LULCC), ozone pollution (Felzer et al., 2009), or managements effects (e.g., thinning, insect control, irrigation (Döll, 2002; Gordon et al., 2005). One of the most important aspects is the intense LULCC and management activities in forest ecosystems. It has been argued that signs of the C sink saturation in Europe have been overlooked due to false attributions of different drivers and the neglect of effects of land-use change and management (Erb et al., 2013; Nabuurs et al., 2013), which alters C-N dynamics and C sink strengths, and hence the accurate assessment of the N deposition effect. This highlights the urgent need to include the LULCC in ecosystem models to enable them to assess accurately the impact of N deposition and other drivers on the C sink. Also, model uncertainties associated with the structure, initialization and input data need further improvements. The quality of global gridded meteorological data sets is a universal problem for global modeling studies (Hicke, 2005; Zhao et al., 2006). The input data source of NCEP radiation and precipitation used in this study is known to have bias (Fekete et al., 2004; Zhao et al., 2006). Moreover, we used a static land cover map (SYNMAP, Jung et al., 2006) during the model initialization and did not account for LULCC, which introduces uncertainty in inter-annual variability in some regions that experienced extensive land use conversions over the last many decades. Also, SYNMAP has no “wetland” class because this class was not consistent with the applied PFTs

(Jung et al., 2006). Uncertainty in simulated fluxes and C stocks might also be caused by errors in the translation of the land cover and vegetation map, SYNMAP into the 9 PFTs for CLASS-CTEM^{N+}. It is possible that bare soil fractions have been overestimated in our simulations. For example, it is not clear whether the ‘‘shrubs and barren’’ vegetation type of SYNMAP should really be translated into 100% bare soil in CLASSCTEM^{N+}, or the “shrubs and grasses” vegetation type of SYNMAP should be translated into 100% of grassland, as the same vegetation densities were prescribed, knowing that under a semi-desert climate, the simulated LAI of the prescribed plants is likely to be low (Krinner et al., 2005). More accurate parameters for C4 grassland and cropland derived from observational data are needed as well as parameters and formulations associated with the effects of tropospheric ozone (Felzer et al., 2007), forest fires (Balshi et al., 2007), and insect outbreaks (Kurz et al., 2008). These aspects have not been explicitly captured in our study. The inclusion of a more detailed soil hydrology, which hopefully will improve the model behavior in arid and tropical regions, will also be an important future development. All these issues have to be explicitly represented in the further model development to improve its performance.

There are uncertainties in observational data sets that are used to compare modeling results. For example, a small but systematic bias in eddy covariance (Lasslop et al., 2008; Richardson et al., 2006) or a biased sampling of ecosystems, may have propagated a bias of 5– 10 Pg C yr^{-1} in the global C budget (Jung et al., 2009; Kuppel et al., 2012). Measured flux data is subject to uncertainty from the limited spatial and temporal coverage of flux tower sites. For example, in our study, the simulation period spanned from 1901-2010, while available observations data were limited and different for each study location. It suggests the need for long-term monitoring networks to measure changes in the vegetation and soil C biomass at the local and regional scales.

4.5 CONCLUSION

This study evaluated the performance of a Carbon-Nitrogen (C-N) coupled dynamic vegetation model, CLASS-CTEM^{N+} in simulating the terrestrial ecosystem’s carbon, water and energy budgets for over ~100 years at 0.5 × 0.5 degree spatial resolution across the globe. It used reanalyzed forcing data from the North American Carbon Program (NACP)-Multi-Scale Synthesis and Terrestrial Model Intercomparison Project (MsTMIP). Two versions of the model (C-N and C-only) were applied to investigate the simulated nitrogen impacts on spatio-temporal patterns of terrestrial carbon cycle. Exploratory and diagnostic analyses were conducted against multiple environmental forcings to assess the nitrogen constraints on terrestrial carbon, water and energy fluxes at various temporal (from months to decades) and spatial (regional, PFTs and global) scales.

Results demonstrated that the CLASS-CTEM^{N+} model simulated global total mean values of C, water and energy fluxes and C pools were broadly in agreement with the observation-based estimates and values reported in previous modeling studies in the literature. The inclusion of the N processes in CLASS-CTEM^{N+} model improved the simulation of the influence of N limitation on the spatial distribution of C uptake and loss, with greater C sink activity occurring in mid-to-high latitudes in response to climate change and smaller C sink occurring in the southern ecosystems and tropical forests due to N limitation associated with increased CO_2 fertilization and forest regrowth. Analysis of long-term annual variations over 1901-2010 periods showed different responses from the two models (C-N and C-only versions) in response to evolving climate, CO_2 concentration levels, and N deposition. For the recent industrial period (1980-2010), the C-N coupled model indicated a strong N attenuation effect when compared with the C-only model. Results suggested that responses of available N in terrestrial ecosystems have not significantly affected the total amount of terrestrial C sequestration over this period, but these N responses showed a strong influence on the spatial distribution of simulated C budgets, especially in high latitude regions during summer months, where N limitation is well documented.

This is first application of the CLASS-CTEM^{N+} model at global scales (at 0.5 x 0.5 spatial resolution) to simulate C, water and energy budgets of terrestrial ecosystems. This work essentially helped to identify and diagnose the impact of N controls on the simulated spatio-temporal patterns of terrestrial C sinks and sources; and helped to evaluate and quantify the variability of simulated N effects on different plant functional types. It increased our confidence in the ability of CLASS-CTEM^{N+} to simulate the spatiotemporal variability of global ecosystem fluxes and stocks at larger scales. There are other biophysical and physiological processes and factors that might affect terrestrial ecosystem C dynamics but this analysis did not consider them, e.g., land use and land cover changes, phosphorous limitation in tropical forests, fires and insect outbreaks. Despite these limitations and challenges, the CLASS-CTEM^{N+} model performed well and provided a realistic simulation of plant productivity at global scale.

This study provides a framework and benchmark for future analysis on the interactive effects of C-N dynamics on terrestrial ecosystems and the carbon-climate feedbacks. Inclusion of a nitrogen cycle in the CLASS-CTEM^{N+} model and it may help the Canadian Earth System Model in simulating multi-century climate scenarios for future IPCC Assessment Report, as well as for policy development and help Canada meet its international obligations to reduce its greenhouse gas emissions.

Acknowledgements

Funding for this study was provided by the Natural Sciences and Engineering Research Council (NSERC) of Canada Discovery and Strategic grants and Ontario Ministry of Environment (MOE). Canadian Foundation of Innovation (CFI) and Ontario Innovation Trust (OIT) provided funds for computational facilities in our lab. Support from Environment Canada is acknowledged for CLASS and CTEM models. Model forcing and input data for this work was provided by the North American Carbon Program (NACP) - Multi-Scale Synthesis and Terrestrial Model Intercomparison Project (MsTMIP). We acknowledge NACP, the National Centers for Environmental Prediction (NCEP) and National Center for Atmospheric Research (NCAR) for these data and support. We acknowledge contributions from many scientists from Environment Canada, who have contributed to the development of CLASS and CTEM models over the past many years. We acknowledge SHARCNET and Compute Canada for providing computational faculties to make these simulations. We greatly appreciate technical support from Sergey Mashchenko at SHARCNET at McMaster University. We would also like to thank Dr. Jing Chen and Dr. Mike Waddington for their advice and comments that led to significant improvements in this work and manuscript.

4.6 Reference

Ajtay, M.J., Ketner, P., Duvigneaud, P., 1979. Terrestrial Primary Production and Phytomass, in: Bolin, B., Degens, E.T., Ketner, P. (Eds.), The Global Carbon Cycle, SCOPE 13. John Wiley & Sons, New York, pp. 129–182.

Arain, M.A., Black, T.A., Barr, A.G., Jarvis, P.G., Massheder, J.M., Verseghy, D.L., Nesic, Z., 2002. Effects of seasonal and interannual climate variability on net ecosystem productivity of boreal deciduous and conifer forests. Can. J. For. Res. Can. Rech. For. 32, 878–891.

Arain, M.A., Yuan, F.M., Black, T.A., 2006. Soil-plant nitrogen cycling modulated carbon exchanges in a western temperate conifer forest in Canada. Agric. For. Meteorol. 140, 171–192.

Arneth, A., Harrison, S.P., Zaehle, S., Tsigaridis, K., Menon, S., Bartlein, P.J., Feichter, J., Korhola, A., Kulmala, M., O'Donnell, D., Schurgers, G., Sorvari, S., Vesala, T., 2011. Terrestrial biogeochemical feedbacks in the climate system. Nat. Geosci 3, 525–532.

Arora, V.K., 2001. Assessment of simulated water balance for continental-scale river basins in an AMIP 2 simulation. J. Geophys. Res. 106, 14827. doi:10.1029/2000JD900698

Arora, V.K., Boer, G.J., 2003. A representation of variable root distribution in dynamic vegetation models. Earth Interact. 7, 6–19.

Arora, V.K., Boer, G.J., 2005a. A parameterization of leaf phenology for the terrestrial ecosystem component of climate models. Glob. Chang. Biol. 11, 39–59.

Arora, V.K., Boer, G.J., 2005b. Fire as an interactive component of dynamic vegetation models. J. Geophys. Res. 110.

Arora, V.K., Boer, G.J., 2006. The Temporal Variability of Soil Moisture and Surface Hydrological Quantities in a Climate Model. J. Clim. 19, 5875–5888. doi:10.1175/JCLI3926.1

Arora, V.K., Boer, G.J., 2006. Simulating competition and coexistence between plant functional types in a dynamic vegetation model. Earth Interact. 10.

Arora, V.K., Boer, G.J., Christian, J.R., Curry, C.L., Denman, K.L., Zahariev, K., Flato, G.M., Scinocca, J.F., Merryfield, W.J., Lee, W.G., 2009. The Effect of Terrestrial Photosynthesis Down Regulation on the Twentieth-Century Carbon Budget Simulated with the CCCma Earth System Model. J. Clim. 22, 6066–6088. doi:doi:10.1175/2009JCLI3037.1

Avissar, R., 2002. Preface to special issue on the Large-Scale Biosphere-Atmosphere Experiment in Amazonia (LBA). J. Geophys. Res. 107, 8034. doi:10.1029/2002JD002507

Baldocchi, D., Falge, E., Gu, L., Olson, R., Hollinger, D., Running, S., Anthoni, P., Bernhofer, C., Davis, K., Evans, R., Fuentes, J., Goldstein, A., Katul, G., Law, B., Lee, X., Malhi, Y., Meyers, T., Munger, W., Oechel, W., Paw, K.T., Pilegaard, K., Schmid, H.P., Valentini, R., Verma, S., Vesala, T., Wilson, K., Wofsy, S., 2001. FLUXNET: A New Tool to Study the Temporal and Spatial Variability of Ecosystem–Scale Carbon Dioxide, Water Vapor, and Energy Flux Densities. Bull. Am. Meteorol. Soc. 82, 2415–2434. doi:10.1175/1520-0477(2001)082<2415:FANTTS>2.3.CO;2

Balshi, M.S., McGuire, A.D., Zhuang, Q., Melillo, J., Kicklighter, D.W., Kasischke, E., Wirth, C., Flannigan, M., Harden, J., Clein, J.S., Burnside, T.J., McAllister, J., Kurz, W.A., Apps, M., Shvidenko, A., 2007. The role of historical fire disturbance in the carbon dynamics of the pan-boreal region: A process-based analysis. J. Geophys. Res. 112, G02029. doi:10.1029/2006JG000380

Beer, C., Reichstein, M., Tomelleri, E., Ciais, P., Jung, M., Carvalhais, N., Rodenbeck, C., Arain, M.A., Baldocchi, D., Bonan, G.B., Bondeau, A., Cescatti, A., Lasslop, G., Lindroth, A., Lomas, M., Luyssaert, S., Margolis, H., Oleson, K.W., Roupsard, O., Veenendaal, E., Viovy, N., Williams, C., Woodward, F.I., Papale, D., 2011. Terrestrial Gross Carbon Dioxide Uptake: Global Distribution and Covariation with Climate. Science (80-.). 329, 834–838. doi:10.1126/science.1184984

Beier, C., Emmett, B.A., Peelas, J., Schmidt, I.K., Tietema, A., Estiarte, M., Gundersen, P., Llorens, L., Riis-Nielsen, T., Sowerby, A., Gorissen, A., 2008. Carbon and nitrogen cycles in European ecosystems respond differently to global warming. Sci. Total Environ. In Press, .

Bonan, G.B., Levis, S., 2010. Quantifying carbon-nitrogen feedbacks in the Community Land Model (CLM4). Geophys. Res. Lett. 37, 1–6. doi:10.1029/2010GL042430

Canadell, J.G., Pataki, D.E., Pitelka, L.F. (Eds.), 2007. Terrestrial Ecosystems in a Changing World, Global Change — The IGBP Series. Springer Berlin Heidelberg, Berlin, Heidelberg. doi:10.1007/978-3-540-32730-1

Carlson, T.N., Ripley, D.A., 1997. On the relation between NDVI, fractional vegetation cover, and leaf area index. Remote Sens. Environ. 62, 241–252. doi:10.1016/S0034-4257(97)00104-1

Chahine, M.T., 1992. The hydrological cycle and its influence on climate. Nature 359, 373–380. doi:10.1038/359373a0

Chen, J.M., Mo, G., Pisek, J., Liu, J., Deng, F., Ishizawa, M., Chan, D., 2012. Effects of foliage clumping on the estimation of global terrestrial gross primary productivity. Global Biogeochem. Cycles 26, n/a–n/a. doi:10.1029/2010GB003996

Churkina, G., Trusilova, K., Vetter, M., Dentener, F., 2007. Contributions of nitrogen deposition and forest regrowth to terrestrial carbon uptake. Carbon Balance Manag. 2, 5. doi:10.1186/1750-0680-2-5

Ciais, P., Reichstein, M., Viovy, N., Granier, A., Ogee, J., Allard, V., Aubinet, M., Buchmann, N., Bernhofer, C., Carrara, A., Chevallier, F., De Noblet, N., Friend, A.D., Friedlingstein, P., Grunwald, T., Heinesch, B., Keronen, P., Knohl, A., Krinner, G., Loustau, D., Manca, G., Matteucci, G., Miglietta, F., Ourcival, J.M., Papale, D., Pilegaard, K., Rambal, S., Seufert, G., Soussana, J.F., Sanz, M.J., Schulze, E.D., Vesala, T., Valentini, R., 2005. Europe-wide reduction in primary productivity caused by the heat and drought in 2003. Nature 437, 529–533.

Ciais, P., Schelhaas, M.J., Zaehle, S., Piao, S.L., Cescatti, A., Liski, J., Luyssaert, S., Le-Maire, G., Schulze, E.D., Bouriaud, O., Freibauer, A., Valentini, R., Nabuurs, G.J., 2008. Carbon accumulation in European forests. Nat. Geosci 1, 425–429.

Collatz, G., Ribas-Carbo, M., Berry, J., 1992. Coupled Photosynthesis-Stomatal Conductance Model for Leaves of C 4 Plants. Aust. J. Plant Physiol. 19, 519. doi:10.1071/PP9920519

Collatz, G.J., Ball, J.T., Grivet, C., Berry, J.A., 1991. Physiological and environmental regulation of stomatal conductance, photosynthesis and transpiration: a model that includes a laminar boundary layer. Agric. For. Meteorol. 54, 107–136. doi:10.1016/0168-1923(91)90002-8

Cramer, W., Kicklighter, D.W., Bondeau, A., Iii, B.M., Churkina, G., Nemry, B., Ruimy, A., Schloss, A.L., Intercomparison, T.P.O.T.P., 1999. Comparing global models of terrestrial net primary productivity (NPP): overview and key results. Glob. Chang. Biol. 5, 1–15. doi:10.1046/j.1365-2486.1999.00009.x

Davidson, E.A., Reis de Carvalho, C.J., Vieira, I.C.G., Figueiredo, R. de O., Moutinho, P., Yoko Ishida, F., Primo dos Santos, M.T., Benito Guerrero, J., Kalif, K., Tuma Sabá, R., 2004. Nitrogen and Phosphorus limitation of biomass growth in a tropical secondary forest. Ecol. Appl. 14, 150–163. doi:10.1890/01-6006

Denman, K.L., 2007. Couplings Between Changes in the Climate System and Biogeochemistry, in: Solomon, S and Qin, D and Manning, M and Marquis, M and Averyt, K and Tignor, MMB and Miller, HL and Chen, Z. (Ed.), CLIMATE CHANGE 2007: THE PHYSICAL SCIENCE BASIS. CAMBRIDGE UNIV PRESS, 32 AVENUE OF THE AMERICAS, NEW YORK, NY 10013-2473 USA, pp. 499–587.

Dentener, F., Drevet, J., Lamarque, J.F., Bey, I., Eickhout, B., Fiore, A.M., 2006. Nitrogen and sulfur deposition on regional and global scales: A multimodel evaluation. Glob. Biogeochem. Cycles.

Dickinson, R.E., Shaikh, M., Bryant, R., Graumlich, L., 1998. Interactive Canopies for a Climate Model. J. Clim. 11, 2823–2836. doi:10.1175/1520-0442(1998)011<2823:ICFACM>2.0.CO;2

Dirmeyer, P.A., Gao, X., Zhao, M., Guo, Z., Oki, T., Hanasaki, N., 2006. GSWP-2: Multimodel Analysis and Implications for Our Perception of the Land Surface. Bull. Am. Meteorol. Soc. 87, 1381–1397. doi:10.1175/BAMS-87-10-1381

Dixon, R.K., Solomon, A.M., Brown, S., Houghton, R.A., Trexier, M.C., Wisniewski, J., 1994. Carbon pools and flux of global forest ecosystems. Science 263, 185–90. doi:10.1126/science.263.5144.185

Döll, P., 2002. Impact of Climate Change and Variability on Irrigation Requirements: A Global Perspective. Clim. Change 54, 269–293. doi:10.1023/A:1016124032231

Dolman, A.J., van der Werf, G.R., van der Molen, M.K., Ganssen, G., Erisman, J.-W., Strengers, B., 2010. A carbon cycle science update since IPCC AR-4. Ambio 39, 402–12.

Erb, K.-H., Haberl, H., Jepsen, M.R., Kuemmerle, T., Lindner, M., Müller, D., Verburg, P.H., Reenberg, A., 2013. A conceptual framework for analysing and measuring land-use intensity. Curr. Opin. Environ. Sustain. 5, 464–470. doi:10.1016/j.cosust.2013.07.010

FAO/IIASA/ISRIC/ISSCAS/JRC, 2012. Harmonized World Soil Database (version 1.2) [WWW Document]. FAO, Rome, Italy IIASA, Laxenburg, Austria. URL http://webarchive.iiasa.ac.at/Research/LUC/External-World-soil-database/HTML/index.html?sb=1 (accessed 4.29.14).

Farquhar, G.D., von Caemmerer, S., Berry, J.A., 1980. A biochemical model of photosynthetic CO2 assimilation in leaves of C 3 species. Planta 149, 78–90. doi:10.1007/BF00386231

Fekete, B.M., Vörösmarty, C.J., Roads, J.O., Willmott, C.J., 2004. Uncertainties in Precipitation and Their Impacts on Runoff Estimates. J. Clim. 17, 294–304. doi:10.1175/1520-0442(2004)017<0294:UIPATI>2.0.CO;2

Felzer, B.S., Cronin, T., Reilly, J.M., Melillo, J.M., Wang, X., 2007. Impacts of ozone on trees and crops. Comptes Rendus Geosci. 339, 784–798. doi:10.1016/j.crte.2007.08.008

Felzer, B.S., Cronin, T.W., Melillo, J.M., Kicklighter, D.W., Schlosser, C.A., 2009. Importance of carbon-nitrogen interactions and ozone on ecosystem hydrology during the 21st century. J. Geophys. Res. 114, G01020. doi:10.1029/2008JG000826

Felzer, B.S., Cronin, T.W., Melillo, J.M., Kicklighter, D.W., Schlosser, C.A., Dangal, S.R.S., 2011. Nitrogen effect on carbon-water coupling in forests, grasslands, and shrublands in the arid western United States. J. Geophys. Res. 116, G03023. doi:10.1029/2010JG001621

Findell, K.L., Gentine, P., Lintner, B.R., Kerr, C., 2011. Probability of afternoon precipitation in eastern United States and Mexico enhanced by high evaporation. Nat. Geosci 4, 434–439.

Fleischer, K., Rebel, K.T., van der Molen, M.K., Erisman, J.W., Wassen, M.J., van Loon, E.E., Montagnani, L., Gough, C.M., Herbst, M., Janssens, I.A., Gianelle, D., Dolman, A.J., 2013. The contribution of nitrogen deposition to the photosynthetic capacity of forests. Global Biogeochem. Cycles 27, 187–199. doi:10.1002/gbc.20026

Frank, D.C., Esper, J., Raible, C.C., Büntgen, U., Trouet, V., Stocker, B., Joos, F., 2010. Ensemble reconstruction constraints on the global carbon cycle sensitivity to climate. Nature 463, 527–30. doi:10.1038/nature08769

Gallardo, A., Schlesinger, W.H., 1992. Carbon and nitrogen limitations of soil microbial biomass in desert ecosystems. Biogeochemistry 18, 1–17. doi:10.1007/BF00000423

Galloway, J.N., Dentener, F.J., Capone, D.G., Boyer, E.W., Howarth, R.W., Seitzinger, S.P., Asner, G.P., Cleveland, C.C., Green, P.A., Holland, E.A., Karl, D.M., Michaels, A.F., Porter, J.H., Townsend, A.R., Vöosmarty, C.J., 2004. Nitrogen Cycles: Past, Present, and Future. Biogeochemistry 70, 153–226.

Gerber, S., Hedin, L.O., Oppenheimer, M., Pacala, S.W., Shevliakova, E., 2010. Nitrogen cycling and feedbacks in a global dynamic land model. Global Biogeochem. Cycles 24, n/a–n/a. doi:10.1029/2008GB003336

Global Soil Data Task Group, 2000. Global Gridded Surfaces of Selected Soil Characteristics (International Geosphere-Biosphere Programme - Data and Information System) [WWW Document]. Available on-line [http//www.daac.ornl.gov] from Oak Ridge Natl. Lab. Distrib. Act. Arch. Center, Oak Ridge, Tennessee, U.S.A. doi:10.3334/ORNLDAAC/569

GLOBALVIEW-CO2, 2013. Cooperative Global Atmospheric Data Integration Project. 2013, updated annually. Multi-laboratory compilation of synchronized and gap-filled atmospheric carbon dioxide records for the period 1979-2012 (obspack_co2_1_GLOBALVIEW-CO2_2013_v1.0.4_2013-12-23).

Goetz, S.J., Prince, S.D., Small, J., Gleason, A.C.R., 2000. Interannual variability of global terrestrial primary production : observations that differed regionally over the 8-year integrated global slight trend toward increased values through with boreal regions increasing regions for each IøC rise in air tempera 105.

Gordon, L.J., Steffen, W., Jönsson, B.F., Folke, C., Falkenmark, M., Johannessen, A., 2005. Human modification of global water vapor flows from the land surface. Proc. Natl. Acad. Sci. U. S. A. 102, 7612–7. doi:10.1073/pnas.0500208102

Gurney, K.R., Baker, D., Rayner, P., Denning, S., 2008. Interannual variations in continental-scale net carbon exchange and sensitivity to observing networks estimated from atmospheric CO 2 inversions for the period 1980 to 2005. Global Biogeochem. Cycles 22, n/a–n/a. doi:10.1029/2007GB003082

Gurney, K.R., Law, R.M., Denning, A.S., Rayner, P.J., Pak, B.C., Baker, D., Bousquet, P., Bruhwiler, L., Chen, Y.-H., Ciais, P., Fung, I.Y., Heimann, M., John, J., Maki, T., Maksyutov, S., Peylin, P., Prather, M., Taguchi, S., 2004. Transcom 3 inversion intercomparison: Model mean results for the estimation of seasonal carbon sources and sinks. Global Biogeochem. Cycles 18, n/a–n/a. doi:10.1029/2003GB002111

Harrington, R.A., Fownes, J.H., Vitousek, P.M., 2001. Production and Resource Use Efficiencies in N- and P-Limited Tropical Forests: A Comparison of Responses to Long-term Fertilization. Ecosystems 4, 646–657. doi:10.1007/s10021-001-0034-z

Hicke, J.A., 2005. NCEP and GISS solar radiation data sets available for ecosystem modeling: Description, differences, and impacts on net primary production. Global Biogeochem. Cycles 19, n/a–n/a. doi:10.1029/2004GB002391

Hietz, P., Turner, B.L., Wanek, W., Richter, A., Nock, C.A., Wright, S.J., 2011. Long-term change in the nitrogen cycle of tropical forests. Science 334, 664–6. doi:10.1126/science.1211979

Hobbie, S.E., Nadelhoffer, K.J., Högberg, P., 2002. A synthesis: The role of nutrients as constraints on carbon balances in boreal and arctic regions. Plant Soil 242, 163–170.

Hoffman, F.M., Covey, C.C., Fung, I.Y., Randerson, J.T., Thornton, P.E., Lee, Y.-H., Rosenbloom, N.A., Stöckli, R.C., Running, S.W., Bernholdt, D.E., Williams, D.N., 2007. Results from the carbon-land model intercomparison project (C-LAMP) and availability of the data on the earth system grid (ESG). J. Phys. Conf. Ser. 78, 012026. doi:10.1088/1742-6596/78/1/012026

Holland, E., Braswell, B., Lamarque, J.F., Townsend, A., Sulzman, J., J.-F, M., uuml, ller, 1997. Variations in the predicted spatial distribution of atmospheric nitrogen deposition and their impact on carbon uptake by terrestrial ecosystems. J. Geophys. Res.

Holland, E.A., Braswell, B.H., Sulzman, J., Lamarque, J.-F., 2005. Nitrogen deposition onto the United States and Western Europe: synthesis of observations and models. Ecol. Appl. 15, 38–57. doi:10.1890/03-5162

Huang, S., Arain, M.A., Arora, V.K., Yuan, F., Brodeur, J., Peichl, M., 2011. Analysis of nitrogen controls on carbon and water exchanges in a conifer forest using the CLASS-CTEMN+ model. Ecol. Modell. 222, 3743–3760. doi:10.1016/j.ecolmodel.2011.09.008

Hudiburg, T., Law, B., Turner, D.P., Campbell, J., Donato, D., Duane, M., 2009. Carbon dynamics of Oregon and Northern California forests and potential land-based carbon storage. Ecol. Appl. 19, 163–180. doi:10.1890/07-2006.1

Hungate, B.A., Dukes, J.S., Shaw, M.R., Luo, Y., Field, C.B., 2003. ATMOSPHERIC SCIENCE: Nitrogen and Climate Change. Science (80-.). 302, 1512–1513. doi:10.1126/science.1091390

Huntzinger, D.N., Schwalm, C., Michalak, A.M., Schaefer, K., King, A.W., Wei, Y., Jacobson, A., Liu, S., Cook, R.B., Post, W.M., Berthier, G., Hayes, D., Huang, M., Ito, A., Lei, H., Lu, C., Mao, J., Peng, C.H., Peng, S., Poulter, B., Riccuito, D., Shi, X., Tian, H., Wang, W., Zeng, N., Zhao, F., Zhu, Q., 2013. The North American Carbon Program Multi-scale synthesis and Terrestrial Model Intercomparison Project – Part 1: Overview and experimental design. Geosci. Model Dev. Discuss. 6, 3977–4008. doi:10.5194/gmdd-6-3977-2013

Huston, M.A., Wolverton, S., 2009. The global distribution of net primary production: resolving the paradox. Ecol. Monogr. 79, 343–377. doi:10.1890/08-0588.1

IPCC, 2007a. AR4 SPM. http://www.ipcc.ch/.

IPCC, 2007b. Climate Change 2007: The Physical Science Basis, Contribution of Working Group I to the Fourth Assessment Report of the Intergovernmental Panel on Climate Change. Cambridge University Press, Cambridge.

Jain, A., Yang, X., Kheshgi, H., McGuire, A.D., Post, W., Kicklighter, D., 2009. Nitrogen attenuation of terrestrial carbon cycle response to global environmental factors. Global Biogeochem. Cycles 23, n/a–n/a. doi:10.1029/2009GB003519

Janssens, I.A., Dieleman, W., Luyssaert, S., Subke, J.A., Reichstein, M., Ceulemans, R., Ciais, P., Dolman, A.J., Grace, J., Matteucci, G., Papale, D., Piao, S.L., Schulze, E.D., Tang, J., Law, B.E., 2011. Reduction of forest soil respiration in response to nitrogen deposition. Nat. Geosci 3, 315–322.

Jarvis, P., Linder, S., 2000. Constraints to growth of boreal forests. Nature 405, 904–5. doi:10.1038/35016154

Jarvis, P.G., 1976. The Interpretation of the Variations in Leaf Water Potential and Stomatal Conductance Found in Canopies in the Field. Philos. Trans. R. Soc. B Biol. Sci. 273, 593–610. doi:10.1098/rstb.1976.0035

Jiménez, C., Prigent, C., Mueller, B., Seneviratne, S.I., McCabe, M.F., Wood, E.F., Rossow, W.B., Balsamo, G., Betts, A.K., Dirmeyer, P.A., Fisher, J.B., Jung, M., Kanamitsu, M., Reichle, R.H., Reichstein, M., Rodell, M., Sheffield, J., Tu, K., Wang, K., 2011. Global intercomparison of 12 land surface heat flux estimates. J. Geophys. Res. 116, D02102. doi:10.1029/2010JD014545

Jones, C.D., Cox, P., Huntingford, C., 2003. Uncertainty in climate-carbon-cycle projections associated with the sensitivity of soil respiration to temperature. Tellus B 55, 642–648. doi:10.1034/j.1600-0889.2003.01440.x

Jung, M., Henkel, K., Herold, M., Churkina, G., 2006. Exploiting synergies of global land cover products for carbon cycle modeling. Remote Sens. Environ. 101, 534–553. doi:10.1016/j.rse.2006.01.020

Jung, M., Reichstein, M., Bondeau, A., 2009. Towards global empirical upscaling of FLUXNET eddy covariance observations: validation of a model tree ensemble approach using a biosphere model. Biogeosciences 6, 2001–2013. doi:10.5194/bg-6-2001-2009

Jung, M., Reichstein, M., Ciais, P., Seneviratne, S.I., Sheffield, J., Goulden, M.L., Bonan, G., Cescatti, A., Chen, J., de Jeu, R., Dolman, A.J., Eugster, W., Gerten, D., Gianelle, D., Gobron, N., Heinke, J., Kimball, J., Law, B.E., Montagnani, L., Mu, Q., Mueller, B., Oleson, K., Papale, D., Richardson, A.D., Roupsard, O., Running, S., Tomelleri, E., Viovy, N., Weber, U., Williams, C., Wood, E., Zaehle, S., Zhang, K., 2010. Recent decline in the global land evapotranspiration trend due to limited moisture supply. Nature 467, 951–4. doi:10.1038/nature09396

Jung, M., Reichstein, M., Margolis, H.A., Cescatti, A., Richardson, A.D., Arain, M.A., Arneth, A., Bernhofer, C., Bonal, D., Chen, J., Gianelle, D., Gobron, N., Kiely, G., Kutsch, W., Lasslop, G., Law, B.E., Lindroth, A., Merbold, L., Montagnani, L., Moors, E.J., Papale, D., Sottocornola, M., Vaccari, F., Williams, C., 2011. Global patterns of land-atmosphere fluxes of carbon dioxide, latent heat, and sensible heat derived from eddy covariance, satellite, and meteorological observations. J. Geophys. Res. 116, G00J07. doi:10.1029/2010JG001566

Kanamitsu, M., Ebisuzaki, W., Woollen, J., Yang, S.-K., Hnilo, J.J., Fiorino, M., Potter, G.L., 2002. NCEP–DOE AMIP-II Reanalysis (R-2). Bull. Am. Meteorol. Soc. 83, 1631–1643. doi:10.1175/BAMS-83-11-1631

Keeling, C.D., Chin, J.F.S., Whorf, T.P., 1996. Increased activity of northern vegetation inferred from atmospheric CO2 measurements. Nature 382, 146–149. doi:10.1038/382146a0

Kothavala, Z., Arain, M.A., Black, T.A., Verseghy, D., 2005. The simulation of energy, water vapor and carbon dioxide fluxes over common crops by the Canadian Land Surface Scheme (CLASS). Agric. For. Meteorol. 133, 89–108. doi:10.1016/j.agrformet.2005.08.007

Krinner, G., Viovy, N., de Noblet-Ducoudré, N., Ogée, J., Polcher, J., Friedlingstein, P., Ciais, P., Sitch, S., Prentice, I.C., 2005. A dynamic global vegetation model for studies of the coupled atmosphere-biosphere system. Global Biogeochem. Cycles 19, n/a–n/a. doi:10.1029/2003GB002199

Kuppel, S., Peylin, P., Chevallier, F., Bacour, C., Maignan, F., Richardson, A.D., 2012. Constraining a global ecosystem model with multi-site eddy-covariance data. Biogeosciences 9, 3757–3776. doi:10.5194/bg-9-3757-2012

Kurz, W.A., Dymond, C.C., Stinson, G., Rampley, G.J., Neilson, E.T., Carroll, A.L., Ebata, T., Safranyik, L., 2008. Mountain pine beetle and forest carbon feedback to climate change. Nature 452, 987–90. doi:10.1038/nature06777

Labat, D., Goddéris, Y., Probst, J.L., Guyot, J.L., 2004. Evidence for global runoff increase related to climate warming. Adv. Water Resour. 27, 631–642. doi:10.1016/j.advwatres.2004.02.020

Lamarque, J.-F., Dentener, F., McConnell, J., Ro, C.-U., Shaw, M., Vet, R., Bergmann, D., Cameron-Smith, P., Dalsoren, S., Doherty, R., Faluvegi, G., Ghan, S.J., Josse, B., Lee, Y.H., MacKenzie, I.A., Plummer, D., Shindell, D.T., Skeie, R.B., Stevenson, D.S., Strode, S., Zeng, G., Curran, M., Dahl-Jensen, D., Das, S., Fritzsche, D., Nolan, M., 2013. Multi-model mean nitrogen and sulfur deposition from the Atmospheric Chemistry and Climate Model Intercomparison Project (ACCMIP): evaluation of historical and projected future changes. Atmos. Chem. Phys. 13, 7997–8018. doi:10.5194/acp-13-7997-2013

Lasslop, G., Reichstein, M., Kattge, J., Papale, D., 2008. Influences of observation errors in eddy flux data on inverse model parameter estimation. Biogeosciences 5, 1311–1324. doi:10.5194/bg-5-1311-2008

Lasslop, G., REICHSTEIN, M., PAPALE, D., RICHARDSON, A.D., ARNETH, A., BARR, A., STOY, P., WOHLFAHRT, G., 2010. Separation of net ecosystem exchange into assimilation and respiration using a light response curve approach: critical issues and global evaluation. Glob. Chang. Biol. 16, 187–208. doi:10.1111/j.1365-2486.2009.02041.x

Le Quere, C., Raupach, M.R., Canadell, J.G., Marland, G., et al., 2009. Trends in the sources and sinks of carbon dioxide. Nat. Geosci 2, 831–836.

Lehmann, J., Skjemstad, J., Sohi, S., Carter, J., Barson, M., Falloon, P., Coleman, K., Woodbury, P., Krull, E., 2008. Australian climate-carbon cycle feedback reduced by soil black carbon. Nat. Geosci 1, 832–835.

Leuning, R., Kelliher, F.M., Pury, D.G.G., Schulze, E.-D., 1995. Leaf nitrogen, photosynthesis, conductance and transpiration: scaling from leaves to canopies. Plant, Cell Environ. 18, 1183–1200.

Leuning, R., Kelliher, F.M., Pury, D.G.G., Schulze, E.-D., 1995. Leaf nitrogen, photosynthesis, conductance and transpiration: scaling from leaves to canopies. Plant, Cell Environ. 18, 1183–1200. doi:10.1111/j.1365-3040.1995.tb00628.x

Liu, L., Greaver, T.L., 2009. A review of nitrogen enrichment effects on three biogenic GHGs: the CO2 sink may be largely offset by stimulated N2O and CH4 emission. Ecol. Lett. 12, 1103–17. doi:10.1111/j.1461-0248.2009.01351.x

Liu, X., Zhang, Y., Han, W., Tang, A., Shen, J., Cui, Z., Vitousek, P., Erisman, J.W., Goulding, K., Christie, P., Fangmeier, A., Zhang, F., 2013. Enhanced nitrogen deposition over China. Nature 494, 459–62. doi:10.1038/nature11917

Luo, Y., Hui, D., Zhang, D., 2006. Elevated CO2 stimulates net accumulations of carbon and nitrogen in land ecosystems: a meta-analysis. Ecology 87, 53–63. doi:10.1890/04-1724

Luo, Y., Su, B.O., Currie, W.S., Dukes, J.S., Finzi, A., Hartwig, U., Hungate, B., Mc Murtrie, R.E., Oren, R.A.M., Parton, W.J., Pataki, D.E., Shaw, M.R., Zak, D.R., Field, C.B., 2004. Progressive Nitrogen Limitation of Ecosystem Responses to Rising Atmospheric Carbon Dioxide. Bioscience 54, 731–739.

Luyssaert, S., Inglima, I., Jung, M., Richardson, A.D., Reichstein, M., Papale, D., Piao, S.L., Schulze, E.-D., Wingate, L., Matteucci, G., Aragao, L., Aubinet, M., Beer, C., Bernhofer, C., Black, K.G., Bonal, D., Bonnefond, J.M., Chambers, J., Ciais, P., Cook, B., Davis, K.J., Dolman, A.J., Gielen, B., Goulden, M., Grace, J., Grrnier, A., Gelle, A., Griffis, T., Grunwald, T., Guidolotti, G., Hanson, P.J., Harding, R., Hollinger, D.Y., Hutyra, L.R., Kolari, P., Kruijt, B., Kutsch, W., Lagergren, F., Laurila, T., Law, B.E., Le Maire, G., Lindroth, A., Loustau, D., Malhi, Y., Mateus, J., Migliavacca, M., Misson, L., Montagnani, L., Moncrieff, J., Moors, E., Munger, J.W., Nikinmaa, E., Ollinger, S. V., Pita, G., Rebmann, C., Roupsard, O., Saigusa, N., Sanz, M.J., Seufert, G., Sierra, C., Smith, M.-L., Tang, J., Valentini, R., Vesala, T., Janssens, I.A., 2007. CO2 balance of boreal, temperate, and tropical forests derived from a global database. Glob. Chang. Biol. 13, 2509–2537. doi:10.1111/j.1365-2486.2007.01439.x

Mahecha, M.D., Reichstein, M., Carvalhais, N., Lasslop, G., Lange, H., Seneviratne, S.I., Vargas, R., Ammann, C., Arain, M.A., Cescatti, A., Janssens, I. a, Migliavacca, M., Montagnani, L., Richardson, A.D., 2010. Global convergence in the temperature sensitivity of respiration at ecosystem level. Science 329, 838–40. doi:10.1126/science.1189587

Marland, G., Boden, T.A., Andres, R.J., 2008. Global, Regional, and National Fossil Fuel CO2 Emissions [WWW Document]. Trends A Compend. Data Glob. Chang. Carbon Dioxide Inf. Anal. Center, Oak Ridge Natl. Lab. U.S. Dep. Energy, Oak Ridge, Tenn., U.S.A. URL http://cdiac.ornl.gov/trends/emis/overview.html (accessed 5.12.14).

Matimati, I., Verboom, G.A., Cramer, M.D., 2014. Nitrogen regulation of transpiration controls mass-flow acquisition of nutrients. J. Exp. Bot. 65, 159–68. doi:10.1093/jxb/ert367

Matthews, E., Fung, I., 1987. Methane emission from natural wetlands: Global distribution, area, and environmental characteristics of sources. Global Biogeochem. Cycles 1, 61–86. doi:10.1029/GB001i001p00061

McGuire, A.D., Chapin III, F.S., Wirth, C., Apps, M., Bhatti, J., Callaghan, T., Christensen, T., Clein, J., Fukuda, M., Maximov, T., Onuchin, A., Shvidenko, A., Vaganov, E., 2007. Responses of High Latitude Ecosystems to Global Change: Potential Consequences for the Climate System, in: Canadell, J., Pataki, D., Pitelka, L. (Eds.), Terrestrial Ecosystems in a Changing World SE - 24, Global Change — The IGBP Series. Springer Berlin Heidelberg, pp. 297–310. doi:10.1007/978-3-540-32730-1_24

Meissner, K.J., Weaver, A.J., Matthews, H.D., Cox, P.M., 2003. The role of land surface dynamics in glacial inception: a study with the UVic Earth System Model. Clim. Dyn. 21, 515–537. doi:10.1007/s00382-003-0352-2

Melton, J.R., Arora, V.K., 2014. Sub-grid scale representation of vegetation in global land surface schemes: implications for estimation of the terrestrial carbon sink. Biogeosciences 11, 1021–1036. doi:10.5194/bg-11-1021-2014

Mitchell, P.J., Veneklaas, E., Lambers, H., Burgess, S.S.O., 2009. Partitioning of evapotranspiration in a semi-arid eucalypt woodland in south-western Australia. Agric. For. Meteorol. 149, 25–37. doi:10.1016/j.agrformet.2008.07.008

Mitchell, T.D., Jones, P.D., 2005. An improved method of constructing a database of monthly climate observations and associated high-resolution grids. Int. J. Climatol. 25, 693–712. doi:10.1002/joc.1181

Monfreda, C., Ramankutty, N., Foley, J.A., 2008. Farming the planet: 2. Geographic distribution of crop areas, yields, physiological types, and net primary production in the year 2000. Global Biogeochem. Cycles 22, n/a–n/a. doi:10.1029/2007GB002947

Muller-Landau, H.C., 2009. Carbon cycle: Sink in the African jungle. Nature 457, 969–970.

Mycroft, E.E., Zhang, J., Adams, G., Reekie, E., 2008. Elevated CO2 will not select for enhanced growth in white spruce despite genotypic variation in response. Basic Appl. Ecol. In Press, .

Nabuurs, G.-J., Lindner, M., Verkerk, P.J., Gunia, K., Deda, P., Michalak, R., Grassi, G., 2013. First signs of carbon sink saturation in European forest biomass. Nat. Clim. Chang. 3, 792–796. doi:10.1038/nclimate1853

Nadelhoffer, K.J., Emmett, B.A., Gundersen, P., Kjonaas, O.J., Koopmans, C.J., Schleppi, P., Tietema, A., Wright, R.F., 1999. Nitrogen deposition makes a minor contribution to carbon sequestration in temperate forests. Nature 398, 145–148.

Oki, T., Kanae, S., 2006. Global hydrological cycles and world water resources. Science 313, 1068–72. doi:10.1126/science.1128845

Pan, Y., Birdsey, R.A., Fang, J., Houghton, R., Kauppi, P.E., Kurz, W.A., Phillips, O.L., Shvidenko, A., Lewis, S.L., Canadell, J.G., Ciais, P., Jackson, R.B., Pacala, S.W., McGuire, A.D., Piao, S., Rautiainen, A., Sitch, S., Hayes, D., 2011. A large and persistent carbon sink in the world's forests. Science 333, 988–93. doi:10.1126/science.1201609

Piao, S., Ciais, P., Friedlingstein, P., de Noblet-Ducoudré, N., Cadule, P., Viovy, N., Wang, T., 2009. Spatiotemporal patterns of terrestrial carbon cycle during the 20th century. Global Biogeochem. Cycles 23, n/a–n/a. doi:10.1029/2008GB003339

Piao, S., Friedlingstein, P., Ciais, P., de Noblet-Ducoudré, N., Labat, D., Zaehle, S., 2007. Changes in climate and land use have a larger direct impact than rising CO2 on global river runoff trends. Proc. Natl. Acad. Sci. U. S. A. 104, 15242–7. doi:10.1073/pnas.0707213104

Post, W.M., Emanuel, W.R., Zinke, P.J., Stangenberger, A.G., 1982. Soil carbon pools and world life zones. Nature 298, 156–159. doi:10.1038/298156a0

Prentice, I.C., 2007. Climate Change 2007 - The Physical Science Basis: Working Group I Contribution to the Fourth Assessment Report of the IPCC. Cambridge University Press.

Quinn Thomas, R., Canham, C.D., Weathers, K.C., Goodale, C.L., 2011. Increased tree carbon storage in response to nitrogen deposition in the US. Nat. Geosci 3, 13–17.

Randerson, J.T., Hoffman, F.M., THORNTON, P.E., MAHOWALD, N.M., LINDSAY, K., LEE, Y.-H., NEVISON, C.D., DONEY, S.C., BONAN, G., STÖCKLI, R., COVEY, C., RUNNING, S.W., FUNG, I.Y., 2009. Systematic assessment of terrestrial biogeochemistry in coupled climate-carbon models. Glob. Chang. Biol. 15, 2462–2484. doi:10.1111/j.1365-2486.2009.01912.x

Reay, D.S., Dentener, F., Smith, P., Grace, J., Feely, R.A., 2008. Global nitrogen deposition and carbon sinks. Nat. Geosci 1, 430–437.

Richardson, A.D., Hollinger, D.Y., Burba, G.G., Davis, K.J., Flanagan, L.B., Katul, G.G., William Munger, J., Ricciuto, D.M., Stoy, P.C., Suyker, A.E., Verma, S.B., Wofsy, S.C., 2006. A multi-site analysis of random error in tower-based measurements of carbon and energy fluxes. Agric. For. Meteorol. 136, 1–18. doi:10.1016/j.agrformet.2006.01.007

Rogers, A., 2014. The use and misuse of V(c,max) in Earth System Models. Photosynth. Res. 119, 15–29. doi:10.1007/s11120-013-9818-1

Ruesch, A., Holly, K., 2008. New IPCC Tier-1 Global Biomass Carbon Map for the Year 2000 [WWW Document]. Available from ftp//cdiac.ornl.gov/pub/global carbon/. URL http://cdiac.ornl.gov/epubs/ndp/global_carbon/carbon_documentation.html (accessed 4.29.14).

Running, S.W., Nemani, R.R., HEINSCH, F.A., ZHAO, M., REEVES, M., HASHIMOTO, H., 2004. A Continuous Satellite-Derived Measure of Global Terrestrial Primary Production. Bioscience 54, 547. doi:10.1641/0006-3568(2004)054[0547:ACSMOG]2.0.CO;2

Saugier, B., Roy, J., Mooney, H.A., 2001. Estimations of global terrestrial productivity: Converging towards a single number?, in: Roy, J., Saugier, B., Mooney, H.A. (Eds.), Terrestrial Global Productivity. Academic Press, San Diego; California, pp. 543–558.

Schlesinger, W.H., 1977. Carbon Balance in Terrestrial Detritus. Annu. Rev. Ecol. Syst. 8, 51–81. doi:10.1146/annurev.es.08.110177.000411

Schwalm, C.R., Williams, C.A., Schaefer, K., Anderson, R., Arain, M.A., Baker, I., Barr, A., Black, T.A., Chen, G., Chen, J.M., Ciais, P., Davis, K.J., Desai, A., Dietze, M., Dragoni, D., Fischer, M.L., Flanagan, L.B., Grant, R., Gu, L., Hollinger, D., Izaurralde, R.C., Kucharik, C., Lafleur, P., Law, B.E., Li, L., Li, Z., Liu, S., Lokupitiya, E., Luo, Y., Ma, S., Margolis, H., Matamala, R., McCaughey, H., Monson, R.K., Oechel, W.C., Peng, C., Poulter, B., Price, D.T., Riciutto, D.M., Riley, W., Sahoo, A.K., Sprintsin, M., Sun, J., Tian, H., Tonitto, C., Verbeeck, H., Verma, S.B., 2010. A model-data intercomparison of CO2 exchange across North America: Results from the North American Carbon Program site synthesis. J. Geophys. Res. 115, G00H05. doi:10.1029/2009JG001229

Shaver, G.R., 1992. Global change and the carbon balance of arctic ecosystems, Bioscience.

Shi, X., Mao, J., Thornton, P.E., Huang, M., 2013. Spatiotemporal patterns of evapotranspiration in response to multiple environmental factors simulated by the Community Land Model. Environ. Res. Lett. 8, 024012. doi:10.1088/1748-9326/8/2/024012

Shimshi, D., 1970. The effect of nitrogen supply on transpiration and stomatal behaviour of Beans (Phaseolus Vulgaris L.). New Phytol. 69, 405–412. doi:10.1111/j.1469-8137.1970.tb02439.x

Sokolov, A.P., Kicklighter, D.W., Melillo, J.M., Felzer, B.S., Schlosser, C.A., Cronin, T.W., 2008. Consequences of Considering Carbon-Nitrogen Interactions on the Feedbacks between Climate and the Terrestrial Carbon Cycle. J. Clim. 21, 3776–3796.

Tarnocai, C., Canadell, J.G., Schuur, E.A.G., Kuhry, P., Mazhitova, G., Zimov, S., 2009. Soil organic carbon pools in the northern circumpolar permafrost region. Global Biogeochem. Cycles 23, n/a–n/a. doi:10.1029/2008GB003327

Thomas, R.Q., Zaehle, S., Templer, P.H., Goodale, C.L., 2013. Global patterns of nitrogen limitation: confronting two global biogeochemical models with observations. Glob. Chang. Biol. 19, 2986–98. doi:10.1111/gcb.12281

Thornton, P.E., Doney, S.C., Lindsay, K., Moore, J.K., Mahowald, N., Randerson, J.T., Fung, I., Lamarque, J.F., Feddema, J.J., Lee, Y.H., 2009. Carbon-nitrogen interactions regulate climate-carbon cycle feedbacks: results from an atmosphere-ocean general circulation model. Biogeosciences Discuss. 6, 3303–3354.

Thornton, P.E., Lamarque, J.-F., Rosenbloom, N.A., Mahowald, N.M., 2007. Influence of carbon-nitrogen cycle coupling on land model response to CO2 fertilization and climate variability. Glob. Biogeochem. Cycles 21.

Townsend, A.R., Braswell, B.H., Holland, E.A., Penner, J.E., 1996. Spatial and Temporal Patterns in Terrestrial Carbon Storage Due to Deposition of Fossil Fuel Nitrogen. Ecol. Appl. 6, 806–814.

Townsend, A.R., Cleveland, C.C., Houlton, B.Z., Alden, C.B., White, J.W., 2011. Multi-element regulation of the tropical forest carbon cycle. Front. Ecol. Environ. 9, 9–17. doi:10.1890/100047

Trenberth, K.E., Fasullo, J.T., Kiehl, J., 2009. Earth's Global Energy Budget. Bull. Am. Meteorol. Soc. 90, 311–323. doi:10.1175/2008BAMS2634.1

Van Aardenne, J.A., Dentener, F.J., Olivier, J.G.J., Goldewijk, C.G.M.K., Lelieveld, J., 2001. A 1°×1° resolution data set of historical anthropogenic trace gas emissions for the period 1890-1990. Global Biogeochem. Cycles 15, 909–928. doi:10.1029/2000GB001265

Verseghy, D.L., 1991. CLASS--A Canadian Land Surface Scheme for GCMS: I. Soil Model Int. J. Climatol. 11, 111–133.

Verseghy, D.L., 2000. The Canadian land surface scheme (CLASS): Its history and future. Atmosphere-Ocean 38, 1–13. doi:10.1080/07055900.2000.9649637

Verseghy, D.L., 2009. Class the canadian land surface scheme (version 3.4).

Verseghy, D.L., Lazare, M., 1993. CLASS-Canadian land surface scheme for GCMS, II. Vegetation model and coupled runs. Int. J. Climatol. 13, 347–370.

Vetter, M., Churkina, G., Jung, M., Reichstein, M., Zaehle, S., Bondeau, A., Chen, Y., Ciais, P., Feser, F., Freibauer, A., Geyer, R., Jones, C., Papale, D., Tenhunen, J., Tomelleri, E., Trusilova, K., Viovy, N., Heimann, M., 2008. Analyzing the causes and spatial pattern of the European 2003 carbon flux anomaly using seven models. Biogeosciences 5, 561–583. doi:10.5194/bg-5-561-2008

Viovy, N., 2012. CRUNCEP Version 4, :, available at: http://dods.extra.cea.fr/data/p529viov/cruncep/2012 (last access: 11 October 2012), 2012. 16011.

Wania, R., Meissner, K.J., Eby, M., Arora, V.K., Ross, I., Weaver, A.J., 2012. Carbon-nitrogen feedbacks in the UVic ESCM. Geosci. Model Dev. 5, 1137–1160. doi:10.5194/gmd-5-1137-2012

Wårlind, D., Smith, B., Hickler, T., Arneth, A., 2014. Nitrogen feedbacks increase future terrestrial ecosystem carbon uptake in an individual-based dynamic vegetation model. Biogeosciences Discuss. 11, 151–185. doi:10.5194/bgd-11-151-2014

Weber, U., Jung, M., Reichstein, M., Beer, C., Braakhekke, M.C., Lehsten, V., Ghent, D., Kaduk, J., Viovy, N., Ciais, P., Gobron, N., Rödenbeck, C., 2009. The interannual variability of Africa's ecosystem productivity: a multi-model analysis. Biogeosciences 6, 285–295. doi:10.5194/bg-6-285-2009

Wei, Y., Liu, S., Huntzinger, D.N., Michalak, A.M., Viovy, N., Post, W.M., Schwalm, C.R., Schaefer, K., Jacobson, A.R., Lu, C., Tian, H., Ricciuto, D.M., Cook, R.B., Mao, J., Shi, X., 2013. The North American Carbon Program Multi-scale Synthesis and Terrestrial Model Intercomparison Project – Part 2: Environmental driver data. Geosci. Model Dev. Discuss. 6, 5375–5422. doi:10.5194/gmdd-6-5375-2013

White, M.A., Thornton, P.E., Running, S.W., Nemani, R.R., 2000. Parameterization and Sensitivity Analysis of the BIOME–BGC Terrestrial Ecosystem Model: Net Primary Production Controls. Earth Interact. 4, 1–85. doi:10.1175/1087-3562(2000)004<0003:PASAOT>2.0.CO;2

Williams, C.A., Hanan, N.P., 2010. ENSO and IOD teleconnections for African ecosystems: evidence of destructive interference between climate oscillations. Biogeosciences Discuss. 7, 6323–6352. doi:10.5194/bgd-7-6323-2010

Winslow, J.C., Hunt, E.R., Piper, S.C., 2003. The influence of seasonal water availability on global C3 versus C4 grassland biomass and its implications for climate change research. Ecol. Modell. 163, 153–173. doi:10.1016/S0304-3800(02)00415-5

Yates, L.R., Rundel, P.W., Sylvester-Bradley, R., Cisternas, R.E., 1982. Report of the work group on savannas and shrublands. Plant Soil 67, 409–413. doi:10.1007/BF02182790

Yuan, F., McCaughey, H., Wofsy, S.C., 2008. Modeling analysis of primary controls on net ecosystem productivity of seven boreal and temperate coniferous forests across a continental transect. Glob. Chang. Biol. 14, 1765–1784.

Zaehle, S., Dalmonech, D., 2011. Carbon–nitrogen interactions on land at global scales: current understanding in modelling climate biosphere feedbacks. Curr. Opin. Environ. Sustain. 3, 311–320. doi:10.1016/j.cosust.2011.08.008

Zaehle, S., Friedlingstein, P., Friend, A.D., 2010. Terrestrial nitrogen feedbacks may accelerate future climate change. Geophys. Res. Lett. 37, L01401.

Zaehle, S., Friend, A.D., Friedlingstein, P., Dentener, F., Peylin, P., Schulz, M., 2010. Carbon and nitrogen cycle dynamics in the O-CN land surface model: 2. Role of the nitrogen cycle in the historical terrestrial carbon balance. Global Biogeochem. Cycles 24, n/a–n/a. doi:10.1029/2009GB003522

Zhao, M., Running, S.W., 2011. Drought-Induced Reduction in Global Terrestrial Net Primary Production from 2000 Through 2009. Science (80-.). 329, 940–943. doi:10.1126/science.1192666

Zhao, M., Running, S.W., Nemani, R.R., 2006. Sensitivity of Moderate Resolution Imaging Spectroradiometer (MODIS) terrestrial primary production to the accuracy of meteorological reanalyses. J. Geophys. Res. 111, G01002. doi:10.1029/2004JG000004

5. CHAPTER 5: CONCLUSION

This thesis presented the CLASS-CTEM^{N+} model development and evaluations in three major steps. The first step was to evaluate the model performance at multiple PFTs using data from 32 North America and 7 South American eddy covariance flux tower sites to improve its algorithms and parameters to simulate C, water and energy processes. The observed flux, meteorological and ancillary data were provided by the North American Carbon Program (NACP) and the Large-Scale Biosphere Atmosphere Experiment in Amazonia (LBA) initiatives. The second step was to evaluate the model performance in simulating C, water and energy fluxes and C stocks at regional and global scales (0.5 × 0.5 degree resolution) from 1901 to 2010 using data from the NACP-Multi-scale Synthesis and Terrestrial Model Intercomparison Project (MsTMIP).

The work presented in three papers includes several critical modifications in model algorithms and processes than those reported in my previously published paper (Huang et al., 2011; although, most of the work reported in that paper was part of my M.Sc thesis, however, I completed and published that paper during initial year of my Ph.D program). A summary of these modifications is given here. First, N/C ratios for leaf, steam and roots, and Rubisco-N related enzyme controls on photosynthesis were parameterized for all PFTs in CLASS-CTEM^{N+}. Second, vegetation and soil hydrology parameterizations were modified to improve evapotranspiration partitioning and to reduce photosynthetic uptake bias in rainforest areas in the tropical region. Third, new set of parameters (Table 2.1) were developed and documented for model application at regional and global scale.

These modifications enabled CLASS-CTEM^{N+} to adequately simulate the N dynamics and surface fluxes for site-level to regional and global scales, Results presented in three separate chapters show that CLASS-CTEM^{N+} model simulated carbon, water and energy exchanges and C stocks reasonably well, from site to regional to global scales. Evaluation of simulated N limitation impacts on global carbon sink and sources showed considerable variability between and within plant functional types such as forest due to non-linearity of N effects and spatiotemporal heterogeneity of C-N interactions. The consideration of N dynamics in the model reduced the terrestrial C uptake compared with the C-only version of the model in those regions, where N may not always be sufficiently available for plant growth, particularly in mid to high latitude boreal forests, tundra and some temperate forest regions. While a smaller N limitation effect was observed in the southern temperate and tropical regions where ecosystem production is limited by phosphorus rather than N. Our study results are comparable with other C-N coupled model estimates in the literature. My study highlights strengths and weaknesses of the CLASS-CTEM^{N+} and illuminates potential improvements and developments. It provides confidence that model is able to simulate interannual variability of the regional and global carbon fluxes and stocks. This capacity is important for coupled climate system modeling studies.

Throughout the development of CLASS-CTEM^{N+}, a main goal was to dynamically integrate a prognostic N cycle with C, water and energy processes simulation, allowing, among others, an explicit representation of nitrogen limitation in the carbon allocation scheme and accurately simulate plant productivity in nitrogen-limited environments. This goal was essentially achieved. However, study results also indicated that more biophysical and physiological processes might have to be explicitly represented to further improve model performance.

Important next steps may include, (1) improved representation of Plant Functional Types (PFTs); (2) inclusion of disturbances e.g., deforestation and fires and land use change; (3) inclusion of prognostic phosphorus cycle for tropical ecosystems; (4) introducing specific processes for peatland or wetland ecosystems; (5) inclusion of a more detailed soil hydrology to improve the model behavior in arid and tropical regions; and (6) extreme weather impact simulation capabilities under future climate change scenarios. These improvements (in both uncoupled and coupled modes), along with better characterization of errors in the climate forcing data sets and lagged environmental effects, would further increase agreement with the atmospheric records, and contribute most to reducing uncertainties.

In conclusion, this is the first attempt to apply and evaluate CLASS-CTEM^{N+} performance from site-to-region-to-global to simulate carbon, water and energy flux and carbon pools in terrestrial ecosystem with improved formulation of model processes and algorithms. The resulting model outputs and parameters serve as a strong foundation for future regional and global scale and long-term modeling studies. Overall, the inclusion of the nitrogen cycle in the CLASS-CTEM^{N+} improved its prediction accuracy. This study also suggested the need for long-term networks of observed data sets that can aid be model process development and their testing. Future implementation of CLASS-CTEM^{N+} in the Canadian GCM or Canadian Erath System Model would provide an assessment tool to generate scenarios for future climate change in support of the IPCC Assessment Reports, as well as for policy development and help Canada meet its international obligations to reduce its greenhouse gas emissions.